Title
High Precision Monte Carlo Event Generation for Particle Colliders

Author
Berggren, Calvin James

Publication Date
2013

Peer reviewed|Thesis/dissertation

High Precision Monte Carlo Event Generation for Particle Colliders

by

Calvin James Berggren

A dissertation submitted in partial satisfaction of the

requirements for the degree of

Doctor of Philosophy

in

Physics

in the

Graduate Division

of the

University of California, Berkeley

Committee in charge:

Dr. Christian W. Bauer, Co-Chair

Professor Lawrence J. Hall, Co-Chair

Professor Marjorie D. Shapiro

Professor Marc A. Rieffel

Fall 2013

High Precision Monte Carlo Event Generation for Particle Colliders

Abstract

High Precision Monte Carlo Event Generation for Particle Colliders

by

Calvin James Berggren

Doctor of Philosophy in Physics

University of California, Berkeley

Dr. Christian W. Bauer, Co-Chair

Professor Lawrence J. Hall, Co-Chair

Matrix-element calculations and parton shower programs are both crucial tools in the analysis of data at modern particle physics experiments at colliders. Finding the most effective ways to combine these complementary, but sometimes conflicting, approaches to simulating physical events has been the subject of much work in the recent decade. This thesis investigates state-of-the-art ways in which the precision of the matrix elements can be extended in combination with the parton shower. We identify three dimensions along which precision can be improved and describe how progress can be made along each one.

First, we present a general method to match fully differential next-to-next-to-leading-order (NNLO) calculations to parton shower (PS) programs, which represents an extension of the successful LO+PS (leading order) and NLO+PS (next-to-leading order) frameworks to NNLO+PS. We discuss in detail the perturbative accuracy criteria a complete NNLO+PS matching has to satisfy, and we give an explicit and general construction of the input "Monte Carlo cross sections" satisfying all required criteria.

Next, we describe how augmenting an NLO calculation with higher-order resummation of large Sudakov logarithms allows one to extend the lowest-order matching of tree-level matrix elements with parton showers to give a complete description at the next higher perturbative accuracy in α_s, at both small and large jet resolutions. As a byproduct, this combination naturally leads to a smooth connection of the NLO calculations for different jet multiplicities. We focus on the general construction of our method and present results of an implementation in the GENEVA Monte Carlo framework. For leptonic collisions, we apply our construction to $e^+e^- \to$ jets and obtain good agreement with LEP data for a variety of 2-jet observables. For hadronic collisions, we look at Drell-Yan production.

Gloria Patri, et Filio, et Spiritui Sancto

Contents

List of Figures

List of Tables

Acknowledgments

I give glory to God for the amazing world that He has made, and I give Him thanks for calling me to this endeavor, leading me through it, and giving me success. I give Him credit for blessing me with the ability to perform the work and the strength to complete it.

I would like to thank my wife Lesli Berggren for being so supportive and patient for these years of graduate school and for encouraging me to come to graduate school in the first place. I am also thankful for being able to have two sons during this time, Isaiah and Judah, who may someday find this interesting reading material. I would also like to thank my parents, Ron and Julia Berggren, for all of the support, stability, and opportunity they have provided for me throughout my life.

I would like to thank my advisor Christian Bauer for his leadership, guidance, caring attitude, and passion for physics and for the investment he has made in me the last few years. I have learned a huge amount about doing physics research from him.

I would also like to thank my collaborators including Andrew Hornig, Frank Tackmann, Chris Vermilion, and Saba Zuberi. I would especially like to thank my collaborators Simone Alioli and Jon Walsh for always being available for questions and spending time to help train me during my time at Berkeley.

Chapter 1

Introduction

In order to conduct an experimental particle collider program, one must have some way to translate both accepted and proposed theories into the backgrounds and signals that will be measured in the detector. Doing this is an involved and many-stage process that has evolved over decades of hard work from many communities. The goal is forming an expectation of what a specific measurement would yield if a certain theory were valid. This is done by simulating possible final-state events of particles that could have appeared in the detector. Once a large set of events has been simulated, they can be run through an analysis similar to that used for real events, and then the results of the simulation and the data can be compared.

At the core of the simulation are calculations of matrix elements using techniques of quantum field theory. Possible configurations of final-state hard partons are generated and weights are assigned to them based on their calculated matrix elements. It is advantageous to calculate these matrix elements as accurately as possible, and improving this is one way of increasing the precision of the simulation.

Calculations in quantum field theory are carried out in a perturbative fashion, where the result is a series of increasing powers of the coupling constants. The most important corrections to the leading order (LO) term come from the strong coupling constant α_s of quantum chromodynamics (QCD). Higher order terms in α_s come from interactions containing loops of strongly interacting particles. Organizing a calculation around powers of α_s is called a fixed-order calculation. The next-to-leading-order term in such a calculation is designated NLO is this document, the next-to-next-to-leading term NNLO, and so on. Leading order terms for events with greater numbers of strongly interacting particles also yield higher powers of α_s.

Unfortunately, proceeding with the calculation for a real event in terms of matrix elements becomes infeasible since real events can contain hundreds of particles and the complexity of the calculation scales factorially with the number of particles. In addition, nonperturbative effects also play a role, which matrix-element techniques are ill-equipped to handle. Fortunately, the interactions in an event tend to factorize into different scales where interactions at each scale are approximately independent

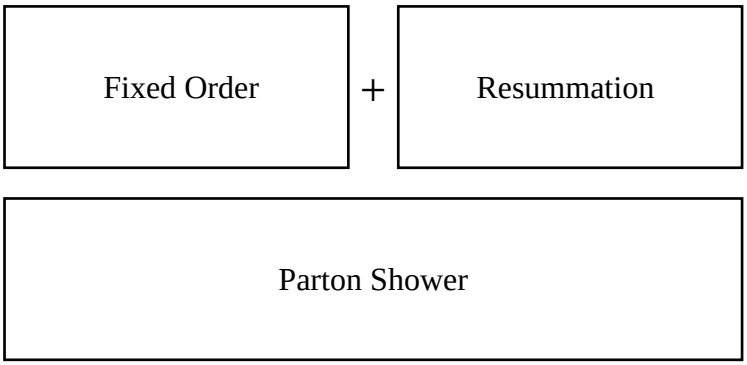

Figure 1.1: Shown above are important components for a Monte Carlo event generator. The top row represents the combination of fixed-order and resummed calculations. The final calculation is then matched onto a parton shower.

from each other. The hard scale interaction typically has only a few particles, and each of these hard particles then fragments into numerous other particles through lower-scale interactions. This factorization in scales led to the development of the parton shower, whose job it is to perform this fragmentation. The parton shower is an approximation to the full calculation and assumes that successive splittings are independent. The approximation of the parton shower tends to be reasonably accurate for soft and collinear splittings and not very accurate for hard splittings. At lower scales still, the partons combine into color-neutral hadrons, and this stage is handled by phenomenological hadronization models.

A central tension throughout this thesis is the one between the field theoretic calculation and the parton shower, as each plays an important role in the process and each imposes constraints on the other. In a sense, one would like to progressively replace more and more of the parton shower with a full calculation, as the parton shower is only an approximation to the full calculation. But as we shall see, making a partial and selective replacement is a delicate task.

Besides the difficulty of having a large multiplicity of particles, one further issue with traditional fixed-order calculations is that the perturbative series is not well behaved in certain regions of phase space. Regions of phase space that introduce a scale which is far below the hard scale of the interaction become problematic due to the appearance of large logarithmic factors in the series. For example, when two hard partons at hard scale Q become close together and are separated by a scale $\mathcal{T}$, then generically, up to two powers of $\log \frac{\mathcal{T}}{Q}$ appear for every power of α_s in the series. For small enough values of $\mathcal{T}$, the logarithm becomes numerically large. These large logarithms appear at all orders and spoil the convergence of the fixed-order series. Meaning can be restored to the series in these problematic regions through a technique called resummation, where sets of these logarithms are resummed to all orders.

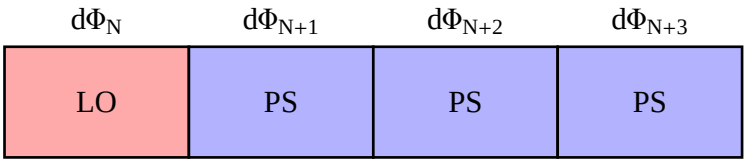

Figure 1.2: A scheme for event generation can be represented using a diagram like the above. This diagram represents a single multiplicity given at LO and all others filled in by the parton shower.

In total, fixed-order matrix elements, resummation, and parton showers are the three major elements that need to be carefully combined into a Monte Carlo event generator (see figure 1.1). The matrix elements and resummation are combined at the level of the theory calculation, and the full calculation is then matched onto the parton shower.

In light of this discussion, three major strategies can be seen for increasing the precision of the event generator.

1. One can add or increase the precision of higher multiplicity matrix elements in the calculation.

2. One can increase the fixed order to which the base-level matrix element is available.

3. One can increase the order of the resummation.

The final crucial note is that when carrying out any combination of the three strategies above, one must not disrupt the link to the parton shower. Each of these strategies presents its own difficulties.

Adding matrix elements for multiple multiplicities in a set of processes, as in strategy 1, requires a careful division of responsibilities between the matrix elements and the parton shower since both sides can give rise to events at the higher multiplicities. The parton shower increases the multiplicity of partons through splittings and can potentially lead to double counting regions of phase space covered by the matrix elements if one is not careful.

Note here that correctly combining matrix elements at multiple multiplicities requires a base level of resummation in order to match onto the parton shower. This is because the parton shower carries out a modest level of resummation itself, and the calculation needs to do the same in order to match up to it correctly. The parton shower provides resummation at the leading logarithmic (LL) level and partial resummation at the next-to-leading logarithmic (NLL) level. See sections 3.2.1.3 and 3.2.1.4 for more discussion of resummation orders.

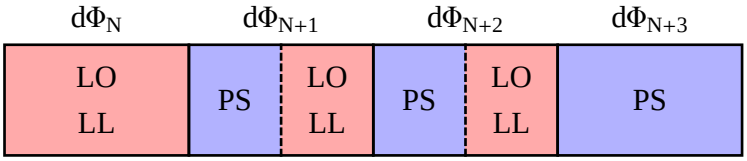

Figure 1.3: In an event generation scheme combining multiple LO matrix elements, each multiplicity is covered by either a matrix element calculation, a parton shower, or a combination of both. Correctly combining matrix elements and parton showers within a multiplicity requires the addition of LL resummation. The dashed line represents a jet resolution variable which divides the phase space into an N-jet-like region covered by the parton shower and an $(N+1)$-jet-like region covered by the matrix element.

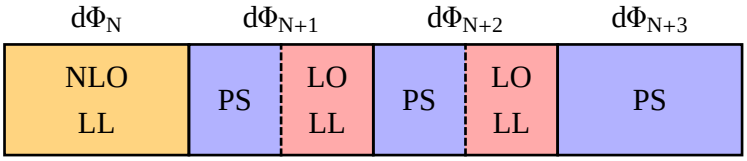

Figure 1.4: This scheme builds on figure 1.3 to include the first multiplicity at higher order.

Strategy 2 complicates things further because the presence of infrared (IR) divergences arising in higher-order matrix elements requires not only the addition of certain higher multiplicities as in strategy 1, but also its own rearrangement of phase space. Pushing to ever higher order in strategy 2 or returning to strategy 1 to increase the order of higher multiplicities creates an increasingly involved interplay between the various terms at different orders and different multiplicities that must align correctly with the base level of resummation required by the presence of the parton shower.

The third strategy above is to increase the level resummation beyond what is required by the parton shower. This requires careful consideration because resummation calculations typically are not fully differential and also because one has to be careful not to double count the effect of the resummation between the calculation and the parton shower.

The past decade has seen substantial improvements in the accuracy of fully exclusive event generators. Using strategy 1 above, matching schemes to simultaneously combine multiple LO matrix elements have been interfaced with parton shower (PS) routines and implemented in many event generators [4, 5, 6, 7, 8, 9, 10, 11, 12]. The combination with the parton shower requires the inclusion of LL resummation in the calculation. A diagrammatic representation of this scheme is shown in figure 1.3.

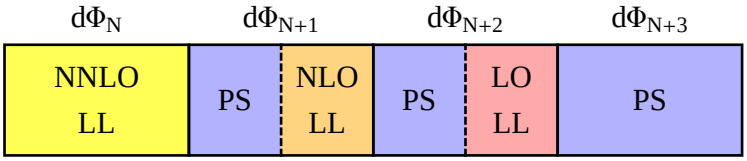

Figure 1.5: An NNLO+LL event generator would further extend the accuracy of certain multiplicities as shown above.

Pushing in direction 2, it has also become possible to match general NLO calculations with a parton shower and produce physical event samples that describe sufficiently inclusive distributions at NLO [13, 14, 15, 16, 17, 18, 19]. These NLO+PS event generators are now part of the standard tool set for experimental analyses and have made significant impact on phenomenology (see figure 1.4).

Calculations at NLO are particularly important because not only do they often produce sizeable corrections to the LO result, but they also introduce a scale parameter into the calculation which can be varied to put a handle on the uncertainty expected at that order. Well-behaved series will display a convergence where the uncertainties shrink at higher orders and where each order falls approximately within the previous order's uncertainties. Obtaining some measure of the theoretical uncertainty along with the central prediction is clearly a crucial part of understanding the theoretical expectations.

The frontier of fixed-order precision is calculations at NNLO in QCD perturbation theory. Fully differential NNLO calculations exist for several important hadron-collider processes involving W, Z, γ, and Higgs bosons as well as top quarks [20, 21, 22, 23, 24, 25, 26, 27, 28], and the technology for these calculations is continually being pushed toward more complex topologies [29, 30, 31]. Although experimental analyses regularly make use of NNLO cross sections and distributions, there are many challenges inherent in directly comparing fixed-order results with data.

As discussed above, an event generator that matches NNLO calculations with a parton shower would be the tool needed to bridge the gap between pure fixed-order calculations and the needs of experimentalists. It would provide hadron-level events that can be more easily interfaced with an analysis while maintaining NNLO accuracy for the underlying hard process, extending the power and flexibility of an NLO+PS generator to NNLO+PS.

In chapter 2, we present a general method for combining NNLO calculations with LL resummation to produce fully differential cross sections, and for attaching a parton shower routine to produce complete events (see figure 1.5). We derive the conditions that an NNLO+LL generator must satisfy and provide a construction that satisfies these.

Another complementary strategy for increasing the precision of an event generator

is by increasing the resummation order (strategy 3 in the list above). Accurate and reliable theoretical predictions for measurements at collider experiments require the inclusion of QCD effects beyond the lowest perturbative accuracy in the strong coupling α_s, and error estimation is also an important part of having reliable predictions. This is especially important in the complex environment of the LHC, which requires precise predictions for a broad spectrum of observables. It is true that higher-order corrections in α_s (strategy 2) are important to predict total cross sections and other inclusive observables. But it is also important to realize that exclusive jet observables, such as jet-vetoed cross sections, require the all-orders resummation of logarithmically enhanced contributions (strategy 3). In fact, for many observables, an accurate description across phase space demands a combination of *both* types of corrections. And as we have been repeating, the presence of the parton shower is crucial for experimental analyses to benefit from these advances.

The goal of modern Monte Carlo programs is to provide a proper description of the physics at every jet resolution scale. Returning to the LO+PS schemes described above (see figure 1.3), we can understand that one of their main advantages is being able to attain the lowest perturbative order accuracy in every region of phase space. Here, the parton shower provides the correct lowest-order description at small jet resolution scales, where the resummation of large Sudakov logarithms is needed, while at large jet resolution scales the exact tree-level matrix elements are needed to provide the correct lowest-order description. Hence, the LO+PS merging provides theoretical predictions at the formally leading $\mathcal{O}(1)$ accuracy relative to the lowest meaningful perturbative order. Once one has a consistent matching between these two limits of phase space, the possibility to include exact tree-level matrix elements for several jet multiplicities (strategy 1) follows almost automatically by iteration.

Given the necessity of higher-order perturbative corrections to make accurate predictions, it is important to extend the perturbative accuracy of the Monte Carlo description to formal $\mathcal{O}(\alpha_s)$ accuracy relative to the lowest order. Constructing a framework to do this is described in detail in chapter 3, along with an implementation of this framework in a new Monte Carlo called GENEVA.

Extending the perturbative accuracy requires including the formally next higher-order corrections that are relevant at each scale. At small scales, i.e., small values of the jet resolution variable, this requires improving the LL parton shower resummation with higher-order logarithmic resummation (strategy 3), while at large scales this requires including the fully differential NLO matrix elements. Assuming that we already have the matrix elements necessary to produce inclusive observables correct to NLO, improving the accuracy at large values of the jet resolution variable corresponds to increasing the order of matrix elements at higher multiplicity as described in strategy 1. Extending the precision of multiple multiplicities is a desirable feature which has recently been addressed by several groups [32, 33, 34, 35, 36, 37, 38, 39]. Our approach in particular focuses on the improvement to the resummation and finds that the extension to higher multiplicities emerges as a byproduct. We show results

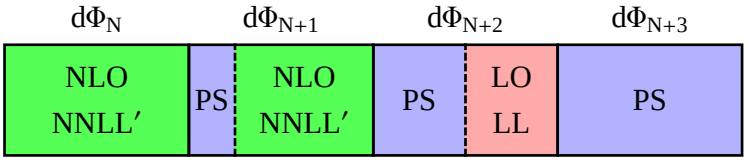

Figure 1.6: The GENEVA Monte Carlo merges two multiplicities at NLO and a third at LO. Resummation is included beyond the leading level, specifically NNLL′. (See sections 3.2.1.3 and 3.2.1.4 for more discussion of resummation orders.) The dashed line in the $(N+1)$-body phase space has shifted to the left compared to figure 1.4 because higher-order resummation has enabled us to use the matrix elements for a greater portion of the $(N+1)$-body phase space and the parton shower for less.

for two multiplicities merged at NLO (see figure 1.6) and describe a straightforward extension for merging an arbitrary number of multiplicities at NLO.

Having higher-order resummation allows GENEVA to push the matrix element calculations into the resummation region. This region has typically been beyond the reach of fixed-order calculations because the low scales encountered give rise to logarithms which are large enough to break down the perturbative expansion. When combined with resummation, one can extend the reach of the matrix-element calculations to these lower scales. This also means that one maintains explicit control of the perturbative uncertainties in this region where the parton shower was once used. This is an important step forward because parton showers do not provide a well-defined and reliable way to estimate uncertainties.

Chapter 3 focuses on the general construction of our method and discusses its application to e^+e^- and pp collisions. We present results of the implementation in the GENEVA Monte Carlo framework. We employ N-jettiness [1] as the jet resolution variable, combining its NNLL′ resummation with fully exclusive NLO matrix elements, and PYTHIA 8 as the backend for further parton showering and hadronization. For leptonic collisions, we take $e^+e^- \to$ jets as an example to apply our construction, and for hadronic collisions, we take Drell-Yan production. For $e^+e^- \to$ jets, together with the PYTHIA 8 hadronization model, we obtain good agreement with LEP data for a variety of 2-jet observables.

The remainder of this introduction provides an overview of Monte Carlo event generation and gives a general setup which is used in later chapters. The subsequent chapters in this thesis describe important progress that has been made along the lines of each of the three strategies outlined above. First, chapter 2 describes the extension of the generic NLO+PS program to NNLO+PS. Next, chapter 3 describes the first attempt to systematically include resummation into an event generator, which in turn yields the ability to fully combine multiple multiplicities at NLO. Finally, conclusions are presented in chapter 4.

1.1 Overview of Monte Carlo event generation

1.1.1 Monte Carlo phase space integration

Consider the cross section for some infrared-safe N-jet measurement M_X, which can contain a number of cuts (θ functions) as well as differential measurements (δ functions) of observables, which we collectively refer to as X. At leading order in perturbation theory, the cross section for measuring X is given by

$$\sigma^{\mathrm{LO}}(X) = \int \mathrm{d}\Phi_N \, B_N(\Phi_N) \, M_X(\Phi_N) \,, \tag{1.1}$$

where $B_N(\Phi_N)$ is the tree-level (Born) squared matrix element for N emissions. In case of hadronic collisions, we assume that the relevant parton densities (PDF) have already been convolved with the matrix elements, and we will therefore avoid writing them out explicitly in our formulae. The measurement function $M_X(\Phi_N)$ implements the measurement on the N-body phase space point Φ_N. In particular, since M_X is infrared safe, it cuts off any possible IR divergences in $B_N(\Phi_N)$. To obtain $\sigma(X)$ from eq. (1.1), one usually performs the phase space integral over Φ_N numerically. Due to the large dimensionality of N-body phase space, the typical method of choice is Monte Carlo integration: we generate points Φ_N with relative weights such that they are distributed according to $B_N(\Phi_N)$.[1] For each generated point Φ_N, we evaluate $M_X(\Phi_N)$ and record the result for X into appropriate histograms with the associated weight of the point Φ_N.

At next-to-leading order in perturbation theory, $\sigma(X)$ is given by

$$\sigma^{\mathrm{NLO}}(X) = \int \mathrm{d}\Phi_N \, (B_N + V_N)(\Phi_N) \, M_X(\Phi_N) + \int \mathrm{d}\Phi_{N+1} \, B_{N+1}(\Phi_{N+1}) \, M_X(\Phi_{N+1}) \,. \tag{1.2}$$

The virtual one-loop contribution V_N and the $(N+1)$-parton real-emission contribution B_{N+1} are separately IR divergent. A convenient way to handle these divergences is the standard subtraction method, where one writes[2]

$$\sigma^{\mathrm{NLO}}(X) = \int \mathrm{d}\Phi_N \, (B_N + V_N^C)(\Phi_N) \, M_X(\Phi_N) \tag{1.3}$$

[1] To be precise, if Φ_N points are generated according to a probability distribution $P(\Phi_N)$, each point gets assigned the weight $w(\Phi_N) = B_N(\Phi_N)/P(\Phi_N)$. The effective distribution of points is then $w(\Phi_N)P(\Phi_N) = B_N(\Phi_N)$, as desired. The simplest would be to use a flat sampling $P(\Phi_N) = 1$, while $P(\Phi_N) \approx B_N(\Phi_N)$ would be statistically more efficient. While the choice for $P(\Phi_N)$ is important for the statistical efficiency of the Monte Carlo integration, it is not relevant for our discussion.

[2] Alternatively, one can keep the Φ_N point fixed during the Φ_{N+1} integration and evaluate the same $M_X(\Phi_N)$ for all the subtraction counterterms and different $M_X[\hat{\Phi}^m_{N+1}(\Phi_N)]$ for each different B^m_{N+1} contribution, where $\sum_m B^m_{N+1} = B_{N+1}$. This approach might be better for efficiency reasons and more suitable for matching with the parton shower.

$$+ \int \mathrm{d}\Phi_{N+1} \left\{ B_{N+1}(\Phi_{N+1})\, M_X(\Phi_{N+1}) - \sum_m C^m_{N+1}(\Phi_{N+1})\, M_X[\hat{\Phi}^m_N(\Phi_{N+1})] \right\}.$$

Here, V^C_N denotes the virtual contribution including the appropriate integrated subtraction terms to render it IR finite. The C^m_{N+1} are the corresponding real-emission subtraction terms. Written in this way, the Φ_N and Φ_{N+1} integrals are separately IR finite and can each be performed numerically by Monte Carlo integration.

The Φ_N integral in eq. (1.3) can be performed as before at LO, except that the Φ_N points are now distributed according to $B_N + V^C_N$. The Φ_{N+1} integral is more involved now due to the presence of the subtraction terms. Their precise form is not important for our discussion. What is relevant is that generically several subtraction terms are needed to remove all possible IR singularities in B_{N+1} and that in each subtraction term, the measurement must be performed on a (in principle) different projected N-body phase space point $\hat{\Phi}^m_N(\Phi_{N+1})$. As a result, each generated point Φ_{N+1} contributes multiple times to each histogram with multiple weights distributed according to B_{N+1} and C^m_{N+1}, which are separately IR divergent. As we approach any IR-singular region, the different X values obtained for the real emission term and the relevant subtraction terms approach each other and eventually fall into the same histogram bin, where the IR-divergent contributions of real emission and subtractions cancel each other.

1.1.2 Monte Carlo event generation

The above Monte Carlo phase space integration is how essentially all (N)NLO programs using subtractions operate. Its main feature is that it allows one to obtain the exact result (up to limitations due to numerical precision) for arbitrary IR-safe observables. It can be contrasted with the event generation used in (parton shower) Monte Carlo event generators. In an event generator, the basic goal is to produce physical events that are generated and stored once and that can be repeatedly processed later, e.g., by performing various measurements on them.

Theoretically, performing a measurement M_X on the stored events is exactly equivalent to making a theoretical prediction for $\sigma(X)$. To illustrate this with a trivial example, imagine we want to compute $\sigma^{\mathrm{LO}}(X)$ in eq. (1.1) by generating events. To do so, we take

$$\frac{\mathrm{d}\sigma^{\mathrm{MC}}_{\geq N}}{\mathrm{d}\Phi_N} = B_N(\Phi_N) \qquad \text{and} \qquad \sigma^{\mathrm{LO}}(X) = \int \mathrm{d}\Phi_N \, \frac{\mathrm{d}\sigma^{\mathrm{MC}}_{\geq N}}{\mathrm{d}\Phi_N} \, M_X(\Phi_N)\,. \tag{1.4}$$

We now first generate a number of points Φ_N (the actual generation routine can be the same as before), call them "N-parton events," and store them together with their weights. These events are distributed according to the "MC cross section" $\mathrm{d}\sigma^{\mathrm{MC}}_{\geq N}/\mathrm{d}\Phi_N$. In the second step, we run over all stored events, evaluate the measurement $M_X(\Phi_N)$, and record the result for X into histograms with the associated weight of each event.

The result for $\sigma^{\mathrm{LO}}(X)$ obtained in this way is obviously identical to that obtained by performing the Monte Carlo integration of eq. (1.1) as described there. We have merely changed from two operations in a single loop into two separate loops with one operation each. In practice, this separation becomes vital as soon as the additional processing steps performed on the events become very involved (theoretically and/or computationally intensive). This is the case when the events are run through a parton shower and hadronization routine, which then also allows one to perform much more detailed measurements, such as propagating them through a complete detector simulation and using them in different experimental analyses.

Now, if we try to perform the NLO calculation in eq. (1.3) with the same approach, then for each generated and stored Φ_{N+1} point with weight proportional to B_{N+1}, we would also have to keep track and store the complete set of associated (correlated) Φ_N^m events with weights $-C_{N+1}^m(\Phi_{N+1})$. In principle, this is possible and would again give the identical result for $\sigma(X)$ as before (some fixed-order programs can indeed be run in this mode). However, for experimental purposes, e.g., when matching onto parton shower routines, it is impractical to deal with such "effective" events that consist of a number of correlated unphysical events with large and opposite weights. The point is that B_{N+1} and C_{N+1}^m separately are not physical cross sections. Their individual contributions are IR divergent, and the divergences only cancel each other to give a physical result once they are combined into a physical measurement, i.e., a single histogram bin.

Therefore, the goal is to generate events that are physical in the sense that the contribution from each event should correspond to an IR-safe cross section; i.e., all IR divergences should cancel on a per-event basis rather than between several unphysical events.[3] Conceptually, this implies that each N-parton event should be considered a "bin entry" in a partonic N-jet measurement, which is IR finite and fully differential in the corresponding partonic N-jet phase space. In other words, the generated N-parton events really represent points in an N-jet phase space rather than an N-parton phase space.

The definition of an N-jet cross section requires the presence of an N-jet resolution variable, which we call $\mathcal{T}_N$. It is defined such that, in the IR-singular region, $\mathcal{T}_N \to 0$. Emissions below $\mathcal{T}_N < \mathcal{T}_N^{\mathrm{cut}}$ are considered unresolved and $\mathcal{T}_N^{\mathrm{cut}}$ is called the N-jet resolution scale. When generating events with N and $N+1$ partons, they are

[3]Note that the problem is not the use of weighted events to obtain the desired distribution, since as long as the weighted events are statistically independent, they can be (partially) unweighted. What is very impractical is to have unphysical events that must be treated as correlated due to their individual weights being IR divergent, since there is no reasonable way to unweight these. One can also have an "intermediate" case, where the final cross section is made up of independent IR-finite parts, some of which still require events with negative weights. This causes much less severe but still important practical complications and so should be avoided if possible.

distributed according to the following Monte Carlo (MC) cross sections:

$$\begin{aligned} \Phi_N \text{ events:} \qquad & \frac{\mathrm{d}\sigma_N^{\mathrm{MC}}}{\mathrm{d}\Phi_N}(\mathcal{T}_N^{\mathrm{cut}})\,, \\ \Phi_{N+1} \text{ events:} \qquad & \frac{\mathrm{d}\sigma_{\geq N+1}^{\mathrm{MC}}}{\mathrm{d}\Phi_{N+1}}(\mathcal{T}_N > \mathcal{T}_N^{\mathrm{cut}})\,. \end{aligned} \tag{1.5}$$

The cross section $\sigma(X)$ measured from these events is given by

$$\sigma(X) = \int \mathrm{d}\Phi_N \, \frac{\mathrm{d}\sigma_N^{\mathrm{MC}}}{\mathrm{d}\Phi_N}(\mathcal{T}_N^{\mathrm{cut}})\, M_X(\Phi_N) + \int \mathrm{d}\Phi_{N+1} \, \frac{\mathrm{d}\sigma_{\geq N+1}^{\mathrm{MC}}}{\mathrm{d}\Phi_{N+1}}(\mathcal{T}_N > \mathcal{T}_N^{\mathrm{cut}})\, M_X(\Phi_{N+1})\,. \tag{1.6}$$

Physically, $\mathrm{d}\sigma_N^{\mathrm{MC}}/\mathrm{d}\Phi_N(\mathcal{T}_N^{\mathrm{cut}})$ is a fully differential, exclusive, partonic, N-jet cross section. Perturbatively, it is the cross section for the emission of N identified partons plus any number of unresolved emissions below the resolution scale $\mathcal{T}_N^{\mathrm{cut}}$. (At higher orders, this includes the necessary virtual corrections to render it IR finite.) Hence, as mentioned already, Φ_N really means Φ_N^{jet} here, and when specifying the jet resolution variable $\mathcal{T}_N$, one also needs to specify how unresolved emissions with $\mathcal{T}_N < \mathcal{T}_N^{\mathrm{cut}}$ are projected onto the partonic N-jet phase space Φ_N^{jet} in which the events are distributed. To avoid cluttering the notation, we suppress the explicit "jet" label from here out.

The cross section $\mathrm{d}\sigma_{\geq N+1}^{\mathrm{MC}}/\mathrm{d}\Phi_{N+1}(\mathcal{T}_N > \mathcal{T}_N^{\mathrm{cut}})$ in eqs. (1.5) and (1.6) is an inclusive partonic $(N+1)$-jet cross section. Perturbatively, it is the cross section for the emission of $N+1$ identified partons above the N-jet resolution scale $\mathcal{T}_N^{\mathrm{cut}}$. It includes any number of additional emissions, which are mapped onto the partonic $(N+1)$-jet phase space $\Phi_{N+1} \equiv \Phi_{N+1}^{\mathrm{jet}}$ of the $N+1$ identified partons (or rather partonic jets). The jet resolution variable $\mathcal{T}_N$ is part of the full Φ_{N+1}, and we use the argument $\mathcal{T}_N > \mathcal{T}_N^{\mathrm{cut}}$ to explicitly indicate the fact that $\mathrm{d}\sigma_{\geq N+1}^{\mathrm{MC}}$ only has support for $\mathcal{T}_N$ above $\mathcal{T}_N^{\mathrm{cut}}$.

This procedure is essentially what every generator of physical events does, either implicitly or explicitly. For example, in a pure parton shower generator, $\mathcal{T}_N$ corresponds to the shower evolution variable, and $\mathcal{T}_N^{\mathrm{cut}}$ is the parton shower cutoff. In this case, $\mathrm{d}\sigma_N^{\mathrm{MC}}/\mathrm{d}\Phi_N(\mathcal{T}_N^{\mathrm{cut}})$ is the no-emission probability, and $\mathrm{d}\sigma_{\geq N+1}^{\mathrm{MC}}/\mathrm{d}\Phi_{N+1}(\mathcal{T}_N > \mathcal{T}_N^{\mathrm{cut}})$ is the probability to have at least one emission above $\mathcal{T}_N^{\mathrm{cut}}$. This is discussed in detail in section 2.2.2.

We now want to cast the FO calculation in eq. (1.2) into a form suitable for event generation by applying the logic in eqs. (1.5) and (1.6) at fixed order. We start by considering the trivial example of an LO calculation. Since at tree level there are no additional emissions, we do not need to specify a resolution variable, the N jets coincide with the N tree-level partons, and measuring the N-jet phase space simply returns the full N-parton information. Thus, at LO, the "MC measurement" function defining the MC cross section is

$$M_{\mathrm{MC}}(\Phi_N') = \delta(\Phi_N - \Phi_N')\,; \tag{1.7}$$

i.e., the partonic phase space point Φ'_N going into the measurement is mapped trivially onto the partonic N-jet phase space $\Phi_N \equiv \Phi_N^{\text{jet}}$ of the Monte Carlo events. Inserting this into the LO calculation in eq. (1.1), we obtain

$$\frac{\mathrm{d}\sigma_{\geq N}^{\text{MC}}}{\mathrm{d}\Phi_N} = \int \mathrm{d}\Phi'_N \, B_N(\Phi'_N) \, M_{\text{MC}}(\Phi'_N) = B_N(\Phi_N) \,, \tag{1.8}$$

which is the obvious result and corresponds to eq. (1.4).

Starting at NLO, the fully differential MC measurement becomes nontrivial. We now need to specify how the measurement function acts on both Φ_N and Φ_{N+1} points. At NLO, the definition of the MC cross sections given below eq. (1.6) corresponds to the fully differential MC measurements

$$\begin{aligned} M_{\text{MC}}(\Phi'_N) &= \delta(\Phi_N - \Phi'_N) \,, \\ M_{\text{MC}}(\Phi'_{N+1}) &= \delta[\Phi_N - \hat{\Phi}_N(\Phi'_{N+1})] \, \theta[\mathcal{T}_N(\Phi'_{N+1}) < \mathcal{T}_N^{\text{cut}}] \\ &\quad + \delta(\Phi_{N+1} - \Phi'_{N+1}) \, \theta[\mathcal{T}_N(\Phi'_{N+1}) > \mathcal{T}_N^{\text{cut}}] \,. \end{aligned} \tag{1.9}$$

For these to be IR safe, $\mathcal{T}_N(\Phi_{N+1})$ can be any IR-safe resolution variable, and $\hat{\Phi}_N(\Phi_{N+1})$ can be any IR-safe projection from Φ_{N+1} to Φ_N. In particular, $\mathcal{T}_N(\Phi_N) = 0$, and $\mathcal{T}_N(\Phi_{N+1}) > \mathcal{T}_N^{\text{cut}}$ cuts off all IR-singular regions in Φ_{N+1}. Below the resolution scale $\mathcal{T}_N^{\text{cut}}$, the additional emission in Φ_{N+1} remains unresolved, and Φ_{N+1} is projected onto a corresponding Φ_N point via $\hat{\Phi}_N(\Phi_{N+1})$. Above $\mathcal{T}_N^{\text{cut}}$, the additional emission is resolved, and we measure the full Φ_{N+1} dependence. Inserting eq. (1.9) into eq. (1.2), we obtain

$$\begin{aligned} \frac{\mathrm{d}\sigma_N^{\text{MC}}}{\mathrm{d}\Phi_N}(\mathcal{T}_N^{\text{cut}}) &= (B_N + V_N)(\Phi_N) \\ &\quad + \int \frac{\mathrm{d}\Phi_{N+1}}{\mathrm{d}\Phi_N} \, B_{N+1}(\Phi_{N+1}) \, \theta[\mathcal{T}_N(\Phi_{N+1}) < \mathcal{T}_N^{\text{cut}}] \,, \\ \frac{\mathrm{d}\sigma_{\geq N+1}^{\text{MC}}}{\mathrm{d}\Phi_{N+1}}(\mathcal{T}_N > \mathcal{T}_N^{\text{cut}}) &= B_{N+1}(\Phi_{N+1}) \, \theta[\mathcal{T}_N(\Phi_{N+1}) > \mathcal{T}_N^{\text{cut}}] \,, \end{aligned} \tag{1.10}$$

where in the first equation, we have abbreviated

$$\frac{\mathrm{d}\Phi_{N+1}}{\mathrm{d}\Phi_N} \equiv \mathrm{d}\Phi_{N+1} \, \delta[\Phi_N - \hat{\Phi}_N(\Phi_{N+1})] \,. \tag{1.11}$$

Using eq. (1.10) as the MC cross sections in eq. (1.5), we can generate physical NLO events. Of course, to distribute our N-parton events, we still have to perform the NLO calculation in $\mathrm{d}\sigma_N^{\text{MC}}/\mathrm{d}\Phi_N(\mathcal{T}_N^{\text{cut}})$ (which may be nontrivial and require subtractions [see eq. (1.3)], but which we will assume exists).

We can ask to what extent other measurements M_X are reproduced at NLO when using eq. (1.10) together with eq. (1.6):

$$\sigma(X) = \int \mathrm{d}\Phi_N \, (B_N + V_N)(\Phi_N) \, M_X(\Phi_N) + \int \mathrm{d}\Phi_{N+1} \, B_{N+1}(\Phi_{N+1}) \tag{1.12}$$
$$\times \left\{ \theta[\mathcal{T}_N(\Phi_{N+1}) < \mathcal{T}_N^{\mathrm{cut}}] \, M_X[\hat{\Phi}_N(\Phi_{N+1})] + \theta[\mathcal{T}_N(\Phi_{N+1}) > \mathcal{T}_N^{\mathrm{cut}}] \, M_X(\Phi_{N+1}) \right\}.$$

Comparing to eq. (1.2), it is clear that observables are correct to the appropriate fixed order if and only if they are insensitive to the unresolved region of phase space below $\mathcal{T}_N^{\mathrm{cut}}$ where the measurement is evaluated on the projected phase space point $\hat{\Phi}_N(\Phi_{N+1})$ rather than the exact Φ_{N+1}. That is,

- N-jet (integrated) observables are correct to NLO_N up to power corrections that scale as $\mathcal{O}(\alpha_s \mathcal{T}_N^{\mathrm{cut}}/\mathcal{T}_N^{\mathrm{eff}})$, where $\mathcal{T}_N^{\mathrm{eff}}$ is the typical resolution scale to which the measurement is sensitive, i.e., up to which it integrates over Φ_{N+1}. In particular, it should contain the complete unresolved region of Φ_{N+1} where $\mathcal{T}_N(\Phi_{N+1}) < \mathcal{T}_N^{\mathrm{cut}}$.

- $(N+1)$-jet (differential) observables are correct to LO_{N+1} if they only include contributions in the resolved region of Φ_{N+1}, i.e., if their $M_X(\Phi_{N+1})$ completely excludes the unresolved $\mathcal{T}_N(\Phi_{N+1}) < \mathcal{T}_N^{\mathrm{cut}}$ region.

Here, M-jet observables are those that receive their first nonzero contribution from an M-parton final state, and $\mathrm{N}^n\mathrm{LO}_M$ refers to the $\mathcal{O}(\alpha_s^n)$ correction relative to the corresponding tree-level M-parton result.

An example of the effective resolution scale $\mathcal{T}_N^{\mathrm{eff}}$ is in Higgs boson production with a veto on extra jets (requiring $p_T^{\mathrm{jet}} < p_T^{\mathrm{cut}}$). If the resolution variable $\mathcal{T}_N$ is chosen to be the transverse momentum of the hardest jet, then $\mathcal{T}_N^{\mathrm{eff}} = p_T^{\mathrm{cut}}$. For a different resolution variable, $\mathcal{T}_N^{\mathrm{eff}}$ corresponds to the effective scale in $\mathcal{T}_N$ to which the cut on p_T^{jet} is sensitive. For example, if $\mathcal{T}_N$ is chosen to be the p_T of the Higgs, then $\mathcal{T}_N^{\mathrm{eff}} \simeq p_T^{\mathrm{cut}}$. If it is chosen to be beam thrust [40], then $\mathcal{T}_N^{\mathrm{eff}} \sim m_H (p_T^{\mathrm{cut}}/m_H)^{\sqrt{2}}$ [41].

The presence of power corrections in $\mathcal{T}_N^{\mathrm{cut}}/\mathcal{T}_N^{\mathrm{eff}}$ clearly highlights the formal limitation fundamental to the event generation method, namely that we inevitably lose the fully differential information below the resolution cutoff. This is the price we have to pay for the event-by-event IR-finiteness. Fortunately, in practice, this is not a problem, since we can always make $\mathcal{T}_N^{\mathrm{cut}}$ small enough such that either power corrections in $\mathcal{T}_N^{\mathrm{cut}}$ are irrelevant or else, if we do probe scales of order $\mathcal{T}_N^{\mathrm{cut}}$, the FO expansion breaks down and resummed perturbation theory is required to obtain a stable prediction. In this case, the only observables for which we cannot obtain an accurate FO result are those for which we would not want to use the FO calculation in the first place.

One might think that the breakdown of the FO expansion indicates that our events also become unphysical again. However, the important point is that the events (or

more precisely the underlying MC cross sections) are still defined in a physical IR-safe way. For very small $\mathcal{T}_N^{\text{cut}}$, we are simply going into an extremely exclusive and thus IR-sensitive region, where the FO calculation itself breaks down, irrespectively of how it is performed. This is precisely the region where improving the FO calculation with the parton-shower LL resummation or a higher-order resummation becomes necessary to obtain a meaningful perturbative result. Rewriting the FO calculation in this way forms the basis (and in fact is a necessary precondition) for combining it with a parton shower event generator. As we will see in the next chapter, after including the LL improvement, $\mathcal{T}_N^{\text{cut}}$ will become equivalent to the parton shower cutoff.

Chapter 2

Matching fully differential NNLO calculations and parton showers[1]

2.1 Introduction

One important frontier in modern event generation is the combination of state-of-the-art NNLO calculations with parton showers. Event generators at NLO+PS are now part of the standard tool set at experiments, but these lack the highest order theory calculations available. Experimental analyses also regularly make use of standalone NNLO cross sections and distributions, but there are many challenges inherent in directly comparing fixed-order results with data. An event generator that matches NNLO calculations with a parton shower would be an ideal tool to bridge the gap between pure fixed-order calculations and the needs of experimentalists. It would provide hadron-level events that can be more easily interfaced with an analysis while maintaining NNLO accuracy for the underlying hard process.

One important first step in this direction has been taken in ref. [43], where a MiNLO-improved Powheg simulation for Higgs plus one jet [38] was used to produce an NNLO+PS event sample for Higgs boson production by reweighting the events to the NNLO Higgs rapidity distribution.

In this chapter, we present a general method for combining NNLO calculations with leading-logarithmic (LL) resummation to produce fully differential cross sections and for attaching a parton shower routine to produce complete events. We derive the conditions that an NNLO+LL generator must satisfy and provide a construction that satisfies these. We also comment on the approach in ref. [43] and show how it can be derived as a special case of our results.

Theoretically, there are two conceptually very distinct aspects to interfacing a fixed-order calculation with a parton shower event generator (see figure 1.1). The

[1] This chapter is a modified version of a paper originally co-written with Simone Alioli, Christian W. Bauer, Frank J. Tackmann, Jonathan R. Walsh, and Saba Zuberi and published in [42].

first aspect is the LL improvement of the fully differential NNLO calculation. This corresponds to matching an LL resummed calculation with an NNLO calculation to obtain a combined NNLO+LL calculation, and doing so at a fully differential level. This aspect is, a priori, completely independent of any particular parton shower algorithm or program and can be performed solely at the partonic (or matrix-element) level. Here, the NNLO calculation first needs to be recast in a way that is suitable for fully differential event generation. Beyond leading order, the cross section for a fixed number of partons is infrared divergent and thus ill defined, meaning that to generate physical events with a given number of partons, the events must correspond to a physically well-defined and infrared-safe partonic jet cross section. In other words, each four-vector in the event should represent a partonic jet, which includes the contribution of an arbitrary number of unresolved emissions below some jet resolution cutoff. The NNLO calculation written in this way is then matched to an LL resummed calculation to obtain a combined fully differential NNLO+LL calculation.

The second aspect is to attach an exclusive parton shower Monte Carlo to this NNLO+LL calculation. In this step, events with N, $N+1$, and $N+2$ partons of the NNLO+LL calculation are handed to a parton shower algorithm, which generates additional emissions. Here, one has to take care of double counting between the shower emissions and the partonic calculation as well as the compatibility of the LL parton shower evolution with the partonic LL resummation.

The conceptual distinction between these two aspects has already been stressed in refs. [44, 45, 46]. It becomes particularly important at NNLO. As we will see, the first aspect of obtaining a consistent fully differential NNLO+LL matched calculation is the more challenging one, which is why most of our discussion will focus on it. Once this step has been carried out, the step of attaching a parton shower algorithm is relatively straightforward.

This chapter is organized as follows. In section 2.2, we discuss in detail the general framework for generating physical events at NNLO and at LL. The main outcome of this section will be to identify the "Monte Carlo (MC) cross sections" $\mathrm{d}\sigma^{\mathrm{MC}}$, which are the partonic jet cross sections according to which the different event multiplicities are distributed. In particular, we show how the fixed-order (FO) calculation is cast into this form to make it suitable for event generation. In section 2.3, we discuss the general procedure and conditions for combining the pure FO and pure LL calculations into a matched FO+LL calculation. As an instructive exercise, we review the corresponding MC cross section for the known cases of LO+LL and NLO+LL calculations. In section 2.4, we then discuss in detail how to construct the MC cross sections for an NNLO+LL calculation. In section 2.5, we discuss how to interface the NNLO+LL calculation with a parton shower, including the conditions needed to avoid any double counting that might arise. In section 2.6, we discuss how our method encompasses proposed and existing approaches [43, 46, 47], and in section 2.7, we give the conclusions for this chapter.

2.2 General setup

2.2.1 Event generation at NNLO

An overview of Monte Carlo event generation was given in the introduction in section 1.1 and included specific examples for the construction of pure LO and NLO Monte Carlos. We seek here to adapt that discussion to the case of NNLO.

To implement an NNLO calculation in the form of event generation, we first have to extend eq. (1.5) to include $(N+2)$-parton events. To do so, we split $\mathrm{d}\sigma^{\mathrm{MC}}_{\geq N+1}$ into an exclusive $\mathrm{d}\sigma^{\mathrm{MC}}_{N+1}$ and an inclusive $\mathrm{d}\sigma^{\mathrm{MC}}_{\geq N+2}$ using an additional $(N+1)$-jet resolution scale $\mathcal{T}^{\mathrm{cut}}_{N+1}$. Events with N, $N+1$, and $N+2$ partons are then distributed according to the following MC cross sections:

$$\begin{aligned}
\Phi_N \text{ events:} &\qquad \frac{\mathrm{d}\sigma^{\mathrm{MC}}_{N}}{\mathrm{d}\Phi_N}(\mathcal{T}^{\mathrm{cut}}_{N})\,, \\
\Phi_{N+1} \text{ events:} &\qquad \frac{\mathrm{d}\sigma^{\mathrm{MC}}_{N+1}}{\mathrm{d}\Phi_{N+1}}(\mathcal{T}_{N} > \mathcal{T}^{\mathrm{cut}}_{N}; \mathcal{T}^{\mathrm{cut}}_{N+1})\,, \\
\Phi_{N+2} \text{ events:} &\qquad \frac{\mathrm{d}\sigma^{\mathrm{MC}}_{\geq N+2}}{\mathrm{d}\Phi_{N+2}}(\mathcal{T}_{N} > \mathcal{T}^{\mathrm{cut}}_{N}, \mathcal{T}_{N+1} > \mathcal{T}^{\mathrm{cut}}_{N+1})\,.
\end{aligned} \tag{2.1}$$

The cross section $\sigma(X)$ measured from these events is given by

$$\begin{aligned}
\sigma(X) = &\int \mathrm{d}\Phi_N \, \frac{\mathrm{d}\sigma^{\mathrm{MC}}_{N}}{\mathrm{d}\Phi_N}(\mathcal{T}^{\mathrm{cut}}_{N})\, M_X(\Phi_N) \\
&+ \int \mathrm{d}\Phi_{N+1} \, \frac{\mathrm{d}\sigma^{\mathrm{MC}}_{N+1}}{\mathrm{d}\Phi_{N+1}}(\mathcal{T}_{N} > \mathcal{T}^{\mathrm{cut}}_{N}; \mathcal{T}^{\mathrm{cut}}_{N+1})\, M_X(\Phi_{N+1}) \\
&+ \int \mathrm{d}\Phi_{N+2} \, \frac{\mathrm{d}\sigma^{\mathrm{MC}}_{\geq N+2}}{\mathrm{d}\Phi_{N+2}}(\mathcal{T}_{N} > \mathcal{T}^{\mathrm{cut}}_{N}, \mathcal{T}_{N+1} > \mathcal{T}^{\mathrm{cut}}_{N+1})\, M_X(\Phi_{N+2})\,.
\end{aligned} \tag{2.2}$$

Here, $\mathrm{d}\sigma^{\mathrm{MC}}_{N}(\mathcal{T}^{\mathrm{cut}}_{N})$ is defined as before as an exclusive partonic N-jet cross section, i.e., the IR-finite cross section for N identified partons plus any number of unresolved emissions below the resolution scale $\mathcal{T}^{\mathrm{cut}}_{N}$. Next, $\mathrm{d}\sigma^{\mathrm{MC}}_{N+1}(\mathcal{T}_{N} > \mathcal{T}^{\mathrm{cut}}_{N}; \mathcal{T}^{\mathrm{cut}}_{N+1})$ is an exclusive partonic $(N+1)$-jet cross section and is also IR finite. It contains $N+1$ identified partons plus any number of unresolved emissions below the resolution scale $\mathcal{T}^{\mathrm{cut}}_{N+1}$. The argument $\mathcal{T}_{N} > \mathcal{T}^{\mathrm{cut}}_{N}$ indicates that the cross section only has support above $\mathcal{T}^{\mathrm{cut}}_{N}$, which acts as the condition to have one additional resolved parton. Finally, $\mathrm{d}\sigma^{\mathrm{MC}}_{\geq N+2}(\mathcal{T}_{N} > \mathcal{T}^{\mathrm{cut}}_{N}, \mathcal{T}_{N+1} > \mathcal{T}^{\mathrm{cut}}_{N+1})$ is an inclusive partonic $(N+2)$-jet cross section and is also IR finite. It contains at least $N+2$ identified partons, where two additional partons are required to be above $\mathcal{T}^{\mathrm{cut}}_{N}$ and $\mathcal{T}^{\mathrm{cut}}_{N+1}$, respectively, as well as any number of additional emissions. Compared to eq. (1.5), where $N+1$ was the highest multiplicity and inclusive over additional emissions, now both N and $N+1$ are exclusive multiplicities, while the highest multiplicity is $N+2$ and is again inclusive over additional emissions. In figure 2.1, we illustrate the regions in $\mathcal{T}_N$ and $\mathcal{T}_{N+1}$ contributing to each multiplicity.

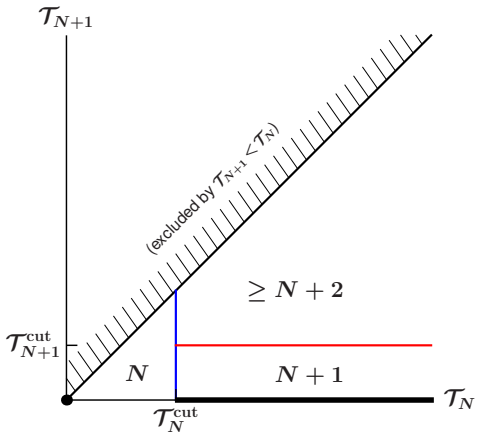

Figure 2.1: Illustration of the N-jet, $(N+1)$-jet, and $(N+2)$-jet regions in eq. (2.1) for resolution variables that satisfy $\mathcal{T}_{N+1} < \mathcal{T}_N$ (e.g., the p_T of the leading and subleading jet or N-jettiness [1]). The N-jet bin has $\mathcal{T}_N < \mathcal{T}_N^{\text{cut}}$ and is represented by N-parton events with $\mathcal{T}_N = \mathcal{T}_{N+1} = 0$ (shown by the black dot at the origin). The $(N+1)$-jet bin has $\mathcal{T}_N > \mathcal{T}_N^{\text{cut}}$ and $\mathcal{T}_{N+1} < \mathcal{T}_{N+1}^{\text{cut}}$ and is represented by $(N+1)$-parton events with $\mathcal{T}_{N+1} = 0$ (shown by the black line on the $\mathcal{T}_N$ axis). The inclusive $(N+2)$-jet bin has $\mathcal{T}_N > \mathcal{T}_N^{\text{cut}}$ and $\mathcal{T}_{N+1} > \mathcal{T}_{N+1}^{\text{cut}}$ and is represented by $(N+2)$-parton events.

At fixed NNLO, the cross section $\sigma(X)$ is given by

$$\begin{aligned}\sigma^{\text{NNLO}}(X) = &\int \mathrm{d}\Phi_N \,(B_N + V_N + W_N)(\Phi_N)\, M_X(\Phi_N) \\ &+ \int \mathrm{d}\Phi_{N+1} \,\big(B_{N+1} + V_{N+1}\big)(\Phi_{N+1})\, M_X(\Phi_{N+1}) \\ &+ \int \mathrm{d}\Phi_{N+2}\, B_{N+2}(\Phi_{N+2})\, M_X(\Phi_{N+2})\,, \end{aligned} \tag{2.3}$$

where W_N contains the two-loop virtual corrections for N partons and V_{N+1} the one-loop virtual corrections for $N+1$ partons. In principle, the phase space integrals in eq. (2.3) can again be performed by Monte Carlo integration using subtractions. Since the singularity structure of the real, virtual, and real-virtual contributions is much more complex than at NLO, the required subtractions are far more intricate.

We now want to recast eq. (2.3) in the form of eq. (2.2). At NNLO, the general definition of the MC cross sections given below eq. (2.2) corresponds to the following MC measurement functions:

$$\begin{aligned} M_{\text{MC}}(\Phi'_N) &= \delta(\Phi_N - \Phi'_N)\,, \\ M_{\text{MC}}(\Phi'_{N+1}) &= \delta[\Phi_N - \hat{\Phi}_N(\Phi'_{N+1})]\,\theta[\mathcal{T}_N(\Phi'_{N+1}) < \mathcal{T}_N^{\text{cut}}] \\ &\quad + \delta(\Phi_{N+1} - \Phi'_{N+1})\,\theta[\mathcal{T}_N(\Phi'_{N+1}) > \mathcal{T}_N^{\text{cut}}]\,, \end{aligned} \tag{2.4}$$

$$
\begin{aligned}
M_{\text{MC}}(\Phi'_{N+2}) &= \delta[\Phi_N - \hat{\Phi}_N(\Phi'_{N+2})]\,\theta[\mathcal{T}_N(\Phi'_{N+2}) < \mathcal{T}_N^{\text{cut}}] \\
&\quad + \delta[\Phi_{N+1} - \hat{\Phi}_{N+1}(\Phi'_{N+2})]\,\theta[\mathcal{T}_N(\Phi'_{N+2}) > \mathcal{T}_N^{\text{cut}}]\,\theta[\mathcal{T}_{N+1}(\Phi'_{N+2}) < \mathcal{T}_{N+1}^{\text{cut}}] \\
&\quad + \delta(\Phi_{N+2} - \Phi'_{N+2})\,\theta[\mathcal{T}_N(\Phi'_{N+2}) > \mathcal{T}_N^{\text{cut}}]\,\theta[\mathcal{T}_{N+1}(\Phi'_{N+2}) > \mathcal{T}_{N+1}^{\text{cut}}]\,.
\end{aligned}
$$

For these measurements to be IR safe, $\mathcal{T}_N$ and $\mathcal{T}_{N+1}$ can be any IR-safe resolution variables, and the various $\hat{\Phi}_N(\Phi_M)$ can be any IR-safe phase space projections. These conditions are much more nontrivial at NNLO compared to NLO, since we now need explicit projections from Φ_{N+2} down to Φ_N, and furthermore, the condition $\mathcal{T}_N(\Phi_{N+2}) > \mathcal{T}_N^{\text{cut}}$ must cut off all double-unresolved IR-singular regions of Φ_{N+2}. For example, at NLO, $\mathcal{T}_N$ could simply be defined as the p_T or virtuality of the one additional emission (which is IR safe at NLO). However, taking $\mathcal{T}_N$ and $\mathcal{T}_{N+1}$ as the p_T or virtuality of each of the two additional emissions is not IR safe at NNLO. Instead, a properly IR-safe NNLO generalization for $\mathcal{T}_N$ would be to define it as the p_T of the additional jet using an explicit jet algorithm with some jet radius R. This corresponds to using a "local" resolution variable. Another choice is to define it as the $\sum p_T$ of all additional emissions or N-jettiness [1]. These correspond to "global" resolution variables.

Plugging eq. (2.4) back into eq. (2.3), we obtain the required MC cross sections,

$$
\begin{aligned}
\frac{\mathrm{d}\sigma_N^{\text{MC}}}{\mathrm{d}\Phi_N}(\mathcal{T}_N^{\text{cut}}) &= (B_N + V_N + W_N)(\Phi_N) \\
&\quad + \int \frac{\mathrm{d}\Phi_{N+1}}{\mathrm{d}\Phi_N}\,(B_{N+1} + V_{N+1})(\Phi_{N+1})\,\theta[\mathcal{T}_N(\Phi_{N+1}) < \mathcal{T}_N^{\text{cut}}] \\
&\quad + \int \frac{\mathrm{d}\Phi_{N+2}}{\mathrm{d}\Phi_N}\,B_{N+2}(\Phi_{N+2})\,\theta[\mathcal{T}_N(\Phi_{N+2}) < \mathcal{T}_N^{\text{cut}}]\,, \\
\frac{\mathrm{d}\sigma_{N+1}^{\text{MC}}}{\mathrm{d}\Phi_{N+1}}(\mathcal{T}_N > \mathcal{T}_N^{\text{cut}}; \mathcal{T}_{N+1}^{\text{cut}}) &= (B_{N+1} + V_{N+1})(\Phi_{N+1})\,\theta[\mathcal{T}_N(\Phi_{N+1}) > \mathcal{T}_N^{\text{cut}}] \\
&\quad + \int \frac{\mathrm{d}\Phi_{N+2}}{\mathrm{d}\Phi_{N+1}}\,B_{N+2}(\Phi_{N+2})\,\theta[\mathcal{T}_N(\Phi_{N+2}) > \mathcal{T}_N^{\text{cut}}]\,\theta[\mathcal{T}_{N+1}(\Phi_{N+2}) < \mathcal{T}_{N+1}^{\text{cut}}]\,, \\
\frac{\mathrm{d}\sigma_{\geq N+2}^{\text{MC}}}{\mathrm{d}\Phi_{N+2}}(\mathcal{T}_N > \mathcal{T}_N^{\text{cut}}, \mathcal{T}_{N+1} > \mathcal{T}_{N+1}^{\text{cut}}) &= B_{N+2}(\Phi_{N+2})\,\theta[\mathcal{T}_N(\Phi_{N+2}) > \mathcal{T}_N^{\text{cut}}]\,\theta[\mathcal{T}_{N+1}(\Phi_{N+2}) > \mathcal{T}_{N+1}^{\text{cut}}]\,,
\end{aligned}
\tag{2.5}
$$

where we have defined the generalization of eq. (1.11),

$$
\frac{\mathrm{d}\Phi_M}{\mathrm{d}\Phi_N} \equiv \mathrm{d}\Phi_M\,\delta[\Phi_N - \hat{\Phi}_N(\Phi_M)]\,. \tag{2.6}
$$

Note that the implementation of the constraint $\mathcal{T}_N > \mathcal{T}_N^{\text{cut}}$ in $\mathrm{d}\sigma_{N+1}^{\text{MC}}$ is nontrivial now. For simplicity, we have not written any subtractions in eq. (2.5), which will be needed in some form when evaluating the cross sections numerically to separate

out and cancel the IR divergences in the virtual and real emission contributions. Applying the MC measurement functions in eq. (2.4) to the required subtraction terms is straightforward. The precise form of the subtractions is, however, not important for our discussion, and one can apply for example the NNLO subtraction techniques in refs. [48, 49, 50, 51].

As at NLO, writing the NNLO calculation in terms of IR-finite MC cross sections, as above, forms the basis for using it in an exclusive event generator for physical events. Using eq. (2.5) together with eq. (2.2), the cross section for some measurement M_X obtained in this way is

$$\begin{aligned}
\sigma(X) = &\int \mathrm{d}\Phi_N \,(B_N + V_N + W_N)(\Phi_N)\, M_X(\Phi_N) \\
&+ \int \mathrm{d}\Phi_{N+1}\,(B_{N+1} + V_{N+1})(\Phi_{N+1}) \\
&\quad \times \Big\{\theta[\mathcal{T}_N(\Phi_{N+1}) < \mathcal{T}_N^{\mathrm{cut}}]\, M_X[\hat{\Phi}_N(\Phi_{N+1})] \\
&\qquad + \theta[\mathcal{T}_N(\Phi_{N+1}) > \mathcal{T}_N^{\mathrm{cut}}]\, M_X(\Phi_{N+1})\Big\} \\
&+ \int \mathrm{d}\Phi_{N+2}\, B_{N+2}(\Phi_{N+2}) \\
&\quad \times \Big\{\theta[\mathcal{T}_N(\Phi_{N+2}) < \mathcal{T}_N^{\mathrm{cut}}]\, M_X[\hat{\Phi}_N(\Phi_{N+2})] \\
&\qquad + \theta[\mathcal{T}_N(\Phi_{N+2}) > \mathcal{T}_N^{\mathrm{cut}}]\, \theta[\mathcal{T}_{N+1}(\Phi_{N+2}) < \mathcal{T}_{N+1}^{\mathrm{cut}}]\, M_X[\hat{\Phi}_{N+1}(\Phi_{N+2})] \\
&\qquad + \theta[\mathcal{T}_N(\Phi_{N+2}) > \mathcal{T}_N^{\mathrm{cut}}]\, \theta[\mathcal{T}_{N+1}(\Phi_{N+2}) > \mathcal{T}_{N+1}^{\mathrm{cut}}]\, M_X(\Phi_{N+2})\Big\}\,. \qquad (2.7)
\end{aligned}$$

This has the same inevitable limitations that we already saw in the NLO case. Since N-parton and $(N+1)$-parton events correspond to partonic N-jet and $(N+1)$-jet cross sections, the measurement is evaluated on the corresponding projected phase space points in the unresolved regions of phase space. Therefore, the cross section $\sigma(X)$ is correct to the required fixed order (up to power corrections in the resolution scales) for measurements X that are insensitive to the unresolved regions of phase space. This means:

- N-jet observables are correct to NNLO_N if they integrate over the complete unresolved regions of Φ_{N+1} and Φ_{N+2}. [Power corrections are at most of relative $\mathcal{O}(\alpha_s \mathcal{T}_N^{\mathrm{cut}}/\mathcal{T}_N^{\mathrm{eff}})$ and $\mathcal{O}(\alpha_s^2 \mathcal{T}_{N+1}^{\mathrm{cut}}/\mathcal{T}_{N+1}^{\mathrm{eff}})$ where $\mathcal{T}_N^{\mathrm{eff}}$ and $\mathcal{T}_{N+1}^{\mathrm{eff}}$ are the typical resolution scales up to which the measurement integrates over Φ_{N+1} and Φ_{N+2}, and generically, $\mathcal{T}_{N+1}^{\mathrm{eff}} \lesssim \mathcal{T}_N^{\mathrm{eff}}$.]

- $(N+1)$-jet observables are correct to NLO_{N+1} if they only include contributions in the resolved region of Φ_{N+1}, while integrating over the complete unresolved region of Φ_{N+2}. [Power corrections are at most of relative $\mathcal{O}(\alpha_s \mathcal{T}_{N+1}^{\mathrm{cut}}/\mathcal{T}_{N+1}^{\mathrm{eff}})$ where $\mathcal{T}_{N+1}^{\mathrm{eff}} \leq \mathcal{T}_N$ is the typical resolution scale up to which the measurement integrates over Φ_{N+2}.]

- $(N+2)$-jet observables are correct to LO_{N+2} if they only include contributions in the resolved region of Φ_{N+2}.

As before, M-jet observables receive their tree-level contribution from an M-parton final state, and $\mathrm{N}^n\mathrm{LO}_M$ refers to the $\mathcal{O}(\alpha_s^n)$ correction relative to that. The definition of $\mathcal{T}_N^{\text{eff}}$ can be understood using an example similar to that used when discussing MC cross sections at NLO. These properties are fundamental to the event generation method and are shared by all implementations. In turn, they will also be the necessary conditions on the FO accuracy that should be maintained by the NNLO+LL calculation.

Although $\mathcal{T}_N^{\text{cut}}$ and $\mathcal{T}_{N+1}^{\text{cut}}$ are jet resolution scales, they will typically not define jets that are reasonable to measure experimentally. They effectively serve as IR cutoffs below which observables should be inclusive over unresolved emissions (which in fact means they should be smaller than the typical scales probed in the experimental jet measurements). In practice, $\mathcal{T}_N^{\text{cut}}$ and $\mathcal{T}_{N+1}^{\text{cut}}$ can again be made sufficiently small such that FO perturbation theory is no longer appropriate to describe observables that probe emissions at or below these scales. As at NLO, at this point, we are not losing any relevant fixed-order information, and the parton shower or higher-order resummation is required to provide a valid perturbative description.

To conclude this subsection, we stress that so far we have not done any showering; we have simply rewritten the FO calculation in a form suitable to generate physical events. This will be our starting point for obtaining a fully differential NNLO_N+LL calculation and defines the partonic jet cross sections that we will require as inputs from the FO calculation. We assume these are available to us, and we will not discuss the techniques used to compute them. For $\mathrm{d}\sigma_{N+1}^{\text{MC}}$ and $\mathrm{d}\sigma_{\geq N+2}^{\text{MC}}$, these are the same inputs that are required in the corresponding NLO_{N+1}+LL calculation. The genuine NNLO input required is the cumulant cross section $\mathrm{d}\sigma_N^{\text{MC}}/\mathrm{d}\Phi_N(\mathcal{T}_N^{\text{cut}})$. We assume that it is provided to us by the FO calculation in a form that allows us to obtain a numerical result for any needed Φ_N point and $\mathcal{T}_N^{\text{cut}}$ value. This is likely to be a challenging part in the practical implementation, and its availability might restrict the possible choices for the concrete definitions of $\mathcal{T}_N(\Phi_{N+2})$ and $\hat{\Phi}_N(\Phi_{N+2})$ that can be used.

2.2.2 Event generation at LL

The parton shower produces events whose cross sections include resummed contributions from all orders in perturbation theory. These resummed rates account for the large cancellations between virtual and real emissions in the IR region of phase space. The shower can therefore describe the resummation region of observables more accurately than FO calculations as well as produce high-multiplicity final states than can be passed through hadronization routines to produce realistic events. In this subsection, we are interested in using the parton shower approximation to obtain a

resummed calculation for the MC cross sections at leading-logarithmic (LL) order. This will serve as the basis for the LL improvement of the FO cross sections to obtain matched FO+LL calculations in sections 2.3 and 2.4. Note that here, we are not interested in the algorithmic construction of the parton shower. Formulating the LL calculation in a parton-shower-like fashion will facilitate attaching an actual parton shower to the matched FO+LL calculation.

The parton shower directly works as an event generator and is fundamentally based on evolution in a resolution variable $\mathcal{T}$, which characterizes the scale of an emission. Subsequent emissions occur at increasingly smaller values of $\mathcal{T}$, down to a low-scale cutoff $\mathcal{T}^{\text{cut}} \sim 1\,\text{GeV}$, where the perturbative parton shower description ceases to be valid. Below this cutoff, one enters the nonperturbative regime, where hadronization models are used. In the leading-logarithmic limit, all emissions are strongly ordered; i.e., each emission occurs at a much smaller value of $\mathcal{T}$ than the previous one, such that all emissions can be considered independent. Due to this single-emission nature, at LL, there is no distinction between global and local resolution variables that are equivalent for a single emission. Hence, we can define the N-jet resolution variable $\mathcal{T}_N$ as the emission scale $\mathcal{T}$ of the $N+1$st emission, with the resolution scale $\mathcal{T}_N^{\text{cut}}$ given by the shower cutoff $\mathcal{T}^{\text{cut}}$; i.e.,

$$\mathcal{T}_N = \mathcal{T}(N \to N+1)\,, \qquad \mathcal{T}_{N+1} = \mathcal{T}(N+1 \to N+2)\,, \qquad \mathcal{T}_N^{\text{cut}} = \mathcal{T}_{N+1}^{\text{cut}} \equiv \mathcal{T}^{\text{cut}}\,. \tag{2.8}$$

To start, we consider an N-jet process (with N partons at the Born level) and are interested in generating events with N and $N+1$ partons as in eqs. (1.5) and (1.6). The MC cross sections using the above N-jet resolution variable are then given at LL order as

$$\begin{aligned}
\frac{\mathrm{d}\sigma_N^{\text{MC}}}{\mathrm{d}\Phi_N}(\mathcal{T}_N^{\text{cut}}) &= B_N(\Phi_N)\,\Delta_N(\Phi_N;\mathcal{T}_N^{\text{cut}})\,,\\
\frac{\mathrm{d}\sigma_{\geq N+1}^{\text{MC}}}{\mathrm{d}\Phi_{N+1}}(\mathcal{T}_N &> \mathcal{T}_N^{\text{cut}})\\
&= \sum_m S_{N+1}^m(\Phi_{N+1})\,\Delta_N[\hat{\Phi}_N^m(\Phi_{N+1});\mathcal{T}_N^m(\Phi_{N+1})]\,\theta[\mathcal{T}_N^m(\Phi_{N+1}) > \mathcal{T}_N^{\text{cut}}]\\
&\equiv \sum_m S_{N+1}^m(\Phi_{N+1})\,\Delta_N(\hat{\Phi}_N^m;\mathcal{T}_N^m)\,\theta(\mathcal{T}_N^m > \mathcal{T}_N^{\text{cut}})\,,
\end{aligned} \tag{2.9}$$

where all ingredients and the notation we have introduced are discussed in detail in the following. To shorten the notation, we will often drop the explicit dependence on Φ_{N+1} for most objects, as in the last line of eq. (2.9), but one should keep in mind that in general, all objects which depend on the emission label m (which is explained below) have Φ_{N+1} as their argument.

First, $\Delta_N(\Phi_N;\mathcal{T}_N^{\text{cut}})$ is the N-parton Sudakov factor, which effectively sums the dominant contribution from an arbitrary number of unresolved emission below $\mathcal{T}_N^{\text{cut}}$

at LL, corresponding to the general definition of $\mathrm{d}\sigma_N^{\mathrm{MC}}/\mathrm{d}\Phi_N(\mathcal{T}_N^{\mathrm{cut}})$ [cf. the discussion below eq. (1.6)]. It can be written as

$$\Delta_N(\Phi_N;\mathcal{T}_N^{\mathrm{cut}}) = \exp\left[-\int \mathrm{d}\mathcal{T}\,\mathcal{P}_N(\Phi_N,\mathcal{T})\,\theta(\mathcal{T}>\mathcal{T}_N^{\mathrm{cut}})\right], \tag{2.10}$$

where $\mathcal{P}_N(\Phi_N,\mathcal{T})$ is a global $N \to N+1$ splitting function which sums over all possible single-parton emissions from each parton in Φ_N at the emission scale $\mathcal{T}$. It arises from projecting the full emission phase space $\mathrm{d}\Phi_{N+1}/\mathrm{d}\Phi_N$, which contains the complete set of splitting variables, onto the resolution variable $\mathcal{T}$,

$$\mathcal{P}_N(\Phi_N,\mathcal{T}) = \sum_m \int \mathrm{d}\Phi_{N+1}\,\mathcal{P}_N^m(\Phi_{N+1})\,\delta[\mathcal{T}-\mathcal{T}^m(\Phi_{N+1})]\,\delta[\Phi_N-\hat{\Phi}_N^m(\Phi_{N+1})]\,. \tag{2.11}$$

The m labels in eqs. (2.9) and (2.11) run over all the possible (IR-singular) emission channels ($q \to qg$, $g \to gg$, $g \to q\bar{q}$, etc.), including the information of which parton in Φ_N was split and which two partons in Φ_{N+1} resulted from the splitting. For each emission channel m, $\mathcal{T}^m(\Phi_{N+1})$ determines the relevant emission scale, and the splitting function $\mathcal{P}_N^m(\Phi_{N+1})$ contains all coupling and kinematic prefactors times the usual Altarelli-Parisi splitting function. For simplicity, we keep the upper limit $\mathcal{T} < \mathcal{T}_{\mathrm{max}}^m$ on the emission scale $\mathcal{T}$ implicit in the definition of $\mathcal{P}_N^m$.[2]

Finally, the projection $\hat{\Phi}_N^m(\Phi_{N+1})$ can be any IR-safe projection and as before, specifies how the partonic Φ_{N+1} is mapped onto the partonic N-jet phase space point $\Phi_N \equiv \Phi_N^{\mathrm{jet}}$, in which the N-parton events are distributed. The projection can be different for each m. (As far as the parton shower goes, $\hat{\Phi}_N^m$ is the inverse of the momentum reshuffling performed when splitting $\Phi_N \to \Phi_{N+1}$ in channel m.)

Coming to $\mathrm{d}\sigma_{\geq N+1}^{\mathrm{MC}}$ in eq. (2.9), the differential parton shower rate for the emission with index m is given by its splitting function times the Born contribution,

$$S_{N+1}^m(\Phi_{N+1}) = B_N[\hat{\Phi}_N^m(\Phi_{N+1})]\,\mathcal{P}_N^m(\Phi_{N+1})\,. \tag{2.12}$$

For future use, we also define

$$S_{N+1}(\Phi_{N+1}) = \sum_m S_{N+1}^m(\Phi_{N+1})\,, \tag{2.13}$$

which is the LL approximation of the full real emission contribution B_{N+1} in the IR-singular limit. The Sudakov factor $\Delta_N(\hat{\Phi}_N^m;\mathcal{T}_N^m)$ appearing in $\mathrm{d}\sigma_{\geq N+1}^{\mathrm{MC}}$ in eq. (2.9) is the same as in eq. (2.10) but evaluated at the emission scale $\mathcal{T}_N^m$. It effectively resums the contributions from arbitrary additional emissions below $\mathcal{T}_N^m$ at LL.

[2] In general, the upper limit $\mathcal{T} < \mathcal{T}_{\mathrm{max}}^m(\Phi_{N+1})$ is a function of the full Φ_{N+1} and can be different for different m. It can be determined purely by phase space limits or by an explicit upper cutoff of some form in order to turn off the resummation above $\mathcal{T}_{\mathrm{max}}$.

The cross section for some measurement M_X obtained from the LL MC cross sections in eq. (2.9) is

$$\sigma(X) = \int \mathrm{d}\Phi_N \, B_N(\Phi_N) \, \Delta_N(\Phi_N; \mathcal{T}_N^{\mathrm{cut}}) \, M_X(\Phi_N) + \int \mathrm{d}\Phi_{N+1} \sum_m S_{N+1}^m(\Phi_{N+1}) \, \Delta_N(\hat{\Phi}_N^m; \mathcal{T}_N^m) \, \theta(\mathcal{T}_N^m > \mathcal{T}_N^{\mathrm{cut}}) \, M_X(\Phi_{N+1}) \,. \quad (2.14)$$

To discuss its perturbative accuracy, we define

$$L = \ln(\mathcal{T}_N/Q) \,, \qquad L_{\mathrm{cut}} = \ln(\mathcal{T}_N^{\mathrm{cut}}/Q) \,, \quad (2.15)$$

where $Q \sim \mathcal{T}_N^{\mathrm{max}}$ is a typical hard scale in the process. Formally, the resummation corresponds to a reorganization of the perturbative series, which is achieved by expanding in α_s while counting[3]

$$\alpha_s L^2 \sim 1 \,, \qquad \alpha_s L_{\mathrm{cut}}^2 \sim 1 \,, \quad \text{or equivalently,} \quad L \sim L_{\mathrm{cut}} \sim \alpha_s^{-1/2} \,. \quad (2.16)$$

The leading-logarithmic order is $\mathcal{O}(1)$ in this counting. For the cumulant cross section integrated up to $\mathcal{T}_N^{\mathrm{cut}}$, this corresponds to resumming all terms $\sim \alpha_s^n L_{\mathrm{cut}}^{2n}$ relative to the Born cross section, while for the cross section differential in $\mathcal{T}_N$, this corresponds to resumming all terms $\sim \alpha_s^n L^{2n-1}/\mathcal{T}_N$. For a general measurement, this means:

- N-jet (integrated) observables are correct to LL resumming all terms $\sim \alpha_s^n \ln^{2n}(\mathcal{T}_N^{\mathrm{eff}}/Q)$, where here, $\mathcal{T}_N^{\mathrm{eff}}$ is the typical resolution up to which the measurement is integrated. (In particular, for $\mathrm{d}\sigma_N^{\mathrm{MC}}/\mathrm{d}\Phi_N(\mathcal{T}_N^{\mathrm{cut}})$, we have $\mathcal{T}_N^{\mathrm{eff}} \equiv \mathcal{T}_N^{\mathrm{cut}}$.)
- $(N+1)$-jet (differential) observables are correct to LL resumming all terms $\sim \alpha_s^n \ln^{2n-1}(\mathcal{T}_N^{\mathrm{eff}}/Q)/\mathcal{T}_N^{\mathrm{eff}}$, where here, $\mathcal{T}_N^{\mathrm{eff}}$ is the typical resolution to which the measurement is sensitive. (In particular, for $\mathrm{d}\sigma_{\geq N+1}^{\mathrm{MC}}/\mathrm{d}\Phi_{N+1}(\mathcal{T}_N)$, we have $\mathcal{T}_N^{\mathrm{eff}} \equiv \mathcal{T}_N$.)

The parton shower intrinsically preserves probability, which is a consequence of the fact that it is formulated as a Markov chain process, with the probability of each emission given by the exact differential of the integrated probability. Taking the special case where $M_X(\Phi_{N+1}) = M_X[\hat{\Phi}_N^m(\Phi_{N+1})]$, we precisely reproduce the total leading-order N-jet cross section from eq. (2.14),

$$\begin{aligned} \sigma(X) &= \int \mathrm{d}\Phi_N \Big\{ B_N(\Phi_N) \, \Delta(\Phi_N; \mathcal{T}_N^{\mathrm{cut}}) \, M_X(\Phi_N) \\ &\qquad + B_N(\Phi_N) \big[1 - \Delta_N(\Phi_N; \mathcal{T}_N^{\mathrm{cut}})\big] M_X(\Phi_N) \Big\} \\ &= \int \mathrm{d}\Phi_N \, B_N(\Phi_N) \, M_X(\Phi_N) \,. \end{aligned} \quad (2.17)$$

[3] We use the simple logarithmic counting for the cross section, so LL stands for LL_σ. Higher-order resummation is usually performed not for the cross section but for the logarithm of the cross section and using the stronger counting $\alpha_s L \sim 1$.

Here, we used the fact that the differential $\mathcal{T}_N$ spectrum is the exact derivative of the integrated $\mathcal{T}_N^{\text{cut}}$ cumulant cross section,

$$\begin{aligned}
&\sum_m \int \mathrm{d}\Phi_{N+1}\, S_{N+1}^m(\Phi_{N+1})\, \Delta_N(\Phi_N; \mathcal{T}_N^m)\, \theta(\mathcal{T}_N^m > \mathcal{T}_N^{\text{cut}})\, \delta(\Phi_N - \hat{\Phi}_N^m) \\
&\qquad = B_N(\Phi_N) \int \mathrm{d}\mathcal{T}\, \mathcal{P}_N(\Phi_N, \mathcal{T})\, \Delta_N(\Phi_N; \mathcal{T})\, \theta(\mathcal{T} > \mathcal{T}_N^{\text{cut}}) \\
&\qquad = B_N(\Phi_N) \big[1 - \Delta_N(\Phi_N; \mathcal{T}_N^{\text{cut}})\big] \,. \qquad (2.18)
\end{aligned}$$

As a result, the $\mathcal{T}_N^{\text{cut}}$ dependence precisely cancels between the cumulant and the integrated spectrum in eq. (2.17). For a general measurement $M_X(\Phi_{N+1})$ that cannot be written in terms of the shower projection $\hat{\Phi}_N^m$, the LO cross section is reproduced up to small power corrections $\sim \mathcal{T}_N^{\text{cut}}/Q$, which introduce a small residual $\mathcal{T}_N^{\text{cut}}$ dependence.

In the resummation counting of eq. (2.16), the Sudakov factors in eqs. (2.14) and (2.17) are $\mathcal{O}(1)$, and in particular, $1 - \Delta_N(\mathcal{T}_N^{\text{cut}}) \sim \mathcal{O}(1)$, despite the fact that its FO expansion would start at α_s, which is essential for eq. (2.17) to work out. What happens is that $S_{N+1} \sim \alpha_s L/\mathcal{T}_N$, which upon integration over $\mathcal{T}_N > \mathcal{T}_N^{\text{cut}}$, becomes $\alpha_s L_{\text{cut}}^2 \sim 1$. In other words, the $\mathcal{T}_N$ spectrum at small $\mathcal{T}_N$ is $\mathcal{O}(1)$ at LL, even though at fixed order, it only starts at α_s.

2.3 Combining fully differential FO calculations with LL resummation

In this section, we discuss the general conditions to combine the fully differential FO and LL calculations in an event generator. After the general discussion in section 2.3.1, we will review the LO+LL and NLO+LL cases in the following subsections. The NNLO+LL case is then discussed in detail in section 2.4.

2.3.1 General discussion

The goal of combining the FO calculation with the LL resummation is to improve the perturbative accuracy in the resummation region, where the FO expansion itself becomes invalid, to attain at least the $\mathcal{O}(1)$ accuracy provided by the LL resummation there. At the same time, the perturbative accuracy of the FO calculation must be maintained in the FO region where the resummation is unimportant.

As a necessary precondition, the combined FO+LL calculation must be simultaneously correct to the desired fixed order (LO, NLO, etc.) and resummation order (LL, NLL, etc.). Here, the fixed order is counted as usual by powers of α_s, while the resummation order is dictated by the logarithmic counting in eq. (2.16),

$$\alpha_s L^2 \sim 1 \,, \qquad \alpha_s L_{\text{cut}}^2 \sim 1 \,, \quad \text{or equivalently,} \quad L \sim L_{\text{cut}} \sim \alpha_s^{-1/2} \,,$$

where $L = \ln(\mathcal{T}_N/Q)$ and $L_{\text{cut}} = \ln(\mathcal{T}_N^{\text{cut}}/Q)$ [see eq. (2.15)]. Therefore, the MC cross sections of the FO+LL calculation have to satisfy the conditions

$$\left[\mathrm{d}\sigma^{\text{MC}}\right]_{\text{FO}} = \mathrm{d}\sigma^{\text{MC-FO}}\,, \qquad \left[\mathrm{d}\sigma^{\text{MC}}\right]_{\text{LL}} = \mathrm{d}\sigma^{\text{MC-LL}}\,, \tag{2.19}$$

which require that, upon expanding/truncating the MC cross sections to either FO or LL, denoted by $[\cdots]_{\text{FO}}$ or $[\cdots]_{\text{LL}}$, the pure FO or LL results appearing on the right-hand sides in eq. (2.19) correctly reproduce the results in section 2.2. These conditions ensure that the input MC cross sections for each event multiplicity have the desired perturbative accuracy in both the resummation and fixed-order regions. For example, at NLO+LL, where we need events with N and $N+1$ partons, the MC cross sections $\mathrm{d}\sigma_N^{\text{MC}}$ and $\mathrm{d}\sigma_{\geq N+1}^{\text{MC}}$ are correct to NLO_N+LL and LO_{N+1}+LL, respectively. Similarly, for NNLO+LL, where we need events with N, $N+1$, and $N+2$ partons, the corresponding $\mathrm{d}\sigma_N^{\text{MC}}$, $\mathrm{d}\sigma_{N+1}^{\text{MC}}$, and $\mathrm{d}\sigma_{\geq N+2}^{\text{MC}}$ are correct to NNLO_N+LL, NLO_{N+1}+LL, and LO_{N+2}+LL, respectively.

We also have to achieve the desired perturbative accuracy at FO and LL for general measurements M_X. As discussed in section 2.2, when generating physical events, $\sigma(X)$ is predicted at the desired accuracy only up to power corrections in the resolution scale $\mathcal{T}_N^{\text{cut}}$, which should therefore be as small as possible. At the same time, for integrated N-jet observables, the residual dependence on the resolution scale $\mathcal{T}_N^{\text{cut}}$ in the pure FO and LL calculations is at most power suppressed. The important condition is now that the same must also hold for the combined FO+LL calculation. Therefore:

- Since $\mathcal{T}_N^{\text{cut}}$ must be taken as small as possible to minimize power corrections, it is imperative that logarithms of $\mathcal{T}_N^{\text{cut}}$ must be counted as in eq. (2.16), for which we adopt the notation $\mathcal{O}_{\text{cut}}$, such that $\alpha_s^n L_{\text{cut}}^m \sim \mathcal{O}_{\text{cut}}(\alpha_s^{n-m/2})$.

- For integrated N-jet and $(N+1)$-jet observables that in fixed order are predicted at α_s^n with corrections starting at $\mathcal{O}(\alpha_s^{n+1})$, any residual logarithmic dependence on the jet resolution scales $\mathcal{T}_N^{\text{cut}}$ and $\mathcal{T}_{N+1}^{\text{cut}}$ must be $\mathcal{O}_{\text{cut}}(\alpha_s^{\geq n+1})$, i.e., only give corrections at the level of accuracy (or higher) as expected from higher FO corrections.

To ensure this, the conditions in eq. (2.19) alone are not sufficient. In addition, the MC cross sections for different multiplicities must be consistent with each other and satisfy the relation[4]

$$\frac{\mathrm{d}}{\mathrm{d}\mathcal{T}_N^{\text{cut}}}\left[\frac{\mathrm{d}\sigma_N^{\text{MC}}}{\mathrm{d}\Phi_N}(\mathcal{T}_N^{\text{cut}})\right]_{\mathcal{T}_N^{\text{cut}}=\mathcal{T}_N} = \int \frac{\mathrm{d}\Phi_{N+1}}{\mathrm{d}\Phi_N}\,\delta[\mathcal{T}_N - \mathcal{T}_N(\Phi_{N+1})]\,\frac{\mathrm{d}\sigma_{\geq N+1}^{\text{MC}}}{\mathrm{d}\Phi_{N+1}}(\mathcal{T}_N > \mathcal{T}_N^{\text{cut}}) \tag{2.20}$$

[4]In general, the projection from Φ_{N+1} to Φ_N and the definition of $\mathcal{T}_N(\Phi_{N+1})$ can depend on the emission channel inside $\mathrm{d}\sigma_{\geq N+1}^{\text{MC}}$, which we have kept implicit in eq. (2.20). In a given implementation, this dependence is naturally accounted for, as we will see in the discussions below.

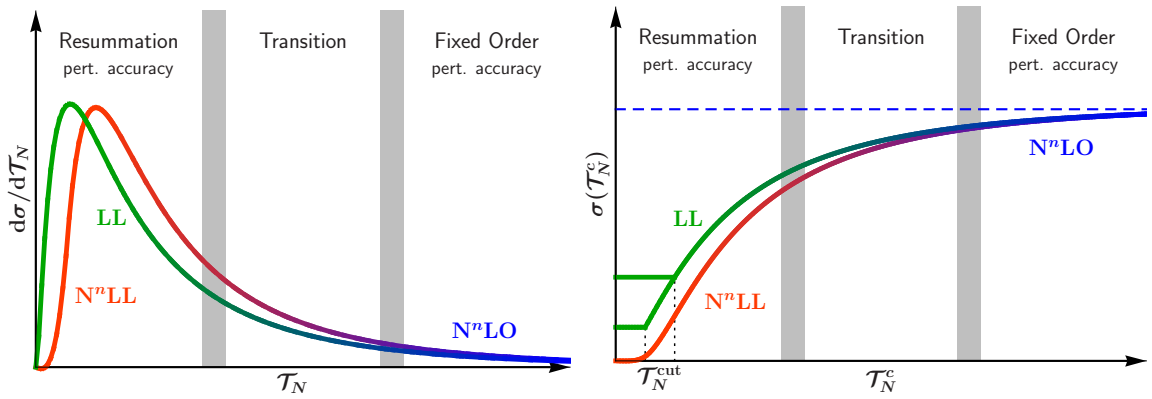

Figure 2.2: Illustration of the perturbative accuracy of the cross section in different regions of the jet resolution variable $\mathcal{T}_N$. On the left, we show the differential spectrum in $\mathcal{T}_N$, and on the right, we show the cumulant as a function of $\mathcal{T}_N^c$, which approaches the total N-jet cross section (blue dashed line) for large $\mathcal{T}_N^c$. For large $\mathcal{T}_N^{(c)}$, the FO contributions (blue) determine the perturbative accuracy. As $\mathcal{T}_N^{(c)}$ decreases into the transition region, the resummed terms become increasingly important. At small $\mathcal{T}_N^{(c)}$, the resummation order determines the perturbative accuracy. The LL accuracy (green) that determines the shape at small $\mathcal{T}_N^{(c)}$ can be improved by higher-order resummation (orange). In the LL cumulant, we show that two different $\mathcal{T}_N^{\mathrm{cut}}$ values (dotted vertical lines) should produce the same cumulant cross section above $\mathcal{T}_N^{\mathrm{cut}}$.

up to $\mathcal{O}_{\mathrm{cut}}(\alpha_s^{\geq n+1})$ violations for an N^{n}LO$_N$+LL calculation. (The missing exact dependence on Φ_{N+1} below $\mathcal{T}_N^{\mathrm{cut}}$ will still introduce the same power corrections in $\mathcal{T}_N^{\mathrm{cut}}$ for general measurements M_X as in the pure FO and LL cases.) On the right-hand side, the fully differential Φ_{N+1} dependence is projected onto $\{\Phi_N, \mathcal{T}_N\}$. The condition then enforces that the resulting differential $\mathcal{T}_N$ spectrum is the derivative of the cumulant with respect to $\mathcal{T}_N^{\mathrm{cut}}$ (for any fixed Φ_N), such that the $\mathcal{T}_N^{\mathrm{cut}}$ dependence between the cumulant and the spectrum cancels to the desired order. Integrating eq. (2.20) over $\mathcal{T}_N$, we obtain the equivalent condition for the cumulant being the integral of the $\mathcal{T}_N$ spectrum. That is, for any $\mathcal{T}_N^c$ (and fixed Φ_N),

$$\frac{\mathrm{d}\sigma_N^{\mathrm{MC}}}{\mathrm{d}\Phi_N}(\mathcal{T}_N^c) = \frac{\mathrm{d}\sigma_N^{\mathrm{MC}}}{\mathrm{d}\Phi_N}(\mathcal{T}_N^{\mathrm{cut}}) + \int \frac{\mathrm{d}\Phi_{N+1}}{\mathrm{d}\Phi_N} \frac{\mathrm{d}\sigma_{\geq N+1}^{\mathrm{MC}}}{\mathrm{d}\Phi_{N+1}}(\mathcal{T}_N > \mathcal{T}_N^{\mathrm{cut}})\,\theta(\mathcal{T}_N < \mathcal{T}_N^c) \tag{2.21}$$

up to $\mathcal{O}_{\mathrm{cut}}(\alpha_s^{\geq n+1})$ violations for an N^{n}LO$_N$+LL calculation.

In figure 2.2, we show how the FO and resummed contributions determine the accuracy of the cross sections in different regions of phase space. In table 2.1, we summarize the perturbative accuracy as well as the size of uncontrolled higher-order corrections from fixed order, resummed, and residual resolution scale dependence for integrated N-jet observables and differential $(N+1)$-jet observables for various

	$\mathcal{T}_N^{\text{eff}} \sim Q$ (fixed order)	$\mathcal{T}_N^{\text{eff}} \ll Q$ (resummation)
	N-jet observables	
LO_N	$1 + \mathcal{O}(\alpha_s)$	$\mathcal{O}(1)$
NLO_N	$1 + \alpha_s + \mathcal{O}(\alpha_s^2)$	$\mathcal{O}(1)$
NNLO_N	$1 + \alpha_s + \alpha_s^2 + \mathcal{O}(\alpha_s^3)$	$\mathcal{O}(1)$
LO_N+LL	$1 + \mathcal{O}(\alpha_s)$	$1 + \mathcal{O}(\alpha_s^{1/2})$
$\text{LO}_{N,N+1}$+LL	$1 + \mathcal{O}(\alpha_s) + \mathcal{O}_{\text{cut}}(\alpha_s^{\geq 1})$	$1 + \mathcal{O}(\alpha_s^{1/2})$
NLO_N+LL	$1 + \alpha_s + \mathcal{O}(\alpha_s^2) + \mathcal{O}_{\text{cut}}(\alpha_s^{\geq 2})$	$1 + \mathcal{O}(\alpha_s^{1/2})$
$\text{NLO}_{N,N+1}$+LL	$1 + \alpha_s + \mathcal{O}(\alpha_s^2) + \mathcal{O}_{\text{cut}}(\alpha_s^{\geq 2})$	$1 + \mathcal{O}(\alpha_s^{1/2})$
NNLO_N+LL	$1 + \alpha_s + \alpha_s^2 + \mathcal{O}(\alpha_s^3) + \mathcal{O}_{\text{cut}}(\alpha_s^{\geq 3})$	$1 + \mathcal{O}(\alpha_s^{1/2})$
	$(N+1)$-jet observables	
LO_N	$\times$	$\times$
NLO_N	$1 + \mathcal{O}(\alpha_s)$	$\mathcal{O}(1)$
NNLO_N	$1 + \alpha_s + \mathcal{O}(\alpha_s^2)$	$\mathcal{O}(1)$
LO_N+LL	$\mathcal{O}(1)$	$1 + \mathcal{O}(\alpha_s^{1/2})$
$\text{LO}_{N,N+1}$+LL	$1 + \mathcal{O}(\alpha_s) + \mathcal{O}_{\text{cut}}(\alpha_s^{\geq 1})$	$1 + \mathcal{O}(\alpha_s^{1/2})$
NLO_N+LL	$1 + \mathcal{O}(\alpha_s) + \mathcal{O}_{\text{cut}}(\alpha_s^{\geq 1})$	$1 + \mathcal{O}(\alpha_s^{1/2})$
$\text{NLO}_{N,N+1}$+LL	$1 + \alpha_s + \mathcal{O}(\alpha_s^2) + \mathcal{O}_{\text{cut}}(\alpha_s^{\geq 2})$	$1 + \mathcal{O}(\alpha_s^{1/2})$
NNLO_N+LL	$1 + \alpha_s + \mathcal{O}(\alpha_s^2) + \mathcal{O}_{\text{cut}}(\alpha_s^{\geq 2})$	$1 + \mathcal{O}(\alpha_s^{1/2})$

Table 2.1: Perturbative accuracy of N-jet (integrated) and $(N+1)$-jet (differential) observables satisfied at different FO and FO+LL. Here, $\mathcal{T}_N^{\text{eff}}$ is the effective scale to which the observables are sensitive. For $\mathcal{T}_N^{\text{eff}} \sim Q$, the perturbative accuracy is set by the FO expansion, with corrections from higher FO contributions as well as residual $\mathcal{T}_N^{\text{cut}}$ dependence. (The latter will depend on the details of the matching, so we show the minimal required accuracy, which has to match the FO level of accuracy; see the discussion of eq. (2.20) for more details.) For $\mathcal{T}_N^{\text{eff}} \ll Q$, the perturbative accuracy is set by the resummation counting in eq. (2.16).

FO+LL orders. To give an example, at NNLO_N+LL, integrated N-jet observables are supposed to get the $\mathcal{O}(\alpha_s^0)$, $\mathcal{O}(\alpha_s^1)$, and $\mathcal{O}(\alpha_s^2)$ terms correct, with corrections starting at $\mathcal{O}(\alpha_s^3)$. This implies that the $\mathcal{T}_N^{\text{cut}}$ dependence must cancel such that it only appears at $\mathcal{O}_{\text{cut}}(\alpha_s^{\geq 3})$, so the lowest-order dependence must be of the form $\alpha_s^n L_{\text{cut}}^{2n-6} \sim \mathcal{O}_{\text{cut}}(\alpha_s^3)$ or higher. A residual $\mathcal{T}_N^{\text{cut}}$ dependence of the form $\alpha_s^2[1 - \Delta_N(\mathcal{T}_N^{\text{cut}})]$, which starts at fixed $\mathcal{O}(\alpha_s^3)$, counts as $\mathcal{O}_{\text{cut}}(\alpha_s^2)$ because $\Delta_N(\mathcal{T}_N^{\text{cut}}) \sim \mathcal{O}_{\text{cut}}(1)$. Hence, such a $\mathcal{T}_N^{\text{cut}}$ dependence would spoil the desired $\mathcal{O}(\alpha_s^2)$ accuracy of the NNLO+LL calculation.

When increasing the FO accuracy, the condition in eq. (2.20) becomes more and more stringent and thus more challenging. As we saw in section 2.2.2, in the LL calculation, the cancellation of the $\mathcal{T}_N^{\text{cut}}$ dependence to all orders is achieved by virtue of the fact that the differential cross section in $\mathcal{T}_N$ is given by the exact derivative of the cumulant cross section with respect to $\mathcal{T}_N^{\text{cut}}$. The same is also obviously true for the pure FO calculation. This demonstrates that a simple and generic method to ensure the cancellation of the resolution scale dependence (up to power corrections) is to explicitly construct the spectrum and cumulant by enforcing eqs. (2.20) and (2.21) exactly. There are different choices for doing so, as we will see in section 2.4, as well as different options for the practical implementation, which we will come back to in section 2.6.

Note that, a priori, we do not require the resummation order to match the perturbative accuracy of the fixed order. For example, the NLL terms in an NNLO+LL cross section are allowed to be incorrectly predicted, even though in the resummation region, they are formally more important than the NNLO terms. These higher-order resummed terms will affect observables in the singular regime at small $\mathcal{T}_N^{\text{eff}}$ but not observables at large $\mathcal{T}_N^{\text{eff}}$, which are controlled by FO corrections. In section 2.4, we will explicitly see how the mismatch between the LL resummation and the NNLO calculation enters. A consistent matching of fixed order and resummation at the same perturbative accuracy would clearly be a desirable feature. As is shown in chapter 3, by performing the resummation at NNLL, the merging of two NLO calculations with different multiplicities arises as a byproduct. Maintaining the perturbative accuracy with higher-order matrix elements and higher-order resummation is obviously more challenging as more ingredients are required and additional complications arise; e.g., one has to employ a resolution variable that is resummable to the desired order. These issues are thoroughly addressed in chapter 3, and we discuss the connection in section 2.6.1.

2.3.2 LO+LL

The LL calculation performs the LL resummation in $\mathcal{T}_N$ and $\mathcal{T}_N^{\text{cut}}$, as outlined in section 2.2.2. It naturally contains the full LO_N contribution, so it is already LO_N+LL correct but does not include the full contribution from the $\text{LO}_{\geq N+1}$ matrix elements for additional jet multiplicities (beyond the shower approximation). The goal of LO+LL matching is to combine the $\text{LO}_{\geq N+1}$ calculations with the LL resummation, an example of which is the CKKW method [4, 5, 6, 10].

Considering the matching of LO_N, LO_{N+1}, and LL, denoted as $\text{LO}_{N,N+1}$+LL, the exclusive N-jet and inclusive $(N+1)$-jet MC cross sections are

$$\frac{\mathrm{d}\sigma_N^{\text{MC}}}{\mathrm{d}\Phi_N}(\mathcal{T}_N^{\text{cut}}) = B_N(\Phi_N)\,\Delta_N(\Phi_N;\mathcal{T}_N^{\text{cut}})\,,$$

$$\frac{\mathrm{d}\sigma^{\mathrm{MC}}_{\geq N+1}}{\mathrm{d}\Phi_{N+1}}(\mathcal{T}_N > \mathcal{T}_N^{\mathrm{cut}}) = \sum_m B^m_{N+1}(\Phi_{N+1})\,\Delta_N(\hat{\Phi}^m_N; \mathcal{T}^m_N)\,\theta(\mathcal{T}^m_N > \mathcal{T}_N^{\mathrm{cut}})\,,$$
$$\equiv \sum_m \Big\{ B_{N+1}(\Phi_{N+1})\,\Delta_N(\hat{\Phi}_N; \mathcal{T}_N)\,\theta(\mathcal{T}_N > \mathcal{T}_N^{\mathrm{cut}}) \Big\}_m\,. \qquad (2.22)$$

Here, the B^m_{N+1} are defined such that $B_{N+1} = \sum_m B^m_{N+1}$, and whenever an emission m becomes IR singular, B^m_{N+1} contains all its divergences. A possible choice would be to take $B^m_{N+1} = B_{N+1}(S^m_{N+1}/S_{N+1})$. For ease of notation, from here on we always group the emission label m on expressions with the notation $\sum_m\{\cdots\}_m$ to denote that all relevant terms within the curly brackets receive a label m.

The cross sections in eq. (2.22) are correct to LO_N and LO_{N+1} respectively, simply because any corrections to B_N or B_{N+1} are of higher fixed order. The Sudakov factors multiplying the Born contributions render the N-jet cumulant correct to LL in $\mathcal{T}_N^{\mathrm{cut}}$ and the $(N+1)$-jet spectrum correct to LL in $\mathcal{T}_N$.

To discuss the perturbative accuracy of integrated N-jet observables from residual $\mathcal{T}_N^{\mathrm{cut}}$ dependence, we rewrite $\mathrm{d}\sigma^{\mathrm{MC}}_{\geq N+1}$ in eq. (2.22) as

$$\frac{\mathrm{d}\sigma^{\mathrm{MC}}_{\geq N+1}}{\mathrm{d}\Phi_{N+1}}(\mathcal{T}_N > \mathcal{T}_N^{\mathrm{cut}}) = \sum_m \Big\{ S_{N+1}(\Phi_{N+1})\,\Delta_N(\hat{\Phi}_N; \mathcal{T}_N)$$
$$+ (B_{N+1} - S_{N+1})(\Phi_{N+1})\,\Delta_N(\hat{\Phi}_N; \mathcal{T}_N) \Big\}_m \theta(\mathcal{T}^m_N > \mathcal{T}_N^{\mathrm{cut}})\,. \qquad (2.23)$$

The first term on the right-hand side is identical to the pure LL cross section, and when projected onto Φ_N and integrated over $\mathcal{T}_N$, it produces $B_N(\Phi_N)[1 - \Delta_N(\Phi_N; \mathcal{T}_N^{\mathrm{cut}})]$, which exactly cancels the $\mathcal{T}_N^{\mathrm{cut}}$ dependence in the cumulant $\mathrm{d}\sigma_N^{\mathrm{MC}}(\mathcal{T}_N^{\mathrm{cut}})$ [see eq. (2.18)]. The second term corresponds to the FO matching correction, making $\mathrm{d}\sigma^{\mathrm{MC}}_{\geq N+1}$ to be LO_{N+1} accurate. Its $\mathcal{T}_N^{\mathrm{cut}}$ dependence is determined by the accuracy of $B_{N+1} - S_{N+1}$. If this difference contains subleading singular dependence on $\mathcal{T}_N$, which would be terms $\sim \alpha_s/\mathcal{T}_N$, then the $\mathcal{T}_N^{\mathrm{cut}}$ dependence in integrated N-jet observables will be of order $\alpha_s^n L_{\mathrm{cut}}^{2n-1} \sim \mathcal{O}_{\mathrm{cut}}(\alpha_s^{1/2})$. Interestingly, this is not actually sufficient to preserve the $1 + \mathcal{O}(\alpha_s)$ accuracy required at LO_N (see table 2.1). In the case that S_{N+1} does reproduce the full singular structure of B_{N+1} (which generically will not be the case for parton showers), then the residual $\mathcal{T}_N^{\mathrm{cut}}$ dependence will only appear as $\mathcal{O}_{\mathrm{cut}}(\alpha_s \mathcal{T}_N^{\mathrm{cut}})$ power corrections. Improved LO+LL methods that explicitly remove this residual $\mathcal{O}_{\mathrm{cut}}(\alpha_s^{1/2})$ dependence and restore the LO_N accuracy have been discussed in detail in refs. [52, 53, 47, 36]. They essentially enforce the consistency conditions in eq. (2.21).

Finally, we note that at $\mathrm{LO}_{N,N+1}$+LL, another possible valid choice for $\mathrm{d}\sigma^{\mathrm{MC}}_{\geq N+1}$ is

to take

$$\begin{aligned}
\frac{\mathrm{d}\sigma_N^{\mathrm{MC}}}{\mathrm{d}\Phi_N}(\mathcal{T}_N^{\mathrm{cut}}) &= B_N(\Phi_N)\,\Delta_N(\Phi_N;\mathcal{T}_N^{\mathrm{cut}})\,,\\
\frac{\mathrm{d}\sigma_{\geq N+1}^{\mathrm{MC}}}{\mathrm{d}\Phi_{N+1}}(\mathcal{T}_N > \mathcal{T}_N^{\mathrm{cut}}) &= \sum_m \Big\{ S_{N+1}(\Phi_{N+1})\,\Delta_N(\hat{\Phi}_N;\mathcal{T}_N)\\
&\qquad + (B_{N+1}-S_{N+1})(\Phi_{N+1})\Big\}_m \theta(\mathcal{T}_N^m > \mathcal{T}_N^{\mathrm{cut}})\,, \qquad (2.24)
\end{aligned}$$

where compared to eq. (2.23), we have dropped the Sudakov factor in the last line. The $\mathcal{T}_N^{\mathrm{cut}}$ dependence in this case is different numerically but of the same accuracy as for eq. (2.23), depending in the same way on the extent to which S_{N+1} reproduces the IR singularities of B_{N+1}.

2.3.3 NLO+LL

The matching of fully differential NLO calculations to parton shower routines has been addressed by several frameworks [13, 15, 54, 55, 18, 46]. Here, we review the general structure of the underlying matched NLO+LL calculation.

The MC cross sections underlying the MC@NLO [13] and POWHEG [15, 16] approaches are given by[5]

$$\begin{aligned}
\frac{\mathrm{d}\sigma_N^{\mathrm{MC}}}{\mathrm{d}\Phi_N}(\mathcal{T}_N^{\mathrm{cut}}) &= \underbrace{\frac{\mathrm{d}\sigma_{\geq N}^{S}}{\mathrm{d}\Phi_N}\,\Delta_N(\Phi_N;\mathcal{T}_N^{\mathrm{cut}})}_{\text{resummed}} + \underbrace{\frac{\mathrm{d}\sigma_N^{B-S}}{\mathrm{d}\Phi_N}(\mathcal{T}_N^{\mathrm{cut}})}_{\text{FO matching}}\,,\\
\frac{\mathrm{d}\sigma_{\geq N+1}^{\mathrm{MC}}}{\mathrm{d}\Phi_{N+1}}(\mathcal{T}_N > \mathcal{T}_N^{\mathrm{cut}}) &= \sum_m \left\{ \left.\frac{\mathrm{d}\sigma_{\geq N}^{S}}{\mathrm{d}\Phi_N}\right|_{\Phi_N=\hat{\Phi}_N} \frac{S_{N+1}(\Phi_{N+1})}{B_N(\hat{\Phi}_N)}\,\Delta_N(\hat{\Phi}_N;\mathcal{T}_N)\,\theta(\mathcal{T}_N > \mathcal{T}_N^{\mathrm{cut}}) \right\}_m\\
&\quad + \frac{\mathrm{d}\sigma_{\geq N+1}^{B-S}}{\mathrm{d}\Phi_{N+1}}(\mathcal{T}_N > \mathcal{T}_N^{\mathrm{cut}})\,, \qquad (2.25)
\end{aligned}$$

where

$$\begin{aligned}
\frac{\mathrm{d}\sigma_N^{B-S}}{\mathrm{d}\Phi_N}(\mathcal{T}_N^{\mathrm{cut}}) &= \sum_m \left\{ \int \frac{\mathrm{d}\Phi_{N+1}}{\mathrm{d}\Phi_N}\,(B_{N+1}-S_{N+1})(\Phi_{N+1})\,\theta(\mathcal{T}_N < \mathcal{T}_N^{\mathrm{cut}}) \right\}_m\,,\\
\frac{\mathrm{d}\sigma_{\geq N+1}^{B-S}}{\mathrm{d}\Phi_{N+1}}(\mathcal{T}_N > \mathcal{T}_N^{\mathrm{cut}}) &= \sum_m \Big\{ (B_{N+1}-S_{N+1})(\Phi_{N+1})\,\theta(\mathcal{T}_N > \mathcal{T}_N^{\mathrm{cut}}) \Big\}_m \qquad (2.26)
\end{aligned}$$

[5] For POWHEG, $\mathrm{d}\sigma_{\geq N}^{S}/\mathrm{d}\Phi_N \equiv \overline{B}_N(\Phi_N)$. In MC@NLO, $\mathbb{S}$ events are generated with a weight determined by $\mathrm{d}\sigma_{\geq N}^{S}/\mathrm{d}\Phi_N$, while $\mathbb{H}$ events are generated according to $\mathrm{d}\sigma_{\geq N+1}^{B-S}/\mathrm{d}\Phi_{N+1} \equiv \sum_m \{(B_{N+1}-S_{N+1})(\Phi_{N+1})\}_m$.

are the FO matching corrections, and

$$\frac{\mathrm{d}\sigma^{S}_{\geq N}}{\mathrm{d}\Phi_N} = (B_N + V_N)(\Phi_N) + \sum_m \left\{ \int \frac{\mathrm{d}\Phi_{N+1}}{\mathrm{d}\Phi_N}\, S_{N+1}(\Phi_{N+1}) \right\}_m \tag{2.27}$$

is essentially the inclusive NLO_N cross section, but using the real emission given by S_{N+1} instead of B_{N+1}. This means that S_{N+1} must contain the full IR singularities of B_{N+1} in the limit $\mathcal{T}_N \to 0$, such that upon integration, the virtual IR divergences of V_N are canceled in eq. (2.27).

We can easily check that eq. (2.25) is correct to NLO and LL, i.e., that it satisfies eq. (2.19). Dropping the NLO corrections, which amounts to taking $\mathrm{d}\sigma^{S}_{\geq N} \to B_N$ and dropping the $\mathrm{d}\sigma^{B-S}_N$ in $\mathrm{d}\sigma^{\mathrm{MC}}_N$, we reproduce the $\mathrm{LO}_{N,N+1}$+LL result in eq. (2.24). Using the fixed $\mathcal{O}(\alpha_s)$ expansion of the Sudakov,

$$\Delta_N(\Phi_N; \mathcal{T}_N^{\mathrm{cut}}) = 1 - \frac{1}{B_N(\Phi_N)} \sum_m \left\{ \int \frac{\mathrm{d}\Phi_{N+1}}{\mathrm{d}\Phi_N}\, S_{N+1}(\Phi_{N+1})\, \theta(\mathcal{T}_N > \mathcal{T}_N^{\mathrm{cut}}) \right\}_m + \mathcal{O}(\alpha_s^2)\,, \tag{2.28}$$

we see that expanding eq. (2.25) to NLO exactly reproduces eq. (1.10) at NLO_N and LO_{N+1}, where the $\mathcal{T}_N$ in the NLO calculation is now the same m-dependent resolution variable that is used in the LL calculation.

As written in eq. (2.25), the MC cross sections exactly satisfy eqs. (2.20) and (2.21). In fact, they do so separately for the resummed contributions proportional to $\mathrm{d}\sigma^{S}_{\geq N}\Delta_N$ and the FO matching corrections $\mathrm{d}\sigma^{B-S}_N$ and $\mathrm{d}\sigma^{B-S}_{\geq N+1}$.

The difference in the MC@NLO and POWHEG implementations lies in the (effective) choice of S_{N+1}. In MC@NLO,

$$\begin{aligned} & S^m_{N+1}(\Phi_{N+1}) = G(\mathcal{T}^m_N)\, \mathrm{PS}^m_{N+1}(\Phi_{N+1}) + [1 - G(\mathcal{T}^m_N)]\, C^m_{N+1}(\Phi_{N+1})\,, \\ \text{with} \qquad & \lim_{\mathcal{T}_N \to 0} G(\mathcal{T}_N) = 0\,, \qquad G(\mathcal{T}_N > \mathcal{T}_N^{\mathrm{cut}}) = 1\,, \end{aligned} \tag{2.29}$$

where PS^m_{N+1} denotes the parton shower approximation to B_{N+1} for channel m as determined by the splitting factors used in an actual parton shower algorithm like HERWIG or PYTHIA, C^m_{N+1} could be used as an NLO subtraction for B^m_{N+1}, and the purpose of $G(\mathcal{T}_N)$ is to smoothly join the two. [In principle, $G(\mathcal{T}_N) \equiv G^m_{N+1}(\Phi_{N+1})$ can depend on m and the full Φ_{N+1}.]

Note that the value of S_{N+1} for $\mathcal{T}_N < \mathcal{T}_N^{\mathrm{cut}}$ was not needed in the LL and LO+LL discussions but is needed here, and the expressions we use are specific to the NLO+LL construction. In our formulation of eq. (2.25), the MC@NLO method corresponds to taking $G(\mathcal{T}_N > \mathcal{T}_N^{\mathrm{cut}}) = 1$, since an actual parton shower is used to generate the Sudakov factor and $\mathcal{T}_N^{\mathrm{cut}}$ is identical to the parton shower cutoff. The condition $\lim_{\mathcal{T}_N \to 0} G(\mathcal{T}_N) = 0$ is necessary to ensure that all IR divergences cancel in the limit $\mathcal{T}_N \to 0$, because PS_{N+1} does not provide a valid NLO subtraction.

Even though there is no explicit $\mathcal{T}_N^{\text{cut}}$ dependence in eq. (2.27), the fact that PS_{N+1} does not reproduce the full IR singularities of B_{N+1} causes an implicit logarithmic sensitivity to scales $\leq \mathcal{T}_N^{\text{cut}}$ in $\mathrm{d}\sigma_{\geq N}^S$. To see this, we rewrite $S_{N+1} = C_{N+1} + G(\mathcal{T}_N)(\text{PS}_{N+1} - C_{N+1})$, such that

$$\begin{aligned}\frac{\mathrm{d}\sigma_{\geq N}^S}{\mathrm{d}\Phi_N} = (B_N + V_N)(\Phi_N) + \sum_m \left\{ \int \frac{\mathrm{d}\Phi_{N+1}}{\mathrm{d}\Phi_N} \, C_{N+1}(\Phi_{N+1}) \right\}_m \\ + \sum_m \left\{ \int \frac{\mathrm{d}\Phi_{N+1}}{\mathrm{d}\Phi_N} \, (\text{PS}_{N+1} - C_{N+1})(\Phi_{N+1}) \, G(\mathcal{T}_N) \right\}_m . \end{aligned} \tag{2.30}$$

The first three terms are IR finite and $\mathcal{T}_N^{\text{cut}}$ independent. The last term is also IR finite since $\lim_{\mathcal{T}_N \to 0} G(\mathcal{T}_N) = 0$. However, since $G(\mathcal{T}_N > \mathcal{T}_N^{\text{cut}}) = 1$, the subleading singular dependence in $\text{PS}_{N+1} - C_{N+1}$ is integrated down to $\mathcal{T}_N^{\text{cut}}$ and only cut off below, which means this last term scales as $\mathcal{O}_{\text{cut}}(\alpha_s^{1/2})$.[6] Taking into account this implicit $\mathcal{T}_N^{\text{cut}}$ dependence, $\mathrm{d}\sigma_{\geq N}^S \equiv \mathrm{d}\sigma_{\geq N}^S(\mathcal{T}_N^{\text{cut}})$, the conditions in eqs. (2.20) and (2.21) are no longer satisfied exactly. Rather, in the FO region, integrated N-jet observables are only accurate to $1 + \alpha_s + \mathcal{O}(\alpha_s^2) + \mathcal{O}_{\text{cut}}(\alpha_s^{3/2})$, while differential $(N+1)$-jet observables are only accurate to $1 + \mathcal{O}(\alpha_s) + \mathcal{O}_{\text{cut}}(\alpha_s^{1/2})$. Formally, this is not sufficient to maintain the perturbative accuracy expected at NLO_N and LO_{N+1}, cf. table 2.1. In practice, the numerical impact depends on how well the employed parton shower algorithm is able to capture the subleading singular structure of the full real emission contribution. In refs. [13, 14], this was shown to be a minor problem.

In POWHEG, S_{N+1} is constructed by dividing the full B_{N+1} between the IR-singular regions for the different emission channels,

$$\begin{aligned} & S_{N+1}^m(\Phi_{N+1}) = B_{N+1}(\Phi_{N+1}) \, \Theta_{N+1}^m(\Phi_{N+1}) \, F(\mathcal{T}_N) \,, \\ \text{with} \qquad & \sum_m \Theta_{N+1}^m = 1 \,, \qquad \lim_{\mathcal{T}_N^m \to 0} \Theta_{N+1}^m = 1 \,, \qquad \lim_{\mathcal{T}_N \to 0} F(\mathcal{T}_N) = 1 \,. \end{aligned} \tag{2.31}$$

The conditions imposed on the Θ_{N+1}^m ensure that the full B_{N+1} is obtained in any singular limit, such that S_{N+1} reproduces the full IR-singular structure and $\mathrm{d}\sigma_{\geq N}^S$ is IR finite. The function $F(\mathcal{T}_N)$ is included so the resummation can be turned off by letting $F(\mathcal{T}_N) \to 0$ at large $\mathcal{T}_N$. [In principle, $F(\mathcal{T}_N) \equiv F_{N+1}^m(\Phi_{N+1})$ can depend on m and the full Φ_{N+1}.] In this case, since S_{N+1} contains the full singular structure also above $\mathcal{T}_N^{\text{cut}}$, there is no implicit $\mathcal{T}_N^{\text{cut}}$ dependence. Strictly speaking, this is true as long as Θ^m and F do not introduce a sensitivity to small $\mathcal{T}_N$.

The full Φ_{N+1} dependence in $\mathrm{d}\sigma_{\geq N+1}^{\text{MC}}$ in eq. (2.25) is determined by $S_{N+1}(\Phi_{N+1})$ in the resummation term, i.e., by the approximate Φ_{N+1} dependence in the splitting factor that determines the Sudakov factor. The FO matching correction, $\mathrm{d}\sigma_{\geq N+1}^{B-S} \sim$

[6] The $\mathcal{T}_N^{\text{cut}}$ dependence becomes explicit if one takes $G(\mathcal{T}_N > \mathcal{T}_N^{\text{cut}}) = \theta(\mathcal{T}_N > \mathcal{T}_N^{\text{cut}})$, in which case the integral would produce an explicit $\ln \mathcal{T}_N^{\text{cut}}$. For a smooth G, this logarithm is smeared out, but the integral has the same scaling.

$(B_{N+1}-S_{N+1})(\Phi_{N+1})$, additively corrects the approximate Φ_{N+1} dependence in S_{N+1} to the full LO_{N+1} dependence given by B_{N+1}. Another possible approach is to also multiply this term by the Sudakov factor, or equivalently, directly use the full B_{N+1} dependence in the resummed spectrum, such that

$$\frac{\mathrm{d}\sigma_N^{\mathrm{MC}}}{\mathrm{d}\Phi_N}(\mathcal{T}_N^{\mathrm{cut}}) = \frac{\mathrm{d}\sigma_{\geq N}^{S}}{\mathrm{d}\Phi_N}\,\Delta_N(\Phi_N;\mathcal{T}_N^{\mathrm{cut}}) + \frac{\mathrm{d}\sigma_N^{B-S}}{\mathrm{d}\Phi_N}(\mathcal{T}_N^{\mathrm{cut}})\,, \tag{2.32}$$

$$\frac{\mathrm{d}\sigma_{\geq N+1}^{\mathrm{MC}}}{\mathrm{d}\Phi_{N+1}}(\mathcal{T}_N > \mathcal{T}_N^{\mathrm{cut}}) = \sum_m \left\{ \frac{\mathrm{d}\sigma_{\geq N}^{S}}{\mathrm{d}\Phi_N}\bigg|_{\Phi_N=\hat{\Phi}_N} \frac{B_{N+1}(\Phi_{N+1})}{B_N(\hat{\Phi}_N)}\,\Delta_N(\hat{\Phi}_N;\mathcal{T}_N)\,\theta(\mathcal{T}_N > \mathcal{T}_N^{\mathrm{cut}}) \right\}_m .$$

This corresponds to the usual CKKW procedure for $\mathrm{LO}_{N,N+1}$+LL in eq. (2.22). It is also analogous to the GENEVA method in ref. [46], where the Φ_{N+1}-differential FO calculation is multiplicatively combined with the $\mathcal{T}_N$ spectrum resummed to higher order. In eq. (2.32), the spectrum is not the exact derivative of the cumulant anymore, resulting in a residual $\mathcal{T}_N^{\mathrm{cut}}$ dependence in the integrated cross section. The effective correction term by which eq. (2.21) is violated and that gets added to the correct NLO_N cross section is given by

$$\int \frac{\mathrm{d}\Phi_{N+1}}{\mathrm{d}\Phi_N}(B_{N+1}-S_{N+1})(\Phi_{N+1})\left[\Delta_N(\hat{\Phi}_N;\mathcal{T}_N)-1\right]\theta(\mathcal{T}_N > \mathcal{T}_N^{\mathrm{cut}})\,. \tag{2.33}$$

In fixed order, this is $\mathcal{O}(\alpha_s^2)$ and beyond NLO_N. However, its impact on the perturbative accuracy depends again on the extent to which the IR singularities of B_{N+1} are correctly reproduced by S_{N+1}. If S_{N+1} contains the full IR singularities, so $B_{N+1}-S_{N+1}$ is finite for $\mathcal{T}_N \to 0$, then the leading term in eq. (2.33) scales as $\mathcal{T}_N^{\mathrm{cut}}\alpha_s^2\ln^2(\mathcal{T}_N^{\mathrm{cut}}/Q)$, which is $\mathcal{O}_{\mathrm{cut}}(\alpha_s\mathcal{T}_N^{\mathrm{cut}})$. Therefore, in this case, the correction can be regarded as a power correction. If S_{N+1} does not reproduce the full IR singularities, so that $B_{N+1}-S_{N+1}$ contains subleading divergences $\sim \alpha_s/\mathcal{T}_N$, then the leading term scales as $\alpha_s^2\ln^3(\mathcal{T}_N^{\mathrm{cut}}/Q)$. Hence, in this case the correction is of $\mathcal{O}_{\mathrm{cut}}(\alpha_s^{1/2})$ and clearly violates the NLO_N+LL accuracy, which allows at most $\mathcal{O}_{\mathrm{cut}}(\alpha_s^2)$ corrections (see the first column of table 2.1). Note that the perturbative accuracy of the residual $\mathcal{T}_N^{\mathrm{cut}}$ dependence in either case here is the same as in eq. (2.22) at $\mathrm{LO}_{N,N+1}$+LL. The reason is that it is determined by the resummation counting and the NLO matching by itself only improves the FO accuracy.

2.4 Combining NNLO calculations with LL resummation

As we saw in section 2.2.1, at NNLO, we need events representing N, $N+1$, and $N+2$ partonic jets, defined through the N-jet and $(N+1)$-jet resolution variables $\mathcal{T}_N$ and $\mathcal{T}_{N+1}$. The same is therefore also the case at NNLO+LL. Hence, we need to

construct expressions for the corresponding fully differential MC cross sections [see eqs. (2.1) and (2.2)]

$$\frac{\mathrm{d}\sigma_N^{\mathrm{MC}}}{\mathrm{d}\Phi_N}(\mathcal{T}_N^{\mathrm{cut}})\,, \quad \frac{\mathrm{d}\sigma_{N+1}^{\mathrm{MC}}}{\mathrm{d}\Phi_{N+1}}(\mathcal{T}_N > \mathcal{T}_N^{\mathrm{cut}}; \mathcal{T}_{N+1}^{\mathrm{cut}})\,, \quad \frac{\mathrm{d}\sigma_{\geq N+2}^{\mathrm{MC}}}{\mathrm{d}\Phi_{N+2}}(\mathcal{T}_N > \mathcal{T}_N^{\mathrm{cut}}, \mathcal{T}_{N+1} > \mathcal{T}_{N+1}^{\mathrm{cut}})\,. \tag{2.34}$$

As discussed in section 2.3.1, at NNLO+LL we require that N-jet observables are correct to NNLO$_N$+LL, $(N+1)$-jet observables to NLO$_{N+1}$+LL, and $(N+2)$-jet observables to LO$_{N+2}$+LL, provided that any observable built from these cross sections is sufficiently inclusive over the unresolved regions of phase space. Since the FO calculation is supplemented with the LL resummation of the jet resolution variables $\mathcal{T}_N$ and $\mathcal{T}_{N+1}$, the perturbative accuracy of the prediction in the IR-singular regime is improved relative to the pure FO calculation, which breaks down in this region. The required perturbative accuracy at NNLO+LL in the FO and resummation regions is summarized in table 2.1.

To construct the NNLO+LL MC cross sections, it will be convenient to proceed in two steps. In section 2.4.1, we first consider the separation between the exclusive N-jet and inclusive $(N+1)$-jet cross sections using $\mathcal{T}_N$ and construct the corresponding exclusive $\mathrm{d}\sigma_N^{\mathrm{MC}}(\mathcal{T}_N^{\mathrm{cut}})$ and inclusive $\mathrm{d}\sigma_{\geq N+1}^{\mathrm{MC}}(\mathcal{T}_N > \mathcal{T}_N^{\mathrm{cut}})$. In section 2.4.2, we then consider the further separation of $\mathrm{d}\sigma_{\geq N+1}^{\mathrm{MC}}(\mathcal{T}_N > \mathcal{T}_N^{\mathrm{cut}})$ into the final exclusive $\mathrm{d}\sigma_{N+1}^{\mathrm{MC}}(\mathcal{T}_N > \mathcal{T}_N^{\mathrm{cut}}; \mathcal{T}_{N+1}^{\mathrm{cut}})$ and inclusive $\mathrm{d}\sigma_{\geq N+2}^{\mathrm{MC}}(\mathcal{T}_N > \mathcal{T}_N^{\mathrm{cut}}, \mathcal{T}_{N+1} > \mathcal{T}_{N+1}^{\mathrm{cut}})$ using $\mathcal{T}_{N+1}$. To make the notation as transparent as possible, we drop the emission labels m throughout this section. They can be inserted straightforwardly into all formulae giving the different contributions to the cross sections.

2.4.1 The exclusive N-jet and inclusive $(N+1)$-jet cross sections

As we have already seen at LO and NLO, it is convenient to divide the full FO exclusive N-jet cross section, $\mathrm{d}\sigma_N^{\mathrm{FO}}(\mathcal{T}_N^{\mathrm{cut}})$, into a singular and a nonsingular contribution,[7]

$$\frac{\mathrm{d}\sigma_N^{\mathrm{FO}}}{\mathrm{d}\Phi_N}(\mathcal{T}_N^{\mathrm{cut}}) = \underbrace{\frac{\mathrm{d}\sigma_N^{C}}{\mathrm{d}\Phi_N}(\mathcal{T}_N^{\mathrm{cut}})}_{\text{FO singular}} + \underbrace{\frac{\mathrm{d}\sigma_N^{B-C}}{\mathrm{d}\Phi_N}(\mathcal{T}_N^{\mathrm{cut}})}_{\text{FO nonsingular}}\,. \tag{2.35}$$

[7] To be precise, singular terms in the cumulant contain logarithms of $\mathcal{T}_N^{\mathrm{cut}}$ or constants, while nonsingular terms vanish as $\mathcal{T}_N^{\mathrm{cut}} \to 0$. In the spectrum, singular terms contain plus distributions or delta functions of $\mathcal{T}_N$, while nonsingular terms contain no singular distributions and at most integrable singularities.

At NNLO, $\mathrm{d}\sigma_N^{\mathrm{FO}}(\mathcal{T}_N^{\mathrm{cut}})$ is given in eq. (2.5). Its singular approximation is given by

$$\begin{aligned}\frac{\mathrm{d}\sigma_N^C}{\mathrm{d}\Phi_N}(\mathcal{T}_N^{\mathrm{cut}}) = (B_N + V_N + W_N)(\Phi_N) \\ + \int \frac{\mathrm{d}\Phi_{N+1}}{\mathrm{d}\Phi_N} (C_{N+1} + VC_{N+1})(\Phi_{N+1})\, \theta[\mathcal{T}_N(\Phi_{N+1}) < \mathcal{T}_N^{\mathrm{cut}}] \\ + \int \frac{\mathrm{d}\Phi_{N+2}}{\mathrm{d}\Phi_N} C_{N+2}(\Phi_{N+2})\, \theta[\mathcal{T}_N(\Phi_{N+2}) < \mathcal{T}_N^{\mathrm{cut}}]\,, \end{aligned} \tag{2.36}$$

where C_{N+1}, VC_{N+1}, and C_{N+2} reproduce the exact IR singularities of B_{N+1}, V_{N+1}, and B_{N+2}, respectively; i.e., they correspond to a valid set of NNLO subtractions, such that eq. (2.36) is IR finite. The full logarithmic $\mathcal{T}_N^{\mathrm{cut}}$ dependence arises from integrating B_{N+1}, V_{N+1}, and B_{N+2}, over the IR-singular region, which is fully reproduced by the C_{N+1}, VC_{N+1}, and C_{N+2} contributions in eq. (2.36). Therefore, $\mathrm{d}\sigma_N^C(\mathcal{T}_N^{\mathrm{cut}})$ contains all logarithms in $\mathcal{T}_N^{\mathrm{cut}}$, while the remainder $\mathrm{d}\sigma_N^{B-C}(\mathcal{T}_N^{\mathrm{cut}})$ in eq. (2.35) is a power correction in $\mathcal{T}_N^{\mathrm{cut}}$.

To identify the relevant terms, we rewrite the N-jet MC cross section in terms of a resummed contribution and FO matching corrections. As we have seen at NLO+LL in section 2.3.3, the LL resummed contribution can be obtained by multiplying an inclusive cross section by the LL Sudakov factor for $\mathcal{T}_N^{\mathrm{cut}}$. The resulting expression in general differs from the correct FO result by both singular and nonsingular terms in $\mathcal{T}_N^{\mathrm{cut}}$, which are accounted for by adding corresponding FO singular and nonsingular matching corrections. This gives

$$\text{Case 1:} \qquad \frac{\mathrm{d}\sigma_N^{\mathrm{MC}}}{\mathrm{d}\Phi_N}(\mathcal{T}_N^{\mathrm{cut}}) = \underbrace{\frac{\mathrm{d}\sigma_{\geq N}^C}{\mathrm{d}\Phi_N}\, \Delta_N(\Phi_N; \mathcal{T}_N^{\mathrm{cut}})}_{\text{resummed}} + \underbrace{\frac{\mathrm{d}\sigma_N^{C-S}}{\mathrm{d}\Phi_N}(\mathcal{T}_N^{\mathrm{cut}})}_{\text{FO singular matching}} + \underbrace{\frac{\mathrm{d}\sigma_N^{B-C}}{\mathrm{d}\Phi_N}(\mathcal{T}_N^{\mathrm{cut}})}_{\substack{\text{FO nonsingular} \\ \text{matching}}}. \tag{2.37}$$

The first term is the resummed contribution, where $\mathrm{d}\sigma_{\geq N}^C$ is the singular approximation of the inclusive FO N-jet cross section, obtained by dropping the $\theta(\mathcal{T}_N < \mathcal{T}_N^{\mathrm{cut}})$ in eq. (2.36). It is by construction $\mathcal{T}_N^{\mathrm{cut}}$ independent, so all dependence on $\mathcal{T}_N^{\mathrm{cut}}$ in the resummed term resides in the Sudakov factor $\Delta_N(\Phi_N; \mathcal{T}_N^{\mathrm{cut}})$, which sums the LL series in $\mathcal{T}_N^{\mathrm{cut}}$. The remaining two terms are FO matching corrections to ensure the correct FO expansion of eq. (2.37).

The last term in eq. (2.37), labeled $B - C$, is the FO nonsingular term from eq. (2.35). It contains the difference between the full FO contribution and its singular limit,

$$\frac{\mathrm{d}\sigma_N^{B-C}}{\mathrm{d}\Phi_N}(\mathcal{T}_N^{\mathrm{cut}}) = \frac{\mathrm{d}\sigma_N^{\mathrm{FO}}}{\mathrm{d}\Phi_N}(\mathcal{T}_N^{\mathrm{cut}}) - \frac{\mathrm{d}\sigma_N^C}{\mathrm{d}\Phi_N}(\mathcal{T}_N^{\mathrm{cut}})\,. \tag{2.38}$$

As discussed above, it contains no logarithmic dependence on $\mathcal{T}_N^{\mathrm{cut}}$.

The second term in eq. (2.37), labeled $C - S$, is the singular FO matching correction. It contains the difference between the singular approximation containing the

full logarithmic $\mathcal{T}_N^{\text{cut}}$ dependence and that obtained by expanding the resummed term in fixed order; i.e.,

$$\begin{aligned}\frac{\mathrm{d}\sigma_N^{C-S}}{\mathrm{d}\Phi_N}(\mathcal{T}_N^{\text{cut}}) &= \frac{\mathrm{d}\sigma_N^{C}}{\mathrm{d}\Phi_N}(\mathcal{T}_N^{\text{cut}}) - \left[\frac{\mathrm{d}\sigma_{\geq N}^{C}}{\mathrm{d}\Phi_N}\,\Delta_N(\Phi_N;\mathcal{T}_N^{\text{cut}})\right]_{\text{FO}} \\ &= -\int\frac{\mathrm{d}\Phi_{N+1}}{\mathrm{d}\Phi_N}\,(C_{N+1}-S_{N+1})(\Phi_{N+1})\,\theta(\mathcal{T}_N>\mathcal{T}_N^{\text{cut}})+\mathcal{O}(\alpha_s^2)\,. \end{aligned} \tag{2.39}$$

Hence, it supplies the FO singular terms in $\mathcal{T}_N^{\text{cut}}$ that are not contained in the resummed contribution. In the second line, we show the NLO result for illustration. As already discussed in section 2.3.3, since the splitting function S_{N+1} generically only reproduces the leading singularities in C_{N+1}, $\mathrm{d}\sigma_N^{C-S}(\mathcal{T}_N^{\text{cut}})$ can in general contain logarithmic dependence as large as $\alpha_s L_{\text{cut}}$ at NLO and $\alpha_s^2 L_{\text{cut}}^3$ at NNLO, which contribute at $\mathcal{O}_{\text{cut}}(\alpha_s^{1/2})$ with the counting of eq. (2.16).

A potential problem with implementing eq. (2.37) is the presence of explicit logarithms in $\mathrm{d}\sigma_N^{C-S}(\mathcal{T}_N^{\text{cut}})$, which become large as $\mathcal{T}_N^{\text{cut}}$ is reduced, meaning in particular $\mathrm{d}\sigma_N^{C-S}(\mathcal{T}_N^{\text{cut}})$ diverges for $\mathcal{T}_N^{\text{cut}}\to 0$. While by construction this divergence cancels in physical observables, it could give rise to events with large or even negative weights. To circumvent this and regulate the logarithmic divergence, we can alternatively choose to multiply the singular matching terms with the Sudakov factor and write

$$\text{Case 2:}\qquad \frac{\mathrm{d}\sigma_N^{\text{MC}}}{\mathrm{d}\Phi_N}(\mathcal{T}_N^{\text{cut}}) = \underbrace{\left[\frac{\mathrm{d}\sigma_{\geq N}^{C}}{\mathrm{d}\Phi_N} + \underbrace{\frac{\mathrm{d}\widetilde{\sigma}_N^{C-S}}{\mathrm{d}\Phi_N}(\mathcal{T}_N^{\text{cut}})}_{\substack{\text{FO singular}\\ \text{matching}}}\right]\Delta_N(\Phi_N;\mathcal{T}_N^{\text{cut}})}_{\text{resummed}} + \underbrace{\frac{\mathrm{d}\sigma_N^{B-C}}{\mathrm{d}\Phi_N}(\mathcal{T}_N^{\text{cut}})}_{\substack{\text{FO nonsingular}\\ \text{matching}}}, \tag{2.40}$$

where the FO singular matching corrections are now given by

$$\begin{aligned}\frac{\mathrm{d}\widetilde{\sigma}_N^{C-S}}{\mathrm{d}\Phi_N}(\mathcal{T}_N^{\text{cut}}) &= \left[\frac{\mathrm{d}\sigma_N^{C-S}}{\mathrm{d}\Phi_N}(\mathcal{T}_N^{\text{cut}})\,\frac{1}{\Delta_N(\Phi_N;\mathcal{T}_N^{\text{cut}})}\right]_{\text{FO}} \\ &= -\int\frac{\mathrm{d}\Phi_{N+1}}{\Phi_N}\,(C_{N+1}-S_{N+1})(\Phi_{N+1})\,\theta(\mathcal{T}_N>\mathcal{T}_N^{\text{cut}})+\mathcal{O}(\alpha_s^2)\,. \end{aligned} \tag{2.41}$$

Note that, while multiplying with the Sudakov factor helps to suppress the FO $\mathcal{T}_N^{\text{cut}}$ logarithms in $\mathrm{d}\widetilde{\sigma}_N^{C-S}(\mathcal{T}_N^{\text{cut}})$, this choice does not amount to an actual resummation of these logarithms. A downside of this choice is that it introduces a more complicated $\mathcal{T}_N^{\text{cut}}$ dependence at all orders that must be canceled in inclusive N-jet observables. Since $\mathrm{d}\widetilde{\sigma}_N^{C-S}(\mathcal{T}_N^{\text{cut}})$ can contain logarithms $\alpha_s^2 L_{\text{cut}}^3$, multiplying with the Sudakov factor introduces terms of order $\alpha_s^n L_{\text{cut}}^{2n-1}$.

The singular matching correction is always required if the resummation term does not contain all logarithms of $\mathcal{T}_N^{\text{cut}}$ to the desired fixed order. Even if S_{N+1} in eq. (2.39) contains the full subleading singularities at NLO (as in POWHEG where

$C_{N+1} = S_{N+1}$, so $\mathrm{d}\sigma_N^{C-S}(\mathcal{T}_N^{\mathrm{cut}}) = 0$), at NNLO, $\mathrm{d}\sigma_N^{C-S}(\mathcal{T}_N^{\mathrm{cut}})$ can still contain terms $\sim \alpha_s^2 L_{\mathrm{cut}}^2 \sim \mathcal{O}_{\mathrm{cut}}(\alpha_s)$. Hence, to achieve NNLO$_N$+LL accuracy, it is essential to enforce the consistency conditions in eqs. (2.20) and (2.21) for the $\mathrm{d}\sigma_N^{C-S}$ or $\mathrm{d}\widetilde{\sigma}_N^{C-S}$ contributions. Otherwise, these terms can easily generate a residual $\mathcal{T}_N^{\mathrm{cut}}$ dependence in inclusive observables that destroys their perturbative accuracy.

To construct the inclusive $(N+1)$-jet MC cross section, $\mathrm{d}\sigma_{\geq N+1}^{\mathrm{MC}}(\mathcal{T}_N > \mathcal{T}_N^{\mathrm{cut}})$, as with $\mathrm{d}\sigma_N^{\mathrm{MC}}$ before, we split it into a resummed contribution and FO singular and nonsingular matching corrections. Following the above discussion, these different contributions are constructed from their corresponding counterparts in eqs. (2.37) and (2.40) by explicitly enforcing eqs. (2.20) and (2.21). This gives

$$\begin{aligned}\text{Case 1: } \frac{\mathrm{d}\sigma_{\geq N+1}^{\mathrm{MC}}}{\mathrm{d}\Phi_{N+1}}(\mathcal{T}_N > \mathcal{T}_N^{\mathrm{cut}}) &= \frac{\mathrm{d}\sigma_{\geq N}^{C}}{\mathrm{d}\Phi_N}\bigg|_{\Phi_N=\hat{\Phi}_N} \frac{S_{N+1}(\Phi_{N+1})}{B_N(\hat{\Phi}_N)}\,\Delta_N(\hat{\Phi}_N;\mathcal{T}_N)\,\theta(\mathcal{T}_N > \mathcal{T}_N^{\mathrm{cut}}) \\ &\quad + \frac{\mathrm{d}\sigma_{\geq N+1}^{C-S}}{\mathrm{d}\Phi_{N+1}}(\mathcal{T}_N > \mathcal{T}_N^{\mathrm{cut}}) + \frac{\mathrm{d}\sigma_{\geq N+1}^{B-C}}{\mathrm{d}\Phi_{N+1}}(\mathcal{T}_N > \mathcal{T}_N^{\mathrm{cut}})\,,\end{aligned} \tag{2.42}$$

$$\begin{aligned}\text{Case 2: } &\frac{\mathrm{d}\sigma_{\geq N+1}^{\mathrm{MC}}}{\mathrm{d}\Phi_{N+1}}(\mathcal{T}_N > \mathcal{T}_N^{\mathrm{cut}}) = \\ &\quad\bigg\{\bigg[\frac{\mathrm{d}\sigma_{\geq N}^{C}}{\mathrm{d}\Phi_N} + \frac{\mathrm{d}\widetilde{\sigma}_N^{C-S}}{\mathrm{d}\Phi_N}(\mathcal{T}_N)\bigg]_{\Phi_N=\hat{\Phi}_N} \frac{S_{N+1}(\Phi_{N+1})}{B_N(\hat{\Phi}_N)}\,\theta(\mathcal{T}_N > \mathcal{T}_N^{\mathrm{cut}}) \\ &\qquad + \frac{\mathrm{d}\widetilde{\sigma}_{\geq N+1}^{C-S}}{\mathrm{d}\Phi_{N+1}}(\mathcal{T}_N > \mathcal{T}_N^{\mathrm{cut}})\bigg\}\Delta_N(\hat{\Phi}_N;\mathcal{T}_N) + \frac{\mathrm{d}\sigma_{\geq N+1}^{B-C}}{\mathrm{d}\Phi_{N+1}}(\mathcal{T}_N > \mathcal{T}_N^{\mathrm{cut}})\,,\end{aligned} \tag{2.43}$$

where the various ingredients are discussed in detail in sections 2.4.1.1 and 2.4.1.2. For case 1, the FO singular and nonsingular matching terms are pure FO corrections, and to obtain them, it is sufficient to enforce that $\mathrm{d}\sigma_{\geq N+1}^{\mathrm{MC}}$ expands to the correct NLO cross section. For case 2, the singular matching correction is more complicated, and its $\mathcal{T}_N$ dependence is obtained by taking the derivative of $\mathrm{d}\widetilde{\sigma}_N^{C-S}(\mathcal{T}_N^{\mathrm{cut}})\,\Delta_N(\mathcal{T}_N^{\mathrm{cut}})$ in eq. (2.40) with respect to $\mathcal{T}_N^{\mathrm{cut}}$. This ensures that the singular matching corrections in the spectrum correctly integrate up to cancel the corresponding $\mathcal{T}_N^{\mathrm{cut}}$ dependence in the cumulant.[8]

Before we give the detailed expressions for all ingredients required to construct eqs. (2.37), (2.40), (2.42), and (2.43), it is instructive to see how the NLO+LL case

[8]Notice that there might be points in Φ_{N+1} for which $B_N(\hat{\Phi}_N) = 0$ due to either kinematical or PDF effects. To avoid that the ratio $S_{N+1}(\Phi_{N+1})/B_N(\hat{\Phi}_N)$ goes to infinity, one has to define S_{N+1} such that it vanishes for these points. This implies that the contributions from these phase space regions are contained in $\mathrm{d}\sigma^{C-S}$ or $\mathrm{d}\widetilde{\sigma}^{C-S}$.

arises from this notation. At NLO, we have

$$\frac{\mathrm{d}\sigma^{C}_{\geq N}}{\mathrm{d}\Phi_N} = (B_N + V_N)(\Phi_N) + \int \frac{\mathrm{d}\Phi_{N+1}}{\mathrm{d}\Phi_N}\, C_{N+1}(\Phi_{N+1})\,, \tag{2.44}$$

and the singular matching corrections for the cumulant, $\mathrm{d}\sigma^{C-S}_N$, are given in the second line of eq. (2.39) [or eq. (2.41) for $\mathrm{d}\widetilde{\sigma}^{C-S}_N$]. The nonsingular matching correction is

$$\frac{\mathrm{d}\sigma^{B-C}_N}{\mathrm{d}\Phi_N}(\mathcal{T}^{\mathrm{cut}}_N) = \int \frac{\mathrm{d}\Phi_{N+1}}{\mathrm{d}\Phi_N}\,(B_{N+1} - C_{N+1})(\Phi_{N+1})\,\theta(\mathcal{T}_N < \mathcal{T}^{\mathrm{cut}}_N)\,. \tag{2.45}$$

The corresponding results for the differential spectrum are

$$\begin{aligned}\frac{\mathrm{d}\sigma^{C-S}_{\geq N+1}}{\mathrm{d}\Phi_{N+1}}(\mathcal{T}_N > \mathcal{T}^{\mathrm{cut}}_N) = \frac{\mathrm{d}\widetilde{\sigma}^{C-S}_{\geq N+1}}{\mathrm{d}\Phi_{N+1}}(\mathcal{T}_N > \mathcal{T}^{\mathrm{cut}}_N) &= (C_{N+1} - S_{N+1})(\Phi_{N+1})\,\theta(\mathcal{T}_N > \mathcal{T}^{\mathrm{cut}}_N)\,,\\ \frac{\mathrm{d}\sigma^{B-C}_{\geq N+1}}{\mathrm{d}\Phi_{N+1}}(\mathcal{T}_N > \mathcal{T}^{\mathrm{cut}}_N) &= (B_{N+1} - C_{N+1})(\Phi_{N+1})\,\theta(\mathcal{T}_N > \mathcal{T}^{\mathrm{cut}}_N)\,.\end{aligned} \tag{2.46}$$

Note that $\mathrm{d}\sigma^{C-S}$ and $\mathrm{d}\widetilde{\sigma}^{C-S}$ are equal at this order. They only start to differ at NNLO, where the cross terms in the FO expansion of the product $\mathrm{d}\widetilde{\sigma}^{C-S}_N\Delta_N$ become relevant.

As discussed in section 2.3.3, the splitting function of POWHEG given in eq. (2.31) reproduces the full singular dependence of the real emission. Thus, one can choose $C_{N+1} = S_{N+1}$, such that $\mathrm{d}\sigma^{C-S}_N = 0$ and $\mathrm{d}\sigma^{C}_{\geq N} = \mathrm{d}\sigma^{S}_{\geq N}$, and cases 1 and 2 both reduce to eq. (2.25).

For MC@NLO, the splitting function is given in eq. (2.29). It depends on a function $G(\mathcal{T}_N)$, which for the sake of illustration we can choose as $G(\mathcal{T}_N) = \theta(\mathcal{T}_N > \mathcal{T}^{\mathrm{cut}}_N)$ (even though this is not the choice made in the MC@NLO implementation). In this case, the expression for $\mathrm{d}\sigma^{S}_{\geq N}$ given in eq. (2.30) is equivalent to $\mathrm{d}\sigma^{S}_{\geq N} = \mathrm{d}\sigma^{C}_{\geq N} + \mathrm{d}\widetilde{\sigma}^{C-S}_N$, which corresponds to case 2 in eq. (2.40) for the cumulant. However, the corresponding spectrum in eq. (2.25) is not that of case 2 in eq. (2.43). This is the origin of the residual $\mathcal{T}^{\mathrm{cut}}_N$ dependence in MC@NLO discussed below eq. (2.30).

It should be clear from the discussion so far that the expressions in eqs. (2.37) and (2.42) for case 1, or alternatively eqs. (2.40) and (2.43) for case 2, provide a completely general result for the FO+LL matching valid to any fixed order. The explicit NNLO+LL expressions are given in detail below in section 2.4.1.1 for case 1 and section 2.4.1.2 for case 2. Besides the choice one has between the two cases, different implementations can be obtained by making different choices for the C_{N+1}, VC_{N+1}, and C_{N+2} contributions that are used to approximate the singular behavior of the full theory, as well as for the splitting function S_{N+1} that is used to define the Sudakov factor. This amounts to shifting nonsingular corrections or subleading logarithms between the resummed contribution and the FO matching corrections.

2.4.1.1 Case 1

Here, we use $\mathrm{d}\sigma_N^{\mathrm{MC}}(\mathcal{T}_N^{\mathrm{cut}})$ as given in eq. (2.37) with its corresponding inclusive $\mathrm{d}\sigma_{\geq N+1}^{\mathrm{MC}}(\mathcal{T}_N > \mathcal{T}_N^{\mathrm{cut}})$ given in eq. (2.42), which we repeat here for completeness:

$$\begin{aligned}
\frac{\mathrm{d}\sigma_N^{\mathrm{MC}}}{\mathrm{d}\Phi_N}(\mathcal{T}_N^{\mathrm{cut}}) &= \frac{\mathrm{d}\sigma_{\geq N}^{C}}{\mathrm{d}\Phi_N}\,\Delta_N(\Phi_N;\mathcal{T}_N^{\mathrm{cut}}) + \frac{\mathrm{d}\sigma_N^{C-S}}{\mathrm{d}\Phi_N}(\mathcal{T}_N^{\mathrm{cut}}) + \frac{\mathrm{d}\sigma_N^{B-C}}{\mathrm{d}\Phi_N}(\mathcal{T}_N^{\mathrm{cut}})\,, \\
\frac{\mathrm{d}\sigma_{\geq N+1}^{\mathrm{MC}}}{\mathrm{d}\Phi_{N+1}}(\mathcal{T}_N > \mathcal{T}_N^{\mathrm{cut}}) &= \frac{\mathrm{d}\sigma_{\geq N}^{C}}{\mathrm{d}\Phi_N}\bigg|_{\Phi_N=\hat{\Phi}_N} \frac{S_{N+1}(\Phi_{N+1})}{B_N(\hat{\Phi}_N)}\,\Delta_N(\hat{\Phi}_N;\mathcal{T}_N)\,\theta(\mathcal{T}_N > \mathcal{T}_N^{\mathrm{cut}}) \\
&\quad + \frac{\mathrm{d}\sigma_{\geq N+1}^{C-S}}{\mathrm{d}\Phi_{N+1}}(\mathcal{T}_N > \mathcal{T}_N^{\mathrm{cut}}) + \frac{\mathrm{d}\sigma_{\geq N+1}^{B-C}}{\mathrm{d}\Phi_{N+1}}(\mathcal{T}_N > \mathcal{T}_N^{\mathrm{cut}})\,.
\end{aligned}$$

The explicit expressions for all ingredients are given in the following. By construction, these are correct to NNLO_N and NLO_{N+1} and include the correct LL resummation for $\mathcal{T}_N^{\mathrm{cut}}$ and $\mathcal{T}_N$, respectively. Also, each of the three terms in the cumulant and spectrum separately satisfy the exact consistency relations in eqs. (2.20) and (2.21) without any residual $\mathcal{T}_N^{\mathrm{cut}}$ dependence.

The singular inclusive cross section, $\mathrm{d}\sigma_{\geq N}^{C}$, appearing in the resummed terms is obtained by removing the constraints on $\mathcal{T}_N$ in eq. (2.36), which gives

$$\begin{aligned}
\frac{\mathrm{d}\sigma_{\geq N}^{C}}{\mathrm{d}\Phi_N} &= (B_N + V_N + W_N)(\Phi_N) + \int \frac{\mathrm{d}\Phi_{N+1}}{\mathrm{d}\Phi_N}\,(C_{N+1} + VC_{N+1})(\Phi_{N+1}) \\
&\quad + \int \frac{\mathrm{d}\Phi_{N+2}}{\mathrm{d}\Phi_N}\,C_{N+2}(\Phi_{N+2})\,. \qquad (2.47)
\end{aligned}$$

Since $\mathrm{d}\sigma_{\geq N}^{C}$ is explicitly $\mathcal{T}_N^{\mathrm{cut}}$ independent, the resummed terms satisfy eq. (2.20) because [see eq. (2.18)]

$$\begin{aligned}
&\frac{\mathrm{d}}{\mathrm{d}\mathcal{T}_N^{\mathrm{cut}}}\Big[\Delta_N(\Phi_N,\mathcal{T}_N^{\mathrm{cut}})\Big]_{\mathcal{T}_N^{\mathrm{cut}}=\mathcal{T}_N} \\
&\qquad = \int \frac{\mathrm{d}\Phi_{N+1}}{\mathrm{d}\Phi_N}\,\delta[\mathcal{T}_N - \mathcal{T}_N(\Phi_{N+1})]\,\frac{S_{N+1}(\Phi_{N+1})}{B_N(\Phi_N)}\,\Delta_N(\Phi_N,\mathcal{T}_N)\,. \qquad (2.48)
\end{aligned}$$

The nonsingular matching correction, $\mathrm{d}\sigma_N^{B-C}$, is defined in eq. (2.38). Taking the difference of eqs. (2.5) and (2.36), we can immediately obtain its NNLO result,

$$\begin{aligned}
\frac{\mathrm{d}\sigma_N^{B-C}}{\mathrm{d}\Phi_N}(\mathcal{T}_N^{\mathrm{cut}}) &\equiv \frac{\mathrm{d}\sigma_N^{\mathrm{NNLO}}}{\mathrm{d}\Phi_N}(\mathcal{T}_N^{\mathrm{cut}}) - \frac{\mathrm{d}\sigma_N^{C}}{\mathrm{d}\Phi_N}(\mathcal{T}_N^{\mathrm{cut}}) = \\
&\int \frac{\mathrm{d}\Phi_{N+1}}{\mathrm{d}\Phi_N}\,(B_{N+1} - C_{N+1} + V_{N+1} - VC_{N+1})(\Phi_{N+1})\,\theta[\mathcal{T}_N(\Phi_{N+1}) < \mathcal{T}_N^{\mathrm{cut}}] \\
&\quad + \int \frac{\mathrm{d}\Phi_{N+2}}{\mathrm{d}\Phi_N}\,(B_{N+2} - C_{N+2})(\Phi_{N+2})\,\theta[\mathcal{T}_N(\Phi_{N+2}) < \mathcal{T}_N^{\mathrm{cut}}]\,. \qquad (2.49)
\end{aligned}$$

The differential equivalent $\mathrm{d}\sigma^{B-C}_{\geq N+1}(\mathcal{T}_N > \mathcal{T}_N^{\mathrm{cut}})$ is defined exactly analogously,

$$\begin{aligned}\frac{\mathrm{d}\sigma^{B-C}_{\geq N+1}}{\mathrm{d}\Phi_{N+1}}(\mathcal{T}_N > \mathcal{T}_N^{\mathrm{cut}}) &\equiv \frac{\mathrm{d}\sigma^{\mathrm{NLO}}_{\geq N+1}}{\mathrm{d}\Phi_{N+1}}(\mathcal{T}_N > \mathcal{T}_N^{\mathrm{cut}}) - \frac{\mathrm{d}\sigma^{C}_{\geq N+1}}{\mathrm{d}\Phi_{N+1}}(\mathcal{T}_N > \mathcal{T}_N^{\mathrm{cut}}) \\ &= (B_{N+1} - C_{N+1} + V_{N+1} - VC_{N+1})(\Phi_{N+1})\,\theta[\mathcal{T}_N(\Phi_{N+1}) > \mathcal{T}_N^{\mathrm{cut}}] \\ &\quad + \int \frac{\mathrm{d}\Phi_{N+2}}{\mathrm{d}\Phi_{N+1}}\,(B_{N+2} - C_{N+2})(\Phi_{N+2})\,\theta[\mathcal{T}_N(\Phi_{N+2}) > \mathcal{T}_N^{\mathrm{cut}}]\,,\end{aligned} \tag{2.50}$$

and one can easily see that eqs. (2.49) and (2.50) explicitly satisfy the consistency condition in eq. (2.21).

Finally, the singular matching corrections, $\mathrm{d}\sigma^{C-S}$, are defined as

$$\begin{aligned}\frac{\mathrm{d}\sigma^{C-S}_{N}}{\mathrm{d}\Phi_{N}}(\mathcal{T}_N^{\mathrm{cut}}) &= \frac{\mathrm{d}\sigma^{C}_{N}}{\mathrm{d}\Phi_{N}}(\mathcal{T}_N^{\mathrm{cut}}) - \left[\frac{\mathrm{d}\sigma^{C}_{\geq N}}{\mathrm{d}\Phi_{N}}\,\Delta_N(\Phi_N;\mathcal{T}_N^{\mathrm{cut}})\right]_{\mathrm{NNLO}_N}, \\ \frac{\mathrm{d}\sigma^{C-S}_{\geq N+1}}{\mathrm{d}\Phi_{N+1}}(\mathcal{T}_N > \mathcal{T}_N^{\mathrm{cut}}) &= \frac{\mathrm{d}\sigma^{C}_{\geq N+1}}{\mathrm{d}\Phi_{N+1}}(\mathcal{T}_N > \mathcal{T}_N^{\mathrm{cut}}) \\ &\quad - \left[\left.\frac{\mathrm{d}\sigma^{C}_{\geq N}}{\mathrm{d}\Phi_{N}}\right|_{\Phi_N=\hat{\Phi}_N} \frac{S_{N+1}(\Phi_{N+1})}{B_N(\hat{\Phi}_N)}\,\Delta_N(\hat{\Phi}_N;\mathcal{T}_N)\,\theta(\mathcal{T}_N > \mathcal{T}_N^{\mathrm{cut}})\right]_{\mathrm{NLO}_{N+1}}.\end{aligned} \tag{2.51}$$

By definition, they satisfy eqs. (2.20) and (2.21) because each of the terms on the right-hand sides do so. To obtain their explicit expressions, we use the NNLO expansion of the Sudakov factor, which we write as

$$\begin{aligned}\Delta_N(\Phi_N;\mathcal{T}_N^{\mathrm{cut}}) &= 1 + \Delta_N^{(1)}(\Phi_N;\mathcal{T}_N^{\mathrm{cut}}) + \Delta_N^{(2)}(\Phi_N;\mathcal{T}_N^{\mathrm{cut}})\,, \\ \Delta_N^{(1)}(\Phi_N;\mathcal{T}_N^{\mathrm{cut}}) &= -\int \frac{\mathrm{d}\Phi_{N+1}}{\mathrm{d}\Phi_N}\,\frac{S^{(1)}_{N+1}(\Phi_{N+1})}{B_N(\Phi_N)}\,\theta(\mathcal{T}_N > \mathcal{T}_N^{\mathrm{cut}})\,, \\ \Delta_N^{(2)}(\Phi_N;\mathcal{T}_N^{\mathrm{cut}}) &= \frac{1}{2}\big[\Delta_N^{(1)}(\Phi_N;\mathcal{T}_N^{\mathrm{cut}})\big]^2 - \int \frac{\mathrm{d}\Phi_{N+1}}{\mathrm{d}\Phi_N}\,\frac{S^{(2)}_{N+1}(\Phi_{N+1})}{B_N(\Phi_N)}\,\theta(\mathcal{T}_N > \mathcal{T}_N^{\mathrm{cut}})\,.\end{aligned} \tag{2.52}$$

Here, we used $S^{(n)}_{N+1}$ to denote the α_s^n contribution to S_{N+1}; i.e.,

$$S_{N+1}(\Phi_{N+1}) = S^{(1)}_{N+1}(\Phi_{N+1}) + S^{(2)}_{N+1}(\Phi_{N+1}) + \cdots\,. \tag{2.53}$$

For convenience, we also define the subtracted one-loop virtual correction, which is the IR-finite NLO term in $\mathrm{d}\sigma^{C}_{\geq N}$,

$$V_N^C(\Phi_N) = V_N(\Phi_N) + \int \frac{\mathrm{d}\Phi_{N+1}}{\mathrm{d}\Phi_N}\,C_{N+1}(\Phi_{N+1})\,. \tag{2.54}$$

The differential version is easier to obtain (since it does not explicitly require $\Delta_N^{(2)}$), and we find

$$\begin{aligned}
&\frac{\mathrm{d}\sigma^{C-S}_{\geq N+1}}{\mathrm{d}\Phi_{N+1}}(\mathcal{T}_N > \mathcal{T}_N^{\mathrm{cut}}) \\
&\quad = (C_{N+1} + VC_{N+1})(\Phi_{N+1})\,\theta(\mathcal{T}_N > \mathcal{T}_N^{\mathrm{cut}}) \\
&\qquad + \int \frac{\mathrm{d}\Phi_{N+2}}{\mathrm{d}\Phi_{N+1}}\, C_{N+2}(\Phi_{N+2})\,\theta[\mathcal{T}_N(\Phi_{N+2}) > \mathcal{T}_N^{\mathrm{cut}}] \\
&\qquad - \left[1 + \frac{S^{(2)}_{N+1}(\Phi_{N+1})}{S^{(1)}_{N+1}(\Phi_{N+1})} + \frac{V_N^C(\hat{\Phi}_N)}{B_N(\hat{\Phi}_N)} + \Delta_N^{(1)}(\hat{\Phi}_N, \mathcal{T}_N)\right] S^{(1)}_{N+1}(\Phi_{N+1})\,\theta(\mathcal{T}_N > \mathcal{T}_N^{\mathrm{cut}})\,.
\end{aligned} \tag{2.55}$$

The cumulant version is given by

$$\begin{aligned}
\frac{\mathrm{d}\sigma_N^{C-S}}{\mathrm{d}\Phi_N}(\mathcal{T}_N^{\mathrm{cut}}) &= -\int \frac{\mathrm{d}\Phi_{N+1}}{\mathrm{d}\Phi_N}\, \frac{\mathrm{d}\sigma^{C-S}_{\geq N+1}}{\mathrm{d}\Phi_{N+1}}(\mathcal{T}_N > \mathcal{T}_N^{\mathrm{cut}}) \\
&= -\int \frac{\mathrm{d}\Phi_{N+1}}{\mathrm{d}\Phi_N}\, (C_{N+1} + VC_{N+1})(\Phi_{N+1})\,\theta[\mathcal{T}_N(\Phi_{N+1}) > \mathcal{T}_N^{\mathrm{cut}}] \\
&\quad - \int \frac{\mathrm{d}\Phi_{N+2}}{\mathrm{d}\Phi_N}\, C_{N+2}(\Phi_{N+2})\,\theta[\mathcal{T}_N(\Phi_{N+2}) > \mathcal{T}_N^{\mathrm{cut}}] \\
&\quad - B_N(\Phi_N)\left[\Delta_N^{(1)}(\Phi_N; \mathcal{T}_N^{\mathrm{cut}}) + \Delta_N^{(2)}(\Phi_N; \mathcal{T}_N^{\mathrm{cut}})\right] \\
&\quad - V_N^C(\Phi_N)\,\Delta_N^{(1)}(\Phi_N; \mathcal{T}_N^{\mathrm{cut}})\,.
\end{aligned} \tag{2.56}$$

The integrals here are explicitly over $\mathcal{T}_N > \mathcal{T}_N^{\mathrm{cut}}$, which cuts off all IR singularities that do not cancel between the full FO singular contributions and their LL approximation arising from the Sudakov expansion, which is given by the last lines in eqs. (2.55) and (2.56). Note that C_{N+2} here fulfills two roles. First, it produces the leading double logarithms $\alpha_s^2(L_{\mathrm{cut}}^4 + L_{\mathrm{cut}}^3)$ (for the cumulant). The $\alpha_s^2 L_{\mathrm{cut}}^4$ is always canceled by the square $[\Delta_N^{(1)}]^2$ inside $\Delta_N^{(2)}$, and the $\alpha_s^2 L_{\mathrm{cut}}^3$ is also canceled if $\Delta_N^{(1)}$ produces the correct single logarithm $\alpha_s L_{\mathrm{cut}}$ at NLO. Second, the $(N+1)$-parton virtual IR divergences in VC_{N+1} are canceled by the $\mathcal{T}_{N+1} \to 0$ limit in the Φ_{N+2} integral over C_{N+2}, where the remainder is an $\alpha_s(\alpha_s L_{\mathrm{cut}}^2 + \alpha_s L_{\mathrm{cut}})$ correction. Generically, these are only partially canceled by the corresponding $V_N^C \Delta_N^{(1)}(\mathcal{T}_N^{\mathrm{cut}})$ term.

2.4.1.2 Case 2

For this case, we use $\mathrm{d}\sigma_N^{\mathrm{MC}}(\mathcal{T}_N^{\mathrm{cut}})$ as given in eq. (2.40), with its corresponding inclusive $\mathrm{d}\sigma^{\mathrm{MC}}_{\geq N+1}(\mathcal{T}_N > \mathcal{T}_N^{\mathrm{cut}})$ given in eq. (2.43), which we repeat here for completeness:

$$\frac{\mathrm{d}\sigma_N^{\mathrm{MC}}}{\mathrm{d}\Phi_N}(\mathcal{T}_N^{\mathrm{cut}}) = \left[\frac{\mathrm{d}\sigma^C_{\geq N}}{\mathrm{d}\Phi_N} + \frac{\mathrm{d}\widetilde{\sigma}_N^{C-S}}{\mathrm{d}\Phi_N}(\mathcal{T}_N^{\mathrm{cut}})\right]\Delta_N(\Phi_N; \mathcal{T}_N^{\mathrm{cut}}) + \frac{\mathrm{d}\sigma_N^{B-C}}{\mathrm{d}\Phi_N}(\mathcal{T}_N^{\mathrm{cut}})\,,$$

$$\frac{\mathrm{d}\sigma^{\mathrm{MC}}_{\geq N+1}}{\mathrm{d}\Phi_{N+1}}(\mathcal{T}_N > \mathcal{T}_N^{\mathrm{cut}}) = \Bigg\{ \Bigg[\frac{\mathrm{d}\sigma^{C}_{\geq N}}{\mathrm{d}\Phi_N} + \frac{\mathrm{d}\widetilde{\sigma}^{C-S}_{N}}{\mathrm{d}\Phi_N}(\mathcal{T}_N) \Bigg]_{\Phi_N=\hat{\Phi}_N} \frac{S_{N+1}(\Phi_{N+1})}{B_N(\hat{\Phi}_N)}\, \theta(\mathcal{T}_N > \mathcal{T}_N^{\mathrm{cut}}) + \frac{\mathrm{d}\widetilde{\sigma}^{C-S}_{\geq N+1}}{\mathrm{d}\Phi_{N+1}}(\mathcal{T}_N > \mathcal{T}_N^{\mathrm{cut}}) \Bigg\} \Delta_N(\hat{\Phi}_N; \mathcal{T}_N) + \frac{\mathrm{d}\sigma^{B-C}_{\geq N+1}}{\mathrm{d}\Phi_{N+1}}(\mathcal{T}_N > \mathcal{T}_N^{\mathrm{cut}})\,.$$

The explicit expressions for all ingredients are given in the following. As for case 1, these are correct to NNLO_N and NLO_{N+1} and include the correct LL resummation for $\mathcal{T}_N^{\mathrm{cut}}$ and $\mathcal{T}_N$, respectively. The resummation terms involving $\mathrm{d}\sigma^{C}_{\geq N}\Delta_N$ and the nonsingular FO matching terms, $\mathrm{d}\sigma^{B-C}$, are the same as in case 1 [see eq. (2.47) and eqs. (2.49) and (2.50)] and separately satisfy the consistency relations in eqs. (2.20) and (2.21).

The difference to case 1 is how the singular matching corrections, $\mathrm{d}\widetilde{\sigma}^{S-C}$, are included. For the cumulant, we have

$$\begin{aligned}
\frac{\mathrm{d}\widetilde{\sigma}^{C-S}_{N}}{\mathrm{d}\Phi_N}(\mathcal{T}_N^{\mathrm{cut}}) &= \Bigg[\frac{\mathrm{d}\sigma^{C-S}_{N}}{\mathrm{d}\Phi_N}(\mathcal{T}_N^{\mathrm{cut}})\, \frac{1}{\Delta_N(\Phi_N; \mathcal{T}_N^{\mathrm{cut}})} \Bigg]_{\mathrm{NNLO}_N} \\
&= \frac{\mathrm{d}\sigma^{C-S}_{N}}{\mathrm{d}\Phi_N}(\mathcal{T}_N^{\mathrm{cut}}) \\
&\quad + \Delta_N^{(1)}(\Phi_N; \mathcal{T}_N^{\mathrm{cut}}) \int \frac{\mathrm{d}\Phi_{N+1}}{\mathrm{d}\Phi_N}\, (C_{N+1} - S^{(1)}_{N+1})(\Phi_{N+1})\, \theta[\mathcal{T}_N(\Phi_{N+1}) > \mathcal{T}_N^{\mathrm{cut}}]\,,
\end{aligned} \tag{2.57}$$

where $\mathrm{d}\sigma^{C-S}_{N}(\mathcal{T}_N^{\mathrm{cut}})$ is given in eq. (2.56). The corresponding differential result in the spectrum is obtained by requiring eq. (2.21),

$$\begin{aligned}
&\frac{\mathrm{d}\widetilde{\sigma}^{C-S}_{\geq N+1}}{\mathrm{d}\Phi_{N+1}}(\mathcal{T}_N > \mathcal{T}_N^{\mathrm{cut}}) \\
&= \frac{\mathrm{d}\sigma^{C-S}_{\geq N+1}}{\mathrm{d}\Phi_{N+1}}(\mathcal{T}_N > \mathcal{T}_N^{\mathrm{cut}}) - \Bigg\{ \Delta_N^{(1)}(\hat{\Phi}_N; \mathcal{T}_N)\, (C_{N+1} - S^{(1)}_{N+1})(\Phi_{N+1}) \\
&\quad + \frac{S^{(1)}_{N+1}(\Phi_{N+1})}{B_N(\hat{\Phi}_N)} \int \frac{\mathrm{d}\Phi'_{N+1}}{\mathrm{d}\Phi_N}\, \big(C_{N+1} - S^{(1)}_{N+1}\big)(\Phi'_{N+1})\, \theta[\mathcal{T}_N(\Phi'_{N+1}) > \mathcal{T}_N] \Bigg\} \theta(\mathcal{T}_N > \mathcal{T}_N^{\mathrm{cut}})\,,
\end{aligned} \tag{2.58}$$

where $\mathrm{d}\sigma^{C-S}_{\geq N+1}(\mathcal{T}_N > \mathcal{T}_N^{\mathrm{cut}})$ is given in eq. (2.55). One can easily check that with this result the expression for $\mathrm{d}\sigma^{\mathrm{MC}}_{\geq N+1}$ in case 2 expands to the correct NLO_{N+1} result.

2.4.2 The exclusive $(N+1)$-jet and inclusive $(N+2)$-jet cross sections

The inclusive $(N+1)$-jet MC cross section is divided into the exclusive $(N+1)$-jet and inclusive $(N+2)$-jet MC cross sections using a resolution scale $\mathcal{T}^{\mathrm{cut}}_{N+1}$,

$$\frac{\mathrm{d}\sigma^{\mathrm{MC}}_{\geq N+1}}{\mathrm{d}\Phi_{N+1}}(\mathcal{T}_N > \mathcal{T}_N^{\mathrm{cut}}) = \frac{\mathrm{d}\sigma^{\mathrm{MC}}_{N+1}}{\mathrm{d}\Phi_{N+1}}(\mathcal{T}_N > \mathcal{T}_N^{\mathrm{cut}}; \mathcal{T}^{\mathrm{cut}}_{N+1})$$

$$+\int \frac{\mathrm{d}\Phi_{N+2}}{\mathrm{d}\Phi_{N+1}} \frac{\mathrm{d}\sigma^{\mathrm{MC}}_{\geq N+2}}{\mathrm{d}\Phi_{N+2}} (\mathcal{T}_N > \mathcal{T}_N^{\mathrm{cut}}, \mathcal{T}_{N+1} > \mathcal{T}_{N+1}^{\mathrm{cut}}) \,. \tag{2.59}$$

Note that this is just a special case of the consistency condition in eq. (2.21) applied to $\mathcal{T}_{N+1}$ and taking $\mathcal{T}^c_{N+1} \equiv \mathcal{T}^{\max}_{N+1}$.

The inclusive $\mathrm{d}\sigma^{\mathrm{MC}}_{\geq N+1}$ already resums the leading logarithms of $\mathcal{T}_N$ in the $(N+1)$-parton phase space. On top of that, we also want to resum the leading logarithms of $\mathcal{T}^{\mathrm{cut}}_{N+1}$ and $\mathcal{T}_{N+1}$ appearing in $\mathrm{d}\sigma^{\mathrm{MC}}_{N+1}(\mathcal{T}^{\mathrm{cut}}_{N+1})$ and $\mathrm{d}\sigma^{\mathrm{MC}}_{\geq N+2}(\mathcal{T}_{N+1})$. The LL resummation for $\mathcal{T}_{N+1}$ is obtained using the $(N+1)$-parton Sudakov factor, Δ_{N+1}, which is defined as

$$\Delta_{N+1}(\Phi_{N+2}; \mathcal{T}^{\mathrm{cut}}_{N+1}) = \exp\left\{ -\int \frac{\mathrm{d}\Phi_{N+2}}{\mathrm{d}\Phi_{N+1}} \frac{S_{N+2}(\Phi_{N+2})}{B_{N+1}(\hat{\Phi}_{N+1})} \theta[\mathcal{T}_{N+1}(\Phi_{N+2}) > \mathcal{T}^{\mathrm{cut}}_{N+1}] \right\}, \tag{2.60}$$

where the upper limit on the integration over $\mathcal{T}_{N+1}$ should be chosen of order $\mathcal{T}_N$. Note that the $(N+1)$-parton splitting function S_{N+2} enters in the Sudakov factor relative to the $(N+1)$-parton Born matrix element B_{N+1}, which is required to correctly sum the logarithms of $\mathcal{T}_{N+1}$ across the whole range of $\mathcal{T}_N$, even for $\mathcal{T}_N \sim \mathcal{T}_N^{\max}$. In terms of the resummation accuracy, achieving (N)LO$_{N+1}$+LL implies that the $(N+1)$-parton Sudakov factor must multiply the complete B_{N+1} matrix element to obtain the LL resummation of $\mathcal{T}_{N+1}$ (or $\mathcal{T}^{\mathrm{cut}}_{N+1}$) in the limit $\mathcal{T}_{N+1} \ll \mathcal{T}_N$ for both $\mathcal{T}_N \ll \mathcal{T}_N^{\max}$ and $\mathcal{T}_N \sim \mathcal{T}_N^{\max}$.

Given these considerations, we again divide the exclusive $(N+1)$-jet and inclusive $(N+2)$-jet MC cross sections into a resummed contribution and FO matching corrections,

$$\begin{aligned}
&\frac{\mathrm{d}\sigma^{\mathrm{MC}}_{N+1}}{\mathrm{d}\Phi_{N+1}}(\mathcal{T}_N > \mathcal{T}_N^{\mathrm{cut}}; \mathcal{T}_{N+1}^{\mathrm{cut}}) \\
&\quad = \underbrace{\frac{\mathrm{d}\sigma'^{C}_{\geq N+1}}{\mathrm{d}\Phi_{N+1}}(\mathcal{T}_N > \mathcal{T}_N^{\mathrm{cut}})\, \Delta_{N+1}(\Phi_{N+1}; \mathcal{T}^{\mathrm{cut}}_{N+1})}_{\text{resummed}} \\
&\qquad + \Bigg(\underbrace{\frac{\mathrm{d}\sigma^{C-S}_{N+1}}{\mathrm{d}\Phi_{N+1}}}_{\substack{\text{FO singular}\\ \text{matching}}} + \underbrace{\frac{\mathrm{d}\sigma^{B-C}_{N+1}}{\mathrm{d}\Phi_{N+1}}}_{\substack{\text{FO nonsing.}\\ \text{matching}}} \Bigg) (\mathcal{T}_N > \mathcal{T}_N^{\mathrm{cut}}; \mathcal{T}_{N+1}^{\mathrm{cut}}) \,, \\
&\frac{\mathrm{d}\sigma^{\mathrm{MC}}_{\geq N+2}}{\mathrm{d}\Phi_{N+2}}(\mathcal{T}_N > \mathcal{T}_N^{\mathrm{cut}}, \mathcal{T}_{N+1} > \mathcal{T}_{N+1}^{\mathrm{cut}}) \\
&\quad = \frac{\mathrm{d}\sigma'^{C}_{\geq N+1}}{\mathrm{d}\Phi_{N+1}}(\mathcal{T}_N > \mathcal{T}_N^{\mathrm{cut}}) \Bigg|_{\Phi_{N+1}=\hat{\Phi}_{N+1}} \frac{S_{N+2}(\Phi_{N+2})}{B_{N+1}(\hat{\Phi}_{N+1})}\, \Delta_{N+1}(\hat{\Phi}_{N+1}; \mathcal{T}_{N+1})\, \theta(\mathcal{T}_{N+1} > \mathcal{T}^{\mathrm{cut}}_{N+1}) \\
&\qquad + \left(\frac{\mathrm{d}\sigma^{C-S}_{\geq N+2}}{\mathrm{d}\Phi_{N+2}} + \frac{\mathrm{d}\sigma^{B-C}_{\geq N+2}}{\mathrm{d}\Phi_{N+2}} \right) (\mathcal{T}_N > \mathcal{T}_N^{\mathrm{cut}}, \mathcal{T}_{N+1} > \mathcal{T}^{\mathrm{cut}}_{N+1}) \,.
\end{aligned} \tag{2.61}$$

This has precisely the structure of the usual NLO$_{N+1}$+LL calculation [see eq. (2.25)], but with the dependence on the singular and nonsingular FO matching corrections, $\mathrm{d}\sigma^{C-S}$ and $\mathrm{d}\sigma^{B-C}$, written out explicitly. Furthermore, $\mathrm{d}\sigma'^{C}_{\geq N+1}(\mathcal{T}_N > \mathcal{T}_N^{\mathrm{cut}})$ is the singular approximation to the full $(N+1)$-jet inclusive cross section on which the $\mathcal{T}_{N+1}$ resummation acts. The crucial difference compared to the usual NLO+LL case discussed in section 2.3.3 is that the NLO$_{N+1}$+LL calculation is used down to very small values $\mathcal{T}_N > \mathcal{T}_N^{\mathrm{cut}}$, and so $\mathrm{d}\sigma'^{C}_{\geq N+1}(\mathcal{T}_N > \mathcal{T}_N^{\mathrm{cut}})$ now has to include the LL resummation in $\mathcal{T}_N$. In terms of the inclusive $\mathrm{d}\sigma^{\mathrm{MC}}_{\geq N+1}(\mathcal{T}_N > \mathcal{T}_N^{\mathrm{cut}})$ [given by either eq. (2.42) or eq. (2.43)], we can write it as

$$\begin{aligned}\frac{\mathrm{d}\sigma'^{C}_{\geq N+1}}{\mathrm{d}\Phi_{N+1}}(\mathcal{T}_N > \mathcal{T}_N^{\mathrm{cut}}) &= \frac{\mathrm{d}\sigma^{\mathrm{MC}}_{\geq N+1}}{\mathrm{d}\Phi_{N+1}}(\mathcal{T}_N > \mathcal{T}_N^{\mathrm{cut}}) \\ &\quad - \int \frac{\mathrm{d}\Phi_{N+2}}{\mathrm{d}\Phi_{N+1}}\,(B_{N+2} - C_{N+2})(\Phi_{N+2})\,\theta[\mathcal{T}_N(\Phi_{N+2}) > \mathcal{T}_N^{\mathrm{cut}}]\,,\end{aligned} \tag{2.62}$$

where the second term on the right-hand side removes the dependence on B_{N+2} from $\mathrm{d}\sigma^{\mathrm{MC}}_{\geq N+1}$; i.e., it removes the last line in $\mathrm{d}\sigma^{B-C}_{\geq N+1}$ in eq. (2.50). By definition of C_{N+2}, this term has no logarithmic dependence on $\mathcal{T}_N$ and therefore does not affect the LL resummation in $\mathcal{T}_N$. Expanding this to fixed NLO$_{N+1}$ reproduces the $N+1$ version of eq. (2.44),

$$\begin{aligned}\left[\frac{\mathrm{d}\sigma'^{C}_{\geq N+1}}{\mathrm{d}\Phi_{N+1}}(\mathcal{T}_N > \mathcal{T}_N^{\mathrm{cut}})\right]_{\mathrm{NLO}_{N+1}} &= (B_{N+1} + V_{N+1})(\Phi_{N+1}) \\ &\quad + \int \frac{\mathrm{d}\Phi_{N+2}}{\mathrm{d}\Phi_{N+1}}\,C_{N+2}(\Phi_{N+2})\,\theta[\mathcal{T}_N(\Phi_{N+2}) > \mathcal{T}_N^{\mathrm{cut}}]\,.\end{aligned} \tag{2.63}$$

This shows that, in the limit of turning off the $\mathcal{T}_N$ resummation, eq. (2.61) reproduces the correct NLO$_{N+1}$+LL result as required.

The FO matching corrections are determined by imposing the correct NLO$_{N+1}$ and LO$_{N+2}$ expansions of eq. (2.61). The nonsingular matching corrections are given as

$$\begin{aligned}&\frac{\mathrm{d}\sigma^{B-C}_{N+1}}{\mathrm{d}\Phi_{N+1}}(\mathcal{T}_N > \mathcal{T}_N^{\mathrm{cut}}; \mathcal{T}_{N+1}^{\mathrm{cut}}) \\ &\quad = \int \frac{\mathrm{d}\Phi_{N+2}}{\mathrm{d}\Phi_{N+1}}\,(B_{N+2} - C_{N+2})(\Phi_{N+2})\,\theta[\mathcal{T}_N(\Phi_{N+2}) > \mathcal{T}_N^{\mathrm{cut}}]\,\theta[\mathcal{T}_{N+1}(\Phi_{N+2}) < \mathcal{T}_{N+1}^{\mathrm{cut}}]\,, \\ &\frac{\mathrm{d}\sigma^{B-C}_{\geq N+2}}{\mathrm{d}\Phi_{N+2}}(\mathcal{T}_N > \mathcal{T}_N^{\mathrm{cut}}, \mathcal{T}_{N+1} > \mathcal{T}_{N+1}^{\mathrm{cut}}) \\ &\quad = (B_{N+2} - C_{N+2})(\Phi_{N+2})\,\theta[\mathcal{T}_N(\Phi_{N+2}) > \mathcal{T}_N^{\mathrm{cut}}]\,\theta[\mathcal{T}_{N+1}(\Phi_{N+2}) > \mathcal{T}_{N+1}^{\mathrm{cut}}]\,,\end{aligned} \tag{2.64}$$

and (again by definition of C_{N+2}) have no logarithmic dependence on $\mathcal{T}_{N+1}^{\text{cut}}$. For the singular matching corrections, we then find

$$\begin{aligned}
&\frac{\mathrm{d}\sigma_{N+1}^{C-S}}{\mathrm{d}\Phi_{N+1}}(\mathcal{T}_N > \mathcal{T}_N^{\text{cut}}; \mathcal{T}_{N+1}^{\text{cut}}) \\
&\quad = -\int \frac{\mathrm{d}\Phi_{N+2}}{\mathrm{d}\Phi_{N+1}} \Big\{ C_{N+2}(\Phi_{N+2})\, \theta[\mathcal{T}_N(\Phi_{N+2}) > \mathcal{T}_N^{\text{cut}}] \\
&\qquad\qquad - S_{N+2}(\Phi_{N+2})\, \theta[\mathcal{T}_N(\hat{\Phi}_{N+1}) > \mathcal{T}_N^{\text{cut}}] \Big\} \times \theta[\mathcal{T}_{N+1}(\Phi_{N+2}) > \mathcal{T}_{N+1}^{\text{cut}}]\,, \\
&\frac{\mathrm{d}\sigma_{\geq N+2}^{C-S}}{\mathrm{d}\Phi_{N+2}}(\mathcal{T}_N > \mathcal{T}_N^{\text{cut}}, \mathcal{T}_{N+1} > \mathcal{T}_{N+1}^{\text{cut}}) \\
&\quad = \Big\{ C_{N+2}(\Phi_{N+2})\, \theta[\mathcal{T}_N(\Phi_{N+2}) > \mathcal{T}_N^{\text{cut}}] - S_{N+2}(\Phi_{N+2})\, \theta[\mathcal{T}_N(\hat{\Phi}_{N+1}) > \mathcal{T}_N^{\text{cut}}] \Big\} \\
&\qquad \times \theta[\mathcal{T}_{N+1}(\Phi_{N+2}) > \mathcal{T}_{N+1}^{\text{cut}}]\,.
\end{aligned} \tag{2.65}$$

Here, we can explicitly see the mismatch between the exact definition of $\mathcal{T}_N(\Phi_{N+2})$ required at NNLO_N and the shower approximation in the S_{N+2} term, which inherits the $\hat{\Phi}_{N+1}(\Phi_{N+2})$ dependence from the projection from Φ_{N+2} to Φ_{N+1} in the $(N+1)$-jet Sudakov factor. Generically, this can introduce a subleading logarithmic dependence on $\mathcal{T}_N^{\text{cut}}$ in $\mathrm{d}\sigma^{C-S}$ (even in the limit $S_{N+2} = C_{N+2}$), whose coefficient scales as $\sim \mathcal{T}_N^{\text{cut}}$.

With the above results, we can check that no residual $\mathcal{T}_{N+1}^{\text{cut}}$ dependence (beyond power corrections) is introduced in physical observables because eqs. (2.20) and (2.21) are explicitly satisfied. For the FO matching corrections, this is clear from their above expressions. The resummed terms also combine correctly to the inclusive $\mathrm{d}\sigma_{\geq N+1}^{C}$ using the equivalent relation to eq. (2.18) for the $(N+1)$-parton Sudakov,

$$\int \frac{\mathrm{d}\Phi_{N+2}}{\mathrm{d}\Phi_{N+1}} \frac{S_{N+2}(\Phi_{N+2})}{B_{N+1}(\hat{\Phi}_{N+1})}\, \Delta_{N+1}(\hat{\Phi}_{N+1}; \mathcal{T}_{N+1})\, \theta(\mathcal{T}_{N+1} > \mathcal{T}_{N+1}^{\text{cut}}) = 1 - \Delta_{N+1}(\Phi_{N+1}; \mathcal{T}_{N+1}^{\text{cut}})\,. \tag{2.66}$$

Using this relation, we can also easily check that eq. (2.59) is satisfied. Upon integration over $\mathrm{d}\Phi_{N+2}/\mathrm{d}\Phi_{N+1}$, the $\mathrm{d}\sigma_{N+1}^{C-S}$ and $\mathrm{d}\sigma_{\geq N+2}^{C-S}$ terms cancel each other, while the $\mathrm{d}\sigma_{N+1}^{B-C}$ and $\mathrm{d}\sigma_{\geq N+2}^{B-C}$ terms combine to precisely cancel the second line in eq. (2.62). Hence, we precisely get back $\mathrm{d}\sigma_{\geq N+1}^{\text{MC}}(\mathcal{T}_N > \mathcal{T}_N^{\text{cut}})$, which shows that no residual $\mathcal{T}_N^{\text{cut}}$ dependence is introduced.

In the above construction, we have the same amount of freedom as in section 2.4.1 in how to implement the $\mathcal{T}_{N+1}$ resummation and where to put the FO singular corrections. Above, we have used the analog of case 1 from section 2.4.1, where $\mathrm{d}\sigma^{C-S}$ is included at fixed order. Various alternatives are:

- One can multiply $\mathrm{d}\sigma_{N+1}^{C-S}$ by the Δ_{N+1} Sudakov, analogous to case 2 in section 2.4.1. In this case, eq. (2.59) is maintained exactly when the corresponding case 2 version is also used for the differential spectrum.

- One has the freedom in eq. (2.62) and all the results following it to use a different C'_{N+2} from the C_{N+2} used in section 2.4.1. This includes whether one uses $\mathcal{T}_N(\Phi_{N+2})$ or $\mathcal{T}_N(\hat{\Phi}_{N+1})$ to implement the $\mathcal{T}_N > \mathcal{T}_N^{\text{cut}}$ constraint for the C'_{N+2} contribution. In particular, one could use a simpler NLO_{N+1} subtraction for C'_{N+2}. (In general, this can change the logarithmic dependence on $\mathcal{T}_N$ at the subleading level.)

- One can use different choices for S_{N+2}. In particular, in conjunction with using an alternative C'_{N+2}, one can use a POWHEG approach for NLO_{N+1}+LL, such that one can take $S_{N+2} = C'_{N+2}$.

2.5 Matching the NNLO+LL calculation with a parton shower

In the previous sections, we have shown how to consistently combine LO, NLO, and NNLO calculations with LL resummation and how to obtain the MC cross sections $\mathrm{d}\sigma_N^{\text{MC}}$, $\mathrm{d}\sigma_{N+1}^{\text{MC}}$, and $\mathrm{d}\sigma_{\geq N+2}^{\text{MC}}$. In this section, we discuss how to interface the corresponding N-parton, $(N+1)$-parton, and $(N+2)$-parton events with a parton shower and avoid any double counting of phase space between the partonic calculation and the parton shower. The resulting NNLO+LL event generator will thus be able to produce events with any parton multiplicity.

The NNLO+LL MC cross sections in section 2.4 provide resummation in the resolution variables $\mathcal{T}_N$ and $\mathcal{T}_{N+1}$, but in general, do not explicitly resum large logarithms arising in singular regions of phase space for other observables. In the resummation regime, the shape of a generic exclusive observable will therefore only be accurately predicted after the addition of the parton shower, which in general provides LL accuracy. Furthermore, care must be taken when interfacing to the parton shower such that the perturbative accuracy provided by the MC cross sections $\mathrm{d}\sigma_M^{\text{MC}}$ is maintained. This includes the FO accuracy, the LL accuracy in the evolution variables, and the absence of residual dependence on the resolution scales $\mathcal{T}_N^{\text{cut}}$ and $\mathcal{T}_{N+1}^{\text{cut}}$. Precisely, the matching with the parton shower must satisfy three conditions:

1. Any exclusive observable must be correct to at least LL in the resummation regime. This includes the resolution variables $\mathcal{T}_N$ and $\mathcal{T}_{N+1}$, for which the LL accuracy of the MC cross sections must be maintained. Additionally, the LL accuracy requirement extends to observables requiring more than $N+2$ jets, for which the parton shower provides the only prediction.

2. The FO accuracy of any observable should be that of the NNLO calculation (see section 2.2.1), which means:

- N-jet observables are correct to NNLO_N up to power corrections of relative order $\mathcal{O}(\alpha_s \mathcal{T}_N^{\text{cut}}/\mathcal{T}_N^{\text{eff}})$ and $\mathcal{O}(\alpha_s^2 \mathcal{T}_{N+1}^{\text{cut}}/\mathcal{T}_{N+1}^{\text{eff}})$, where $\mathcal{T}_N^{\text{eff}}$ and $\mathcal{T}_{N+1}^{\text{eff}}$ are the effective resolution scales to which the observable is sensitive.
- $(N+1)$-jet observables are correct to NLO_{N+1} if they only include contributions in the resolved region of Φ_{N+1}, up to power corrections of relative order $\mathcal{O}(\alpha_s \mathcal{T}_{N+1}^{\text{cut}}/\mathcal{T}_{N+1}^{\text{eff}})$, where $\mathcal{T}_{N+1}^{\text{eff}}$ is the effective resolution scale to which the observable is sensitive.
- $(N+2)$-jet observables are correct to LO_{N+2} if they only include contributions in the resolved region of Φ_{N+2}.

Note that no FO accuracy is implied for observables sensitive to the unresolved regions of phase space, $\mathcal{T}_N < \mathcal{T}_N^{\text{cut}}$ and $\mathcal{T}_{N+1} < \mathcal{T}_{N+1}^{\text{cut}}$, as the parton shower provides the only prediction in these regions (see below).

3. For observables that must be correct to N^nLO, any residual dependence on the resolution scales $\mathcal{T}_N^{\text{cut}}$ and $\mathcal{T}_{N+1}^{\text{cut}}$ must enter at $\mathcal{O}_{\text{cut}}(\alpha_s^{\geq n+1})$.

The conditions above naturally echo those imposed on the MC cross sections in section 2.3.1, and in particular, ensure that no double counting occurs in the matching. In fact, in cases where the parton shower yields events with $\leq N+2$ partons, the exact phase space constraints implemented by the MC cross section definitions can be used on the shower (see figure 2.1). In cases with more emissions, one must develop analogous constraints making sure the above conditions remain satisfied.

2.5.1 LL shower constraints

Condition 1 above requires us to maintain the LL accuracy of the event sample and combine it with the parton shower LL resummation for additional emissions. For this purpose, the identical considerations apply to our NNLO+LL calculation as in the case of interfacing a merged $\text{LO}_{N,N+1,N+2}$+LL calculation with a parton shower [4, 5, 6, 8, 7, 9, 10, 11, 12]. The reason is that, as far as the LL structure is concerned, the only relevance of the higher FO accuracy in our case is that it imposes a tighter constraint in condition 3 above. However, since the parton shower is formulated such that the probability of an emission is the exact differential of the no-emission probability [i.e., of the Sudakov factor, see eq. (2.18)], condition 3 will be satisfied as long as any additional constraints imposed on the parton shower do not spoil this relation.

The simultaneous LL resummation of $\mathcal{T}_N$ and $\mathcal{T}_{N+1}$ in the NNLO+LL calculation can be achieved by choosing both variables to be equivalent (at the single-emission/LL level) to the same local shower evolution variable $\mathcal{T}$ [see eq. (2.8)], in which case we can assume that they are ordered as $\mathcal{T}_{N+1} < \mathcal{T}_N$.

2.5.1.1 Equivalent resummation and shower evolution variables

The simplest case is when the evolution variable of the parton shower is equivalent to $\mathcal{T}$ (i.e., it has the same LL structure). The event sample with N, $N+1$, and $N+2$ partons can then be viewed as the result of the first two steps in the normal parton shower evolution in $\mathcal{T}$, and attaching the parton shower simply corresponds to continuing this evolution down to the shower cutoff, where the relevant starting scale, $\mathcal{T}_{\text{res}}$, is given by the scale of the last emission or the resolution scale, namely

- $\mathcal{T}_{\text{res}} \equiv \mathcal{T}_N^{\text{cut}}$ for the N-parton events
- $\mathcal{T}_{\text{res}} \equiv \mathcal{T}_{N+1}^{\text{cut}}$ for the $(N+1)$-parton events
- $\mathcal{T}_{\text{res}} \equiv \mathcal{T}_{N+1}(\Phi_{N+2})$ for the $(N+2)$-parton events

In this case, conditions 1 and 3 are automatically satisfied because the parton shower itself respects them.

This is precisely consistent with the physical interpretation of the MC cross sections. The $\mathrm{d}\sigma_N^{\text{MC}}(\mathcal{T}_N^{\text{cut}})$ and $\mathrm{d}\sigma_{N+1}^{\text{MC}}(\mathcal{T}_N > \mathcal{T}_N^{\text{cut}}; \mathcal{T}_{N+1}^{\text{cut}})$ cross sections represented by the N-parton and $(N+1)$-parton events are exclusive jet cross sections defined to only include additional emissions below $\mathcal{T}_N^{\text{cut}}$ and $\mathcal{T}_{N+1}^{\text{cut}}$. The $\mathrm{d}\sigma_{\geq N+2}^{\text{MC}}(\mathcal{T}_N > \mathcal{T}_N^{\text{cut}}, \mathcal{T}_{N+1} > \mathcal{T}_{N+1}^{\text{cut}})$ cross section represented by the $(N+2)$-parton events is an inclusive cross section defined to contain any number of additional emissions below $\mathcal{T}_{N+1}$.

Note also that, in principle, one can choose $\mathcal{T}_N^{\text{cut}} = \mathcal{T}_{N+1}^{\text{cut}}$ to be equal (or very close) to the actual shower cutoff $\mathcal{T}^{\text{cut}}$, such that no (or very few) additional emissions need to be generated for the N-jet and $(N+1)$-jet samples.

2.5.1.2 Different resummation and shower evolution variables

If the local evolution variable $\mathcal{T}'$ of the parton shower differs in its LL structure from the variable $\mathcal{T}$ used to implement the LL resummation in the partonic FO+LL calculation, one has to utilize a veto procedure on the shower to achieve condition 1. In principle, two approaches may be used here, using either a vetoed shower algorithm or a global veto procedure. Additionally, one has to specify the starting scale of the shower evolution.

The use of a vetoed parton shower was discussed in detail in refs. [4, 15] for the case where $\mathcal{T}$ is the p_T of an emission and using an angular-ordered parton shower where $\mathcal{T}'$ is the emission angle. The same veto procedure can be applied here. The vetoed shower works by evolving in $\mathcal{T}'$, and in each emission step, only emissions satisfying the constraint $\mathcal{T} < \mathcal{T}_{\text{res}}$ are allowed, where $\mathcal{T}_{\text{res}}$ is given as above. If an emission at some $\mathcal{T}'$ violates this constraint, it is vetoed, and the evolution continues from $\mathcal{T}'$. This vetoed shower exponentiates the $\mathcal{T} < \mathcal{T}_{\text{res}}$ constraint, which effectively transforms the shower evolution variable from $\mathcal{T}'$ into $\mathcal{T}$.

In the global veto procedure, one lets the evolution proceed undisturbed. After the showering is done, the showered event is accepted if the condition $\mathcal{T} < \mathcal{T}_{\rm res}$ is satisfied for all emissions. If this is not the case, the showering is repeated from the start on the same partonic event, and this is done until an acceptable showered event is generated. This second approach is certainly less efficient, but it has the advantage that one does not need to modify the parton shower algorithm at all.

In either vetoing approach, one has to choose appropriate starting scales for the $\mathcal{T}'$ evolution. First, one determines the maximal starting scale $\mathcal{T}'_{\rm max}$, which should be either the value $\mathcal{T}'_{\rm max}(\Phi_N)$ that one would normally choose when starting the shower directly from $B_N(\Phi_N)$, or the maximum value of $\mathcal{T}'$ kinematically allowed for a given $\mathcal{T}_{\rm res}$, whichever is smaller. The simplest approach is then to start the shower at $\mathcal{T}'_{\rm max}$ for all partons. A somewhat better approach is to choose the starting scale according to the emission history.[9] For partons that had no emissions, the shower is started at $\mathcal{T}'_{\rm max}$. For the daughter partons of an extra emission step in the $(N+1)$-jet and $(N+2)$-jet samples, the shower is started from the scale $\mathcal{T}'_{\rm res}$ of the emission. The possible additional emissions for $\mathcal{T}'_{\rm max} > \mathcal{T}' > \mathcal{T}'_{\rm res}$ are then added by running a truncated shower [15] from $\mathcal{T}'_{\rm max}$ to $\mathcal{T}'_{\rm res}$ along the parent parton line of the emission.

2.5.2 FO shower constraints

The constraints on the shower implied by condition 2 are simpler for event samples with higher jet multiplicity, as the desired perturbative accuracy is lower. Therefore, we start by discussing the $(N+2)$-jet sample, working our way down to the N-jet sample. Note that if the shower evolves directly in $\mathcal{T}$ and both $\mathcal{T}_N^{\rm cut}$ and $\mathcal{T}_{N+1}^{\rm cut}$ are set to the shower cutoff, only the $(N+2)$-jet sample gets showered, and the additional complications arising for the $(N+1)$-jet and N-jet samples become irrelevant.

2.5.2.1 Showering the $(N+2)$-jet event sample

The MC cross section $\mathrm{d}\sigma^{\rm MC}_{\geq N+2}$ of the NNLO+LL calculation is given in eq. (2.61). Its perturbative accuracy is LO_{N+2}+LL, which the parton shower can easily maintain by applying constraints analogous to those applied to the highest jet multiplicity in an LO+LL matched event sample. The LO_{N+2} accuracy of the cross section is automatically guaranteed by the fact that additional emissions from the parton shower are higher order in α_s. Therefore, there are no additional FO constraints on the shower. (Strictly speaking, the showered events in this sample must still satisfy the constraints $\mathcal{T}_N > \mathcal{T}_N^{\rm cut}$ and $\mathcal{T}_{N+1} > \mathcal{T}_{N+1}^{\rm cut}$. If $\mathcal{T}_{N+1} < \mathcal{T}_N$, ignoring this gives rise to at most power corrections.)

[9] The LL resummation in $\mathcal{T}_N$ and $\mathcal{T}_{N+1}$ is formulated as a consecutive sum over emission channels m when splitting from N to $N+1$ partons (in the construction of $\mathrm{d}\sigma^{\rm MC}_{\geq N+1}$) and from $N+1$ to $N+2$ partons (in the construction of $\mathrm{d}\sigma^{\rm MC}_{\geq N+2}$). Hence, we can naturally associate each contribution in this sum with an emission history for going from the underlying Φ_N to the final Φ_{N+1} or Φ_{N+2} point.

2.5.2.2 Showering the $(N+1)$-jet event sample

The MC cross section $\mathrm{d}\sigma^{\mathrm{MC}}_{N+1}(\mathcal{T}_N > \mathcal{T}^{\mathrm{cut}}_N; \mathcal{T}^{\mathrm{cut}}_{N+1})$ of the NNLO+LL calculation is given in eq. (2.61). It contains the integrated cross section for $\mathcal{T}_{N+1} < \mathcal{T}^{\mathrm{cut}}_{N+1}$ calculated to NLO_{N+1}+LL. Before adding the parton shower, it is represented by $(N+1)$-parton events, which have $\mathcal{T}_{N+1} = 0$ (see figure 2.1). By adding emissions, the parton shower distributes the events located at $\mathcal{T}_{N+1} = 0$ to nonzero $\mathcal{T}_{N+1}$ values. In doing so, it must respect the exclusive $(N+1)$-jet definition of the cross section; i.e., the cross section for $\mathcal{T}_{N+1} < \mathcal{T}^{\mathrm{cut}}_{N+1}$ after showering has to remain accurate to NLO_{N+1}+LL. Since the parton shower preserves the total cross section, this means it is only allowed to fill out the region $0 < \mathcal{T}_{N+1} < \mathcal{T}^{\mathrm{cut}}_{N+1}$. [The cross section for $\mathcal{T}_{N+1}(\Phi_{N+2}) > \mathcal{T}^{\mathrm{cut}}_{N+1}$ is already included in the inclusive $(N+2)$-jet sample generated from $\mathrm{d}\sigma^{\mathrm{MC}}_{\geq N+2}(\mathcal{T}_N > \mathcal{T}^{\mathrm{cut}}_N, \mathcal{T}_{N+1} > \mathcal{T}^{\mathrm{cut}}_{N+1})$.]

At LL accuracy, this is achieved by vetoing shower emissions with $\mathcal{T} > \mathcal{T}^{\mathrm{cut}}_{N+1}$, as discussed in section 2.5.1. In addition, to satisfy condition 2, it is also necessary that the cross section for $\mathcal{T}_{N+1} < \mathcal{T}^{\mathrm{cut}}_{N+1}$ remains correct to NLO_{N+1}. The veto on single emissions with $\mathcal{T} > \mathcal{T}^{\mathrm{cut}}_{N+1}$ is sufficient for this purpose as well, so we do not require an additional constraint on the shower. To see this, consider the shower emission with the largest value of $\mathcal{T}$, and sum over all other emissions. Strictly speaking, we need the emission to satisfy $\mathcal{T}_{N+1}[\hat{\Phi}_{N+2}(\Phi_{N+1}, \Phi_{\mathrm{rad}})] < \mathcal{T}^{\mathrm{cut}}_{N+1}$, where Φ_{rad} is the emission phase space and $\hat{\Phi}_{N+2}$ is the inverse of the phase space projection $\hat{\Phi}_{N+1}(\Phi_{N+2})$ that is used in the NLO_{N+1} calculation. The single-emission veto in the shower corresponds to imposing the constraint $\mathcal{T} \equiv \mathcal{T}_{N+1}[\hat{\Phi}^{\mathrm{PS}}_{N+2}(\Phi_{N+1}, \Phi_{\mathrm{rad}})] < \mathcal{T}^{\mathrm{cut}}_{N+1}$, where $\hat{\Phi}^{\mathrm{PS}}_{N+2}$ is the phase space map used in the parton shower. In principle, the two constraints can be different since the two phase space maps can be different. However, both maps have to be IR safe and must agree in the IR limit $\mathcal{T}^{\mathrm{cut}}_{N+1} \to 0$. Therefore, the difference can be at most a power correction in $\mathcal{T}^{\mathrm{cut}}_{N+1}$.

From this discussion, it follows that a generic $(N+1)$-jet observable receives at most power corrections from showering of $\mathcal{O}(\alpha_s \mathcal{T}^{\mathrm{cut}}_{N+1}/\mathcal{T}^{\mathrm{eff}}_{N+1})$, where $\mathcal{T}^{\mathrm{eff}}_{N+1}$ is the effective scale that the observable is sensitive to. Similarly, since $\mathrm{d}\sigma^{\mathrm{MC}}_{\geq N+1}$ contributes at $\mathcal{O}(\alpha_s)$ to generic N-jet observables, they receive at most power corrections of $\mathcal{O}(\alpha_s^2 \mathcal{T}^{\mathrm{cut}}_{N+1}/\mathcal{T}^{\mathrm{eff}}_{N+1})$. Hence, condition 2 is satisfied. In fact, as long as the $\mathcal{T}^{\mathrm{cut}}_{N+1}$ value is kept small, the spectrum for $\mathcal{T}_{N+1} < \mathcal{T}^{\mathrm{cut}}_{N+1}$ is correctly described by the shower. The parton shower therefore improves the description of the previously unresolved region $\mathcal{T}_{N+1} < \mathcal{T}^{\mathrm{cut}}_{N+1}$. As a result, the power corrections induced by the shower actually compensate for the power corrections in the partonic calculation arising from the unresolved region below $\mathcal{T}^{\mathrm{cut}}_{N+1}$. Of course, this is only true if the shower cutoff is lower than $\mathcal{T}^{\mathrm{cut}}_{N+1}$.

2.5.2.3 Showering the N-jet event sample

The MC cross section $\mathrm{d}\sigma_N^{\mathrm{MC}}(\mathcal{T}_N^{\mathrm{cut}})$ of the NNLO+LL calculation is given in eq. (2.37) or eq. (2.40). It contains the integrated cross section for $\mathcal{T}_N < \mathcal{T}_N^{\mathrm{cut}}$ calculated to NNLO$_N$+LL, which before showering, is represented by N-parton events with $\mathcal{T}_N = 0$.

The basic considerations here are similar as for the $(N+1)$-jet case. Repeating the discussion in section 2.5.2.2, the shower must be constrained not to change the cross section for $\mathcal{T}_N < \mathcal{T}_N^{\mathrm{cut}}$, but only to fill out the $\mathcal{T}_N$ spectrum below $\mathcal{T}_N^{\mathrm{cut}}$. Since the action of the parton shower is entirely within the N-jet cumulant bin, the induced power corrections of $\mathcal{O}(\alpha_s \mathcal{T}_N^{\mathrm{cut}}/\mathcal{T}_N^{\mathrm{eff}})$ are again at the level allowed by condition 2 and will actually improve the prediction of observables, because the unshowered events at $\mathcal{T}_N = 0$ are distributed over the previously unresolved region $\mathcal{T}_N < \mathcal{T}_N^{\mathrm{cut}}$ with an LL-accurate shape.

There is a further complication, however, that arises starting at NNLO. At NLO+LL, the resolution variable must have two properties: it must realize an IR-safe separation of the phase space at the level of a single emission, and it must have an LL resummation. Because LL resummation arises from exponentiating independent emissions, these two properties are essentially one and the same. For example, in an NLO+LL calculation of vector boson production, the resolution variable separating events with 0 jets and 1 jet can be chosen as the transverse momentum of the leading parton, with 0-jet events corresponding to $p_T < p_T^{\mathrm{cut}}$ and 1-jet events corresponding to $p_T > p_T^{\mathrm{cut}}$. At NNLO+LL, however, the story is different: defining the jet resolution variable analogous to the shower evolution in terms of independent single-parton variables is no longer sufficient to also ensure the IR safety of the NNLO 0-jet cross section. To see how the problem arises, it is instructive to consider again the example of vector boson production with two emissions illustrated in figure 2.3. Demanding that the transverse momentum of each emitted parton is below p_T^{cut} (dashed lines) does not yield an IR-safe definition for the 0-jet cross section. If the two partons are collinear to each other and each satisfies $p_T^{(i)} < p_T^{\mathrm{cut}}$, while their sum gives $p_T^{(1)} + p_T^{(2)} > p_T^{\mathrm{cut}}$, this IR-divergent contribution would be included in the 0-jet cross section, while the corresponding IR-divergent virtual diagram on the right would contribute to the 1-jet cross section. As already discussed in section 2.2.1, we must use a resolution variable which is properly IR-safe at NNLO. For example, we can sum over all emissions ($\mathcal{T}_N = \sum p_T$) or combine them using an IR-safe jet-clustering procedure ($\mathcal{T}_N = p_T^{\mathrm{jet}}$).

From this discussion, it is clear that the constraint $\mathcal{T}_N < \mathcal{T}_N^{\mathrm{cut}}$ that the parton shower needs to satisfy cannot be formulated in terms of individual emissions but must take at least two emissions into account. Generally, it is not sufficient to only consider the two hardest emissions, since they do not necessarily correspond to the hardest jet of the NNLO calculation. Therefore, the NNLO constraint can only be imposed via a global veto after the showering. In case one uses a vetoed shower with a single-emission local veto to enforce the LL constraints as described in section 2.5.1,

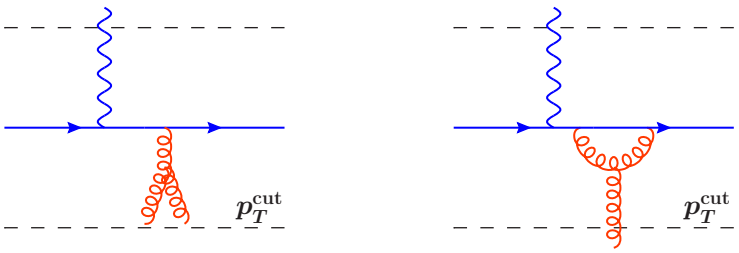

Figure 2.3: Illustration of the issues in defining an IR-safe phase space separation at NNLO using single-parton variables in the case of vector boson production. Limiting each emission to be below p_T^{cut} (dashed lines) results in a miscancellation of IR divergences between the tree-level contribution on the left, which would contribute to $\mathrm{d}\sigma_0^{\text{MC}}(p_T^{\text{cut}})$, and the corresponding one-loop contribution on the right, which would contribute to $\mathrm{d}\sigma_{\geq 1}^{\text{MC}}(p_T > p_T^{\text{cut}})$.

the additional NNLO constraint should be enforced separately.

2.6 Implementation and relation to existing approaches

In this section, we discuss the relation of our framework to recent related work and the NNLO+PS implementation given in ref. [43]. This will show that our method is indeed quite general and encompasses these other approaches. It also illustrates that an actual implementation of our results is indeed feasible.

2.6.1 GENEVA

The motivation to build an NNLO+LL event generator is to interface the most precise FO calculations available with a parton shower routine to be able to simulate realistic events with high perturbative accuracy. Whenever higher logarithmic resummation is also available (NLL for several resolution variables, NNLL for certain resolution variables such as N-jettiness, and NNLL$'$ for select processes[10]), it can be implemented to also improve the perturbative accuracy in the resummation region (see figure 2.2) following the GENEVA approach. The GENEVA approach is detailed in chapter 3, but we provide a brief discussion here to show the connection.

If NNLL$'$ resummation is available, the resummation order matches the fixed NNLO accuracy in the sense that all NNLO singular terms are naturally included in

[10]While NNLL resummation includes all logarithmic terms through NNLO, NNLL$'$ also includes delta function terms to capture all NNLO singular terms including the 2-loop virtual corrections.

the resummation. Hence, the FO singular matching correction vanishes,

$$\frac{\mathrm{d}\sigma_N^{C-S}}{\mathrm{d}\Phi_N}(\mathcal{T}_N^{\mathrm{cut}}) = 0\,, \tag{2.67}$$

because the FO expansion of the NNLL′ resummed result reproduces the full NNLO singular corrections. The remaining contributions in the N-jet MC cross section can then be associated as follows:

$$\begin{aligned} \frac{\mathrm{d}\sigma_{\geq N}^{C}}{\mathrm{d}\Phi_N}\,\Delta_N(\Phi_N;\mathcal{T}_N^{\mathrm{cut}}) \quad &\to \quad \frac{\mathrm{d}\sigma_N^{\mathrm{resummed}}}{\mathrm{d}\Phi_N}(\mathcal{T}_N^{\mathrm{cut}})\,, \\ \frac{\mathrm{d}\sigma_N^{B-C}}{\mathrm{d}\Phi_N}(\mathcal{T}_N^{\mathrm{cut}}) \quad &\to \quad \frac{\mathrm{d}\sigma_N^{\mathrm{nonsingular}}}{\mathrm{d}\Phi_N}(\mathcal{T}_N^{\mathrm{cut}})\,. \end{aligned} \tag{2.68}$$

That is, the cross section takes the form of a traditional resummed calculation, with the FO nonsingular corrections corresponding to $\mathrm{d}\sigma_N^{B-C}$ and the higher-order resummed cumulant replacing the resummation term $\mathrm{d}\sigma_{\geq N}^{C}\Delta_N(\mathcal{T}_N^{\mathrm{cut}})$. The same relations also apply for the exclusive $(N+1)$-jet and inclusive $(N+2)$-jet cross sections.

The results in chapter 3 take this approach, using a jet resolution variable $\mathcal{T}_2$ for which higher-order logarithmic resummation is available. There, the NNLL′ resummation for $e^+e^- \to$ jets for small $\mathcal{T}_2$ are used together with the NLO_2 nonsingular terms, combined with the fully differential 3-jet cross section at NLO_3, and interfaced with a parton shower algorithm. As discussed above, the resummation to NNLL′ already incorporates the full singular contributions up to NNLO, including the two-loop virtual corrections. Thus, the only missing contributions to make the calculation in chapter 3 correct to full NNLO_2 are the nonsingular corrections at NNLO_2. Since they scale as a power correction in $\mathcal{T}_2^{\mathrm{cut}}$, one could also take the value of $\mathcal{T}_2^{\mathrm{cut}}$ small enough to make their numerical impact small.

2.6.2 NNLO+PS using HJ-MiNLO

Results combining the inclusive NNLO Higgs cross section with a parton shower algorithm were presented recently in ref. [43]. This approach uses the Multi-Scale Improved NLO (MiNLO) calculation for the production of Higgs in association with a jet [56], in which the Powheg HJ calculation [57] is supplemented by an analytic Sudakov resummation factor, which includes logarithmic terms that become large as the transverse momentum of the Higgs boson tends to zero. The Sudakov factor effectively regulates the divergences in the Powheg HJ calculation when the transverse momentum of the Higgs boson, q_T, goes to zero. As a result, the HJ-MiNLO sample can be used over the whole phase space even in the limit $q_T \to 0$. In practice, it is used down to q_T of order $\Lambda_{\mathrm{QCD}} \sim 1\,\mathrm{GeV}$.

It was shown in ref. [38] that by explicitly including NNLL information in the Sudakov factor, the HJ-MiNLO cross section integrates up to the correct inclusive

Higgs cross section at NLO_0. The HJ-MiNLO sample is then reweighted to the differential NNLO_0 Higgs cross section, which is facilitated by the fact that it is only singly differential in the Higgs rapidity. This provides NNLO_0 accurate predictions for 0-jet observables without spoiling the NLO_1 accuracy of 1-jet observables. One feature of this approach is that it does not require a Higgs + 0-jet sample, since the full NNLO_0 information of inclusive Higgs production is explicitly included through the reweighting factor.

While this approach seems at first sight quite different from the discussion in the present chapter, we will now show that it directly follows as a special case from our results in section 2.4. Hence, it can be viewed as a specific implementation of the general method developed in this chapter. We first write the results of ref. [43] in terms of the MC cross sections $\mathrm{d}\sigma_0^{\text{MC}}(\mathcal{T}_0^{\text{cut}})$ and $\mathrm{d}\sigma_{\geq 1}^{\text{MC}}(\mathcal{T}_0 > \mathcal{T}_0^{\text{cut}})$, corresponding to the exclusive Higgs + 0-jet and inclusive Higgs + 1-jet cross sections. We then show how these expressions follow directly from our general results by making specific choices.

The 0-jet resolution variable used in ref. [43] to separate 0 from 1 or more extra jets is the transverse momentum of the Higgs boson, so

$$\mathcal{T}_0 \equiv q_T \,. \tag{2.69}$$

We do not need to discuss how to separate the inclusive 1-jet sample into an exclusive 1-jet and an inclusive 2-jet sample. For this purpose, ref. [43] uses the standard Powheg approach, which we have already shown in section 2.3.3 to be a special case of our approach.

As mentioned already, the Higgs + 0-jet cross section is not included in ref. [43], since it vanishes in the limit $\mathcal{T}_0^{\text{cut}} \to 0$. The inclusive MC cross section for one or more jets is then given by

$$\frac{\mathrm{d}\sigma_{\geq 1}^{\text{ref. [43]}}}{\mathrm{d}\Phi_1}(\mathcal{T}_0 > \mathcal{T}_0^{\text{cut}}) = \widetilde{R}(\Phi_0; \mathcal{T}_0^{\text{cut}}) \, \frac{\mathrm{d}\sigma_{\geq 1}^{\text{HJ-MiNLO}}}{\mathrm{d}\Phi_1} \, \theta(\mathcal{T}_0 > \mathcal{T}_0^{\text{cut}}) \,. \tag{2.70}$$

Here, the inclusive 1-jet cross section, $\mathrm{d}\sigma_{\geq 1}^{\text{HJ-MiNLO}}$, is equivalent to the modified $\bar{B}$ function from HJ-MiNLO, which is obtained from the usual $\bar{B}$ function in Powheg by multiplying with the Sudakov factor $\widetilde{\Delta}_0(\mathcal{T}_0)$ and subtracting its first-order expansion to maintain the NLO_1 accuracy,

$$\frac{\mathrm{d}\sigma_{\geq 1}^{\text{HJ-MiNLO}}}{\mathrm{d}\Phi_1} = \left\{ B_1(\Phi_1)\big[1 - \widetilde{\Delta}_0^{(1)}(\hat{\Phi}_0; \mathcal{T}_0)\big] + V_1(\Phi_1) + \int \frac{\mathrm{d}\Phi_2}{\mathrm{d}\Phi_1} \, B_2(\Phi_2) \right\} \widetilde{\Delta}_0(\hat{\Phi}_0, \mathcal{T}_0) \,. \tag{2.71}$$

The term in curly brackets contains the full singular $\mathcal{T}_0$ dependence at NLO_1. The crucial ingredient [38] is the fact that the exponent of the Sudakov factor $\widetilde{\Delta}_0(\mathcal{T}_0)$ contains the full NNLL set of $\mathcal{T}_0$ logarithms to $\mathcal{O}(\alpha_s^2)$. This causes the spectrum to become the total derivative of the NLO_0-correct 0-jet cumulant, $\mathrm{d}\sigma_{\geq 0}^{\text{NLO}} \, \widetilde{\Delta}_0(\mathcal{T}_0^{\text{cut}})$, up to nonsingular corrections in $\mathcal{T}_0$ and higher orders in α_s. As a result, the spectrum

integrates to the correct NLO_0 cross section up to power corrections that vanish as $\mathcal{T}_0^{\text{cut}} \to 0$,

$$\int \frac{\mathrm{d}\Phi_1}{\mathrm{d}\Phi_0} \frac{\mathrm{d}\sigma_{\geq 1}^{\text{HJ-MiNLO}}}{\mathrm{d}\Phi_1} \theta(\mathcal{T}_0 > \mathcal{T}_0^{\text{cut}}) = \frac{\mathrm{d}\sigma_{\geq 0}^{\text{NLO}}}{\mathrm{d}\Phi_0} + \mathcal{O}(\alpha_s \mathcal{T}_0^{\text{cut}}) + \mathcal{O}(\alpha_s^2)\,. \tag{2.72}$$

The reweighting factor $\widetilde{R}(\Phi_0; \mathcal{T}_0^{\text{cut}})$ in eq. (2.70) is then given by the ratio

$$\widetilde{R}(\Phi_0; \mathcal{T}_0^{\text{cut}}) = \frac{\mathrm{d}\sigma_{\geq 0}^{\text{NNLO}}}{\mathrm{d}\Phi_0} \Bigg/ \int \frac{\mathrm{d}\Phi_1}{\mathrm{d}\Phi_0} \frac{\mathrm{d}\sigma_{\geq 1}^{\text{HJ-MiNLO}}}{\mathrm{d}\Phi_1} \theta(\mathcal{T}_0 > \mathcal{T}_0^{\text{cut}})\,, \tag{2.73}$$

and by construction, ensures that the Higgs + 1-jet spectrum in eq. (2.70) integrates to the correct NNLO_0 inclusive Higgs cross section. At the same time, because of eq. (2.72), the reweighting factor has the form

$$\widetilde{R}(\Phi_0; \mathcal{T}_0) = 1 + \mathcal{O}(\alpha_s \mathcal{T}_0^{\text{cut}}) + \mathcal{O}(\alpha_s^2)\,, \tag{2.74}$$

and therefore does not affect the NLO_1 accuracy of the inclusive 1-jet cross section up to power corrections in $\mathcal{T}_0^{\text{cut}}$. By taking $\mathcal{T}_0^{\text{cut}} \to \Lambda_{\text{QCD}}$, these become negligible, and the result becomes a valid NNLO+LL implementation.

To derive this result as a special case of our framework, we make the following two choices:

1. Choose all singular terms equal to the exact tree-level and one-loop contributions,

$$C_1(\Phi_1) = B_1(\Phi_1)\,, \qquad C_2(\Phi_2) = B_2(\Phi_2)\,, \qquad VC_1(\Phi_1) = V_1(\Phi_1)\,. \tag{2.75}$$

2. Choose the splitting functions as

$$\begin{aligned} S_1^{(1)}(\Phi_1) &= B_1(\Phi_1)\,, \\ S_1^{(2)}(\Phi_1) &= V_1(\Phi_1) + \int \frac{\mathrm{d}\Phi_2}{\mathrm{d}\Phi_1} B_2(\Phi_2) - B_1(\Phi_1) \left[\frac{V_0^C(\hat{\Phi}_0)}{B_0(\hat{\Phi}_0)} + \Delta_0^{(1)}(\hat{\Phi}_0; \mathcal{T}_0) \right]. \end{aligned} \tag{2.76}$$

With these two choices, the singular inclusive cross section defined in eq. (2.47) is given by the full NNLO_0 expression,

$$\frac{\mathrm{d}\sigma_{\geq 0}^{C}}{\mathrm{d}\Phi_0} = \frac{\mathrm{d}\sigma_{\geq 0}^{\text{NNLO}}}{\mathrm{d}\Phi_0}\,, \tag{2.77}$$

while all FO matching corrections vanish,

$$\frac{\mathrm{d}\sigma_0^{C-S}}{\mathrm{d}\Phi_0}(\mathcal{T}_0^{\text{cut}}) = \frac{\mathrm{d}\sigma_0^{B-C}}{\mathrm{d}\Phi_0}(\mathcal{T}_0^{\text{cut}}) = 0\,, \quad \frac{\mathrm{d}\sigma_{\geq 1}^{C-S}}{\mathrm{d}\Phi_1}(\mathcal{T}_0 > \mathcal{T}_0^{\text{cut}}) = \frac{\mathrm{d}\sigma_{\geq 1}^{B-C}}{\mathrm{d}\Phi_1}(\mathcal{T}_0 > \mathcal{T}_0^{\text{cut}}) = 0\,. \tag{2.78}$$

The choice of the splitting function $S_2(\Phi_2)$ is not relevant for this discussion since its purpose is to determine how to split the inclusive 1-jet cross section into an exclusive 1-jet and an inclusive 2-jet cross section.

Using the results of section 2.4.1.1 (or section 2.4.1.2, which are identical in this case), we then find for the exclusive 0-jet and inclusive 1-jet MC cross sections

$$\begin{aligned}
\frac{\mathrm{d}\sigma_0^{\mathrm{MC}}}{\mathrm{d}\Phi_0}(\mathcal{T}_0^{\mathrm{cut}}) &= \frac{\mathrm{d}\sigma_{\geq 0}^{\mathrm{NNLO}}}{\mathrm{d}\Phi_0}\,\Delta_0(\Phi_0;\mathcal{T}_0^{\mathrm{cut}})\,,\\
\frac{\mathrm{d}\sigma_{\geq 1}^{\mathrm{MC}}}{\mathrm{d}\Phi_1}(\mathcal{T}_0 > \mathcal{T}_0^{\mathrm{cut}}) &= \frac{\mathrm{d}\sigma_{\geq 0}^{\mathrm{NNLO}}}{\mathrm{d}\Phi_0}\bigg|_{\Phi_0=\hat{\Phi}_0}\frac{S_1(\Phi_1)}{B_0(\hat{\Phi}_0)}\,\Delta_0(\hat{\Phi}_0;\mathcal{T}_0)\,\theta(\mathcal{T}_0 > \mathcal{T}_0^{\mathrm{cut}})\\
&= \frac{\mathrm{d}\sigma_{\geq 0}^{\mathrm{NNLO}}}{\mathrm{d}\Phi_0}\bigg|_{\Phi_0=\hat{\Phi}_0}\frac{1}{B_0(\hat{\Phi}_0)}\bigg\{B_1(\Phi_1)\bigg[1-\Delta_0^{(1)}(\hat{\Phi}_0;\mathcal{T}_0)-\frac{V_0^C(\hat{\Phi}_0)}{B_0(\hat{\Phi}_0)}\bigg]\\
&\quad + V_1(\Phi_1) + \int\frac{\mathrm{d}\Phi_2}{\mathrm{d}\Phi_1}\,B_2(\Phi_2)\bigg\}\,\Delta_0(\hat{\Phi}_0;\mathcal{T}_0)\,\theta(\mathcal{T}_0 > \mathcal{T}_0^{\mathrm{cut}})\,, \qquad (2.79)
\end{aligned}$$

where in the last equation, we inserted the explicit expression for $S_1(\Phi_1)$ from eq. (2.76). We can now compare this to the HJ-MiNLO result in eq. (2.70). Since the exclusive 0-jet cross section is proportional to the Sudakov factor $\Delta_0(\Phi_0;\mathcal{T}_0^{\mathrm{cut}})$, it vanishes in the limit $\mathcal{T}_0^{\mathrm{cut}} \to 0$. Thus, in this limit, the entire 0-jet cross section can be obtained by integrating the inclusive 1-jet result over all values of $\mathcal{T}_0$, precisely analogous to what happens in refs. [38, 43]. Since in practice, $\mathcal{T}_0^{\mathrm{cut}} \sim \Lambda_{\mathrm{QCD}} \sim 1\,\mathrm{GeV}$, one could also keep the 0-jet cumulant, which would avoid introducing any additional power corrections in $\mathcal{T}_0^{\mathrm{cut}}$. The term in curly brackets times the Sudakov factor $\Delta_0(\hat{\Phi}_0;\mathcal{T}_0)$ is equivalent to $\mathrm{d}\sigma_{\geq 1}^{\text{HJ-MiNLO}}/\mathrm{d}\Phi_1$ in eq. (2.71), except for the additional $V_0^C(\hat{\Phi}_0)$ term. By including this term, the prefactor in $\mathrm{d}\sigma_{\geq 1}^{\mathrm{MC}}$ becomes simply the inclusive NNLO cross section normalized to the tree-level result, $\mathrm{d}\sigma_{\geq 0}^{\mathrm{NNLO}}/B_0(\Phi_0)$, without any need to reweight the events.

With the choice $C_1(\Phi_1) = B_1(\Phi_1)$ from above, $V_0^C(\Phi_0)$ is the NLO correction to the inclusive cross section [see eq. (2.54)],

$$\frac{\mathrm{d}\sigma_{\geq 0}^{\mathrm{NLO}}}{\mathrm{d}\Phi_0} = B_0(\Phi_0) + V_0^C(\Phi_0)\,, \qquad (2.80)$$

and is in particular $\mathcal{T}_0$ independent. Although in principle there is no need to do so, we can rewrite $\mathrm{d}\sigma_{\geq 1}^{\mathrm{MC}}$ and pull this term outside into the prefactor, which gives

$$\begin{aligned}
\frac{\mathrm{d}\sigma_{\geq 1}^{\mathrm{MC}}}{\mathrm{d}\Phi_1}(\mathcal{T}_0 > \mathcal{T}_0^{\mathrm{cut}}) &= R(\hat{\Phi}_0)\bigg\{B_1(\Phi_1)\big[1-\Delta_0^{(1)}(\hat{\Phi}_0;\mathcal{T}_0)\big] + V_1(\Phi_1) + \int\frac{\mathrm{d}\Phi_2}{\mathrm{d}\Phi_1}\,B_2(\Phi_2)\bigg\}\\
&\quad\times\ \Delta_0(\hat{\Phi}_0;\mathcal{T}_0)\,\theta(\mathcal{T}_0 > \mathcal{T}_0^{\mathrm{cut}})\,, \qquad (2.81)
\end{aligned}$$

with the rescaling factor

$$R(\Phi_0) = \frac{\mathrm{d}\sigma_{\geq 0}^{\mathrm{NNLO}}}{\mathrm{d}\Phi_0}\bigg/\bigg\{\frac{\mathrm{d}\sigma_{\geq 0}^{\mathrm{NLO}}}{\mathrm{d}\Phi_0} - \frac{V_0^C(\Phi_0)}{B_0(\Phi_0)}\int\frac{\mathrm{d}\Phi_1}{\mathrm{d}\Phi_0}\,S_1^{(2)}(\Phi_1)\,\Delta_0(\Phi_0,\mathcal{T}_0)\bigg\}\,. \qquad (2.82)$$

The last term in the denominator here is the $\mathcal{O}(\alpha_s^3)$ cross term that arises from pulling $V_0^C(\Phi_0)$ out into the rescaling factor. It must be kept because it scales as $\alpha_s^3(\ln \mathcal{T}_0)/\mathcal{T}_0$, which upon integration over $\mathcal{T}_0$, becomes an α_s^2 correction. Equations (2.81) and (2.82) are now the exact equivalent of the expressions in eqs. (2.70), (2.71), and (2.73). By writing the factor in curly brackets in eq. (2.81) as $S_1(1+V_0^C/B_0)-(V_0^C/B_0)S_1^{(2)}$, one can easily check that the denominator in eq. (2.82) is exactly the integral of eq. (2.81) modulo the $R(\Phi_0)$ prefactor.

As we have seen, with the two choices given above, our method gives an expression with an analogous structure as in ref. [43]. In fact, the result in eq. (2.79) that follows immediately from our approach is automatically correct to NNLO_0 without requiring an additional reweighting. Another difference is the precise form of the Sudakov factors, $\Delta_0(\Phi_0;\mathcal{T}_0)$ and $\widetilde{\Delta}_0(\Phi_0;\mathcal{T}_0)$. In our approach, Δ_0 is constructed from the splitting functions $S_1^{(i)}(\Phi_1)$, while in ref. [38], $\widetilde{\Delta}_0$ is obtained from the analytic q_T NNLL resummation formula. Both expressions have the same logarithmic dependence on $\mathcal{T}_0$ expanded to $\mathcal{O}(\alpha_s^2)$ in the exponent. We also point out that, in the approach of refs. [38, 43], the known NNLL structure of the $\mathcal{T}_0 = q_T$ spectrum is essential to analytically control all singular logarithms through $\mathcal{O}(\alpha_s^2)$. In this respect, this approach is closely related to the GENEVA approach [46] discussed in chapter 3 and section 2.6.1.

2.6.3 UNLOPS

In section 2.4, we have explicitly constructed the required exclusive N-jet and $(N+1)$-jet MC cross sections to satisfy all the requirements to obtain a correct NNLO+LL event sample discussed in section 2.3.1. Alternatively, one could also start from the inclusive FO+LL M-jet cross sections and generate the exclusive MC cross sections numerically,

$$\begin{aligned}
\frac{\mathrm{d}\sigma_N^{\text{MC}}}{\mathrm{d}\Phi_N}(\mathcal{T}_N^{\text{cut}}) &= \frac{\mathrm{d}\sigma_{\geq N}^{\text{MC}}}{\mathrm{d}\Phi_N} - \int \frac{\mathrm{d}\Phi_{N+1}}{\mathrm{d}\Phi_N}\,\frac{\mathrm{d}\sigma_{\geq N+1}^{\text{MC}}}{\mathrm{d}\Phi_N}(\mathcal{T}_N > \mathcal{T}_N^{\text{cut}})\,, \\
\frac{\mathrm{d}\sigma_{N+1}^{\text{MC}}}{\mathrm{d}\Phi_{N+1}}(\mathcal{T}_N > \mathcal{T}_N^{\text{cut}}; \mathcal{T}_{N+1}^{\text{cut}}) &= \frac{\mathrm{d}\sigma_{\geq N+1}^{\text{MC}}}{\mathrm{d}\Phi_{N+1}}(\mathcal{T}_N > \mathcal{T}_N^{\text{cut}}) \\
&\quad - \int \frac{\mathrm{d}\Phi_{N+2}}{\mathrm{d}\Phi_{N+2}}\,\frac{\mathrm{d}\sigma_{\geq N+2}^{\text{MC}}}{\mathrm{d}\Phi_{N+1}}(\mathcal{T}_N > \mathcal{T}_N^{\text{cut}}, \mathcal{T}_{N+1} > \mathcal{T}_{N+1}^{\text{cut}})\,. \quad (2.83)
\end{aligned}$$

This method has been applied to merge multiple NLO+LL calculations in refs. [47, 37, 58], where it is referred to as UNLOPS.

Using eq. (2.83), the consistency conditions in eqs. (2.20) and (2.21) between different multiplicities is automatically enforced. The inclusive MC cross sections that are used as inputs must be correct at the relevant FO+LL accuracy according to eq. (2.19). For $\mathrm{d}\sigma_{\geq N}^{\text{MC}}$, this means it has to be correct to NNLO_N, so it is simply

given by the inclusive NNLO_N cross section,

$$\frac{\mathrm{d}\sigma^{\text{MC}}_{\geq N}}{\mathrm{d}\Phi_N} = \frac{\mathrm{d}\sigma^{\text{NNLO}}_{\geq N}}{\mathrm{d}\Phi_N}\,. \tag{2.84}$$

The inclusive $(N+1)$-jet cross section must be correct to NLO_{N+1} with the $\mathcal{T}_N$ dependence resummed to LL, and the inclusive $(N+2)$-jet cross section must be correct to LO_{N+2} with the dependence on both $\mathcal{T}_N$ and $\mathcal{T}_{N+1}$ resummed to LL, for which our general results in section 2.4 [see eqs. (2.42) and (2.61)] can be used.

The major drawback of subtracting the integrals over the inclusive cross sections in eq. (2.83) numerically is that one has to generate events with negative weights. The advantage is that the expressions for the inclusive cross sections can be simplified substantially by dropping all higher-order dependence inherited from lower multiplicities. For the inclusive $(N+1)$-jet cross section, one could then use, for example,

$$\begin{aligned}\frac{\mathrm{d}\sigma^{\text{MC}}_{\geq N+1}}{\mathrm{d}\Phi_{N+1}}(\mathcal{T}_N > \mathcal{T}_N^{\text{cut}}) = \Bigg[&\frac{\mathrm{d}\sigma^{\text{NLO}}_{\geq N+1}}{\mathrm{d}\Phi_{N+1}}(\mathcal{T}_N > \mathcal{T}_N^{\text{cut}}) \\ &- B_{N+1}(\Phi_{N+1})\,\Delta_N^{(1)}(\hat{\Phi}_N;\mathcal{T}_N)\,\theta(\mathcal{T}_N > \mathcal{T}_N^{\text{cut}})\Bigg] \times \Delta_N(\hat{\Phi}_N;\mathcal{T}_N)\,,\end{aligned} \tag{2.85}$$

which includes the correct LL resummation and expands to the correct NLO_{N+1} result. One could also have written this result using a singular approximation to the inclusive cross section and added an FO matching correction, or only have the Born-level result multiply the Sudakov factors, and then add all higher-order terms in the FO matching correction. This last choice corresponds to what is done in refs. [58, 47, 37]. For the inclusive $(N+2)$-jet MC cross section, one could use the equivalent of the CKKW result,

$$\begin{aligned}\frac{\mathrm{d}\sigma^{\text{MC}}_{\geq N+2}}{\mathrm{d}\Phi_{N+2}}(\mathcal{T}_N > \mathcal{T}_N^{\text{cut}}, \mathcal{T}_{N+1} > \mathcal{T}_{N+1}^{\text{cut}}) = {}& B_{N+2}(\Phi_{N+2})\,\theta(\mathcal{T}_N > \mathcal{T}_N^{\text{cut}})\,\theta(\mathcal{T}_{N+1} > \mathcal{T}_{N+1}^{\text{cut}}) \\ &\times \Delta_N(\hat{\Phi}_N;\mathcal{T}_N)\,\Delta_{N+1}(\hat{\Phi}_{N+1};\mathcal{T}_{N+1})\,.\end{aligned} \tag{2.86}$$

2.7 Conclusions

In this chapter, we have developed a general method to combine fully differential NNLO calculations with LL resummation in the form of an event generator for physical events that can be directly interfaced with a parton shower. The basic quantities in our construction are Monte Carlo (MC) cross sections

$$\frac{\mathrm{d}\sigma^{\text{MC}}_{N}}{\mathrm{d}\Phi_N}(\mathcal{T}_N^{\text{cut}})\,, \quad \frac{\mathrm{d}\sigma^{\text{MC}}_{N+1}}{\mathrm{d}\Phi_{N+1}}(\mathcal{T}_N > \mathcal{T}_N^{\text{cut}};\mathcal{T}_{N+1}^{\text{cut}})\,, \quad \frac{\mathrm{d}\sigma^{\text{MC}}_{\geq N+2}}{\mathrm{d}\Phi_{N+2}}(\mathcal{T}_N > \mathcal{T}_N^{\text{cut}}, \mathcal{T}_{N+1} > \mathcal{T}_{N+1}^{\text{cut}})\,, \tag{2.87}$$

representing an exclusive partonic N-jet cross section, calculated to NNLO$_N$+LL; an exclusive partonic $(N+1)$-jet cross section, calculated to NLO$_{N+1}$+LL; and an inclusive partonic $(N+2)$-jet cross section, calculated to LO$_{N+2}$+LL. We use N^{n}LL$_M$ to refer to the $\mathcal{O}(\alpha_s^n)$ result relative to an M-parton tree-level result. These MC cross sections are represented in the generator by events with N, $N+1$, and $N+2$ partons. They are characterized by N-jet and $(N+1)$-jet resolution variables $\mathcal{T}_N$ and $\mathcal{T}_{N+1}$, with resolution scales $\mathcal{T}_N^{\text{cut}}$ and $\mathcal{T}_{N+1}^{\text{cut}}$ defining the separation between them. We stress that these are not jet-merging scales but IR cutoffs equivalent to a parton shower cutoff.

We have formulated the general conditions on the perturbative accuracy that a complete and fully differential NNLO+LL calculation must satisfy. They require that the MC cross sections must have the correct FO expansion (NNLO$_N$ for $\mathrm{d}\sigma_N^{\text{MC}}$, NLO$_{N+1}$ for $\mathrm{d}\sigma_{N+1}^{\text{MC}}$, and LO$_{N+2}$ for $\mathrm{d}\sigma_{\geq N+2}^{\text{MC}}$), as well as include the LL resummation of the resolution variables and scales ($\mathcal{T}_N^{\text{cut}}$ for $\mathrm{d}\sigma_N^{\text{MC}}$, $\mathcal{T}_N$ and $\mathcal{T}_{N+1}^{\text{cut}}$ for $\mathrm{d}\sigma_{N+1}^{\text{MC}}$, and $\mathcal{T}_N$ and $\mathcal{T}_{N+1}$ for $\mathrm{d}\sigma_{\geq N+2}^{\text{MC}}$). In addition, the consistent combination of FO and LL requires that all observables that are expected to be correctly predicted at $\mathcal{O}(\alpha_s^n)$ at fixed order must be independent of the resolution scales $\mathcal{T}_N^{\text{cut}}$ and $\mathcal{T}_{N+1}^{\text{cut}}$ up to residual corrections of $\mathcal{O}_{\text{cut}}(\alpha_s^{\geq n+1})$ [using the LL counting in eq. (2.16)] to maintain their expected perturbative accuracy. We have shown that this can be achieved in general by enforcing a derivative relationship between M-jet exclusive and $(M+1)$-jet inclusive cross sections.

Our main results are given in section 2.4, where we derive in detail the MC cross sections needed to construct the NNLO+LL event generator. The MC cross sections are explicitly given in terms of the constituent matrix elements used in FO calculations and the parton shower. Our results are general, and we make no choices about the techniques used to evaluate the FO contributions in the MC cross sections. The primary and only NNLO ingredients that are required are a singular approximation of the inclusive NNLO N-jet cross section, $\mathrm{d}\sigma_{\geq N}^{C}$, and the corresponding NNLO subtractions, both of which are naturally part of existing NNLO calculations. All other ingredients are NLO in nature and therefore obtainable as in existing NLO+LL implementations. We proved that our construction explicitly satisfies all required conditions on the perturbative accuracy of an NNLO+LL event generator.

We have discussed how the partonic NNLO+LL event generator can be interfaced with standard parton showers using existing technologies, as well as the constraints that must be placed on the parton shower routine. This matching must preserve the FO and LL accuracy of the MC partonic jet cross sections, and the parton shower will provide LL accuracy for general N-jet, $(N+1)$-jet, and $(N+2)$-jet observables, producing events at all parton multiplicities. For the $(N+1)$-jet and $(N+2)$-jet samples, which are needed to NLO$_{N+1}$+LL and LO$_{N+2}$+LL accuracy respectively, the constraints are essentially the same as for the well-known case of NLO+PS matching. For the showering of the exclusive N-jet sample, which is needed at NNLO$_N$+LL accuracy, we showed that the constraints on the parton shower cannot be implemented

at the level of individual emissions as was possible for the other multiplicities. However, a global veto on the parton shower can still be used in this case. Alternatively, if the shower evolution variable coincides with the $\mathcal{T}_N$ and $\mathcal{T}_{N+1}$ resummation variables, the resolution scales $\mathcal{T}_N^{\text{cut}}$ and $\mathcal{T}_{N+1}^{\text{cut}}$ can be set equal to the parton shower cutoff itself, in which case only the inclusive $(N+2)$-jet sample must be showered.

Finally, we have discussed how other methods for matching higher-order perturbative calculations with parton showers fit into our general framework. For the well-known case of NLO+LL matching, the POWHEG and MC@NLO approaches naturally follow as special cases. When employing the higher-order resummation at NNLL$'$ as in GENEVA, the only missing ingredients to achieve full NNLO accuracy are power-suppressed nonsingular contributions. We have also shown explicitly how the recent results for NNLO+PS using HJ-MiNLO arise as a special case from our general results. We also commented how the ideas of UNLOPS fit into our method.

Our results provide a path for combining the precision frontier of fixed-order calculations with the flexibility and versatility of parton shower Monte Carlo programs. There are various steps that should be taken next toward a practical implementation. While the comparison to existing approaches makes it clear that the implementation is feasible, it remains to be seen what the optimal choices are to make the implementation sufficiently generic so that new NNLO calculations can be incorporated with limited effort. Finally, it should be clear from our discussion that our general setup not only applies to NNLO calculations, but can also be extended to even higher order, should such results become available, though the details remain to be worked out in this case.

Chapter 3

Combining higher-order resummation with multiple NLO calculations and parton showers in GENEVA[1]

3.1 Introduction

As we emphasized in chapter 1, accurate and reliable theoretical predictions for measurements at collider experiments require the inclusion of QCD effects beyond the lowest perturbative accuracy in every region of phase space. This includes higher-order corrections in α_s in some regions of phase space, all-orders resummation of logarithmically enhanced contributions in other regions, and a combination of both types of corrections in intermediate regions. In addition, for experimental analyses to benefit from these advances, it is crucial to provide the best possible theoretical predictions in the context of fully exclusive Monte Carlo event generators.

Given the necessity of higher-order perturbative corrections to make accurate predictions, it is important to extend the perturbative accuracy of the Monte Carlo description to formal $\mathcal{O}(\alpha_s)$ accuracy relative to the lowest order. This requires including the formally next higher-order corrections that are relevant at each scale. At small scales, i.e., small values of the jet resolution variable, this requires improving the LL parton shower resummation with higher-order logarithmic resummation, while at large scales this requires including the fully differential NLO matrix elements. It is important to realize that typically a large part of phase space, often including the experimentally relevant region, is characterized by intermediate scales, i.e., by a

[1]This chapter is a modified version of a paper originally co-written with Simone Alioli, Christian W. Bauer, Andrew Hornig, Frank J. Tackmann, Christopher K. Vermilion, Jonathan R. Walsh, and Saba Zuberi and published in [46].

transition from small to large scales. In the end, providing an accurate description of this transition region requires a careful combination of both types of corrections.

Such a Monte Carlo description at relative $\mathcal{O}(\alpha_s)$ accuracy across phase space was first achieved in GENEVA and is the subject of this chapter. (We briefly summarize the existing efforts to combine NLO corrections with parton showers in section 3.1.1 below.) The crucial starting point in our approach is that all perturbative inputs to the Monte Carlo are formulated in terms of well-defined physical jet cross sections [44, 45]. This allows us to systematically increase the perturbative accuracy by incorporating results for the relevant ingredients to the desired order in fixed-order and resummed perturbation theory.

An essential aspect of any higher-order prediction is a reliable estimate of its perturbative uncertainty due to neglected higher-order corrections. To the extent that parton shower Monte Carlos provide perturbative predictions, they should be held to the same standards. An important benefit in our approach is that we have explicit control of the perturbative uncertainties and are able to estimate reliable fixed-order and resummation uncertainties. As a result, in GENEVA each event comes with an estimate of its perturbative uncertainty; i.e., GENEVA provides event-by-event theory uncertainties.[2]

In our approach, the Monte Carlo not only benefits from the resummation, but in turn also provides important benefits to analytic resummed predictions. For one, it greatly facilitates the comparison with experimental data, as it allows easy application of arbitrary kinematic selection cuts, which can often be tedious to take into account in analytic predictions. More importantly, resummed predictions require nonperturbative inputs which can be treated as power corrections at intermediate scales but become $\mathcal{O}(1)$ corrections at very small scales. Here, these are provided "on-the-fly" by the nonperturbative hadronization model. In essence, we are able to combine the precision and theoretical control offered by higher-order resummed predictions with the versatility and flexibility offered by fully exclusive Monte Carlos.

In this chapter, we focus on the theoretical construction.[3] We will however highlight some of the main technical issues we had to overcome and discuss some implementation details in the application sections. In the remainder of this section, we briefly summarize the existing efforts to include NLO corrections in parton shower Monte Carlos and give a short overview of our basic construction. In section 3.2, we discuss in detail the requirements to obtain full α_s accuracy as well as our method to achieve it. In section 3.3, we discuss the application to $e^+e^- \to$ jets, where we combine next-to-next-to-leading logarithmic (NNLL) resummation with NLO matrix elements, and present results from the implementation in GENEVA together with a comparison to LEP measurements. In section 3.4, we discuss the application to hadronic collisions

[2]Further uncertainties, e.g. due to nonperturbative effects such as hadronization, must be evaluated as well for a complete uncertainty analysis.

[3]The current GENEVA framework and implementation is new and independent of the earlier work in refs. [44, 45].

and show first results for Drell-Yan production, $pp \to Z/\gamma^* \to \ell^+\ell^-+$ jets, obtained with GENEVA. We give conclusions for the chapter in section 3.5.

3.1.1 Previous approaches combining NLO corrections with parton showers

As previously discussed, many steps have been taken over the past decade to include NLO corrections into Monte Carlo programs [59, 60, 61, 62, 13, 14, 63, 64, 65, 66, 15, 16, 17, 54, 18, 55, 67, 68]. By now, the MC@NLO [13, 14] and POWHEG [15, 16, 17] methods are routinely able to consistently combine the fixed NLO calculation of an inclusive jet cross section for a given jet multiplicity with additional parton showering. These methods have also been extended to include the full tree-level matrix elements for additional jet multiplicities [44, 69, 70, 53].

Recently, efforts have been made to extend these approaches in order to combine NLO matrix elements for several jet multiplicities with parton showers [71, 32, 33, 34, 35, 36, 37]. We will discuss some issues faced by some of these approaches in section 3.2.1.5. Here, we would like to stress that including several NLO matrix elements by itself does not provide a full extension of the lowest-order ME/PS matching to relative $\mathcal{O}(\alpha_s)$ perturbative accuracy, since the fixed NLO corrections only suffice to increase the perturbative accuracy in the region of large jet resolution scales. To the same extent that the inclusion of the LL Sudakov factors in the ME/PS merging are needed to get meaningful results at intermediate and small jet scales, higher-order resummation is necessary to improve the perturbative accuracy in this region.

In our approach, the full information from NLO matrix elements for several jet multiplicities is automatically included as follows: For a given Born process with N partons, a small jet scale corresponds to the exclusive N-jet region, and here the N-parton virtual NLO corrections are incorporated in conjunction with the higher-order resummation; in fact, they are a natural ingredient of it. On the other hand, a large jet scale corresponds to the inclusive $(N+1)$-jet region with additional hard emissions. Here, the $(N+1)$-parton virtual NLO corrections are included in the usual way by the fixed NLO calculation for $N+1$ jets.

3.1.2 Brief overview of our construction

The starting point of our approach is the separation of the inclusive N-jet cross section into an exclusive N-jet region and an inclusive $(N+1)$-jet region,

$$\sigma_{\geq N} = \int \mathrm{d}\Phi_N \, \frac{\mathrm{d}\sigma}{\mathrm{d}\Phi_N}(\mathcal{T}^{\mathrm{cut}}) + \int \mathrm{d}\Phi_{N+1} \, \frac{\mathrm{d}\sigma}{\mathrm{d}\Phi_{N+1}}(\mathcal{T}) \, \theta(\mathcal{T} > \mathcal{T}^{\mathrm{cut}}) \,. \tag{3.1}$$

Here $\mathcal{T} \equiv \mathcal{T}(\Phi_{N+1})$ is a suitable resolution variable, which is a function of Φ_{N+1}, and $\mathrm{d}\sigma^{\mathrm{MC}}_{\geq N+1}/\mathrm{d}\Phi_{N+1}(\mathcal{T})$ denotes the fully differential cross section for a given $\mathcal{T}$. In

ME/PS merging, this role is played by the variable that determines the merging scale. However, in our case the parameter $\mathcal{T}^{\text{cut}}$ is not a jet-merging cut but instead serves as an infrared cutoff for the calculation of $\mathrm{d}\sigma^{\text{MC}}_{\geq N+1}/\mathrm{d}\Phi_{N+1}(\mathcal{T})$ and ideally is taken as small as possible.

In the N-jet region at small $\mathcal{T}$ (both above and below $\mathcal{T}^{\text{cut}}$), logarithms of $\mathcal{T}$ become large and must be resummed to maintain consistent perturbative accuracy to some order in α_s. On the other hand, in the $(N+1)$-jet region at large $\mathcal{T}$, a fixed-order expansion in α_s will suffice. To consistently match the resummed and fixed-order calculations, we use the following prescription for the jet cross sections entering in eq. (3.1):

$$\begin{aligned}
\frac{\mathrm{d}\sigma}{\mathrm{d}\Phi_N}(\mathcal{T}^{\text{cut}}) &= \frac{\mathrm{d}\sigma^{\text{resum}}}{\mathrm{d}\Phi_N}(\mathcal{T}^{\text{cut}}) + \left[\frac{\mathrm{d}\sigma^{\text{FO}}}{\mathrm{d}\Phi_N}(\mathcal{T}^{\text{cut}}) - \frac{\mathrm{d}\sigma^{\text{resum}}}{\mathrm{d}\Phi_N}(\mathcal{T}^{\text{cut}})\bigg|_{\text{FO}}\right], \\
\frac{\mathrm{d}\sigma}{\mathrm{d}\Phi_{N+1}}(\mathcal{T}) &= \frac{\mathrm{d}\sigma^{\text{FO}}}{\mathrm{d}\Phi_{N+1}}(\mathcal{T})\left[\frac{\mathrm{d}\sigma^{\text{resum}}}{\mathrm{d}\Phi_N \mathrm{d}\mathcal{T}} \Big/ \frac{\mathrm{d}\sigma^{\text{resum}}}{\mathrm{d}\Phi_N\, \mathrm{d}\mathcal{T}}\bigg|_{\text{FO}}\right].
\end{aligned} \tag{3.2}$$

The superscript "resum" indicates an analytically resummed calculation and "FO" indicates a fixed-order calculation or expansion. This construction properly reproduces the fixed-order calculation at large $\mathcal{T}$, the resummed calculation at small $\mathcal{T}$, and smoothly interpolates between them.

It is straightforward to extend our formulation to combine higher jet multiplicities at NLO with higher-order resummation, as we will show. This is done by replacing $\mathrm{d}\sigma^{\text{FO}}/\mathrm{d}\Phi_{N+1}$ in eq. (3.2) with an inclusive $(N+1)$-jet cross section separated into the exclusive $(N+1)$-jet and inclusive $(N+2)$-jet cross sections and iteratively applying eq. (3.2).

The key ingredients in our approach are the higher-order resummation of the jet resolution variable, the fully differential fixed-order calculation, and the parton shower and hadronization. While each of these components is known, there is a sensitive interplay of constraints between them that must be satisfied to achieve a consistent combination. This is precisely what is accomplished in the GENEVA framework and is the focus of this section.

3.2 General construction

In this section, we derive our theoretical construction in a process-independent manner. We start in section 3.2.1 with a slightly simplified setup, considering the singly differential spectrum in the jet resolution variable. We use this to discuss in detail the perturbative structure and the accuracy in the different phase space regions. In section 3.2.2, we discuss the extension to the fully differential case and how to combine the fixed-order expansion and resummation in this situation. In section 3.2.3, we further generalize these results to include several jet multiplicities

by iteration. Finally, in section 3.2.4, we discuss the Monte Carlo implementation and how to attach parton showering and hadronization.

3.2.1 What resummation can do for Monte Carlo

3.2.1.1 Basic setup

As discussed in section 1.1, the basic idea of Monte Carlo integration is to randomly generate points in phase space ("events") that are distributed according to some differential (probability) distribution. By summing over all points that satisfy certain selection criteria, we are able to perform arbitrary integrals of the distribution. In our case, that distribution is the fully differential cross section, allowing one to compute arbitrary observables. For simplicity, we will first focus on the singly differential cross section in some phase space resolution (or jet resolution) variable $\mathcal{T}$ of dimension one. The precise definition of $\mathcal{T}$ is not important at the moment, so we keep it generic for now. We use the convention that the limit $\mathcal{T} \to 0$ corresponds to Born kinematics, i.e., the tree-level cross section is $\sim \delta(\mathcal{T})$. We also require that $\mathcal{T}$ is an IR-safe observable, such that the differential cross section $\mathrm{d}\sigma/\mathrm{d}\mathcal{T}$ can in principle be well defined to all orders in perturbation theory and for $\mathcal{T} > 0$ contains no IR divergences.

To give an example, for our application to $e^+e^- \to 2/3$ jets in section 3.3, we will use 2-jettiness $\mathcal{T}_2 = E_{\mathrm{cm}}(1-T)$, where T is the usual thrust [72]. Alternatives include other 2-jet event shapes. For Drell-Yan in section 3.4, we will use beam thrust [40]. An alternative would be the p_T of the leading jet. If the Born cross section we are interested in has N signal jets,[4] then $\mathcal{T}$ could be N-jettiness or the largest p_T of any additional jet. The important point is that we can think of $\mathcal{T}$ as a resolution variable which determines the scale of additional emissions in the $\Phi_{\geq N+1}$ phase space, such that for $\mathcal{T} \leq \mathcal{T}^{\mathrm{cut}}$ there are no emissions above the scale $\mathcal{T}^{\mathrm{cut}}$. For later convenience, we also define the dimensionless equivalent of $\mathcal{T}$ as

$$\tau = \frac{\mathcal{T}}{Q}\,. \tag{3.3}$$

Here, Q is the relevant hard-interaction scale in the Born process, e.g., $Q \equiv E_{\mathrm{cm}}$ for $e^+e^- \to$ jets or $Q \equiv m_{\ell^+\ell^-}$ for Drell-Yan $pp \to Z/\gamma^* \to \ell^+\ell^-$. In terms of τ, the limit $\tau \ll 1$ corresponds to the exclusive limit close to Born kinematics. For $\tau \sim 1$, there are additional emissions at the hard scale $\mathcal{T} \sim Q$, which means we are far away from Born kinematics and we should switch the description to consider the corresponding Born process with one additional hard jet.

To describe the differential $\mathcal{T}$ spectrum, we want the Monte Carlo to generate events at specific values of $\mathcal{T}$, which are distributed according to the differential cross

[4] As usual, we assume that the Born cross section is defined with appropriate cuts on the N signal jets, so that it does not contain any IR divergences by itself.

section $\mathrm{d}\sigma/\mathrm{d}\mathcal{T}$. The total cross section is then simply given by summing over all events,

$$\sigma = \int \mathrm{d}\mathcal{T}\, \frac{\mathrm{d}\sigma}{\mathrm{d}\mathcal{T}}\,. \tag{3.4}$$

The essential problem every Monte Carlo generator faces is that in perturbation theory the differential cross section $\mathrm{d}\sigma/\mathrm{d}\mathcal{T}$ contains IR divergences from real emissions for $\mathcal{T} \to 0$, which only cancel against the corresponding virtual IR divergences upon integration over the $\mathcal{T} \to 0$ region. As a result, the perturbative spectrum for $\mathcal{T} \to 0$ can only be defined in a distributional sense in terms of plus and delta distributions [see eq. (3.8) below]. To deal with this, we have to introduce a small cutoff $\mathcal{T}^{\mathrm{cut}}$ and define the cumulant of the spectrum as

$$\sigma(\mathcal{T}^{\mathrm{cut}}) = \int \mathrm{d}\mathcal{T}\, \frac{\mathrm{d}\sigma}{\mathrm{d}\mathcal{T}}\, \theta(\mathcal{T} < \mathcal{T}^{\mathrm{cut}})\,. \tag{3.5}$$

In the Monte Carlo, the total cross section is then obtained by combining the cumulant and spectrum as

$$\sigma = \sigma(\mathcal{T}^{\mathrm{cut}}) + \int \mathrm{d}\mathcal{T}\, \frac{\mathrm{d}\sigma}{\mathrm{d}\mathcal{T}}\, \theta(\mathcal{T} > \mathcal{T}^{\mathrm{cut}})\,. \tag{3.6}$$

In practice, this is implemented by generating two distinct types of events: (i) events that have $\mathcal{T} = 0$ and relative weights given by $\sigma(\mathcal{T}^{\mathrm{cut}})$, and (ii) events that have nonzero values $\mathcal{T} > \mathcal{T}^{\mathrm{cut}}$ and relative weights given by $\mathrm{d}\sigma/\mathrm{d}\mathcal{T}$. The first type of events have Born kinematics and represents the tree-level and virtual corrections together with the corresponding real emissions integrated below $\mathcal{T}^{\mathrm{cut}}$. The second type of events contains one or more partons in the final state, since the real-emission corrections determine the shape of the spectrum for nonzero $\mathcal{T}$. We now have two basic conditions:

1. From a numerical point of view, we want the value of $\mathcal{T}^{\mathrm{cut}}$ to be as small as possible, so as to describe as much differential information as possible. In practice, our ability to reliably compute the cumulant $\sigma(\mathcal{T}^{\mathrm{cut}})$ in perturbation theory sets a lower limit on the possible value of $\mathcal{T}^{\mathrm{cut}} \gtrsim$ few times Λ_{QCD}.

2. Since $\mathcal{T}^{\mathrm{cut}}$ is an unphysical parameter, we want the dependence on it to drop out (to the order we are working at). In practice, this is guaranteed by including the corresponding dominant higher-order corrections in the cumulant and spectrum.

3.2.1.2 Perturbative expansion and order counting

In perturbation theory, the differential cross section in τ and the cumulant in τ^{cut} have the general form

$$\frac{\mathrm{d}\sigma}{\mathrm{d}\tau} = \frac{\mathrm{d}\sigma^{\mathrm{sing}}}{\mathrm{d}\tau} + \frac{\mathrm{d}\sigma^{\mathrm{nons}}}{\mathrm{d}\tau}\,, \qquad \sigma(\tau^{\mathrm{cut}}) = \int_0^{\tau^{\mathrm{cut}}} \mathrm{d}\tau\, \frac{\mathrm{d}\sigma}{\mathrm{d}\tau} = \sigma^{\mathrm{sing}}(\tau^{\mathrm{cut}}) + \sigma^{\mathrm{nons}}(\tau^{\mathrm{cut}})\,, \tag{3.7}$$

where we have distinguished "singular" and "nonsingular" contributions. For $\tau \to 0$, the singular terms in $\mathrm{d}\sigma^{\mathrm{sing}}/\mathrm{d}\tau$ scale like $1/\tau$, while the nonsingular terms in $\mathrm{d}\sigma^{\mathrm{nons}}/\mathrm{d}\tau$ contain at most integrable singularities. For the cumulant, this means that $\sigma^{\mathrm{sing}}(\tau^{\mathrm{cut}})$ contains all terms in $\sigma(\tau^{\mathrm{cut}})$ enhanced by logarithms $\ln^k(\tau^{\mathrm{cut}})$, while $\sigma^{\mathrm{nons}}(\tau^{\mathrm{cut}} = 0) = 0$.

The singular part of the spectrum is given by

$$\frac{\mathrm{d}\sigma^{\mathrm{sing}}}{\mathrm{d}\tau} = \sigma_B \Big[C_{-1}(\alpha_s)\, \delta(\tau) + \sum_{n\geq 0} C_n(\alpha_s)\, \mathcal{L}_n(\tau) \Big] , \tag{3.8}$$

where σ_B denotes the Born cross section, and we denote the usual plus distributions as

$$\mathcal{L}_n(x) = \left[\frac{\theta(x) \ln^n(x)}{x} \right]_+ , \qquad \int_0^{x^{\mathrm{cut}}} \mathrm{d}x\, \mathcal{L}_n(x) = \frac{\ln^{n+1}(x^{\mathrm{cut}})}{n+1} . \tag{3.9}$$

They encode the cancellation between real and virtual IR divergences. The corresponding singular contribution to the cumulant cross section integrated up to $\tau \leq \tau^{\mathrm{cut}}$ is

$$\sigma^{\mathrm{sing}}(\tau^{\mathrm{cut}}) = \sigma_B \left[C_{-1}(\alpha_s) + \sum_{n\geq 0} C_n(\alpha_s)\, \frac{\ln^{n+1}(\tau^{\mathrm{cut}})}{n+1} \right] . \tag{3.10}$$

At $\mathcal{O}(\alpha_s^k)$, only the coefficients $C_n(\alpha_s)$ with $n \leq 2k-1$ contribute, so $\mathrm{d}\sigma/\mathrm{d}\tau$ has logarithms up to $\alpha_s^n L^{2n-1}/\tau$, while $\sigma(\tau^{\mathrm{cut}})$ has logarithms up to $\alpha_s^n L_{\mathrm{cut}}^{2n}$, where we use the abbreviations

$$L \equiv \ln(\tau) , \qquad L_{\mathrm{cut}} \equiv \ln(\tau^{\mathrm{cut}}) . \tag{3.11}$$

The α_s expansion of the coefficients $C_{-1}(\alpha_s)$ and $C_n(\alpha_s)$ in the singular contributions can be written as

$$C_{-1}(\alpha_s) = 1 + \sum_{k\geq 1} c_{k,-1}\, \alpha_s^k , \qquad C_n(\alpha_s) = \sum_{2k\geq n+1} c_{kn}\, \alpha_s^k . \tag{3.12}$$

Similarly, the α_s expansion of the nonsingular contributions can be written as

$$\frac{\mathrm{d}\sigma^{\mathrm{nons}}}{\mathrm{d}\tau} = \sigma_B \sum_{k\geq 1} f_k^{\mathrm{nons}}(\tau)\, \alpha_s^k , \qquad F_k^{\mathrm{nons}}(\tau^{\mathrm{cut}}) = \int_0^{\tau^{\mathrm{cut}}} \mathrm{d}\tau\, f_k^{\mathrm{nons}}(\tau) . \tag{3.13}$$

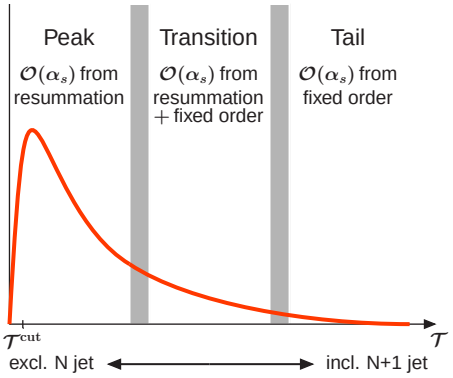

Figure 3.1: Illustration of the different parametric regions in the jet resolution.

Using eqs. (3.12) and (3.13), the spectrum and cumulant up to $\mathcal{O}(\alpha_s^2)$ are given by

$$\begin{aligned}\frac{1}{\sigma_B}\frac{\mathrm{d}\sigma}{\mathrm{d}\tau}\bigg|_{\tau>0} = \quad & \frac{\alpha_s}{\tau}\Big[c_{11}L \;+c_{10} \qquad\qquad\qquad\qquad +\tau f_1^{\rm nons}(\tau)\Big] \\ & + \frac{\alpha_s^2}{\tau}\Big[c_{23}L^3 + c_{22}L^2 + c_{21}L + c_{20} + \tau f_2^{\rm nons}(\tau)\Big] + \mathcal{O}(\alpha_s^3)\,, \qquad (3.14)\\ \frac{1}{\sigma_B}\sigma(\tau^{\rm cut}) = 1 + \alpha_s & \Big[\frac{c_{11}}{2}L_{\rm cut}^2 + c_{10}L_{\rm cut} \;+c_{1,-1} \qquad\qquad +F_1^{\rm nons}(\tau^{\rm cut})\Big] \\ & + \alpha_s^2\Big[\frac{c_{23}}{4}L_{\rm cut}^4 + \frac{c_{22}}{3}L_{\rm cut}^3 + \frac{c_{21}}{2}L_{\rm cut}^2 + c_{20}L_{\rm cut} + c_{2,-1} + F_2^{\rm nons}(\tau^{\rm cut})\Big] \\ & + \mathcal{O}(\alpha_s^3)\,.\end{aligned}$$

Note that the $c_{k,-1}$ constant term in the singular corrections, which contains the finite virtual corrections to the Born process, only appears in the cumulant.

We now distinguish three parametrically different regions in τ, which are illustrated in figure 3.1:

- *Resummation ("peak") region* $\tau \ll 1$: In this limit, the logarithms in the singular contributions are large, such that parametrically one has to count[5]

$$\alpha_s L^2 \sim 1\,, \qquad \alpha_s L_{\rm cut}^2 \sim 1\,. \qquad (3.15)$$

  This means one has to resum the towers of logarithms $(\alpha_s L^2)^n$ in the spectrum and $(\alpha_s L_{\rm cut}^2)^n$ in the cumulant in eq. (3.14) to all orders in α_s to obtain a

[5]In analytic resummation, the counting and resummation of logarithms is performed in the exponent of the cross section, where one counts $\alpha_s L \sim 1$. For the purpose of our argument in this section, it is sufficient to adopt the weaker scaling in eq. (3.15) and only count logarithms in the cross section. In our results, we always perform the full resummation in the exponent, as discussed in section 3.3.1.1.

meaningful perturbative approximation at some order. At the same time, the nonsingular corrections can be regarded as power suppressed, since they are of relative $\mathcal{O}(\tau)$.

- *Fixed-order ("tail") region* $\tau \sim 1$: In this limit, the logarithms are not enhanced, and a fixed-order expansion in α_s is applicable. The singular and nonsingular contributions are equally important and both must be included at the same order in α_s. In particular, there are typically large cancellations between these for $\tau \sim 1$, so it is actually crucial not to resum the singular contributions in this region, since otherwise this cancellation would be spoiled.

- *Transition region*: The transition between the resummation and fixed-order regions.

There are of course no strict boundaries between the different regions. This is why it is important to have a proper description not just in the two limits but also in the transition region, which connects the resummation and fixed-order regions. In fact, in practice the experimentally relevant region is often somewhere in the transition region, where both types of perturbative corrections can be important.

3.2.1.3 Lowest perturbative accuracy

For the Monte Carlo to provide a proper description at all values of $\mathcal{T}$, it has to include at least the lowest-order terms relevant for each region. Keeping only these, and dropping all other terms, the spectrum and the cumulant are given by

$$\begin{aligned}
\frac{1}{\sigma_B}\frac{\mathrm{d}\sigma}{\mathrm{d}\tau}\bigg|_{\tau>0} &= \frac{\alpha_s}{\tau}\Big[L\, f_0(\alpha_s L^2) + f_1(\alpha_s L^2) + \tau f_1^{\text{nons}}(\tau)\Big]\,, \\
\frac{1}{\sigma_B}\sigma(\tau^{\text{cut}}) &= 1 + \alpha_s\Big[L_{\text{cut}}^2\, F_0(\alpha_s L_{\text{cut}}^2) + L_{\text{cut}}\, F_1(\alpha_s L_{\text{cut}}^2)\Big]\,.
\end{aligned} \tag{3.16}$$

where the functions $f_{0,1}$ and $F_{0,1}$ are given in terms of the coefficients c_{ij} in eq. (3.12) as

$$\begin{aligned}
\text{LL}_\sigma: \quad & f_0(\alpha_s L^2) = \sum_{n\geq 0} c_{n+1,2n+1}(\alpha_s L^2)^n\,, \quad F_0(\alpha_s L^2) = \sum_{n\geq 0}\frac{c_{n+1,2n+1}}{2(n+1)}(\alpha_s L_{\text{cut}}^2)^n\,, \\
\text{NLL}_\sigma: \quad & f_1(\alpha_s L^2) = \sum_{n\geq 0} c_{n+1,2n}(\alpha_s L^2)^n\,, \qquad F_1(\alpha_s L^2) = \sum_{n\geq 0}\frac{c_{n+1,2n}}{2n+1}(\alpha_s L_{\text{cut}}^2)^n\,.
\end{aligned} \tag{3.17}$$

The f_0 and F_0 resum the leading-logarithmic series in the cross section, which we denote as LL_σ. The functions f_1 and F_1 resum the next-to-leading-logarithmic series in the cross section, which we denote as NLL_σ.

In the resummation region at $\tau \ll 1$, the LL_σ terms in the spectrum scale as $L \sim 1/\sqrt{\alpha_s}$ (relative to the overall α_s/τ scaling) and provide the lowest level of approximation. The NLL_σ terms scale as ~ 1, and one can argue about whether they are needed as well in order to get a meaningful lowest-order prediction. Formally, they are necessary to obtain the spectrum at $\sim \alpha_s/\tau$, which one might consider the natural leading-order scaling of the spectrum (or equivalently if one does not want to rely on the $\sim 1/\sqrt{\alpha_s}$ enhancement of the LL series). Experience shows that the NLL terms are indeed numerically important. For example, in analytic resummations, one rarely gets a sensible prediction without going at least to NLL. Similarly, to obtain sensible predictions from a parton shower, it is almost mandatory to include important physical effects such as momentum conservation in the parton splitting and the choice of α_s scale [73]. In the cumulant, the LL_σ series in F_0 scales as ~ 1 and must be included. The NLL_σ series in F_1 scales as $\sim \sqrt{\alpha_s}$ and, for consistency, should be included in the cumulant if it is included in the spectrum.

In the fixed-order region at $\tau \sim 1$, the lowest meaningful order in the spectrum is given by the complete $\mathcal{O}(\alpha_s)$ terms, requiring one to include the c_{11} and c_{10} terms, which are part of the f_0 and f_1 functions, as well as the nonsingular corrections $f_1^{\mathrm{nons}}(\tau)$. Since we take τ^{cut} to be small, the cumulant is always in the resummation region. Hence, its nonsingular corrections $F_1^{\mathrm{nons}}(\tau)$ [see eq. (3.14)] are suppressed by $\mathcal{O}(\alpha_s \tau^{\mathrm{cut}})$ and can be safely neglected.

The leading level of accuracy in eq. (3.16) closely corresponds to what is achieved in the standard ME/PS matching. In this case, the LL resummation is provided by the parton shower Sudakov factors (either generated by the shower or multiplied by hand), where the jet resolution variable corresponds to the shower evolution variable, since that is the variable for which the shower directly resums the correct LL_σ series. The LL_σ series has a well-known and simple exponential structure,

$$c_{n+1,2n+1} = \frac{c_{11}^{n+1}}{2^n n!} \qquad \Rightarrow \qquad f_0(\alpha_s L^2) = \exp\Big[\frac{c_{11}}{2}\,\alpha_s L^2\Big]\,, \tag{3.18}$$

such that

$$\frac{1}{\sigma_B}\frac{\mathrm{d}\sigma}{\mathrm{d}\tau}\bigg|_{\tau>0} = c_{11}\,\alpha_s \frac{L}{\tau}\,\exp\Big[\frac{c_{11}}{2}\,\alpha_s L^2\Big]\,, \qquad \frac{1}{\sigma_B}\sigma(\tau^{\mathrm{cut}}) = \exp\Big[\frac{c_{11}}{2}\,\alpha_s L_{\mathrm{cut}}^2\Big]\,. \tag{3.19}$$

The resummation exponent at LL_σ is given by the integral over the leading $c_{11}\,\alpha_s L/\tau$ term in the spectrum. This is precisely what the standard parton shower veto algorithm exploits to generate the resummation exponent. The analogous structure does not hold at NLL_σ, which is why the parton shower cannot resum the NLL_σ series by exponentiating the integral of the $c_{10}\,\alpha_s/\tau$ term. As already mentioned, in practice, parton showers include important partial NLL effects, so practically this provides a numerically close approximation to the correct NLL_σ series. The nonsingular corrections in the spectrum, $f_1^{\mathrm{nons}}(\tau)$, are obtained by including the full tree-level matrix

element for one additional emission. Since the full matrix element also includes the c_{11} and c_{10} terms, this requires a proper matching procedure to avoid double counting these terms. At LL_σ, a simple way to do this is to multiply the full fixed-order result from the matrix element with the shower's LL_σ resummation exponent,

$$\frac{1}{\sigma_B}\frac{\mathrm{d}\sigma}{\mathrm{d}\tau}\bigg|_{\tau>0} = \frac{\alpha_s}{\tau}\Big[c_{11}L + c_{10} + \tau f_1^{\mathrm{nons}}(\tau)\Big]\exp\Big[\frac{c_{11}}{2}\,\alpha_s L^2\Big]\,, \tag{3.20}$$

which corresponds to the CKKW-L [4, 5, 6, 10] procedure. The reason this gives the spectrum correctly at LL_σ is the simple structure in eq. (3.19), where the LL_σ exponent multiplies the c_{11} term in the spectrum.[6] At large $\tau \sim 1$, the exponent in eq. (3.20) can be expanded as $1 + \mathcal{O}(\alpha_s)$, so eq. (3.20) gives the correct leading fixed-order result.

Compared to eq. (3.16), the NLO matching performed in MC@NLO and POWHEG amounts to adding to the cumulant the $c_{1,-1}$ singular constant, containing the $\mathcal{O}(\alpha_s)$ virtual corrections, as well as the nonsingular contributions $F_1^{\mathrm{nons}}(\tau)$. Assuming the same set of NLL terms are included in the cumulant and spectrum, this achieves that inclusive quantities that are integrated over a large range of τ, such as the total cross section, are correctly reproduced at fixed NLO, which provides them with $\mathcal{O}(\alpha_s)$ accuracy. In these approaches, the goal is not to improve the perturbative accuracy of the spectrum (or the cumulant at small τ^{cut}), which has the same leading accuracy as in eq. (3.20).

3.2.1.4 Next-to-lowest perturbative accuracy

We now want to improve the Monte Carlo description in eq. (3.6) from the lowest-order accuracy, given by eq. (3.16), to the next-to-lowest perturbative accuracy in α_s. This requires us to include the appropriate higher-order corrections in each region, which gives

$$\begin{aligned}
\frac{1}{\sigma_B}\frac{\mathrm{d}\sigma}{\mathrm{d}\tau}\bigg|_{\tau>0} &= \frac{\alpha_s}{\tau}\Big[L\,f_0(\alpha_s L^2) + f_1(\alpha_s L^2) + \tau f_1^{\mathrm{nons}}(\tau)\Big] \\
&\quad + \frac{\alpha_s^2}{\tau}\Big[L\,f_2(\alpha_s L^2) + f_3(\alpha_s L^2) + \tau f_2^{\mathrm{nons}}(\tau)\Big]\,, \\
\frac{1}{\sigma_B}\sigma(\tau^{\mathrm{cut}}) &= 1 + \alpha_s\Big[L_{\mathrm{cut}}^2\,F_0(\alpha_s L_{\mathrm{cut}}^2) + L_{\mathrm{cut}}\,F_1(\alpha_s L_{\mathrm{cut}}^2) + c_{1,-1} + F_1^{\mathrm{nons}}(\tau^{\mathrm{cut}})\Big] \\
&\quad + \alpha_s^2\Big[L_{\mathrm{cut}}^2\,F_2(\alpha_s L_{\mathrm{cut}}^2) + L_{\mathrm{cut}}\,F_3(\alpha_s L_{\mathrm{cut}}^2)\Big]\,,
\end{aligned} \tag{3.21}$$

[6] As before, since this simple LL_σ structure does not hold in general at NLL_σ, this procedure does not yield the resummed spectrum at NLL_σ, even if one were to multiply the spectrum with the NLL_σ resummation exponent

where we denote the series of logarithms resummed by the functions f_2 and F_2 by NLL'_σ and the series resummed by f_3 and F_3 by NNLL_σ. They can again be written in terms of the c_{ij} coefficients in eq. (3.12) as

$$\begin{aligned}
\mathrm{NLL}'_\sigma: \quad & f_2(\alpha_s L^2) = \sum_{n\geq 0} c_{n+2,2n+1} (\alpha_s L^2)^n\,, \quad F_2(\alpha_s L^2) = \sum_{n\geq 0} \frac{c_{n+2,2n+1}}{2(n+1)} (\alpha_s L_{\mathrm{cut}}^2)^n\,, \\
\mathrm{NNLL}_\sigma: \quad & f_3(\alpha_s L^2) = \sum_{n\geq 0} c_{n+2,2n} (\alpha_s L^2)^n\,, \qquad F_3(\alpha_s L^2) = \sum_{n\geq 0} \frac{c_{n+2,2n}}{2n+1} (\alpha_s L_{\mathrm{cut}}^2)^n\,.
\end{aligned} \tag{3.22}$$

In the resummation region, the NLL'_σ series in the spectrum scales as $\sim \alpha_s^{3/2}$ and thus provides the $\sim \alpha_s$ correction to the LL_σ series in f_0. Similarly, the NNLL_σ series scales as $\sim \alpha_s^2$ providing the $\sim \alpha_s$ correction to the NLL_σ series in f_1. They can again be obtained by performing the standard resummation in the exponent of the cross section to NLL′ and NNLL respectively. (Here, NLL′ refers to those parts of the full NNLL resummation that arise from the combination of the one-loop matching corrections with the NLL resummation, see section 3.3.1.1 and table 3.2.)

In the fixed-order region, increasing the perturbative accuracy by $\sim \alpha_s$ requires the complete $\mathcal{O}(\alpha_s^2)$ corrections, including the $f_2^{\mathrm{nons}}(\tau)$ nonsingular corrections. Similarly, for the cumulant, F_2 and F_3 resum the NLL'_σ and NNLL_σ series of logarithms, which scale as $\sim \alpha_s$ and $\sim \alpha_s^{3/2}$, respectively, and provide the $\sim \alpha_s$ improvement over the LL_σ and NLL_σ series in F_0 and F_1. In addition, going to the next higher order in the cumulant requires including the full singular constant $c_{1,-1}$,[7] as well as the nonsingular corrections $F_1^{\mathrm{nons}}(\tau)$, which both scale as $\sim \alpha_s$.

It is instructive to see where the information from the virtual NLO matrix elements enters in eq. (3.21). As already mentioned, the virtual NLO corrections to the Born process are given by $c_{1,-1}$. In addition, by multiplying the LL series it contributes part of f_2 and F_2. Hence, consistently combining the virtual corrections with the resummation requires one to go to at least NLL′. The virtual NLO corrections with one extra emission (plus the integral over the two-emission tree-level matrix element) yield the full $\mathcal{O}(\alpha_s^2)$ corrections in the spectrum, i.e., both the singular c_{2k} terms as well as the nonsingular f_2^{nons} terms in eq. (3.14). Adding these corrections again requires one to avoid double counting the singular c_{2k} terms that are already included in the resummation. In analytic resummation, it is well known how to do this, namely by simply adding the nonsingular corrections. These are obtained by taking the difference of the full NLO corrections and the singular NLO corrections, where the latter are given by expanding the resummed result to fixed order. Since this construction involves the virtual contribution to both the Born process and the process with one extra emission, we see that going consistently to higher order in

[7] Formally, $c_{1,-1}$ belongs to the NLL'_σ series in the cumulant, but for the sake of discussion, we keep it explicit.

both the resummation and fixed-order regions naturally leads to a combination of the information from two successive NLO matrix elements.

3.2.1.5 Merging NLO matrix elements with parton shower resummation only

We stress that, for a description at the next-higher perturbative accuracy across the whole range in τ, it is not sufficient to include the fixed NLO corrections to the spectrum and take care of the double counting with the parton shower resummation. This only provides the proper NLO description in the fixed-order region at large τ. In the transition and resummation regions, a proper higher-order description necessitates higher-order resummation. Of course, this is not a problem if the only goal is to improve the fixed-order region at large τ, as is the case for example in a recent MC@NLO publication [35].

However, including the fixed NLO corrections outside the fixed-order region, as is done in SHERPA's recent NLO merging [33, 34], can actually make things worse in two respects: First, numerically this will typically force the spectrum to shift toward the fixed-order result and away from the resummed one. Since this can shift the spectrum in the wrong direction, it can potentially make the result *less* accurate.[8] At the same time, the perturbative uncertainties from fixed-order scale variation decrease, which only aggravates this problem. Multiplying the NLO corrections to the spectrum with LL parton shower Sudakov factors (see, e.g., ref. [56]) can mitigate this to some extent but does not solve the problem. The only consistent way to include the fixed NLO corrections to the spectrum outside the fixed-order region, and in particular obtain reliable perturbative uncertainties, is to properly combine them with a higher-order resummation.

Second, this explicitly spoils the formal $\mathcal{O}(\alpha_s)$ accuracy of the inclusive cross section. To see this, consider adding the fixed NLO corrections to the lowest-order spectrum and cumulant in eq. (3.16), properly taking care of the double counting at $\mathcal{O}(\alpha_s^2)$, which gives

$$\begin{aligned}
\frac{1}{\sigma_B}\frac{\mathrm{d}\sigma}{\mathrm{d}\tau}\bigg|_{\tau>0} &= \frac{\alpha_s}{\tau}\Big[L\,f_0(\alpha_s L^2) + f_1(\alpha_s L^2) + \tau f_1^{\mathrm{nons}}(\tau)\Big] + \frac{\alpha_s^2}{\tau}\Big[c_{21}L + c_{20} + \tau f_2^{\mathrm{nons}}(\tau)\Big]\,, \\
\frac{1}{\sigma_B}\sigma(\tau^{\mathrm{cut}}) &= 1 + \alpha_s\Big[L_{\mathrm{cut}}^2\,F_0(\alpha_s L_{\mathrm{cut}}^2) + L_{\mathrm{cut}}\,F_1(\alpha_s L_{\mathrm{cut}}^2) + c_{1,-1} + F_1^{\mathrm{nons}}(\tau^{\mathrm{cut}})\Big]\,. \qquad (3.23)
\end{aligned}$$

[8] One can see this for example in the case of 2-jettiness in figure 3.3 in section 3.3. Here, the NLL′+LO$_3$ result is much closer to the slightly higher NNLL′+NLO$_3$ best prediction than the fixed NLO$_3$ result. We have checked that in this case, adding the NLO$_3$ to the NLL′+LO$_3$ by expanding it to $\mathcal{O}(\alpha_s^2)$ forces the result to move in the wrong direction toward the lower NLO$_3$.

Using these expressions yields for the inclusive cross section

$$\begin{aligned}\frac{1}{\sigma_B}\sigma &= \frac{1}{\sigma_B}\sigma(\tau^{\text{cut}}) + \int_{\tau^{\text{cut}}}^{1} \mathrm{d}\tau \frac{1}{\sigma_B}\frac{\mathrm{d}\sigma}{\mathrm{d}\tau} \\ &= 1 + \alpha_s\Big[c_{1,-1} + F_1^{\text{nons}}(1)\Big] - \alpha_s^2\Big[\frac{c_{21}}{2}L_{\text{cut}}^2 + c_{20}L_{\text{cut}}\Big]\,. \end{aligned} \tag{3.24}$$

While the first two terms give the correct NLO inclusive cross section, the $\mathcal{O}(\alpha_s^2)$ terms induced by the fixed NLO corrections in the spectrum formally scale as α_s and $\alpha_s^{3/2}$ and therefore spoil the formal $\mathcal{O}(\alpha_s)$ perturbative accuracy for the inclusive cross section and in fact for any inclusive observable. This directly contradicts the claim in refs. [33, 34] that this description maintains the higher-order accuracy of the underlying matrix elements in their respective phase space range. It only preserves the fixed $\mathcal{O}(\alpha_s)$ terms, which in the context of combining fixed-order corrections with a logarithmic resummation is necessary but not sufficient to preserve the higher perturbative accuracy.

This problem cannot be avoided by multiplying the α_s^2 corrections in the spectrum with the LL parton shower Sudakov factors, since this does not provide the proper NLL'_σ and NNLL_σ series. Note also that we have already assumed in eq. (3.24) that the full NLL_σ series is included in the spectrum and cumulant. In general, the parton shower cannot provide this, which means there will be even $\alpha_s^2 L_{\text{cut}}^3 \sim \sqrt{\alpha_s}$ terms induced in eq. (3.24).

Pragmatically, the inclusive cross section can be restored to formal $\mathcal{O}(\alpha_s)$ accuracy by either explicitly including the corresponding α_s^2 corrections in the cumulant to cancel these terms, where numerical methods to do so have been described very recently in refs. [47, 36, 37], or alternatively by explicitly restricting the fixed NLO corrections in the spectrum to the fixed-order region at large τ, such that the induced $\mathcal{O}(\alpha_s^2)$ terms in the total cross section are not logarithmically enhanced and are formally $\mathcal{O}(\alpha_s^2)$. This is essentially the approach taken in ref. [35]. However, neither of these approaches improves the perturbative accuracy in the spectrum outside the fixed-order region.

3.2.2 What Monte Carlo can do for resummation

For $\mathcal{T}$ being the resolution variable between N and more than N jets, we showed in the previous subsection that combining the NLO matrix-element corrections for N and $N+1$ partons at the level of the singly differential $\mathcal{T}$ spectrum is equivalent to combining the NNLL resummation of the singular contributions with the higher-order nonsingular contributions. Our goal now is to extend this singly differential description to the fully differential case, in order to use the full N-parton and $(N+1)$-parton information of the matrix elements. We will use the notation $(\text{N})\text{LO}_N$ or $(\text{N})\text{LO}_{N+1}$ to indicate up to which fixed order in α_s the N-parton or $(N+1)$-parton matrix elements are included.

To start with, it is straightforward to generalize the jet resolution spectrum $\mathrm{d}\sigma/\mathrm{d}\mathcal{T}$ and its cumulant $\sigma(\mathcal{T}^{\mathrm{cut}})$ to include the full dependence on the N-body Born phase space,

$$\begin{aligned} \frac{\mathrm{d}\sigma}{\mathrm{d}\mathcal{T}} &\to \frac{\mathrm{d}\sigma}{\mathrm{d}\Phi_N \mathrm{d}\mathcal{T}}\,, \\ \sigma(\mathcal{T}^{\mathrm{cut}}) &\to \frac{\mathrm{d}\sigma}{\mathrm{d}\Phi_N}(\mathcal{T}^{\mathrm{cut}}) = \int \mathrm{d}\mathcal{T}\, \frac{\mathrm{d}\sigma}{\mathrm{d}\Phi_N \mathrm{d}\mathcal{T}}\, \theta(\mathcal{T} < \mathcal{T}^{\mathrm{cut}})\,, \end{aligned} \tag{3.25}$$

such that eq. (3.6) becomes

$$\frac{\mathrm{d}\sigma_{\mathrm{incl}}}{\mathrm{d}\Phi_N} = \frac{\mathrm{d}\sigma}{\mathrm{d}\Phi_N}(\mathcal{T}^{\mathrm{cut}}) + \int \mathrm{d}\mathcal{T}\, \frac{\mathrm{d}\sigma}{\mathrm{d}\Phi_N \mathrm{d}\mathcal{T}}\, \theta(\mathcal{T} > \mathcal{T}^{\mathrm{cut}})\,. \tag{3.26}$$

Here, $\mathrm{d}\sigma_{\mathrm{incl}}/\mathrm{d}\Phi_N$ is the *inclusive* N-jet cross section. The discussion in section 3.2.1 can be precisely repeated in this case, since the perturbative structure of the differential spectrum $\mathrm{d}\sigma/\mathrm{d}\Phi_N \mathrm{d}\mathcal{T}$ with respect to $\mathcal{T}$ is precisely the same as in eqs. (3.7) and (3.8). Namely, we can write it as the sum of singular and nonsingular contributions,

$$\frac{\mathrm{d}\sigma}{\mathrm{d}\Phi_N \mathrm{d}\mathcal{T}} = \frac{\mathrm{d}\sigma^{\mathrm{sing}}}{\mathrm{d}\Phi_N \mathrm{d}\mathcal{T}} + \frac{\mathrm{d}\sigma^{\mathrm{nons}}}{\mathrm{d}\Phi_N \mathrm{d}\mathcal{T}}\,. \tag{3.27}$$

The nonsingular contributions are general functions of Φ_N and $\mathcal{T}$, but as before are integrable in $\mathcal{T}$ for $\mathcal{T} \to 0$. The singular contributions have the structure

$$\frac{\mathrm{d}\sigma^{\mathrm{sing}}}{\mathrm{d}\Phi_N \mathrm{d}\mathcal{T}} = \frac{\mathrm{d}\sigma_B}{\mathrm{d}\Phi_N}\left[C_{-1}(\Phi_N, \alpha_s)\, \delta(\mathcal{T}) + \sum_{n\geq 0} C_n(\Phi_N, \alpha_s)\, \frac{1}{Q} \mathcal{L}_n\Big(\frac{\mathcal{T}}{Q}\Big)\right], \tag{3.28}$$

where $\mathrm{d}\sigma_B/\mathrm{d}\Phi_N$ is now the fully differential Born cross section. Since the singular contributions arise from the cancellation of virtual and real IR singularities, which only know about Φ_N, their $\mathcal{T}$ dependence naturally factorizes from the Φ_N kinematics of the underlying hard process. This is what allows the resummation of the singular terms to higher orders for a given point in Φ_N. At LL, the entire Φ_N dependence is that of the Born cross section. At higher logarithmic orders, this is not the case anymore, since the coefficients C_n can have nontrivial Φ_N dependence. In addition, the precise definition of $\mathcal{T}$ also becomes important. Depending on its definition, the higher-order singular coefficients can depend on clustering effects or other types of nonglobal logarithms [74, 75, 76, 77, 78, 79], which can be difficult to resum to high enough order with currently available methods. Therefore, it is important to choose a resolution variable with simple resummation properties. An example is N-jettiness, for which the complete NNLL resummation for arbitrary N is known [1, 80]. For the purpose of our discussion below, we will assume that a resummed result for the spectrum and its cumulant in eq. (3.26) at sufficiently high order is available to us.

We can think of the cumulant $\mathrm{d}\sigma/\mathrm{d}\Phi_N(\mathcal{T}_{\mathrm{cut}})$ in eq. (3.26) as the *exclusive* N-jet cross section with no additional emissions (jets) above the scale $\mathcal{T}^{\mathrm{cut}}$, while the

spectrum $\mathrm{d}\sigma/\mathrm{d}\Phi_N\mathrm{d}\mathcal{T}$ for $\mathcal{T} > \mathcal{T}^{\mathrm{cut}}$ is the corresponding *inclusive* $(N+1)$-jet cross section. While the cumulant $\mathrm{d}\sigma/\mathrm{d}\Phi_N(\mathcal{T}^{\mathrm{cut}})$ is differential in $\mathrm{d}\Phi_N$ and thus already as differential as it can be, the spectrum contains a projection from the full $\mathrm{d}\Phi_{\geq N+1}$ phase space down to $\mathrm{d}\Phi_N\mathrm{d}\mathcal{T}$. To also be fully differential in the $(N+1)$-jet phase space, we can generalize eq. (3.26) to

$$\frac{\mathrm{d}\sigma_{\mathrm{incl}}}{\mathrm{d}\Phi_N} = \frac{\mathrm{d}\sigma}{\mathrm{d}\Phi_N}(\mathcal{T}^{\mathrm{cut}}) + \int \frac{\mathrm{d}\Phi_{N+1}}{\mathrm{d}\Phi_N} \frac{\mathrm{d}\sigma}{\mathrm{d}\Phi_{N+1}}(\mathcal{T})\, \theta(\mathcal{T} > \mathcal{T}^{\mathrm{cut}})\,, \tag{3.29}$$

where $\mathrm{d}\sigma/\mathrm{d}\Phi_{N+1}(\mathcal{T})$ denotes the fully differential spectrum for a given $\mathcal{T} \equiv \mathcal{T}(\Phi_{N+1})$. We explicitly denote the dependence on $\mathcal{T}$ and $\mathcal{T}^{\mathrm{cut}}$ to clearly distinguish the spectrum from the cumulant. We have also used the same shorthand as given in eq. (1.11). The projection from an $(N+1)$-body phase space point to an N-body phase space point defines what we mean by N jets at higher orders in perturbation theory. Note that beyond LO, both the cumulant $\mathrm{d}\sigma/\mathrm{d}\Phi_N(\mathcal{T}^{\mathrm{cut}})$ and spectrum $\mathrm{d}\sigma/\mathrm{d}\Phi_{N+1}(\mathcal{T})$ must be well-defined jet cross sections; i.e., they require a specific IR-safe projection from $\Phi_{\geq k+1}$ to Φ_k for both $k = N$ and $k = N+1$. We will see below where this definition enters. Using eq. (3.29) at the next-higher perturbative accuracy requires us to combine the higher-order resummation in $\mathcal{T}$ for the cumulant and spectrum with the fully exclusive N-jet and $(N+1)$-jet fixed-order calculations at NLO_N and NLO_{N+1}. To achieve this, we have to construct appropriate expressions for the cumulant $\mathrm{d}\sigma/\mathrm{d}\Phi_N(\mathcal{T}^{\mathrm{cut}})$ and the spectrum $\mathrm{d}\sigma/\mathrm{d}\Phi_{N+1}(\mathcal{T})$, which we do in the next two subsections.

3.2.2.1 Matched cumulant

We start by discussing the cumulant in eq. (3.29). Since the resummation is naturally differential in the $\mathrm{d}\Phi_N$ of the underlying Born process, we can combine the resummed result with the fixed-order one by adding the fixed-order nonsingular contributions to it,

$$\frac{\mathrm{d}\sigma}{\mathrm{d}\Phi_N}(\mathcal{T}^{\mathrm{cut}}) = \frac{\mathrm{d}\sigma^{\mathrm{resum}}}{\mathrm{d}\Phi_N}(\mathcal{T}^{\mathrm{cut}}) + \left[\frac{\mathrm{d}\sigma^{\mathrm{FO}}}{\mathrm{d}\Phi_N}(\mathcal{T}^{\mathrm{cut}}) - \frac{\mathrm{d}\sigma^{\mathrm{resum}}}{\mathrm{d}\Phi_N}(\mathcal{T}^{\mathrm{cut}})\bigg|_{\mathrm{FO}}\right]. \tag{3.30}$$

The first term contains the resummed contributions, while the difference of the two terms in square brackets provides the remaining nonsingular corrections that have not already been included in the resummation. The NLO_N fixed-order result is given by

$$\frac{\mathrm{d}\sigma^{\mathrm{NLO}}}{\mathrm{d}\Phi_N}(\mathcal{T}^{\mathrm{cut}}) = B_N(\Phi_N) + V_N(\Phi_N) + \int \mathrm{d}\mathcal{T}\theta(\mathcal{T} < \mathcal{T}^{\mathrm{cut}}) \int \frac{\mathrm{d}\Phi_{N+1}}{\mathrm{d}\Phi_N \mathrm{d}\mathcal{T}}\, B_{N+1}(\Phi_{N+1})\,, \tag{3.31}$$

where B_N and B_{N+1} are the N-parton and $(N+1)$-parton tree-level (Born) contributions, V_N is the N-parton one-loop virtual correction, and we abbreviated

$$\frac{\mathrm{d}\Phi_{N+1}}{\mathrm{d}\Phi_N \mathrm{d}\mathcal{T}} \equiv \mathrm{d}\Phi_{N+1}\, \delta[\mathcal{T} - \mathcal{T}(\Phi_{N+1})]\, \delta[\Phi_N - \Phi_N(\Phi_{N+1})]\,. \tag{3.32}$$

Here, $\mathcal{T}(\Phi_{N+1})$ implements the definition of $\mathcal{T}$. The NLO_N result also depends on the projection from Φ_{N+1} to Φ_N, i.e., the precise NLO definition of Φ_N. However, this dependence only appears in the nonsingular corrections. For a given definition of $\mathcal{T}$, the singular NLO corrections do not depend on how the remaining Φ_{N+1} phase space is projected onto Φ_N, since they arise from the IR limit in which all (IR-safe) definitions agree. In eq. (3.30), the singular contributions inside the full fixed-order cumulant, $\mathrm{d}\sigma^{\mathrm{FO}}/\mathrm{d}\Phi_N(\mathcal{T}^{\mathrm{cut}})$ are canceled by the NLO expansion of the resummed result at NLL'_σ or higher, leaving only the nonsingular fixed-order contributions in square brackets.

3.2.2.2 Matched spectrum

To properly combine the higher-order resummation in $\mathcal{T}$ with the fully differential $(N+1)$-jet fixed-order calculation, the inclusive $(N+1)$-jet spectrum $\mathrm{d}\sigma/\mathrm{d}\Phi_{N+1}(\mathcal{T})$ in eq. (3.29) has to fulfill two basic matching conditions,

$$\text{Condition 1:} \qquad \int \frac{\mathrm{d}\Phi_{N+1}}{\mathrm{d}\Phi_N \mathrm{d}\mathcal{T}} \frac{\mathrm{d}\sigma}{\mathrm{d}\Phi_{N+1}}(\mathcal{T}) = \frac{\mathrm{d}\sigma}{\mathrm{d}\Phi_N\, \mathrm{d}\mathcal{T}}\,, \tag{3.33}$$

$$\text{Condition 2:} \qquad \frac{\mathrm{d}\sigma}{\mathrm{d}\Phi_{N+1}}(\mathcal{T})\bigg|_{\mathrm{FO}} = \frac{\mathrm{d}\sigma^{\mathrm{FO}}}{\mathrm{d}\Phi_{N+1}}\,. \tag{3.34}$$

The first condition states that integrating the fully differential spectrum over the additional radiative phase space has to reproduce the correct spectrum in $\mathcal{T}$ including the desired resummation and fixed-order nonsingular corrections, such that eq. (3.29) reproduces eq. (3.26). The second condition states that the fixed-order expansion of the fully differential spectrum has to reproduce the full $(N+1)$-jet fixed-order calculation, where at NLO_{N+1},

$$\frac{\mathrm{d}\sigma^{\mathrm{NLO}}}{\mathrm{d}\Phi_{N+1}} = B_{N+1}(\Phi_{N+1}) + V_{N+1}(\Phi_{N+1}) + \int \frac{\mathrm{d}\Phi_{N+2}}{\mathrm{d}\Phi_{N+1}}\, B_{N+2}(\Phi_{N+2})\,. \tag{3.35}$$

Here, B_{N+1} and B_{N+2} are the $(N+1)$-parton and $(N+2)$-parton tree-level (Born) contributions, and V_{N+1} is the $(N+1)$-parton one-loop virtual correction. Integrating over $\mathrm{d}\Phi_{N+2}$ in the last term now requires a projection from Φ_{N+2} to Φ_{N+1},

$$\frac{\mathrm{d}\Phi_{N+2}}{\mathrm{d}\Phi_{N+1}} \equiv \mathrm{d}\Phi_{N+2}\, \delta[\Phi_{N+1} - \Phi_{N+1}(\Phi_{N+2})]\,, \tag{3.36}$$

analogous to eq. (1.11), which now defines precisely what we mean by $N+1$ jets at NLO.

In principle, there is some freedom to construct an expression for $\mathrm{d}\sigma/\mathrm{d}\Phi_{N+1}(\mathcal{T})$ that satisfies both conditions to the order one is working. Our master formula to combine the resummed spectrum $\mathrm{d}\sigma^{\mathrm{resum}}/\mathrm{d}\Phi_N\mathrm{d}\mathcal{T}$ with the fully differential $\mathrm{d}\sigma^{\mathrm{FO}}/\mathrm{d}\Phi_{N+1}$ is given by

$$\frac{\mathrm{d}\sigma}{\mathrm{d}\Phi_{N+1}}(\mathcal{T}) = \frac{\mathrm{d}\sigma^{\mathrm{FO}}}{\mathrm{d}\Phi_{N+1}}\left[\frac{\mathrm{d}\sigma^{\mathrm{resum}}}{\mathrm{d}\Phi_N\mathrm{d}\mathcal{T}}\bigg/\frac{\mathrm{d}\sigma^{\mathrm{resum}}}{\mathrm{d}\Phi_N\,\mathrm{d}\mathcal{T}}\bigg|_{\mathrm{FO}}\right]. \tag{3.37}$$

Expanding the right-hand side to a given fixed order, we can see immediately that Condition 2 is satisfied by construction. Imposing Condition 1 yields the consistency (or "matching") condition

$$\frac{\mathrm{d}\sigma}{\mathrm{d}\Phi_N\mathrm{d}\mathcal{T}} = \left[\frac{\mathrm{d}\sigma^{\mathrm{FO}}}{\mathrm{d}\Phi_N\mathrm{d}\mathcal{T}}\bigg/\frac{\mathrm{d}\sigma^{\mathrm{resum}}}{\mathrm{d}\Phi_N\mathrm{d}\mathcal{T}}\bigg|_{\mathrm{FO}}\right]\frac{\mathrm{d}\sigma^{\mathrm{resum}}}{\mathrm{d}\Phi_N\mathrm{d}\mathcal{T}}\,. \tag{3.38}$$

If the resummed result already has the nonsingular contributions at the desired fixed order added in, then the term in brackets is by construction equal to unity for any value of $\mathcal{T}$. Otherwise, the expansion of the resummed result reproduces the singular terms of the full fixed-order result, leaving the nonsingular fixed-order contributions, such that we get

$$\frac{\mathrm{d}\sigma}{\mathrm{d}\Phi_N\mathrm{d}\mathcal{T}} = \frac{\mathrm{d}\sigma^{\mathrm{sing,resum}}}{\mathrm{d}\Phi_N\mathrm{d}\mathcal{T}} + \frac{\mathrm{d}\sigma^{\mathrm{nons}}}{\mathrm{d}\Phi_N\mathrm{d}\mathcal{T}}\left[\frac{\mathrm{d}\sigma^{\mathrm{sing,resum}}}{\mathrm{d}\Phi_N\mathrm{d}\mathcal{T}}\bigg/\frac{\mathrm{d}\sigma^{\mathrm{sing}}}{\mathrm{d}\Phi_N\mathrm{d}\mathcal{T}}\right]. \tag{3.39}$$

Here, $\mathrm{d}\sigma^{\mathrm{sing,resum}}$ denotes the pure resummed result only containing the resummation of the singular contributions. Hence, eq. (3.37) not only multiplies in the additional dependence on Φ_{N+1}/Φ_N at fixed order, but if needed also adds the nonsingular corrections to the spectrum multiplied by the higher-order resummation factor. (Note that for the expansion of the resummed result to indeed reproduce all the singular terms at the desired fixed order, the resummation has to be carried out to sufficiently high order, which we have already seen in section 3.2.1.)

To apply Condition 1, we have to integrate eq. (3.35) using the projection onto Φ_N and $\mathcal{T}$ in eq. (3.32). Therefore, to get the correct $\mathcal{T}$ spectrum at NLO_{N+1}, the projection in eq. (3.36) has to satisfy

$$\mathcal{T}[\Phi_{N+1}(\Phi_{N+2})] = \mathcal{T}(\Phi_{N+2})\,; \tag{3.40}$$

i.e., it has to preserve the value of $\mathcal{T}$ when constructing the projected Φ_{N+1} point. Usually, the simplest way to handle this would be to use the left-hand side to define $\mathcal{T}(\Phi_{N+2})$. However, in our case, eq. (3.40) provides a very nontrivial condition on the projection since $\mathcal{T}(\Phi_{N+2})$ is already defined by our choice of jet resolution variable, which in particular has to be resummable. This turns out to be a nontrivial technical challenge one has to overcome to be able to satisfy Condition 1. We will see where this enters in section 3.3.1.2 and section 3.4.1.2.

	inclusive N-jet		exclusive N-jet		inclusive $(N+1)$-jet	
notation	fixed order	accuracy	log. order	accuracy	fixed order	accuracy
$\mathrm{LL}_{\mathcal{T}}$+$\mathrm{LO}_{N+1}$	LO_N	~ 1	LL	$\sim \alpha_s^{-1/2}$	LO_{N+1}	~ 1
$\mathrm{NLL}_{\mathcal{T}}$	LO_N	~ 1	NLL	~ 1	-	-
$\mathrm{NLL}_{\mathcal{T}}$+$\mathrm{LO}_{N+1}$	LO_N	~ 1	NLL	~ 1	LO_{N+1}	~ 1
$\mathrm{NLL}'_{\mathcal{T}}$+$\mathrm{LO}_{N+1}$	NLO_N	$\sim \alpha_s$	NLL$'$	$\sim \alpha_s^{1/2}$	LO_{N+1}	~ 1
$\mathrm{NNLL}_{\mathcal{T}}$+$\mathrm{NLO}_{N+1}$	NLO_N	$\sim \alpha_s$	NNLL	$\sim \alpha_s$	NLO_{N+1}	$\sim \alpha_s$
$\mathrm{NNLL}'_{\mathcal{T}}$+$\mathrm{NLO}_{N+1}$	NLO_N	$\sim \alpha_s$	NNLL$'$	$\sim \alpha_s^{3/2}$	NLO_{N+1}	$\sim \alpha_s$

Table 3.1: Fixed and resummation orders and their achieved accuracy in α_s.

Note that to ensure that the resummation factor in square brackets in eq. (3.37) is well behaved in the fixed-order region at large $\mathcal{T}$, it is important to turn off the resummation such that the ratio of the resummed spectrum and its expansion becomes $\mathcal{O}(1)$ up to higher fixed-order corrections. In principle, the fixed-order result in the denominator can also become negative at very small values of $\mathcal{T}$. This is not a problem in practice, since this region is explicitly avoided by imposing the cut $\mathcal{T} > \mathcal{T}^{\mathrm{cut}}$.

3.2.2.3 Perturbative accuracy and order counting

The appropriate order counting in the resummation and fixed-order regions is precisely the same as in section 3.2.1, so there is no need to repeat it here. Applying eq. (3.37) at the very lowest order, namely LL_σ resummation with LO_{N+1} fixed-order corrections, we get

$$\left.\frac{\mathrm{d}\sigma_{\geq N+1}}{\mathrm{d}\Phi_{N+1}}\right|_{\mathcal{T}>0} = B_{N+1}(\Phi_{N+1})\,\exp\Big[\frac{c_{11}}{2}\,\alpha_s L^2\Big]\,, \tag{3.41}$$

where $B_{N+1}(\Phi_{N+1})$ scales as $\alpha_s/\mathcal{T}$ relative to $B_N(\Phi_N)$ at small $\mathcal{T}$, and we used that at LL_σ the ratio in brackets in eq. (3.37) is just the resummation exponent. This directly corresponds to the CKKW-L procedure [4, 5, 6, 10], which multiplies the tree-level matrix elements with the shower Sudakov factors. Hence, we can think of our master formula eq. (3.37) as a consistent extension of this to higher orders.

As demonstrated in section 3.2.1, going to the next higher perturbative accuracy in all phase space regions requires the NLL'_σ and NNLL_σ series of logarithms. We obtain these by performing the full NLL$'$ and NNLL resummation in the exponent, as well as the fixed NLO_N and NLO_{N+1} corrections in the cumulant and spectrum, respectively. The resummation naturally connects both jet multiplicities, since the NLO_N corrections are included in the cumulant and are part of the resummation for the spectrum starting at NLL$'$, where they effectively predict the singular NLO_{N+1} contributions, and the full NLO_{N+1} corrections are obtained by adding the nonsingular corrections to the spectrum. In the following, we will use the notation (N)$\mathrm{NLL}'_{\mathcal{T}}$+(N)$\mathrm{LO}_{N+1}$ to

indicate the resummation order for the employed jet resolution variable together with the $(N+1)$-jet fixed order. For simplicity, we do not explicitly denote the N-jet fixed order and keep it implicit in the resummation order, i.e., LO_N at (N)LL and NLO_N at NLL$'$ and above. This is summarized in Table 3.1.

An immediate and important question to ask is to what accuracy resummed spectra for jet resolution variables other than $\mathcal{T}$ are predicted in our approach. A detailed theoretical investigation of the formal resummation order one attains for other variables would be very interesting but is beyond the scope of this thesis. What is certainly clear is that other variables will not be resummed at the same formal level as the primary jet resolution variable $\mathcal{T}$ itself. However, we know that other variables are correct to NLO_{N+1}, while at the same time, the inclusive cross section is not changed, as it is independent of which variable one integrates over. This implies that the NLO_{N+1} corrections for other variables do not induce uncanceled, higher-order logarithmic terms as in eq. (3.24), and hence, some higher-order resummation must be partially retained for other observables as well. Numerically, the higher-order resummation in $\mathcal{T}$ provides an improved weighting of the IR region of phase space, from which other variables are expected to benefit as well. We can validate to what accuracy other variables are obtained by comparing predictions from our highest order to the analytically resummed results for other observables, which we do in section 3.3.3.

3.2.3 Extension to more jet multiplicities

The method proposed in this chapter is completely general and can be extended to more jet multiplicities essentially by iterating the procedure discussed in section 3.2.2. We start by introducing separate jet resolution variables $\mathcal{T}_N$ to distinguish N from $N+1$ jets, $\mathcal{T}_{N+1}$ to distinguish $N+1$ from $N+2$ jets, and so on. One can choose any IR-safe observable that goes to zero in the limit of N pencil-like jets. For each N, the inclusive N-jet cross section is obtained by combining the cumulant and spectrum for $\mathcal{T}_N$ as in eq. (3.29),

$$\begin{aligned}
\frac{\mathrm{d}\sigma_{\mathrm{incl}}}{\mathrm{d}\Phi_N} &= \frac{\mathrm{d}\sigma}{\mathrm{d}\Phi_N}(\mathcal{T}_N^{\mathrm{cut}}) + \int \frac{\mathrm{d}\Phi_{N+1}}{\mathrm{d}\Phi_N}\,\frac{\mathrm{d}\sigma}{\mathrm{d}\Phi_{N+1}}(\mathcal{T}_N)\,\theta(\mathcal{T}_N > \mathcal{T}_N^{\mathrm{cut}})\,,\\
\frac{\mathrm{d}\sigma_{\mathrm{incl}}}{\mathrm{d}\Phi_{N+1}} &= \frac{\mathrm{d}\sigma}{\mathrm{d}\Phi_{N+1}}(\mathcal{T}_{N+1}^{\mathrm{cut}}) + \int \frac{\mathrm{d}\Phi_{N+2}}{\mathrm{d}\Phi_{N+1}}\,\frac{\mathrm{d}\sigma}{\mathrm{d}\Phi_{N+2}}(\mathcal{T}_{N+1})\,\theta(\mathcal{T}_{N+1} > \mathcal{T}_{N+1}^{\mathrm{cut}})\,,\\
&\vdots\\
\frac{\mathrm{d}\sigma_{\mathrm{incl}}}{\mathrm{d}\Phi_{N_{\mathrm{max}}}} &= \frac{\mathrm{d}\sigma}{\mathrm{d}\Phi_{N_{\mathrm{max}}}}(\mathcal{T}_{N_{\mathrm{max}}}^{\mathrm{cut}} \to \infty)\,.
\end{aligned} \tag{3.42}$$

The exception is the highest jet multiplicity, N_{max}, for which $\mathcal{T}_{N_{\mathrm{max}}}^{\mathrm{cut}} = \infty$, corresponding to the fact that no additional jets are resolved.

For the cumulants in eq. (3.42), the discussion in section 3.2.2.1 applies separately for each N, so the cumulants matched to higher resummed and fixed order are given,

as in eq. (3.30), by

$$\frac{\mathrm{d}\sigma}{\mathrm{d}\Phi_N}(\mathcal{T}_N^{\mathrm{cut}}) = \frac{\mathrm{d}\sigma^{\mathrm{resum}}}{\mathrm{d}\Phi_N}(\mathcal{T}_N^{\mathrm{cut}}) + \left[\frac{\mathrm{d}\sigma^{\mathrm{FO}}}{\mathrm{d}\Phi_N}(\mathcal{T}_N^{\mathrm{cut}}) - \frac{\mathrm{d}\sigma^{\mathrm{resum}}}{\mathrm{d}\Phi_N}(\mathcal{T}_N^{\mathrm{cut}})\bigg|_{\mathrm{FO}}\right]. \tag{3.43}$$

The fully differential $\mathcal{T}_N$ spectra $\mathrm{d}\sigma/\mathrm{d}\Phi_{N+1}(\mathcal{T}_N)$ are now obtained recursively as follows. We start with the highest jet multiplicity, $N_{\max}$, for which no resummation is needed since $\mathcal{T}_{N_{\max}}^{\mathrm{cut}}$ is essentially removed. Furthermore, the highest jet multiplicity is, by construction, only required at leading order, where the result is simply given by the Born contribution,

$$\frac{\mathrm{d}\sigma}{\mathrm{d}\Phi_{N_{\max}}}(\mathcal{T}_{N_{\max}}^{\mathrm{cut}} \to \infty) = \frac{\mathrm{d}\sigma^{\mathrm{LO}}}{\mathrm{d}\Phi_{N_{\max}}} = B_{N_{\max}}(\Phi_{N_{\max}})\,. \tag{3.44}$$

For each $N < N_{\max}$, we apply the discussion in section 3.2.2.2. To combine the resummation in $\mathcal{T}_N$ with the $(N+1)$-jet fixed-order calculation, the fully differential $\mathcal{T}_N$ spectrum $\mathrm{d}\sigma/\mathrm{d}\Phi_{N+1}(\mathcal{T}_N)$ must satisfy the matching conditions as in eqs. (3.33) and (3.34),

$$\int \frac{\mathrm{d}\Phi_{N+1}}{\mathrm{d}\Phi_N \mathrm{d}\mathcal{T}_N} \frac{\mathrm{d}\sigma}{\mathrm{d}\Phi_{N+1}}(\mathcal{T}_N) = \frac{\mathrm{d}\sigma}{\mathrm{d}\Phi_N \mathrm{d}\mathcal{T}_N}\,, \tag{3.45}$$

$$\frac{\mathrm{d}\sigma}{\mathrm{d}\Phi_{N+1}}(\mathcal{T}_N)\bigg|_{\mathrm{FO}} = \frac{\mathrm{d}\sigma^{\mathrm{FO}}}{\mathrm{d}\Phi_{N+1}}\,. \tag{3.46}$$

These can be satisfied by a straightforward generalization of eq. (3.37),

$$\frac{\mathrm{d}\sigma}{\mathrm{d}\Phi_{N+1}}(\mathcal{T}_N) = \frac{\mathrm{d}\sigma_{\mathrm{incl}}}{\mathrm{d}\Phi_{N+1}} \left[\frac{\mathrm{d}\sigma^{\mathrm{resum}}}{\mathrm{d}\Phi_N \mathrm{d}\mathcal{T}_N} \bigg/ \frac{\mathrm{d}\sigma^{\mathrm{resum}}}{\mathrm{d}\Phi_N \mathrm{d}\mathcal{T}_N}\bigg|_{\mathrm{FO}}\right]. \tag{3.47}$$

The prefactor on the right-hand side is now the inclusive $(N+1)$-jet cross section from eq. (3.42). This is what ties together the different jet multiplicities. The condition in eq. (3.46) now leads to the consistency condition

$$\frac{\mathrm{d}\sigma_{\mathrm{incl}}}{\mathrm{d}\Phi_{N+1}}\bigg|_{\mathrm{FO}} = \frac{\mathrm{d}\sigma^{\mathrm{FO}}}{\mathrm{d}\Phi_{N+1}}\,, \tag{3.48}$$

which states that for each N, the cumulant and spectrum in $\mathcal{T}_{N+1}$ must be included to sufficiently high order so as to reproduce the $(N+1)$-jet fixed order that is required by the $\mathcal{T}_N$ spectrum. Imposing the condition in eq. (3.45) yields the consistency condition for the $\mathcal{T}_N$ spectrum,

$$\frac{\mathrm{d}\sigma}{\mathrm{d}\Phi_N \mathrm{d}\mathcal{T}_N} = \left[\int \frac{\mathrm{d}\Phi_{N+1}}{\mathrm{d}\Phi_N \mathrm{d}\mathcal{T}_N} \frac{\mathrm{d}\sigma_{\mathrm{incl}}}{\mathrm{d}\Phi_{N+1}} \bigg/ \frac{\mathrm{d}\sigma^{\mathrm{resum}}}{\mathrm{d}\Phi_N \mathrm{d}\mathcal{T}_N}\bigg|_{\mathrm{FO}}\right] \frac{\mathrm{d}\sigma^{\mathrm{resum}}}{\mathrm{d}\Phi_N \mathrm{d}\mathcal{T}_N}\,, \tag{3.49}$$

which is the generalization of eq. (3.38). To satisfy eq. (3.48) at NLO_{N+1}, it requires that

$$\mathcal{T}_N[\Phi_{N+1}(\Phi_{N+2})] = \mathcal{T}_N(\Phi_{N+2})\,, \tag{3.50}$$

as in eq. (3.40). That is, for each N, the projection from Φ_{N+2} to Φ_{N+1} which defines the $(N+1)$-jet cross section at NLO has to preserve the value of $\mathcal{T}_N$. In addition, eq. (3.49) requires that, upon integration, the $\mathcal{T}_{N+1}$ resummation contained in $\mathrm{d}\sigma_{\mathrm{incl}}/\mathrm{d}\Phi_{N+1}$ does not interfere with the $\mathcal{T}_N$ resummation, e.g., by inducing higher-order logarithms in $\mathcal{T}_N$. Since eq. (3.42) relates the $\mathrm{d}\sigma^{\mathrm{incl}}/\mathrm{d}\Phi_N$ to $\mathrm{d}\sigma/\mathrm{d}\Phi_{N+1}(\mathcal{T}_N)$, the relationship in eq. (3.47) gives rise to a recursive definition, which when combined with the result for the highest jet multiplicity in eq. (3.44) determines $\mathrm{d}\sigma/\mathrm{d}\Phi_{N+1}(\mathcal{T}_N)$ for all N.

In the Monte Carlo implementation, the phase space is split up recursively as

$$\begin{aligned}
\frac{\mathrm{d}\sigma^{\mathrm{MC}}_{\geq N}}{\mathrm{d}\Phi_N} &= \frac{\mathrm{d}\sigma^{\mathrm{MC}}_{N}}{\mathrm{d}\Phi_N}(\mathcal{T}_N^{\mathrm{cut}}) + \int \frac{\mathrm{d}\Phi_{N+1}}{\mathrm{d}\Phi_N}\,\frac{\mathrm{d}\sigma^{\mathrm{MC}}_{\geq N+1}}{\mathrm{d}\Phi_{N+1}}\,\theta(\mathcal{T}_N > \mathcal{T}_N^{\mathrm{cut}})\,,\\
\frac{\mathrm{d}\sigma^{\mathrm{MC}}_{\geq N+1}}{\mathrm{d}\Phi_{N+1}} &= \frac{\mathrm{d}\sigma^{\mathrm{MC}}_{N+1}}{\mathrm{d}\Phi_{N+1}}(\mathcal{T}_{N+1}^{\mathrm{cut}}) + \int \frac{\mathrm{d}\Phi_{N+2}}{\mathrm{d}\Phi_{N+1}}\,\frac{\mathrm{d}\sigma^{\mathrm{MC}}_{\geq N+2}}{\mathrm{d}\Phi_{N+2}}\,\theta(\mathcal{T}_{N+1} > \mathcal{T}_{N+1}^{\mathrm{cut}})\,,\\
&\vdots\,,
\end{aligned} \tag{3.51}$$

where in each step, the total cross section for N or more jets is separated into an exclusive N-jet cross section, which is assigned to partonic events with N final-state partons, and the integral over the remaining cross section for $N+1$ or more jets. For the highest multiplicity, N_{max}, the remaining cross section for N_{max} or more jets is represented by events with N_{max} final-state partons.

Note that the structure of eq. (3.51) is very similar to eq. (3.42). The crucial difference is that in eq. (3.51), each inclusive cross section on the left-hand side is the same that appears under the integral on the right-hand side in the line above. By comparing eq. (3.51) with eq. (3.42) and repeatedly inserting eq. (3.47), we obtain the higher-order, "fully resummed," exclusive N-jet cross sections that serve as inputs to the Monte Carlo. Abbreviating the resummation factor in eq. (3.47) as

$$U_N(\Phi_N, \mathcal{T}_N) = \frac{\mathrm{d}\sigma^{\mathrm{resum}}}{\mathrm{d}\Phi_N \mathrm{d}\mathcal{T}_N} \Bigg/ \left.\frac{\mathrm{d}\sigma^{\mathrm{resum}}}{\mathrm{d}\Phi_N \mathrm{d}\mathcal{T}_N}\right|_{\mathrm{FO}}\,, \tag{3.52}$$

we obtain

$$\begin{aligned}
\frac{\mathrm{d}\sigma^{\mathrm{MC}}_{N}}{\mathrm{d}\Phi_N}(\mathcal{T}_N^{\mathrm{cut}}) &= \frac{\mathrm{d}\sigma}{\mathrm{d}\Phi_N}(\mathcal{T}_N^{\mathrm{cut}})\,,\\
\frac{\mathrm{d}\sigma^{\mathrm{MC}}_{N+1}}{\mathrm{d}\Phi_{N+1}}(\mathcal{T}_{N+1}^{\mathrm{cut}}) &= \frac{\mathrm{d}\sigma}{\mathrm{d}\Phi_{N+1}}(\mathcal{T}_{N+1}^{\mathrm{cut}})\,U_N(\Phi_N, \mathcal{T}_N)\,,\\
&\vdots
\end{aligned}$$

$$\frac{\mathrm{d}\sigma^{\mathrm{MC}}_{\geq N_{\max}}}{\mathrm{d}\Phi_{N_{\max}}} = \frac{\mathrm{d}\sigma}{\mathrm{d}\Phi_{N_{\max}}}(\mathcal{T}^{\mathrm{cut}}_{N_{\max}} \to \infty)\, U_N(\Phi_N, \mathcal{T}_N)\, U_{N+1}(\Phi_{N+1}, \mathcal{T}_{N+1}) \times \cdots \times U_{N_{\max}-1}(\Phi_{N_{\max}-1}, \mathcal{T}_{N_{\max}-1})\,. \tag{3.53}$$

The careful reader will have noticed that the above is in one-to-one correspondence to the structure generated by a parton shower with up to $N_{\max}$ emissions. The crucial difference is that, in our case, all ingredients are well-defined physical jet cross sections defined in terms of a global jet resolution variable. This allows us to systematically increase the perturbative accuracy by computing the relevant ingredients to higher order in resummed and fixed-order perturbation theory as well as to systematically estimate the perturbative uncertainties. The analogous parton-shower-like structure underlies the CKKW-L ME/PS merging, which replaces the splitting functions in the shower with the full tree-level matrix elements. Restricting eq. (3.53) to the lowest order as in eq. (3.41), it reduces to the ME/PS merging as a special case.

In principle, the above construction allows us to go to even higher fixed and resummation order, as long as the fixed-order ingredients are available and the resummation is known to a correspondingly high enough order. It also lets us combine as many jet multiplicities as we like at the order they are available. In particular, it is straightforward to add additional multiplicities at the lowest accuracy in a CKKW-L-like fashion.

3.2.4 Attaching parton showering and hadronization

In the Monte Carlo, a point in Φ_N is represented by N (massless) four-vectors together with the appropriate flavor information. We then generate events with N to $N_{\max}$ partons and assign the N-parton events the weight $\mathrm{d}\sigma^{\mathrm{MC}}_N/\mathrm{d}\Phi_N(\mathcal{T}^{\mathrm{cut}}_N)$, the $(N+1)$-parton events the weight $\mathrm{d}\sigma^{\mathrm{MC}}_{N+1}/\mathrm{d}\Phi_{N+1}(\mathcal{T}^{\mathrm{cut}}_{N+1})$, and so on. The events with $N_{\max}$ partons are assigned the weight $\mathrm{d}\sigma^{\mathrm{MC}}_{\geq N_{\max}}/\mathrm{d}\Phi_{N_{\max}} = B_{N_{\max}}(\Phi_{N_{\max}})$. The $\theta(\mathcal{T}_N > \mathcal{T}^{\mathrm{cut}}_N)$ functions in eq. (3.51) are included in the weight, which means that all events with $\geq N+1$ partons that have $\mathcal{T}_N < \mathcal{T}^{\mathrm{cut}}_N$ get zero weight.[9] In this way, by summing up the weights of all events, we can integrate up the cross sections in eq. (3.51), including arbitrary kinematic cuts in Φ_N, Φ_{N+1}, etc. What is important is that, although the events contain massless partons, they represent the exclusive jet cross sections of eq. (3.53). (From the resummation point of view, the massless partons represent the kinematics of the hard function.)

In the next step, the events are given as a starting point to a parton shower, whose purpose it is to fill up the jets with additional emissions inside the jets without changing the weight of the event. Formally, this means that the shower should not be allowed to change the underlying distribution in the jet resolution variable,

[9] Technically, the split up of phase space is usually flavor-aware. This means that an event with $\mathcal{T}_N < \mathcal{T}^{\mathrm{cut}}_N$ is only set to zero if the closest two partons produce a QCD singularity.

since this has already been computed at the higher perturbative accuracy. For example, starting from an event with $N+1$ partons with kinematics Φ_{N+1} and weight $\mathrm{d}\sigma^{\mathrm{MC}}_{N+1}/\mathrm{d}\Phi_{N+1}(\mathcal{T}^{\mathrm{cut}}_{N+1})$, the fully showered event should have the same jet kinematics Φ_{N+1} as the unshowered event from which it originated. Most importantly, the showered event should have the same value of $\mathcal{T}_N(\Phi_{N+1})$ and should have $\mathcal{T}_{N+1} < \mathcal{T}^{\mathrm{cut}}_{N+1}$ so it still has the correct weight $\mathrm{d}\sigma^{\mathrm{MC}}_{N+1}/\mathrm{d}\Phi_{N+1}(\mathcal{T}^{\mathrm{cut}}_{N+1})$. In the cumulant N-jet bin, the shower is allowed to fill out the phase space from $\mathcal{T}_N = 0$ to $\mathcal{T}^{\mathrm{cut}}_N$. Since for the highest jet multiplicity, $\mathcal{T}^{\mathrm{cut}}_{N_{\mathrm{max}}} \to \infty$, the shower fills out the remaining phase space. In practice, these are quite nontrivial constraints on the shower. The easiest way to enforce them is to repeatedly run the shower on the same event until it produces an acceptable showered event, where we allow the value of $\mathcal{T}_N$ to be changed at most by a numerically small amount consistent with a power correction. This method is of course computationally intensive (though it is not computationally prohibitive), since one may have to rerun the shower many times, and it would be interesting to develop a more efficient way of constraining the shower for this purpose. Notice that in this procedure no events are discarded, so the cross section is not changed.

In the final step, the showered event is passed to the hadronization routine. In this case, there are no constraints on the kinematics of the hadronized event; i.e., the hadronization is allowed to smear out the $\mathcal{T}_N$ spectrum. The reason is that our perturbative calculation does not take into account nonperturbative effects, which are instead supplied by the hadronization. This is discussed in more detail in section 3.3.1.3.

3.3 Application to e^+e^- collisions

In this section, we apply the framework described in section 3.2 to $e^+e^- \to 2/3$ jets, implemented in the GENEVA Monte Carlo. The higher-order resummation for 2-jet event shapes in e^+e^- collisions is very well understood and many precise measurements from LEP exist, which are used, for example, for precise determinations of the strong coupling constant α_s [81, 82, 83, 84, 85, 86, 87].

In this context, one important aspect is the interplay between both resummed and fixed-order perturbative contributions with the nonperturbative corrections. Here, the GENEVA framework provides an important development by being able to combine the perturbative higher-order resummation with the nonperturbative information provided by PYTHIA's hadronization model [88, 89]. For example, this allows us to use a common theoretical framework to make predictions for different phase space regions and different observables.

The e^+e^- implementation also provides an important and powerful validation of our approach and its practical feasibility, while avoiding the additional complications arising for hadronic collisions, such as initial-state radiation and parton distribution functions (PDFs). The implementation and first results for pp collisions are presented

in section 3.4.

In our e^+e^- implementation, we use 2-jettiness, $\mathcal{T}_2$, as the 2-jet resolution variable, which is defined as [1]

$$\mathcal{T}_2 = E_{\text{cm}}\left(1 - \max_{\hat{n}} \frac{\sum_k |\hat{n}\cdot\vec{p}_k|}{\sum_k |\vec{p}_k|}\right), \tag{3.54}$$

and is simply related to thrust T [72] by $\mathcal{T}_2 = E_{\text{cm}}(1-T)$. Its kinematic limits are $0 \leq \mathcal{T}_2 \leq E_{\text{cm}}/2$. In the limit $\mathcal{T}_2 \to 0$, there are precisely 2 pencil-like jets in the final state, while for $\mathcal{T}_2 \sim E_{\text{cm}}$, there are 3 or more jets. We perform the resummation in $\mathcal{T}_2$ to NNLL$'$ and include the full NLO_2, NLO_3, and LO_4 fixed-order matrix elements, i.e., we obtain $\text{NNLL}'_{\mathcal{T}}$+$\text{NLO}_3$ predictions.

The default running parameters for our e^+e^- studies are $E_{\text{cm}} = 91.2\,\text{GeV}$, $\alpha_s(m_Z) = 0.1135$, and Pythia 8.170 with e^+e^- tune 1.[10] Using this value of $\alpha_s(m_Z)$ is motivated by the fact that it was obtained from fits to the thrust spectrum using $\text{N}^3\text{LL}'$ resummation. These fits were performed in a region (corresponding to $6\,\text{GeV} \leq \mathcal{T}_2 \leq 30\,\text{GeV}$ for our E_{cm}) where the nonperturbative corrections due to hadronization are power suppressed and can be described by a single nonperturbative parameter, which leads to a shift in the spectrum and is included in the fit in ref. [85]. We find that this value of $\alpha_s(m_Z)$, in conjunction with Pythia's tune 1, provides overall the best description of the data, including the peak region below $\mathcal{T}_2 \leq 6\,\text{GeV}$ and other 2-jet event shapes. For comparison, we show results using the world average $\alpha_s(m_Z) = 0.1184$ [90] as well as from using Pythia tune 3.

In the next subsection, we summarize the various ingredients that go into the master formula, with the intention of giving a concise and informative overview, while leaving a detailed discussion of our implementation to a separate publication. In section 3.3.2, we discuss the $\mathcal{T}_2$ spectrum, validating our implementation using analytic predictions as well as comparing our results to LEP data. In section 3.3.3, we present our results for other 2-jet variables, namely C-parameter, heavy jet mass, and jet broadening, comparing Geneva's predictions at $\text{NNLL}'_{\mathcal{T}}$+$\text{NLO}_3$ to the analytic higher-order resummation for each variable as well as to the experimental measurements. In all cases, we find good consistency and agreement with the data.

3.3.1 Ingredients

The master formula is given by

$$\frac{\mathrm{d}\sigma_{\text{incl}}}{\mathrm{d}\Phi_2} = \frac{\mathrm{d}\sigma}{\mathrm{d}\Phi_2}(\mathcal{T}_2^{\text{cut}}) + \int \frac{\mathrm{d}\Phi_3}{\mathrm{d}\Phi_2}\,\frac{\mathrm{d}\sigma}{\mathrm{d}\Phi_3}(\mathcal{T}_2)\,\theta(\mathcal{T}_2 > \mathcal{T}_2^{\text{cut}})\,, \tag{3.55}$$

[10] The α_s value used inside Pythia's parton shower is not changed from the value set in the tune. This is not inconsistent, since here the strong coupling functions as a phenomenological parameter, regulating the amount of showering.

where

$$\frac{\mathrm{d}\sigma}{\mathrm{d}\Phi_2}(\mathcal{T}_2^{\mathrm{cut}}) = \frac{\mathrm{d}\sigma^{\mathrm{resum}}}{\mathrm{d}\Phi_2}(\mathcal{T}_2^{\mathrm{cut}})\,,$$
$$\frac{\mathrm{d}\sigma}{\mathrm{d}\Phi_3}(\mathcal{T}_2) = \frac{\mathrm{d}\sigma_{\mathrm{incl}}}{\mathrm{d}\Phi_3}\left(\frac{\mathrm{d}\sigma^{\mathrm{resum}}}{\mathrm{d}\Phi_2\mathrm{d}\mathcal{T}_2}\Big/\frac{\mathrm{d}\sigma^{\mathrm{resum}}}{\mathrm{d}\Phi_2\,\mathrm{d}\mathcal{T}_2}\Big|_{\mathrm{FO}}\right). \tag{3.56}$$

Its three key ingredients are the higher-order resummation of 2-jettiness, which we include at NNLL$'_{\mathcal{T}}$+LO$_3$, the full fixed-order matrix elements at NLO$_2$, NLO$_3$, and LO$_4$, and the interface to parton showering and hadronization, for which we use Pythia 8.

Following the construction in section 3.2.3 with $N_{\mathrm{max}} = 4$, the inclusive 3-jet cross section is separated into 3 and 4 or more jet contributions using 3-jettiness, $\mathcal{T}_3$, as our 3-jet resolution variable,

$$\frac{\mathrm{d}\sigma_{\mathrm{incl}}}{\mathrm{d}\Phi_3} = \frac{\mathrm{d}\sigma}{\mathrm{d}\Phi_3}(\mathcal{T}_3^{\mathrm{cut}}) + \int\frac{\mathrm{d}\Phi_4}{\mathrm{d}\Phi_3}\,\frac{\mathrm{d}\sigma}{\mathrm{d}\Phi_4}(\mathcal{T}_3)\,\theta(\mathcal{T}_3 > \mathcal{T}_3^{\mathrm{cut}})\,. \tag{3.57}$$

For e^+e^- collisions, N-jettiness is defined by [1]

$$\mathcal{T}_N = \sum_k \min_i\big(E_k - \hat{n}_i\cdot\vec{p}_k\big)\,, \tag{3.58}$$

where $i = 1, \cdots, N$ and $\hat{n}_i$ is a unit vector along the direction of the ith jet, where the jet directions can be determined by a jet algorithm or by directly minimizing $\mathcal{T}_N$.[11] There are N pencil-like jets in the limit $\mathcal{T}_N \to 0$ and N or more jets in the limit $\mathcal{T}_N \sim E_{\mathrm{cm}}$.

As discussed in section 3.2.3, the master formula naturally incorporates the resummation of the 3-jet resolution variable in eq. (3.57) and extends to higher jet multiplicities, i.e., $N_{\mathrm{max}} > 4$. However, since our current focus is on the main conceptual development of combining the higher-order resummation with the fixed NLO matrix elements for 2 and 3 jets, we leave these extensions to future work. As we will not be interested in the $\mathcal{T}_3$ spectrum or other exclusive 3-jet observables, it is sufficient for our purposes to calculate the two terms on the right-hand side of eq. (3.57) at fixed order (i.e., we do not include resummation for $\mathcal{T}_3$). Thus, we use

$$\frac{\mathrm{d}\sigma}{\mathrm{d}\Phi_3}(\mathcal{T}_3^{\mathrm{cut}}) = \frac{\mathrm{d}\sigma^{\mathrm{FO}}}{\mathrm{d}\Phi_3}(\mathcal{T}_3^{\mathrm{cut}})\,, \qquad \frac{\mathrm{d}\sigma}{\mathrm{d}\Phi_4} = B_4(\Phi_4)\,. \tag{3.59}$$

In the results that follow, we use $\mathcal{T}_2^{\mathrm{cut}}$ value between $0.5 - 1\,\mathrm{GeV}$, which is selected randomly from a flat distribution. This smoothing out of $\mathcal{T}_2^{\mathrm{cut}}$ avoids small numerical

[11] This definition agrees with $\mathcal{T}_2$ in eq. (3.54) for massless final-state particles, which is the limit in which resummation is carried out. It does affect the nonperturbative corrections when including hadron masses [91, 92]. We use the definition of $\mathcal{T}_2$ in eq. (3.54) to be able to directly compare to the experimental data for thrust.

	Fixed-order corrections		Resummation input		
	singular	nonsingular	γ_x	Γ_{cusp}	β
LL	LO_2	-	-	1-loop	1-loop
NLL	LO_2	-	1-loop	2-loop	2-loop
NLL$'$	NLO_2	-	1-loop	2-loop	2-loop
NLL$'$+LO_3	NLO_2	LO_3	1-loop	2-loop	2-loop
NNLL+LO_3	NLO_2	LO_3	2-loop	3-loop	3-loop
NNLL$'$	NNLO_2	-	2-loop	3-loop	3-loop
NNLL$'$+NLO_3	NNLO_2	NLO_3	2-loop	3-loop	3-loop

Table 3.2: Perturbative inputs included at a given order in resummed and fixed-order perturbation theory. The columns in the resummation input refer to the noncusp anomalous dimension (γ_x), the cusp anomalous dimension (Γ_{cusp}), and the QCD beta function (β).

discontinuities that can arise with a sharp cutoff. For $\mathcal{T}_3^{\text{cut}}$, we use $\mathcal{T}_3^{\text{cut}} = 2\,\text{GeV}$. This value is chosen small enough that the NLO_3 calculation is fully exclusive and our results are insensitive to scales below $\mathcal{T}_3^{\text{cut}}$. Changing $\mathcal{T}_3^{\text{cut}}$ by a factor of two up and down, the results remain unchanged, with any variations well within our perturbative uncertainties.

3.3.1.1 Resummation

Our jet resolution variable, $\mathcal{T}_2$, has the important property that it can be factorized. The factorization theorem for the $\mathcal{T}_2$ spectrum provides the resummed prediction that is one of the primary inputs to our master formula in eq. (3.56). It is obtained by using the framework of Soft Collinear Effective Theory (SCET) [93, 94, 95, 96] and allows the resummation to be systematically carried out to higher orders and combined with the nonsingular fixed-order result. Our highest-order resummed input to the master formula has NNLL$'$ resummation. We use the standard resummation formalism, where the large logarithms are resummed in the exponent of the cross section, with the corresponding resummation orders summarized in table 3.2.

We write the jet resolution distribution in $\mathcal{T}_2$ as

$$\frac{\mathrm{d}\sigma_2^{\text{resum}}}{\mathrm{d}\Phi_2\,\mathrm{d}\mathcal{T}_2} = \frac{\mathrm{d}\sigma_2^{\text{sing}}}{\mathrm{d}\Omega_2\,\mathrm{d}\mathcal{T}_2} + \frac{\mathrm{d}\sigma_2^{\text{nons}}}{\mathrm{d}\Omega_2\,\mathrm{d}\mathcal{T}_2}\,, \tag{3.60}$$

where the separation into singular and nonsingular contributions was discussed in

section 3.2.2 [see eq. (3.27)]. The singular contribution is given by [97, 98]

$$\frac{\mathrm{d}\sigma_2^{\mathrm{sing}}}{\mathrm{d}\Omega_2\,\mathrm{d}\mathcal{T}_2} = \frac{\mathrm{d}\sigma_B}{\mathrm{d}\Omega_2}\,H_2(E_{\mathrm{cm}}^2,\mu)\int \mathrm{d}s_1\mathrm{d}s_2\,J_1(s_1,\mu)\,J_2(s_2,\mu)\,S_2\Big(\mathcal{T}_2-\frac{s_1}{E_{\mathrm{cm}}}-\frac{s_2}{E_{\mathrm{cm}}},\mu\Big)\,. \tag{3.61}$$

Here, $\mathrm{d}\Phi_2 = \mathrm{d}\Omega_2 = \mathrm{d}\cos\theta\mathrm{d}\phi$ is the angular phase space for the orientation of the thrust axis with respect to the beam, and $\mathrm{d}\sigma_B/\mathrm{d}\Omega_2$ is the tree-level 2-parton cross section. Note that the overall dependence on Ω_2 here is that of the Born cross section, which is correct in the limit $\mathcal{T}_2 \to 0$ in which eq. (3.61) is obtained. The hard function H_2 in eq. (3.61) contains the fixed-order 2-parton matrix elements, which describe the short-distance corrections at the scale E_{cm}. The jet functions J_1 and J_2 describe the back-to-back collinear final-state radiation along the thrust axis, and the soft function S_2 describes the soft radiation between the jets. The soft function contains perturbative and nonperturbative components, which can be separated as [99, 100, 101]

$$S_2(\mathcal{T}_2,\mu) = \int \mathrm{d}k\,S_2^{\mathrm{pert}}(\mathcal{T}_2-k,\mu)\,f(k,\mu)\,, \tag{3.62}$$

where $S_2^{\mathrm{pert}}(\mathcal{T}_2-k,\mu)$ is the perturbative soft function, while the shape function $f(k,\mu)$ describes the nonperturbative hadronization corrections. For $\mathcal{T}_2 \sim \Lambda_{\mathrm{QCD}}$, the shape function gives an $\mathcal{O}(1)$ contribution to the cross section, while for $\mathcal{T}_2 \gg \Lambda_{\mathrm{QCD}}$ it can be expanded, and only the leading $\mathcal{O}(\Lambda_{\mathrm{QCD}}/\mathcal{T}_2)$ nonperturbative power correction is relevant. For further discussion and the derivation of the factorization theorem, see refs. [97, 98]. The resummed prediction used in GENEVA only includes the perturbative soft function, while the nonperturbative corrections are provided by the hadronization in PYTHIA.

The nonsingular contribution in eq. (3.60) is given by the spectrum at fixed order with the singular terms subtracted. It includes all $\mathcal{O}(\mathcal{T}_2/E_{\mathrm{cm}})$ corrections to the singular distribution to a given order in α_s. The $\mathcal{O}(\alpha_s)$ nonsingular corrections in $\mathcal{T}_2$ are known analytically and can be taken from ref. [85], so we include them in our resummed result. Each function in eq. (3.61) depends on the renormalization scale μ and the characteristic scale of the physics it describes. These are $\mu_H \sim E_{\mathrm{cm}}$, $\mu_J \sim \sqrt{\mathcal{T}_2 E_{\mathrm{cm}}}$, and $\mu_S \sim \mathcal{T}_2$ for the hard, jet, and soft functions, respectively. Renormalization group evolution (RGE) between the soft, collinear, and hard scales resums the logarithms of the form $\ln\mu_S/\mu_H \sim \ln\mathcal{T}_2/E_{\mathrm{cm}}$ and $\ln\mu_J^2/\mu_H^2 \sim \ln\mathcal{T}_2/E_{\mathrm{cm}}$ in the factorized singular distribution in eq. (3.61). The anomalous dimensions and singular fixed-order corrections required at a given resummation order are summarized in table 3.2.

The resummed cumulant in eq. (3.56) is obtained in an analogous way to the resummed $\mathcal{T}_2$ distribution. It is given by a singular and nonsingular component,

$$\frac{\mathrm{d}\sigma_2^{\mathrm{resum}}}{\mathrm{d}\Phi_2}(\mathcal{T}_2^{\mathrm{cut}}) = \frac{\mathrm{d}\sigma_2^{\mathrm{sing}}}{\mathrm{d}\Omega_2}(\mathcal{T}_2^{\mathrm{cut}}) + \frac{\mathrm{d}\sigma_2^{\mathrm{nons}}}{\mathrm{d}\Omega_2}(\mathcal{T}_2^{\mathrm{cut}})\,, \tag{3.63}$$

where the singular contribution is obtained by integrating eq. (3.61) over $\mathcal{T}_2$ from 0 to $\mathcal{T}_2^{\text{cut}}$. The nonsingular contribution to the cumulant is given by the difference between the fixed-order result and the resummed singular terms expanded to fixed order.

The perturbative uncertainties in the resummed spectrum are estimated by scale variation and receive a contribution from two distinct sources, the fixed-order corrections and the higher-order logarithmic resummation. The fixed-order uncertainties are estimated by a correlated overall variation of all scales by factors of two. The resummation uncertainties are instead estimated by varying the lower scales $\mu_J(\mathcal{T}_2)$ and $\mu_S(\mathcal{T}_2)$, which are functions of $\mathcal{T}_2$, and are referred to as profile scales [101, 85, 41]. The profile scales satisfy the criteria that, in the resummation region, $\mu_{J,S}(\mathcal{T}_2)$ have their canonical scaling (given above) and in the fixed-order region, $\mu_{J,S}(\mathcal{T}_2) \sim \mu_H$, which turns off the resummation. In the transition region, the profile scales provide a smooth interpolation between the resummation and fixed-order regions. These three regions are determined based on where the fixed-order singular contributions dominate over the nonsingular ones. The variations in the profile scales subject to the above constraints determine the resummation uncertainty, where we take the largest absolute variation from the central scale. The resummation uncertainties are combined in quadrature with the fixed-order uncertainties to generate our theory uncertainty estimate. For a given partonic event in GENEVA, each profile scale variation gives rise to a different event weight, which is computed analytically. Hence, we can provide each event with its own perturbative uncertainty estimate by assigning it several weights from the profile scale variation in addition to its central weight.

3.3.1.2 Fixed order

As we can see from eqs. (3.57) and (3.59), we need the 3-jet cumulant $\mathrm{d}\sigma/\mathrm{d}\Phi_3(\mathcal{T}_3^{\text{cut}})$ as well as the Born 4-parton cross section $B_4(\Phi_4)$. The Born 4-parton cross section is trivial and requires no further discussion. To calculate the 3-jet cumulant at NLO_3, we use the generic formula given in eq. (3.35),

$$\frac{\mathrm{d}\sigma}{\mathrm{d}\Phi_3} = B_3(\Phi_3) + V_3(\Phi_3) + \int \frac{\mathrm{d}\Phi_4}{\mathrm{d}\Phi_3}\, B_4(\Phi_4)\, \theta(\mathcal{T}_3 < \mathcal{T}_3^{\text{cut}})\,, \tag{3.64}$$

where

$$\frac{\mathrm{d}\Phi_4}{\mathrm{d}\Phi_3} \equiv \mathrm{d}\Phi_4\, \delta[\Phi_3 - \Phi_3^{\mathcal{T}}(\Phi_4)]\,. \tag{3.65}$$

The projection $\Phi_3^{\mathcal{T}}(\Phi_4)$ defines what we mean by Φ_3 at NLO_3. It implicitly depends on our choice of resolution variable since eq. (3.40) requires it to satisfy

$$\mathcal{T}_2[\Phi_3^{\mathcal{T}}(\Phi_4)] = \mathcal{T}_2(\Phi_4)\,. \tag{3.66}$$

To deal with the IR singularities that are present both in V_3 and in the integral of B_4 over Φ_4, we use the FKS subtraction method [102]. We introduce a set of projecting

functions, $\theta_m^{\mathcal{T}}(\Phi_4)$, that partition the phase space into nonoverlapping regions, such that $\sum_m \theta_m^{\mathcal{T}}(\Phi_4) = 1$. In our case, this partition is effectively determined by the resolution variable, which is indicated by the superscript. The resulting partition must be such that each region m contains at most one collinear and one soft singularity. Then, we can write

$$\mathrm{d}\Phi_4 = \sum_m \mathrm{d}\Phi_3 \, \mathrm{d}\Phi_{\mathrm{rad}}^m \, \theta_m^{\mathcal{T}}(\Phi_3, \Phi_{\mathrm{rad}}^m) \,, \tag{3.67}$$

where Φ_{rad}^m denotes the radiative phase space describing a $1 \to 2$ splitting in each region.

For each region m, we define a mapping that identifies which particle in Φ_3 is undergoing the $1 \to 2$ splitting, which generates the

$$\Phi_4^m \equiv \Phi_4^m(\Phi_3, \Phi_{\mathrm{rad}}^m) \tag{3.68}$$

phase space point. It also unequivocally defines how the recoil is shared amongst the remaining particles in the event, which is needed to enforce total momentum conservation. Notice that our definition of the $\theta_m^{\mathcal{T}}$-functions leaves us the freedom to include phase space regions in the partition which do not contain any IR singularity. This freedom is in fact essential to be able to satisfy Condition 1 in eq. (3.33), namely, to ensure that in each phase space region the correct functional form for the resolution variable $\mathcal{T}_2(\Phi_4)$ is used. For example, in $e^+e^- \to q\bar{q}g$ production, the region in which the quark and antiquark are closest to each other does not contain any QCD singularity. Nevertheless, it must be treated as a separate region in the phase space partition, since in this region the invariant mass between the quark and antiquark determines the value of $\mathcal{T}_2$.

With this notation, one can write

$$\frac{\mathrm{d}\sigma}{\mathrm{d}\Phi_3} = B_3(\Phi_3) + V_3(\Phi_3) + \sum_m \int \mathrm{d}\Phi_{\mathrm{rad}}^m B_4(\Phi_4^m) \theta_m^{\mathcal{T}}(\Phi_3, \Phi_{\mathrm{rad}}^m) \theta(\mathcal{T}_3 < \mathcal{T}_3^{\mathrm{cut}}) \,. \tag{3.69}$$

If the region m contains an IR divergence, the FKS subtraction requires one to define the soft, collinear, and soft-collinear limits of Φ_{rad}^m, which we denote as $\Phi_{\mathrm{rad}}^{m,\mathrm{s}}$, $\Phi_{\mathrm{rad}}^{m,\mathrm{c}}$, and $\Phi_{\mathrm{rad}}^{m,\mathrm{cs}}$, respectively, together with the resulting points in the 4-body phase space $\Phi_4^{m,\mathrm{s}}$, $\Phi_4^{m,\mathrm{c}}$, and $\Phi_4^{m,\mathrm{cs}}$. We can then write

$$\begin{aligned} \frac{\mathrm{d}\sigma}{\mathrm{d}\Phi_3} =& B_3(\Phi_3) + V_3(\Phi_3) + I(\Phi_3) + \sum_m \int \mathrm{d}\Phi_{\mathrm{rad}}^m \Bigg[B_4(\Phi_4^m) \theta_m^{\mathcal{T}}(\Phi_3, \Phi_{\mathrm{rad}}^m) \theta(\mathcal{T}_3 < \mathcal{T}_3^{\mathrm{cut}}) \\ & - \frac{\mathrm{d}\Phi_{\mathrm{rad}}^{m,\mathrm{s}}}{\mathrm{d}\Phi_{\mathrm{rad}}^m} B_4(\Phi_4^{m,\mathrm{s}}) \theta_m^{\mathrm{s}}(\Phi_3, \Phi_{\mathrm{rad}}^{m,\mathrm{s}}) - \frac{\mathrm{d}\Phi_{\mathrm{rad}}^{m,\mathrm{c}}}{\mathrm{d}\Phi_{\mathrm{rad}}^m} B_4(\Phi_4^{m,\mathrm{c}}) + \frac{\mathrm{d}\Phi_{\mathrm{rad}}^{m,\mathrm{cs}}}{\mathrm{d}\Phi_{\mathrm{rad}}^m} B_4(\Phi_4^{m,\mathrm{cs}}) \Bigg] \,, \end{aligned} \tag{3.70}$$

where θ_m^{s} encodes the soft limit of the $\theta_m^{\mathcal{T}}$-functions and we have used the fact that in the collinear and soft-collinear limits the $\theta_m^{\mathcal{T}}$-functions are trivially satisfied. Also,

since in each of these limits $\mathcal{T}_3 \equiv 0$, the $\theta(\mathcal{T}_3 < \mathcal{T}_3^{\text{cut}})$ functions are satisfied by construction.

If m is not singular, in principle, no such subtraction is needed, and one could simply evaluate the 4-parton tree-level matrix element $B_4(\Phi_4^m)$. However, given that the integral of the subtraction counterterms over the whole phase space is known analytically for both massless and massive partons [102, 103, 17],

$$I(\Phi_3) = \sum_m \Big[\int \mathrm{d}\Phi_{\text{rad}}^{m,\text{s}} B_4(\Phi_4^{m,\text{s}}) \theta_m^{\text{s}}(\Phi_3, \Phi_{\text{rad}}^{m,\text{s}}) + \int \mathrm{d}\Phi_{\text{rad}}^{m,\text{c}} B_4(\Phi_4^{m,\text{c}}) - \int \mathrm{d}\Phi_{\text{rad}}^{m,\text{cs}} B_4(\Phi_4^{m,\text{cs}}) \Big] , \tag{3.71}$$

we found it easier not to restrict the integration of the subtraction counterterms only in the singular regions of phase space but to extend it across all of phase space.[12] This ensures the complete cancellation of and the independence of the final results from the subtraction terms. The procedure outlined above takes care of all IR divergences, making the integrand in the square brackets of eq. (3.70) as well as the sum of $V(\Phi_3) + I(\Phi_3)$ IR finite.

The crucial point, discussed in section 3.2.2.2, is that our construction requires the phase space map that generates $\Phi_4^m(\Phi_3, \Phi_{\text{rad}}^m)$ to preserve the value of $\mathcal{T}_2$; i.e.,

$$\mathcal{T}_2[\Phi_4^m(\Phi_3, \Phi_{\text{rad}}^m)] = \mathcal{T}_2(\Phi_3) \, . \tag{3.72}$$

Comparing this to eq. (3.66), we see that the map $\Phi_4^m(\Phi_3, \Phi_{\text{rad}}^m)$ must be precisely the inverse of $\Phi_3^{\mathcal{T}}(\Phi_4)$ in the region m. In principle, this condition can be relaxed to only hold up to power corrections. Additionally, the map can fail to preserve $\mathcal{T}_2$ in a region of phase space that gives a power-suppressed contribution to the cross section. The phase space maps used in the standard FKS implementations [102, 16] were not designed to preserve the value of $\mathcal{T}_2$, and thus, they change its value by an $\mathcal{O}(\mathcal{T}_3/\mathcal{T}_2)$ amount over a large region of phase space.[13] Since 4-parton events with $\mathcal{T}_3 < \mathcal{T}_3^{\text{cut}}$ and $\mathcal{T}_2 > \mathcal{T}_2^{\text{cut}}$ are the only real emission contributions included in the NLO calculation for the 3-jet cumulant, eq. (3.64), one can impose the restriction $\mathcal{T}_3^{\text{cut}} \ll \mathcal{T}_2^{\text{cut}}$ and use the standard FKS phase space maps. However, this hierarchy strongly restricts $\mathcal{T}_3^{\text{cut}}$, and it is preferable to define a map that is specifically designed for our goals. We have constructed such a map, which preserves the exact value of $\mathcal{T}_2$ up to power corrections, except in a region of phase space whose contribution to the cross section scales as $\mathcal{O}(\mathcal{T}_2/E_{\text{cm}})$. In this region, the value of $\mathcal{T}_2$ is altered by an $\mathcal{O}(\mathcal{T}_3/\mathcal{T}_2)$ amount, meaning the net correction scales as $\mathcal{O}(\mathcal{T}_3/E_{\text{cm}})$. Therefore, enforcing the much looser

[12] These integrals can also easily be defined by restricting the integration of the FKS variable ξ up to some ξ_{cut} value. These are, however, not in direct correspondence to the partition of phase space we are considering.

[13] Generically, an emission that takes a 3-parton event to a 4-parton event will change $\mathcal{T}_2$ by the scaling $\mathcal{T}_2(\Phi_4) - \mathcal{T}_2(\Phi_3) \sim \mathcal{T}_3$.

constraint $\mathcal{T}_3^{\text{cut}} \ll E_{\text{cm}}$ is sufficient to achieve our purposes. We postpone the detailed discussion of this map to a dedicated publication describing the implementation of GENEVA.

3.3.1.3 Parton shower and hadronization

The phase space points Φ_2 and Φ_3 represent jet kinematics, which are defined by the jet resolution variable 2-jettiness. As discussed in section 3.2.4, we require that the parton shower does not change the underlying hard jet distribution so that the higher-order weights we calculate, $\mathrm{d}\sigma/\mathrm{d}\Phi_2(\mathcal{T}_2^{\text{cut}})$ and $\mathrm{d}\sigma/\mathrm{d}\Phi_3(\mathcal{T}_2)$, are correctly assigned. Without any constraints the parton shower will not preserve the value of $\mathcal{T}_2$. We address this problem in our current implementation in a physically motivated way. For small $\mathcal{T}_2$, the resummed singular jet resolution spectrum dominates and is determined up to power corrections of order $\lambda \sim \mathcal{T}_2/E_{\text{cm}}$. We require that for $\Phi_{\geq 3}$ events, the change in $\mathcal{T}_2$ due to showering, $\Delta\mathcal{T}_2$, satisfies $\Delta\mathcal{T}_2/\mathcal{T}_2 < \lambda$. This represents a power correction to the 2-jettiness spectrum, which scales as $1/\mathcal{T}_2$ for small $\mathcal{T}_2$. For the 2-jet cumulant bin, we require that Φ_2 events, which have $\mathcal{T}_2 = 0$ when unshowered, remain in the 2-jet bin after showering up to a power suppressed correction, with $\mathcal{T}_2 < \mathcal{T}_2^{\text{cut}}(1 + \lambda')$. Here, the effect of a small nonzero λ' induces a change to the shape of the distribution generated by PYTHIA that scales as a power correction and does not affect the formal accuracy of the spectrum. Formally, we work in the limit where λ and λ' are effectively taken to zero. For $\lambda = 0$, the shower would be required to exactly preserve $\mathcal{T}_2$, making it maximally inefficient. Therefore, for the results shown in this section, we use small nonzero values $\lambda = 2\,\lambda' = 0.05$. We have checked that these are small enough to be in the asymptotic region where the results become independent of the precise value.

Furthermore, the shower must also be restricted to not change the NLO_3 result. This requires that, for 3-parton events, we effectively only allow showers to start from $\mathcal{T}_3^{\text{cut}}$. Likewise, we limit the showering of 4-partons events down from their $\mathcal{T}_3(\Phi_4)$ value. This can be seen as a proxy for what would be the correct approach in a $\mathcal{T}_N$-ordered shower.

We use PYTHIA 8.170 with e^+e^- tune 1 for showering and hadronization. The choice of tune for e^+e^- data in PYTHIA affects both the time-like showering and hadronization model. However, since in our implementation we restrict the shower from changing the $\mathcal{T}_2$ spectrum, the effect of changing the tune in PYTHIA primarily reflects the uncertainty from hadronization in GENEVA. We have checked that this is also the case for observables other than $\mathcal{T}_2$ by verifying that the effect of the tune on the showered GENEVA predictions is very small compared to the change due to hadronization. The uncertainty from hadronization is associated with the nonperturbative contribution to the soft function in eq. (3.62) in our framework and is not included in our event-by-event perturbative uncertainties, which are derived from the analytical resummation and fixed-order matching. A complete uncertainty

analysis should also include uncertainties due to hadronization as well as due to the remaining amount of parton showering. As an indication of the size of the uncertainty from hadronization, we also show GENEVA hadronized results using e^+e^- tune 3. The shift from the partonic to the showered results could be taken as a conservative upper limit on the remaining showering uncertainty.

It is important to note that we use the standard tunes in PYTHIA, without changing any internal parameters. Since in our approach the shower evolution in standalone PYTHIA 8 is substituted with higher-order resummation above the 2-jet resolution scale, we advocate that a separate tuning of GENEVA + PYTHIA 8 should be employed to obtain the best results. This would also allow one to obtain meaningful estimates of hadronization and remaining showering uncertainties.

3.3.2 Validation using the jet resolution spectrum

Before comparing the GENEVA prediction for various e^+e^- spectra to analytic predictions and LEP data, we first validate the implementation of our procedure to combine higher-order resummation and full NLO matrix-element corrections by using the jet resolution spectrum. At the level of the singly differential $\mathcal{T}_2$ spectrum only, the standard approach to resummation achieves the same matching between resummation and fixed order by adding the nonsingular contribution to the resummed result. This provides a nontrivial crosscheck of the master formula and in particular validates the event-by-event theory uncertainties generated by GENEVA. For each comparison in this section, we show the peak, transition, and tail regions, described in section 3.2.1, at the LEP center-of-mass energy $E_{\mathrm{cm}} = 91.2\,\mathrm{GeV}$. In all cases, the error bars or bands on the GENEVA histograms are built from its event-by-event perturbative uncertainties. The statistical uncertainties from Monte Carlo integration are much smaller and are not shown.

3.3.2.1 Partonic results

The analytic resummed $\mathcal{T}_2$ spectrum is shown in figure 3.2 at successively higher orders: NLL, NLL′+LO_3, and NNLL′+NLO_3 (see table 3.2 for the order-counting definitions). The perturbative uncertainties are generated by using the same profile scale variations employed in GENEVA and discussed in section 3.3.1.1. The theory uncertainties decrease at increasing order and demonstrate excellent convergence at all values of $\mathcal{T}_2$. Below $\mathcal{T}_2 < 0.5\,\mathrm{GeV}$, we enter the purely nonperturbative region, and the scale uncertainties diverge since even resummed perturbation theory breaks down. In the far tail, the scale uncertainties also grow rapidly, which reflects missing higher fixed-order corrections. The uncertainties in the NNLL′+NLO_3 prediction diverge past the 3-parton endpoint at $E_{\mathrm{cm}}/3$, where the fixed-order prediction is only correct at leading order for 4 partons. In the transition region, there is a smooth interpolation between the resummation and fixed-order regions.

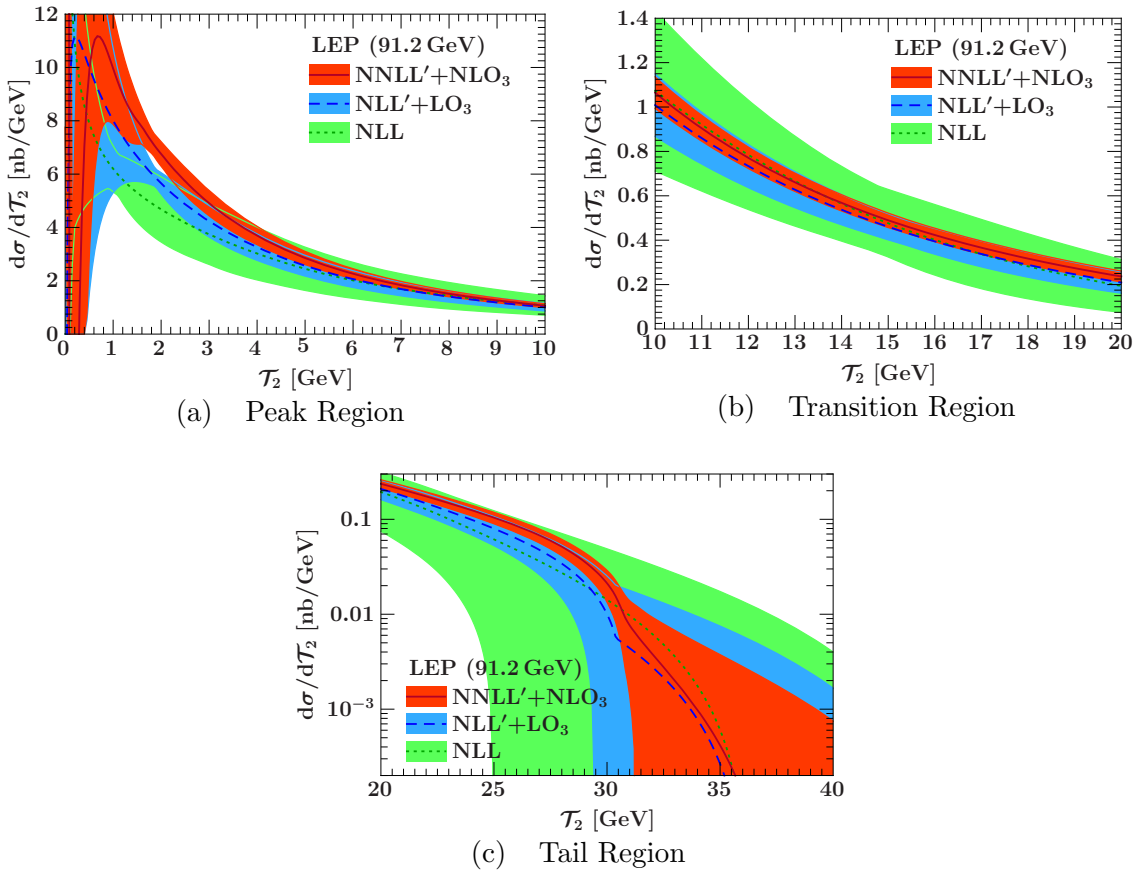

(a) Peak Region

(b) Transition Region

(c) Tail Region

Figure 3.2: Analytic resummation of $\mathcal{T}_2$ matched to fixed order. The central value is shown along with the band from scale uncertainties, as discussed in section 3.3.1.1, at NLL, NLL′+LO_3, and NNLL′+NLO_3.

In figure 3.3, we compare the partonic $\mathcal{T}_2$ spectrum from GENEVA with $\mathcal{T}_2^{\text{cut}} = 1\,\text{GeV}$ to the analytic resummed results from figure 3.2. To illustrate the interpolation between resummed and fixed-order results, we also show the pure resummed results at NLL′ and NNLL′ and the pure fixed-order contribution at LO_3 and NLO_3. The latter are calculated using EVENT2 [104, 105], which serves as an independent crosscheck of our NLO_3 implementation. Using the NLL′+LO_3 resummation of $\mathcal{T}_2$ and the LO_3 fixed-order contribution as inputs to our master formula for the spectrum in eq. (3.56), the $\mathrm{d}\sigma^{\text{FO}}/\mathrm{d}\Phi_3$ and $\mathrm{d}\sigma^{\text{resum}}/\mathrm{d}\Phi_2\mathrm{d}\mathcal{T}_2\big|_{\text{FO}}$ contributions exactly cancel for the $\mathcal{T}_2$ spectrum. As a result, we see precise agreement between GENEVA and the analytic NLL′+LO_3 result in figure 3.3(a)-3.3(c) in the peak, transition, and tail regions. This result agrees well with the pure NLL′ resummed contribution in the peak, while in the tail, it is consistent within uncertainties with the LO_3 result, where the latter clearly underestimates the full perturbative uncertainties.

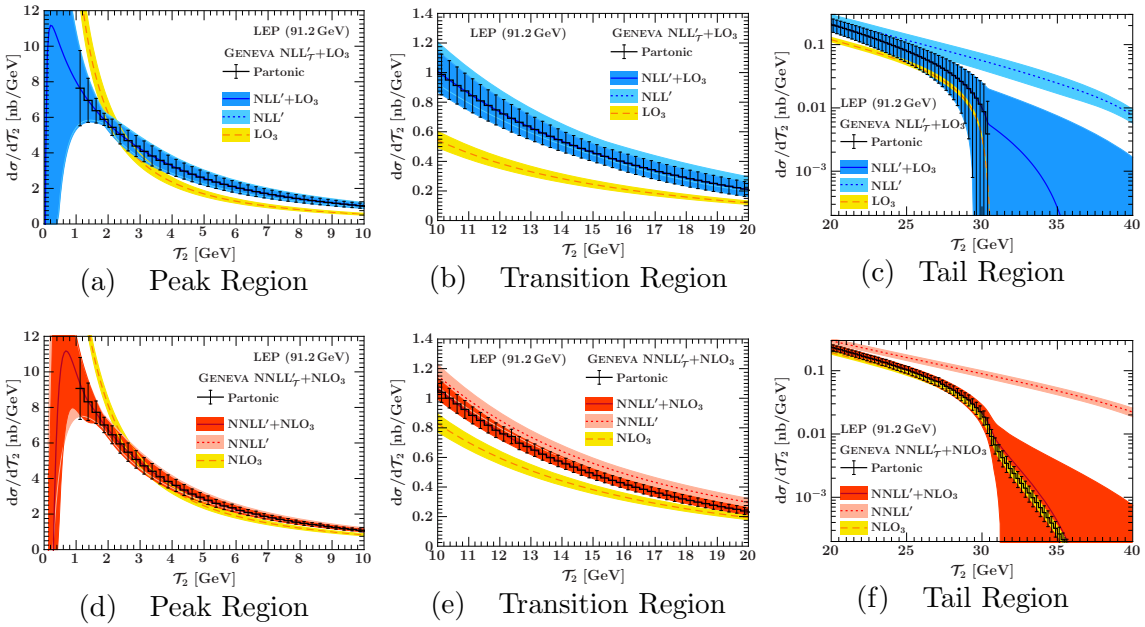

(a) Peak Region (b) Transition Region (c) Tail Region

(d) Peak Region (e) Transition Region (f) Tail Region

Figure 3.3: The GENEVA partonic NLL′+LO$_3$ result is shown compared to the analytic resummation of $\mathcal{T}_2$ matched to fixed order at NLL′+LO$_3$ in the (a) peak, (b) transition, and (c) tail regions. Also shown for comparison is the pure resummed result at NLL′ and the fixed-order LO$_3$ contribution. Figures (d), (e), and (f) show the GENEVA partonic result at NNLL′+NLO$_3$ compared to the analytic resummation of $\mathcal{T}_2$ matched to fixed order at NNLL′+NLO$_3$. The pure NNLL′ resummation and fixed-order NLO$_3$ result are also shown for comparison.

At next higher order, using as inputs to the master formula the NNLL′+LO$_3$ resummation of $\mathcal{T}_2$ and the NLO$_3$ fixed-order calculation, we see that the central value and event-by-event uncertainties in GENEVA agree very well with the full analytic NNLL′+NLO$_3$ resummed prediction in the peak and transition regions, as shown in figures 3.3(d) and 3.3(e). In the tail region, figure 3.3(f), GENEVA has significantly smaller uncertainties of the same size as the pure fixed-order contribution. This is because there is a substantial cancellation between singular and nonsingular contributions in this region, which is incorporated differently in the analytic resummation and the master formula at NNLL′+NLO$_3$. For the former, the nonsingular α_s^2 contributions are added. This preserves the absolute size of residual resummation uncertainties, which are very small relative to the singular contributions but large relative to the total result after cancellation. In the master formula in eq. (3.56), the nonsingular contributions are incorporated multiplicatively through the ratio of $\mathrm{d}\sigma^{\mathrm{FO}}/\mathrm{d}\Phi_3$ and $\mathrm{d}\sigma^{\mathrm{resum}}/\mathrm{d}\Phi_2\mathrm{d}\mathcal{T}_2\big|_{\mathrm{FO}}$. This preserves the relative size of residual resummation uncertainties, thus leading to much smaller absolute variations when compared to the final result. Comparing the GENEVA prediction with the pure NNLL′ resummed and

NLO_3 fixed-order results, we see that the master formula precisely interpolates as expected between the fixed-order and resummation regions, with the transition region properly describing the transition between the two, including uncertainties.

Combining the exclusive 2-jet cross section with the integral of the inclusive 3-jet cross section, the GENEVA prediction at $\text{NNLL}'+\text{NLO}_3$ formally reproduces the total inclusive cross section at NLO. Numerically, we have $\sigma_{\text{tot}}^{\text{NLO}} = 44.1 \pm 0.2\,\text{nb}$. With $\mathcal{T}_2^{\text{cut}}$ smeared between $0.5-1\,\text{GeV}$, the total inclusive cross section in GENEVA is $\sigma_{\text{tot}}^{\text{GENEVA}} = 42.5 \pm 1.6\,\text{nb}$, where the uncertainties are given by integrating over the different profile scale variations. The central value is 3.8% low and agrees within the uncertainties of $\pm 3.8\%$. The uncertainty in GENEVA that comes from integrating the spectrum over $\mathcal{T}_2 > \mathcal{T}_2^{\text{cut}}$, as in eq. (3.6), is much larger than the fixed-order uncertainty. The reason is that, at any given point in the spectrum, but especially in the peak region, the relative uncertainties, reflecting both shape and normalization, are larger than in the total cross section. Hence, when integrating the spectrum to obtain the total cross section, the uncertainties in the spectrum must cancel each other, meaning there is a negative correlation in the uncertainties between different regions in the spectrum. When the resummation and matching to fixed order is performed for the spectrum, this correlation and cancellation is numerically not exact for the total cross section. This is a well-known limitation of analytic resummation [85]. In fact, the result from GENEVA is completely consistent with the inclusive cross section obtained using the analytic resummed result in eq. (3.6) with $\sigma(\mathcal{T}_2^{\text{cut}})$ calculated at $\text{NNLL}'+\text{LO}_3$ and $\mathrm{d}\sigma/\mathrm{d}\mathcal{T}_2$ calculated at $\text{NNLL}'+\text{NLO}_3$. In this case, with $\mathcal{T}_2^{\text{cut}} = 1\,\text{GeV}$, the central value is 3.5% low with uncertainties of $\pm 3.7\%$. One way to solve this problem would be to enforce a (highly nontrivial) constraint on the profile scale variation to reproduce the required correlation exactly, in which case the total cross section would come out exactly right. In practice, a simpler way to enforce this is to compute the result for the resummed cumulant as the difference between the total cross section and the integrated resummed spectrum. (This is similar in spirit to the method proposed in refs. [47, 36, 37].) Since the focus in this thesis is the differential spectrum, which serves as the primary input to the Monte Carlo, rather than the total cross section, we leave this for future improvement.

3.3.2.2 Showered results

Next, we validate our interface with the parton shower. In figure 3.4, we compare the $\text{NNLL}'+\text{NLO}_3$ partonic and showered GENEVA predictions with $\mathcal{T}_2^{\text{cut}}$ smeared between $0.5 - 1\,\text{GeV}$. We also show the analytic resummed $\text{NNLL}'+\text{NLO}_3$ and pure fixed-order NLO_3 spectra for comparison. Before showering, the cumulant $\mathrm{d}\sigma/\mathrm{d}\Phi_2(\mathcal{T}_2^{\text{cut}})$ is in the $\mathcal{T}_2 = 0\,\text{GeV}$ bin, and we see the effect of the smeared $\mathcal{T}_2^{\text{cut}}$ on the spectrum in the GENEVA partonic histogram in figure 3.4(a). The parton shower generates emissions inside the 2-jet bin, which fills out and determines the shape of the GENEVA showered result in the region below $\mathcal{T}_2^{\text{cut}}$ and agrees remarkably

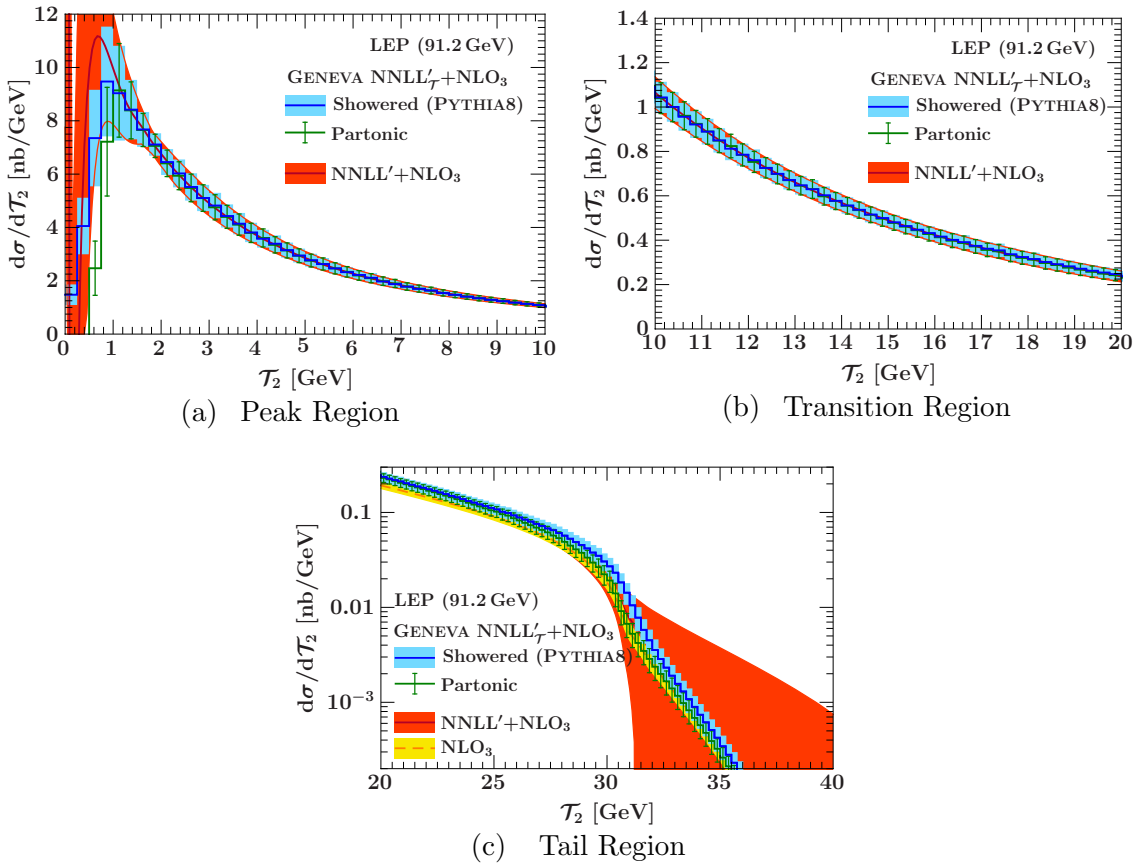

(a) Peak Region

(b) Transition Region

(c) Tail Region

Figure 3.4: The $\mathcal{T}_2$ distribution at NNLL′+NLO$_3$ from GENEVA before and after showering with PYTHIA 8 in the (a) peak, (b) transition, and (c) tail regions of the distribution. The analytic resummed result at NNLL′+NLO$_3$ and the fixed-order NLO$_3$ contribution are shown for comparison.

well with the analytic resummed spectrum below the cut. While the shape of the spectrum here is determined only by PYTHIA, the cross section below $\mathcal{T}_2^{\text{cut}}$ is still accurate to NNLL′+LO$_3$. We can see this explicitly in figure 3.5 from the separate contribution of 2-, 3-, and 4-parton events before and after showering for the central value in the peak region. The shape of the 2-parton showered histogram is determined by PYTHIA, and the area under the histogram is the cumulant $\mathrm{d}\sigma/\mathrm{d}\Phi_2(\mathcal{T}_2^{\text{cut}})$ calculated at NNLL′+LO$_3$. The relative contribution of 3-parton and 4-parton events is determined by $\mathcal{T}_3^{\text{cut}} = 2\,\text{GeV}$, for which the 4-parton contribution is well behaved, giving 15% of the total cross section and no large cancellation with 3-parton events. These contributions all combine smoothly to generate the total GENEVA showered result.

The action of the shower on 3-parton and 4-parton events, which make up the spectrum above $\mathcal{T}_2^{\text{cut}}$, is restricted to not change $\mathcal{T}_2$ by more than a power suppressed

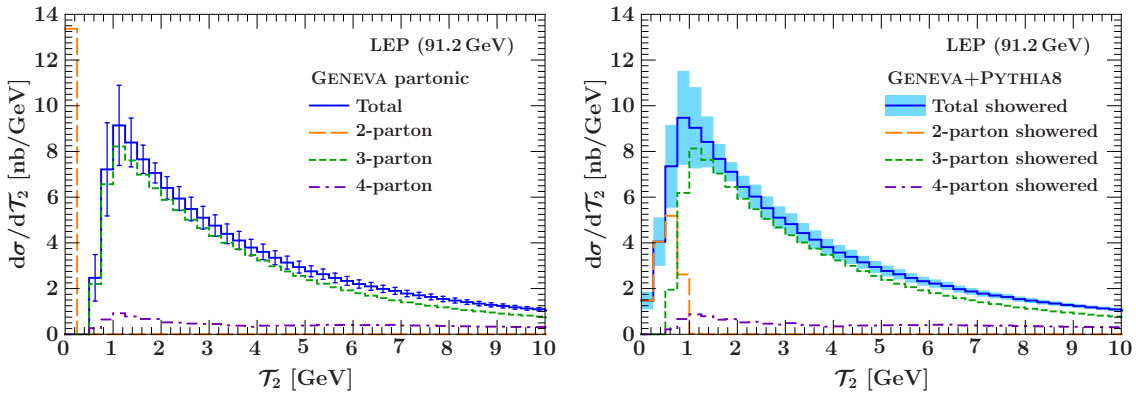

Figure 3.5: The peak region of the $\mathcal{T}_2$ distribution from GENEVA partonic (left) and after showering with PYTHIA 8 (right). The contribution from events originating from 2-, 3-, and 4-parton events is shown along with their sum (solid blue histogram), including the perturbative uncertainties shown by the error bars or band.

amount $\lambda\mathcal{T}_2$, as discussed in section 3.3.1.3. This controls the allowed shift from the GENEVA partonic to showered histograms in figure 3.4. We can see that there is excellent agreement, including uncertainties, between the two in the peak and transition regions. This validates that, with our choice of λ, the higher-order accuracy of the resummed $\mathcal{T}_2$ spectrum is not compromised by the shower. (Increasing λ, we do observe, at some point, a shift of showered results away from partonic.) The showering does shift the $\mathcal{T}_2$ spectrum in the far tail away from the partonic result, which matches the NLO_3 curve, as can be seen in figure 3.4(c). This is allowed, since our partonic prediction in this region becomes only leading order for 4 partons.

3.3.2.3 Hadronized results and comparison to data

The full prediction for the jet resolution spectrum is obtained by turning on the hadronization in PYTHIA. This gives rise to a shift in the $\mathcal{T}_2$ spectrum, shown in figure 3.6, where "default" refers to the default running parameters $\alpha_s(m_Z) = 0.1135$ and PYTHIA e^+e^- tune 1. As discussed in section 3.3.1.3, we use the standard PYTHIA 8 tunes without modifying any internal parameters. For comparison, we show the GENEVA hadronized result for tune 3 with our default α_s value as well as for tune 1 with the world average value $\alpha_s(m_Z) = 0.1184$. We also show a comparison to experimental data from ALEPH [2] and OPAL [3]. We only show ALEPH data in the tail since the OPAL data in this region is sparse. These measurements are fully corrected to the particle level, allowing us to directly compare to our hadronized predictions. Since the data are normalized to the total cross section, we rescale them to the total NNLO cross section and convert from thrust T to $\mathcal{T}_2 = E_{\text{cm}}(1 - T)$. This allows us to directly compare the data to the absolute cross section predictions in GENEVA, unlike a comparison between normalized spectra, which would only test

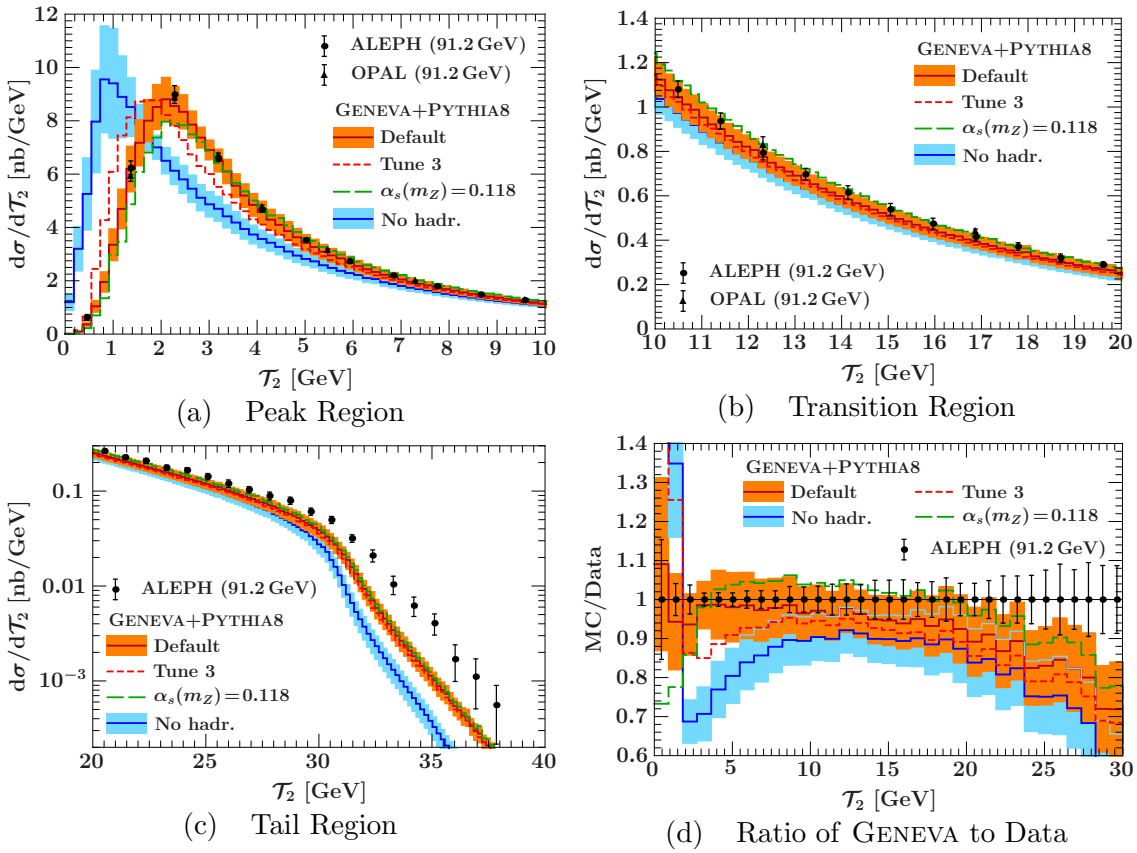

(a) Peak Region (b) Transition Region

(c) Tail Region (d) Ratio of GENEVA to Data

Figure 3.6: The showered NNLL′+NLO$_3$ GENEVA prediction with and without hadronization using the default values PYTHIA 8 e^+e^- tune 1 and $\alpha_s(m_Z) = 0.1135$ compared to data from ALEPH [2] in the (a) peak, (b) transition, and (c) tail regions and to OPAL [3] in the peak and transition regions. The ratio of GENEVA predictions to the ALEPH data is shown in (d). Also shown is the GENEVA prediction at the central scale with $\alpha_s(m_Z) = 0.1184$ and e^+e^- tune 3.

the shape. The GENEVA prediction at the default values agrees impressively well with the data within uncertainties across the peak and transition regions and into the tail. The difference in the far tail is expected since here fixed-order contributions beyond LO$_4$ are important and are not yet included in our results.

The partonic GENEVA prediction does not include nonperturbative effects in the soft function of $\mathcal{O}(\Lambda_{\mathrm{QCD}}/\mathcal{T}_2)$, nor power corrections of the form $\mathcal{O}(\Lambda_{\mathrm{QCD}}/E_{\mathrm{cm}})$. Since we strongly constrain the action of the PYTHIA parton shower to not change the analytic resummed NNLL′+NLO$_3$ result, as discussed in section 3.3.1.3 and demonstrated in figure 3.4, we expect the hadronization in PYTHIA to supply these missing nonperturbative effects. In effect, PYTHIA provides a well-tested model of the nonperturbative soft function in eq. (3.62). We show the hadronized GENEVA result with PYTHIA e^+e^- tune 3 at the central scale in figure 3.6 as a measure of the uncertainty

from hadronization. Tune 3 turns out to give a smaller shift due to hadronization than tune 1, which makes a significant difference in the peak below $\lesssim 3\,\text{GeV}$, where nonperturbative corrections are $\mathcal{O}(1)$ and depend on the details of the hadronization model. In the transition and tail regions, we see a smaller difference, with tune 3 being systematically lower than tune 1. This is consistent with the fact that the transition and tail regions are sensitive only to the first nonperturbative power correction in the soft function of $\mathcal{O}(\Lambda_{\text{QCD}}/\mathcal{T}_2)$.

There is an important interplay between the effect of hadronization and the value of $\alpha_s(m_Z)$, as discussed in ref. [85], where a simultaneous fit to $\alpha_s(m_Z)$ and the first nonperturbative correction to the soft function of $\mathcal{O}(\Lambda_{\text{QCD}}/\mathcal{T}_2)$ was carried out. Generically, larger nonperturbative corrections shift the partonic spectrum to larger values of $\mathcal{T}_2$, while a smaller value of $\alpha_s(m_Z)$ shifts the 2-jettiness spectrum downward. This gives rise to compensating effects. Since tune 3 gives a smaller shift due to hadronization than tune 1, the combination of tune 3 and $\alpha_s(m_Z) = 0.1135$ gives an estimate of the lower bound on the combined uncertainty of these two effects in the transition and tail regions, while the combination of tune 1 and $\alpha_s(m_Z) = 0.1184$ gives an estimate of the upper bound. This is illustrated very well in the ratio of GENEVA to ALEPH data in figure 3.6(d). Both are, however, still within the perturbative uncertainties from GENEVA across most of the transition and tail regions.

We have also checked that the nonperturbative shift from PYTHIA tune 1 is of similar size as expected from the fit results in ref. [85]. This is consistent with the fact that it gives a good description of the data when used together with their fitted value of $\alpha_s(m_Z)$. Hence, we use tune 1 with $\alpha_s(m_Z) = 0.1135$ as the default since it agrees best with the data in the peak and provides a consistent description of the data across larger values of $\mathcal{T}_2$.

3.3.3 Predictions for other event shapes

In this section, we present GENEVA's predictions for a variety of dijet event shape variables. Examining observables other than the jet resolution variable we use as input serves to validate our master formula at the fully differential $\Phi_{2,3}$ level [see eq. (3.55)] rather than its projection onto the $\mathcal{T}_2$ spectrum [see eq. (3.26)]. Event shapes are particularly useful to consider because there exist both higher-order resummed results and precision LEP data with which we can compare.

By construction, GENEVA correctly predicts other observables at NLO_3, while maintaining the correct inclusive cross section. However, as discussed in section 3.2.2.3, it is an important open question to what extent the $\text{NNLL}'_{\mathcal{T}}+\text{NLO}_3$ resummation of the $\mathcal{T}_2$ spectrum increases the accuracy of resummed predictions for the other observables (beyond the partial NLL order naively expected by interfacing with the parton shower). While other observables will not be predicted at the same resummed order as $\mathcal{T}_2$, the accuracy of the predictions for event shapes is expected to increase as a function of their correlation with 2-jettiness. The comparison of

GENEVA to the higher-order analytic resummation of event shapes plays a crucial role in numerically testing the accuracy achieved in our approach and validating the event-by-event perturbative uncertainties.

We present results for the C-parameter [106, 107, 108], heavy jet mass (ρ) [109, 110], and jet broadening (B) [111, 112] event shapes. These are defined as follows:

$$\begin{aligned} C &= \frac{3}{2}\frac{1}{\left(\sum_k |\vec{p}_k|\right)^2}\sum_{i,j}|\vec{p}_i||\vec{p}_j|\sin^2\theta_{ij}\,, \\ \rho &= \frac{1}{E_{\rm cm}^2}\max\left(M_1^2, M_2^2\right)\,, \quad \text{where} \quad M_i^2 = \left(\sum_{k\in \text{hemi}_i} p_k\right)^2 \quad \text{for} \quad i=1,2\,, \\ B &= \frac{1}{2\sum_k|\vec{p}_k|}\sum_i |\vec{p}_i\times\hat{n}_T|\,, \end{aligned} \tag{3.73}$$

where $\hat{n}_T$ is the thrust axis and is used in heavy jet mass to divide the event into two hemispheres, $\text{hemi}_{1,2}$, with respect to which the masses $M_{1,2}$ are measured. C, ρ, and B provide a useful range of event shapes to compare to since their resummation structure is increasingly different from that of $\mathcal{T}_2$. The resummation of C-parameter is precisely the same as $\mathcal{T}_2$ to NLL and has the same convolution structure as eq. (3.61) beyond. Heavy jet mass has a different convolution structure from $\mathcal{T}_2$. Both ρ and $\mathcal{T}_2$ are projections of the same doubly differential spectrum $\mathrm{d}\sigma/\mathrm{d}M_1^2\mathrm{d}M_2^2$, where $\mathcal{T}_2$ is related to the sum and heavy jet mass to the maximum of the hemisphere masses. Of the event shapes we consider, jet broadening is most different from $\mathcal{T}_2$; it measures momentum transverse to the thrust axis and, in the dijet limit, is sensitive to the recoil of the thrust axis due to soft emissions [113], unlike $\mathcal{T}_2$. This complicates the higher-order resummation of jet broadening, which was only recently extended to NNLL_B [114] and gives a logarithmic structure that is very different from $\mathcal{T}_2$. As a result, jet broadening provides a highly nontrivial test of the accuracy and theory uncertainties of the GENEVA prediction.

For each of these observables, we compare to analytic resummed predictions as well as the NLO_3 fixed-order contribution from EVENT2. We present new results for the analytic resummation of C-parameter at $\text{NNLL}'_C{+}\text{NLO}_3$, extending the previous NLL_C resummation of [115].[14] Note the subscript on the order of resummation indicates the observable for which analytic resummation was carried out. Since resummed results for jet broadening do not exist at NNLL'_B, we compare to the highest available resummation $\text{NNLL}_B{+}\text{LO}_3$, where we use the results of [114], which we extend to include fixed-order matching that is necessary to describe the tail and transition regions. Finally, for heavy jet mass, N^3LL_ρ resummed results exist [84]; however, we show the $\text{NNLL}'_\rho{+}\text{NLO}_3$ resummation since this is consistent with the highest $\mathcal{T}_2$ resummation we use.

[14] We thank Vicent Mateu and Iain Stewart for pointing out to us the relationship between thrust and C-parameter in SCET.

It is important to note that all running parameters were set based on the $\mathcal{T}_2$ spectrum alone, and no further optimization was carried out for other observables. This ensures that our results for other observables are true predictions of the GENEVA framework.

3.3.3.1 C-parameter

In figure 3.7, we show the GENEVA prediction for C-parameter both at the partonic level and showered, using NLL$'_{\mathcal{T}}$+LO$_3$ resummation as input to our master formula in figures 3.7(a) and 3.7(b) and at next higher order NNLL$'_{\mathcal{T}}$+NLO$_3$ in figures 3.7(c) and 3.7(d). We compare this to the analytic resummed C-parameter prediction at the same order as the $\mathcal{T}_2$ resummation we input, as well as one order lower. The comparison of the GENEVA prediction at different orders in the peak and transition regions is useful because it highlights the features of resummation that are consistently captured by our implementation. In the tail region, figure 3.7(e), where the comparison to the NLO$_3$ fixed-order result is most relevant, we only show our highest order NNLL$'_{\mathcal{T}}$+NLO$_3$ GENEVA result.

We see the effect of the cut on 2-jettiness of $\mathcal{T}_2^{\text{cut}} = 0.5 - 1\,\text{GeV}$ up to $C = 0.066$ in the partonic prediction from GENEVA in figures 3.7(a) and 3.7(c) since $C \leq 6\mathcal{T}_2/Q$ [115]. Interfacing with the shower generates emissions inside the jets and fills out the region below $C = 0.066$. The action of the parton shower is restricted based on the constraints on $\mathcal{T}_2$ discussed in section 3.3.1.3. This effectively constrains the C-parameter distribution as well, giving very little change from the partonic to showered predictions at both resummation orders except in the multijet region of the far tail. Here, the constraints on the shower are looser, reflecting the fact that our prediction is correct at LO$_4$. The size of the shift from the partonic to the showered result in the peak and transition regions is a measure of the correlation between the C and $\mathcal{T}_2$ event shapes, where, although the two differ beyond NLL, their logarithmic structure is the same. It is worth noting however, that despite the similarity of the resummation structure between C and $\mathcal{T}_2$, the shape of the C-parameter spectrum is very different, with the singular terms dominating the nonsingular for a much larger region of the spectrum.

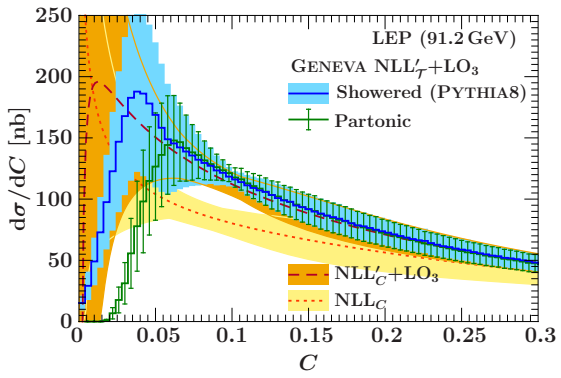

(a) GENEVA NLL′$_\mathcal{T}$+LO$_3$ Peak Region

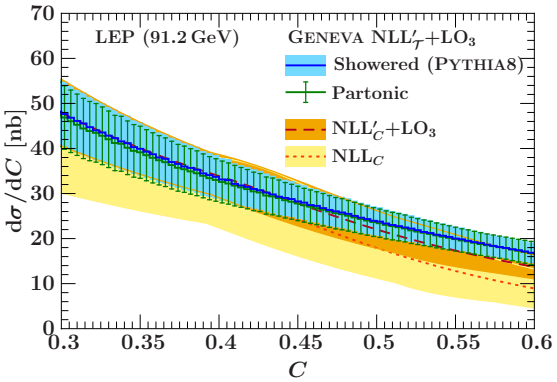

(b) GENEVA NLL′$_\mathcal{T}$+LO$_3$ Transition Region

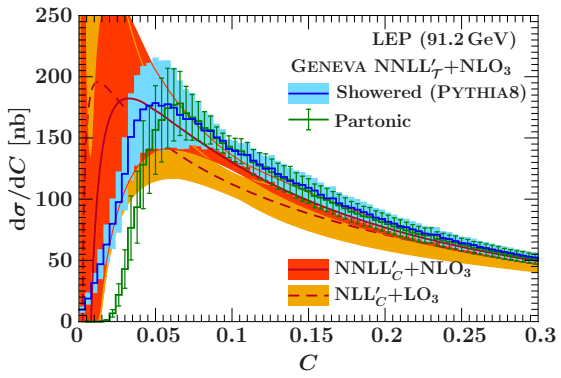

(c) GENEVA NNLL′$_\mathcal{T}$+NLO$_3$ Peak Region

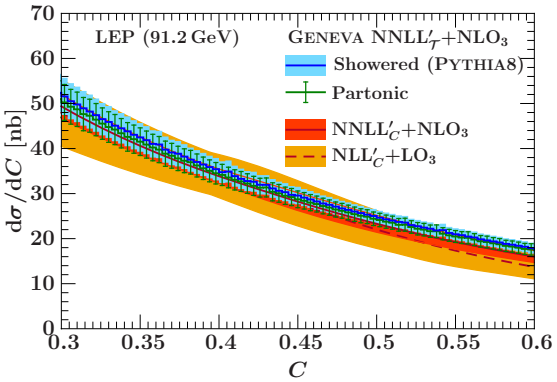

(d) GENEVA NNLL′$_\mathcal{T}$+NLO$_3$ Transition Region

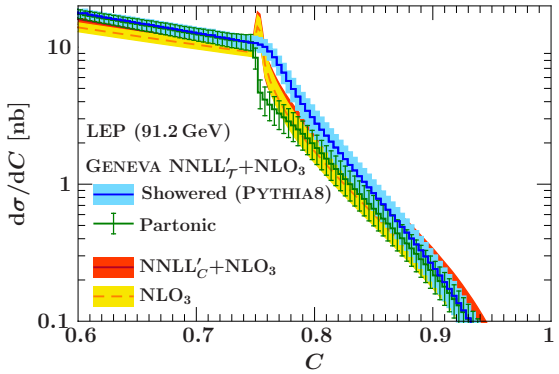

(e) GENEVA NNLL′$_\mathcal{T}$+NLO$_3$ Tail Region

Figure 3.7: The C-parameter partonic and showered GENEVA predictions are shown compared to the analytic resummation of C-parameter at different orders. The GENEVA result at NLL′$_\mathcal{T}$+LO$_3$ is compared to NLL$_C$ and NLL′$_C$+LO$_3$ in (a) and (b). In (c) and (d), the GENEVA prediction at one order higher, NNLL′$_\mathcal{T}$+NLO$_3$, is compared to NLL′$_C$+LO$_3$ and NNLL′$_C$+NLO$_3$, while in the tail (e), we also show the fixed-order NLO$_3$ prediction from EVENT2.

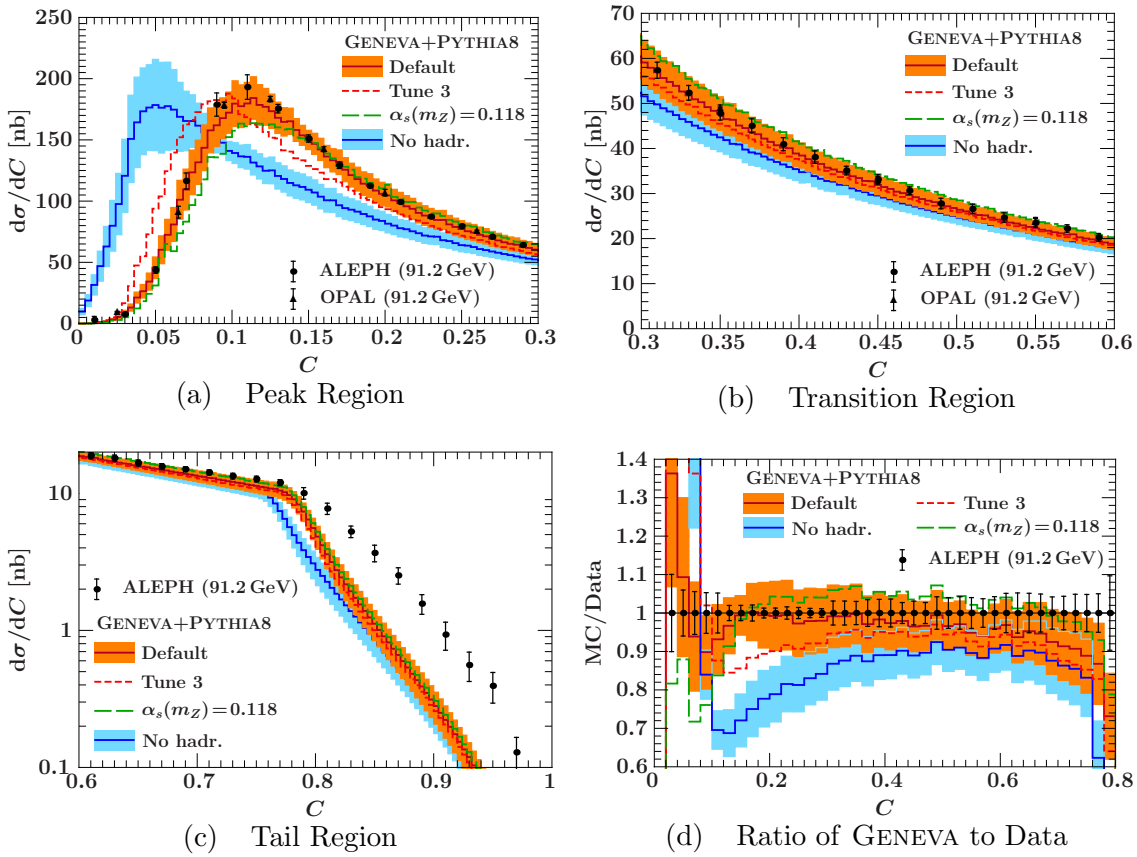

(a) Peak Region (b) Transition Region

(c) Tail Region (d) Ratio of GENEVA to Data

Figure 3.8: The C-parameter distribution comparing GENEVA with and without hadronization using PYTHIA 8 e^+e^- tune 1 and $\alpha_s(m_Z) = 0.1135$ is shown compared to ALEPH data in the (a) peak, (b) transition, and (c) tail regions and to OPAL data in the peak and transition regions. The ratio of the GENEVA predictions to ALEPH data is shown in (d). Also shown are the GENEVA predictions at the central scale with $\alpha_s(m_Z) = 0.1184$ and e^+e^- tune 3.

One might naively expect that the accuracy of the resummation achieved in GENEVA for any observable other than $\mathcal{T}_2$ would only be the partial NLL of the parton shower. However, it is clear that the GENEVA prediction at NLL$'_{\mathcal{T}}$+LO$_3$ in the peak and into the transition region, figures 3.7(a) and 3.7(b), is much more consistent with NLL$'_C$+LO$_3$ than NLL$_C$ resummation, both in its central value and also in the size of the perturbative uncertainties it predicts. This appears to hold even in the peak region below $C \sim 0.05$, where the parton shower determines the shape of the spectrum. Going to one higher order in figures 3.7(c) and 3.7(d), we see that the same pattern holds: the GENEVA prediction is consistent with the higher-order NNLL$'_C$+NLO$_3$ resummation rather than NLL$'_C$+LO$_3$, including uncertainties. This is particularly clear in the peak region where the central values of the two analytic

resummation orders are significantly different and GENEVA tracks the NNLL$'_C$+NLO$_3$ prediction. The convergence of the GENEVA result for C-parameter from NLL$'_{\mathcal{T}}$+LO$_3$ to NNLL$'_{\mathcal{T}}$+NLO$_3$ demonstrates the consistency of the GENEVA implementation including the event-by-event uncertainties for this observable. Although the accuracy of the GENEVA prediction for C-parameter is not formally of the same order as the $\mathcal{T}_2$ resummation we used as input to the master formula, the fact that it matches the analytic C-parameter resummation remarkably well both at NLL$'_C$+LO$_3$ and at NNLL$'_C$+NLO$_3$ shows that numerically the accuracy achieved is very close.

The GENEVA uncertainties in the transition region start to shrink relative to the analytic resummation as we interpolate to the fixed-order NLO$_3$ result. In the tail region, the partonic GENEVA prediction matches smoothly to the fixed-order NLO$_3$ result past the Sudakov shoulder at $C = 0.75$ [116], demonstrating the validity of the multiplicative implementation of $\mathrm{d}\sigma/\mathrm{d}\Phi_3(\mathcal{T}_2)$ in eq. (3.56) in this limit.

The GENEVA prediction including hadronization with the default running values of PYTHIA e^+e^- tune 1 and $\alpha_s(m_Z) = 0.1135$ is shown in figure 3.8 compared to ALEPH and OPAL data rescaled to the NNLO inclusive cross section. GENEVA agrees with the data remarkably well across the entire distribution up to the multijet region in the tail. We show the effect of $\alpha_s(m_Z) = 0.1135$ with tune 3, which gives a smaller correction from hadronization than tune 1, as seen from the size of the shift from the GENEVA unhadronized result to the hadronized in figure 3.8. We also show the GENEVA prediction at the central scale using the world average $\alpha_s(m_Z) = 0.1184$ and tune 1. These two combinations provide an estimate of the upper and lower bounds on the combined uncertainty of the nonperturbative effect and $\alpha_s(m_Z)$ value in the transition and tail regions, as discussed in section 3.3.2. The ratio of the Monte Carlo to data in figure 3.8(d) shows that they are both largely within the perturbative uncertainties from GENEVA in these regions. Of the values we consider, the default tune 1 with $\alpha_s(m_Z) = 0.1135$ gives the best agreement with the data across the C spectrum and is consistent with our findings for the $\mathcal{T}_2$ distribution.

3.3.3.2 Heavy jet mass

The GENEVA prediction for heavy jet mass is shown in figure 3.9, where we compare the partonic and showered results using NLL$'_{\mathcal{T}}$+LO$_3$ resummation in the master formula in figures 3.9(a) and 3.9(b) to the analytic resummation of ρ at NLL$_\rho$ and NLL$'_\rho$+LO$_3$. In figures 3.9(c) and 3.9(d), we show the same results at one order higher, comparing NNLL$'_{\mathcal{T}}$+NLO$_3$ GENEVA results to NLL$'_\rho$+LO$_3$ and NNLL$'_\rho$+NLO$_3$ analytic ρ resummation. In the tail, we show only the highest-order GENEVA and resummed results along with the pure fixed-order NLO$_3$ contribution, since this is sufficient to demonstrate the behavior in this region.

In the peak region, figures 3.9(a) and 3.9(c), we see the effect of $\mathcal{T}_2^{\mathrm{cut}}$ on the partonic ρ spectrum up to $\rho = 1\,\mathrm{GeV}/E_{\mathrm{cm}} = 0.011$, which is smoothly filled out by interfacing with the parton shower. The GENEVA showered prediction in figure 3.9(a)

shows impressive agreement with the NLL$'_\rho$+LO$_3$ resummed result in the peak region, including uncertainties. The improvement in accuracy of the GENEVA prediction for heavy jet mass over the partial NLL resummation provided by the parton shower is clear. Going to one higher order in figure 3.9(c), the GENEVA prediction is more consistent with the NNLL$'_\rho$+NLO$_3$, with which it agrees within uncertainties, rather than the NLL$'_\rho$+LO$_3$ result.

The perturbative uncertainties of the GENEVA showered prediction are larger than those at NNLL$'_\rho$+NLO$_3$ and smaller than at NLL$'_\rho$+LO$_3$. This is consistent with the fact that, while the GENEVA prediction for ρ is not formally of the same order as the $\mathcal{T}_2$ resummation that is input into the master formula, there is a gain in accuracy going from GENEVA at NLL$'_\mathcal{T}$+LO$_3$ to NNLL$'_\mathcal{T}$+NLO$_3$ that is transferred to the ρ prediction.

In the transition region, both at NLL$'_\mathcal{T}$+LO$_3$ and NNLL$'_\mathcal{T}$+NLO$_3$, adding the parton shower gives rise to a larger shift from the partonic spectrum than for the C-parameter, because heavy jet mass is less correlated with $\mathcal{T}_2$ than C. This shift is necessary to obtain agreement with the NNLL$'_\rho$+NLO$_3$ resummation within uncertainties in figure 3.9(d). The partonic GENEVA prediction in this region is more consistent with NLL$'_\rho$+LO$_3$ analytic resummation, which is higher than the NNLL$'_\rho$+NLO$_3$ result. By restricting the change in $\mathcal{T}_2$ due to the shower, we are constraining the sum of the hemisphere masses, $M^2_{1,2}$ in eq. (3.73). For a given value of $\mathcal{T}_2$, ρ is largest when either hemisphere mass is zero, and so $\rho = \mathcal{T}_2$. Adding the parton shower tends to make this mass nonzero (while constraining the sum) and therefore gives an overall shift of the spectrum to lower values of ρ. In the tail region, the partonic spectrum interpolates to the fixed-order NLO$_3$ result, as expected, with the shower giving rise to a larger shift in the multijet region where our constraints are looser.

In figure 3.10, we show the showered GENEVA prediction with and without hadronization, with our default parameters. As before, we compare to ALEPH and OPAL data, which shows impressive agreement with the data within uncertainties across all three regions of the ρ spectrum, with the expected deviation in the multijet region of the far tail. As discussed previously, tune 3 with $\alpha_s(m_Z) = 0.1135$ and tune 1 with $\alpha_s(m_Z) = 0.1184$ provide bounds on the estimate of the combined uncertainty from these two inputs. It is interesting to note that heavy jet mass is relatively insensitive to hadronization in the transition and tail regions. This is demonstrated by the shift from the shower-only to the fully hadronized result in figures 3.10(b) and 3.10(c), as well as the small change in the default central value from using tune 1 to tune 3 above $\rho \sim 0.1$ seen in figure 3.10(d). This breaks the coupling in some respect between the nonperturbative effects and the value of α_s in this region and suggests that $\alpha_s(m_Z) = 0.1135$ provides better agreement with the data.

3.3.3.3 Jet broadening

Finally, we turn to the results of GENEVA for jet broadening, which is the most orthogonal event shape to our jet resolution variable that we consider. In figure 3.11, we show the GENEVA partonic and showered results using NLL$'_{\mathcal{T}}$+LO$_3$ resummation in figures 3.11(a) and 3.11(b) and NNLL$'_{\mathcal{T}}$+NLO$_3$ resummation in figures 3.11(c) and 3.11(d). We compare these to the analytic NLL$_B$ and the best available NNLL$_B$+LO$_3$ resummed prediction. Note that we would like to compare the NLL$'_{\mathcal{T}}$+LO$_3$ resummation in GENEVA to the resummation of B at the same order. However, since going from NLL$'_B$ to NNLL$_B$ (which incorporates $\alpha_s^2 \ln B$ terms into the resummation) is a comparatively small effect in this case, we will find it useful to compare the NLL$'_{\mathcal{T}}$+LO$_3$ prediction with the analytic NNLL$_B$+LO$_3$ result. In the tail, we compare to the fixed-order NLO$_3$ result from EVENT2, which is the more relevant comparison in this region.

The effect of the cut on $\mathcal{T}_2$ extends up to $B \simeq 0.055$ in the peak region and is smoothly removed by attaching the parton shower. Both at NLL$'_{\mathcal{T}}$+LO$_3$ and NNLL$'_{\mathcal{T}}$+NLO$_3$, there is a significant shift induced by the parton shower across the jet broadening spectrum toward larger values of B. The size of this shift is a measure of the lack of correlation between B and $\mathcal{T}_2$, the variable used to constrain the parton shower, and is therefore progressively larger for C, ρ, and B, as we have seen.

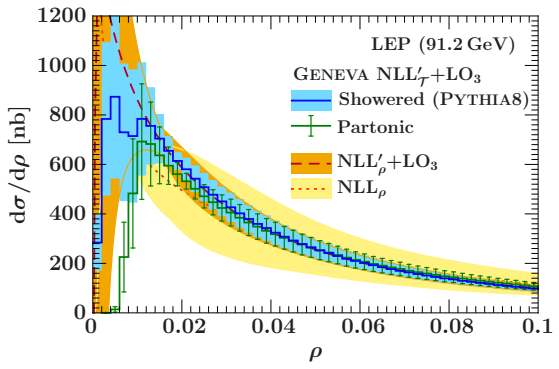

(a) GENEVA NLL′$_\mathcal{T}$+LO$_3$ Peak Region

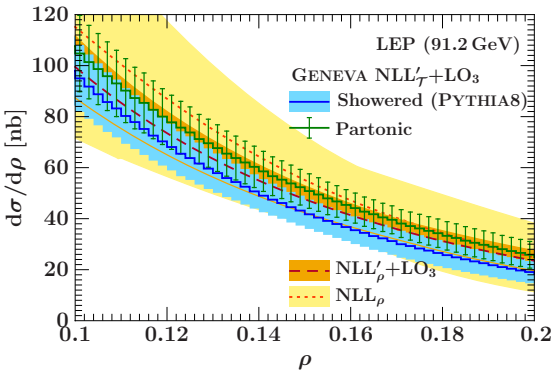

(b) GENEVA NLL′$_\mathcal{T}$+LO$_3$ Transition Region

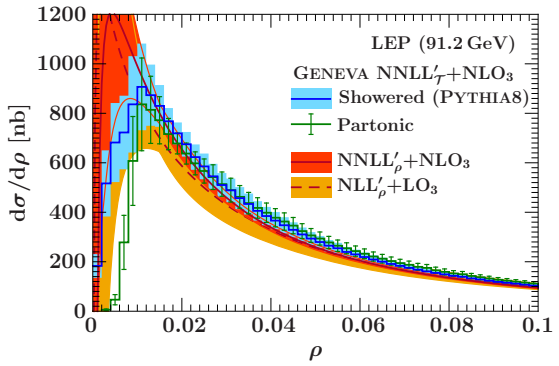

(c) GENEVA NNLL′$_\mathcal{T}$+NLO$_3$ Peak Region

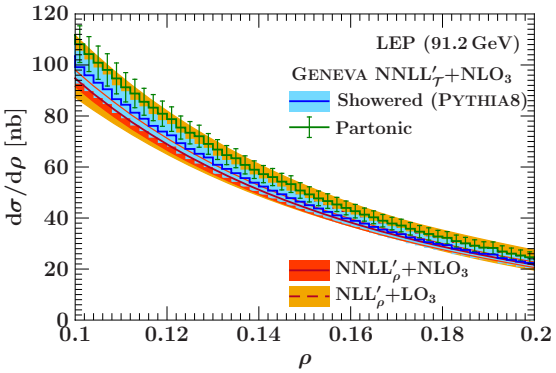

(d) GENEVA NNLL′$_\mathcal{T}$+NLO$_3$ Transition Region

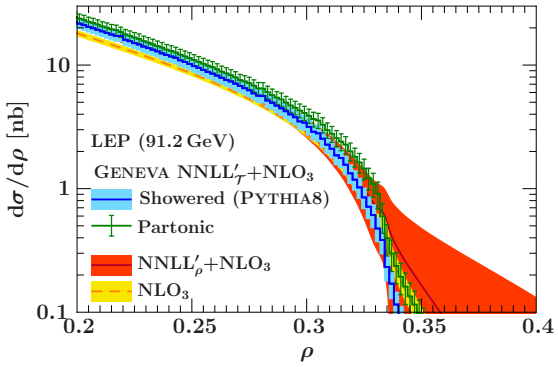

(e) GENEVA NNLL′$_\mathcal{T}$+NLO$_3$ Tail Region

Figure 3.9: The heavy jet mass partonic and showered GENEVA predictions are shown compared to the analytic resummation of ρ at different orders. The GENEVA result at NLL′$_\mathcal{T}$+LO$_3$ is compared to NLL$_\rho$ and NLL′$_\rho$+LO$_3$ in (a) and (b). In (c) and (d), the GENEVA prediction at one order higher, NNLL′$_\mathcal{T}$+NLO$_3$, is compared to NLL′$_\rho$+LO$_3$ and NNLL′$_\rho$+NLO$_3$, while in the tail (e), we also show the fixed-order NLO$_3$ prediction from EVENT2.

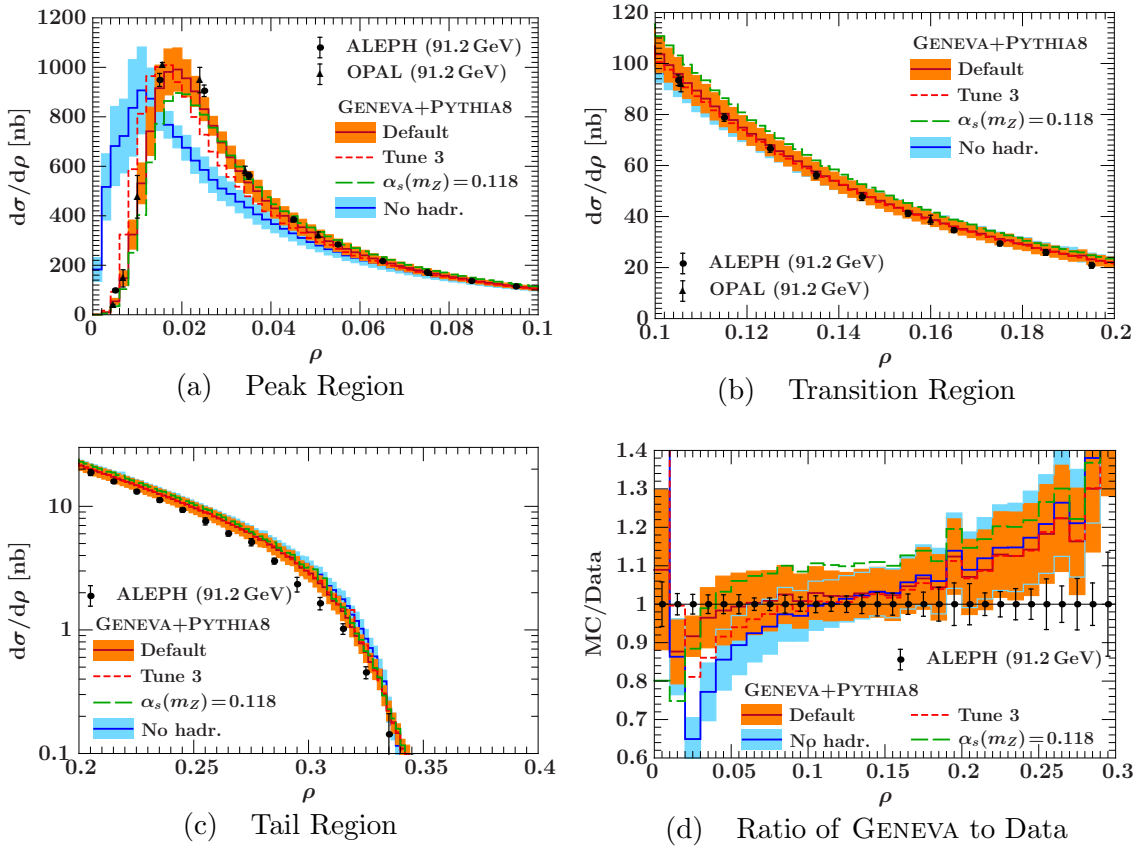

(a) Peak Region (b) Transition Region

(c) Tail Region (d) Ratio of GENEVA to Data

Figure 3.10: The heavy jet mass distribution comparing GENEVA with and without hadronization using PYTHIA 8 e^+e^- tune 1 and $\alpha_s(m_Z) = 0.1135$ is shown compared to ALEPH data in the (a) peak, (b) transition, and (c) tail regions and to OPAL data in the peak and transition regions. The ratio of the GENEVA predictions to ALEPH data is shown in (d). Also shown are the GENEVA predictions at the central scale with $\alpha_s(m_Z) = 0.1184$ and e^+e^- tune 3.

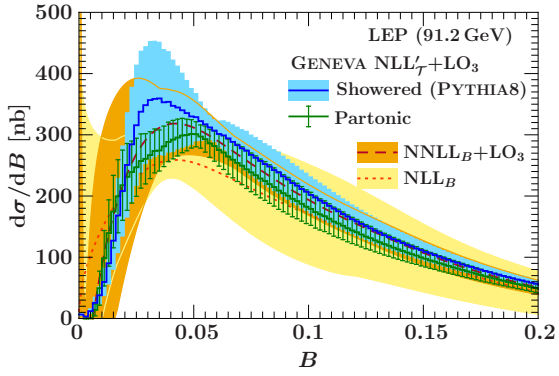

(a) GENEVA NLL′$_\mathcal{T}$+LO$_3$ Peak Region

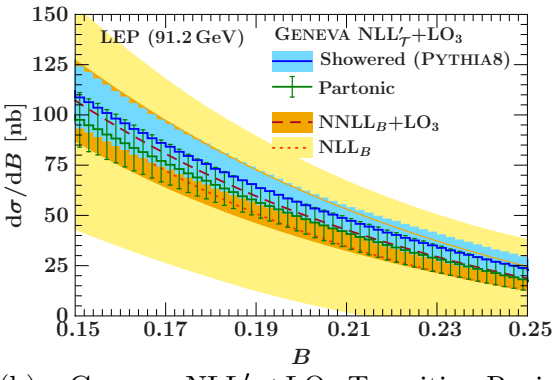

(b) GENEVA NLL′$_\mathcal{T}$+LO$_3$ Transition Region

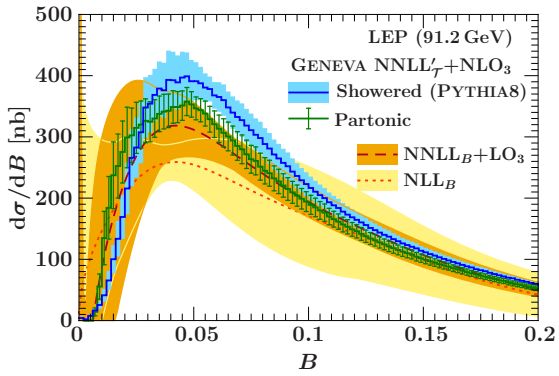

(c) GENEVA NNLL′$_\mathcal{T}$+NLO$_3$ Peak Region

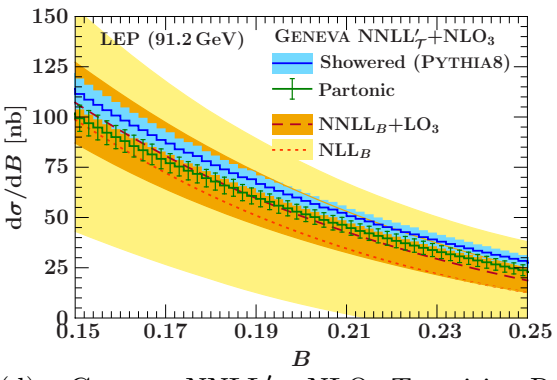

(d) GENEVA NNLL′$_\mathcal{T}$+NLO$_3$ Transition Region

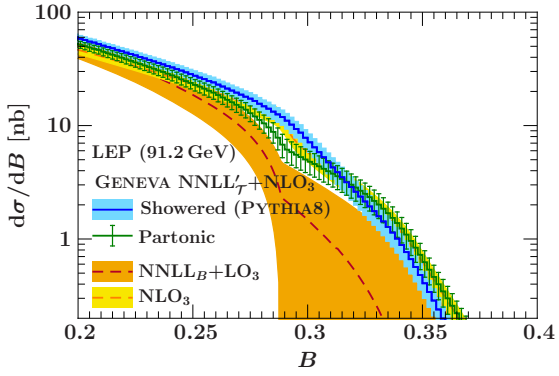

(e) GENEVA NNLL′$_\mathcal{T}$+NLO$_3$ Tail Region

Figure 3.11: The jet broadening partonic and showered GENEVA predictions are shown compared to the analytic resummation of B at NLL$_B$ and NNLL$_B$+LO$_3$. The GENEVA result at NLL′$_\mathcal{T}$+LO$_3$ is shown in (a) and (b), and at one order higher, NNLL′$_\mathcal{T}$+NLO$_3$, in (c) and (d). In the tail (e), we also show the fixed-order NLO$_3$ prediction from EVENT2.

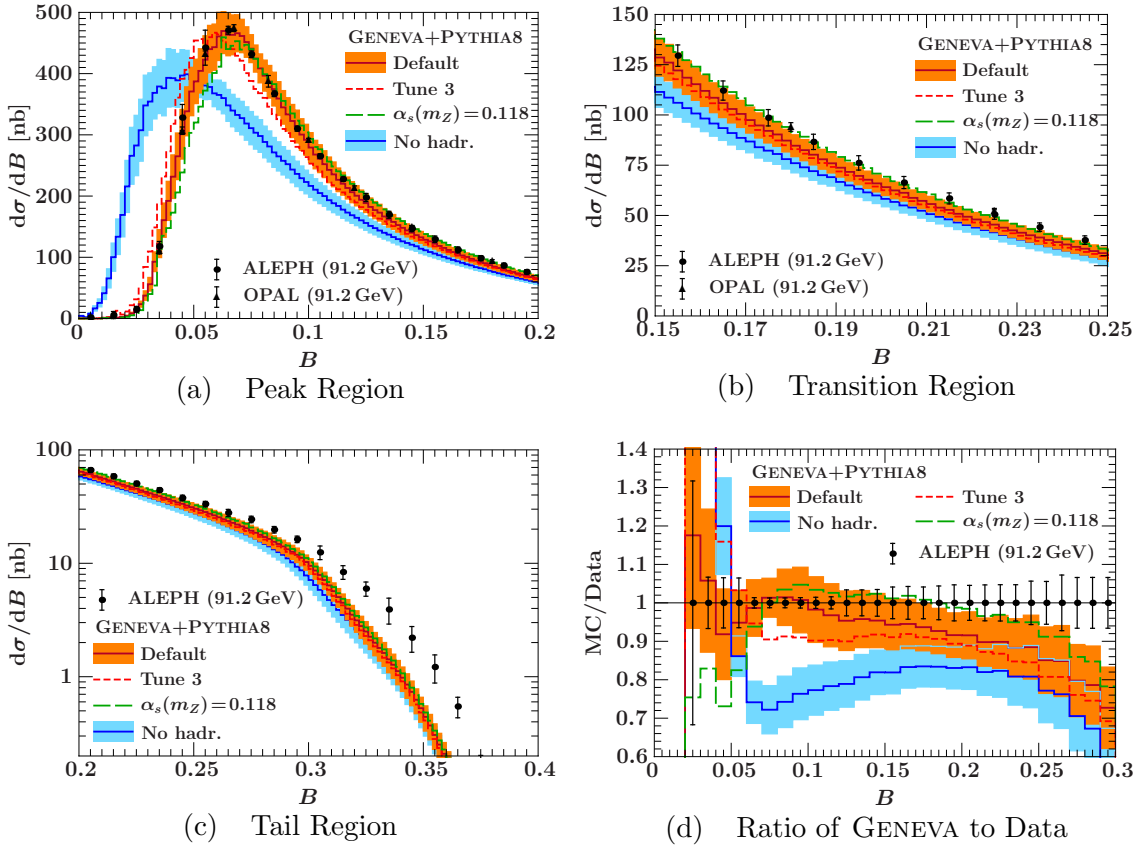

(a) Peak Region (b) Transition Region

(c) Tail Region (d) Ratio of GENEVA to Data

Figure 3.12: The jet broadening distribution comparing GENEVA with and without hadronization using PYTHIA 8 e^+e^- tune 1 and $\alpha_s(m_Z) = 0.1135$ is shown compared to ALEPH data in the (a) peak, (b) transition, and (c) tail regions and OPAL data in the peak and transition regions. The ratio of the GENEVA predictions to ALEPH data is shown in (d). Also shown are the GENEVA predictions at the central scale with $\alpha_s(m_Z) = 0.1184$ and e^+e^- tune 3.

As discussed in section 3.2.2.3, in the IR limit where both $\mathcal{T}_2, B \to 0$, one might expect to see some improved accuracy of the GENEVA prediction over the partial NLL of the parton shower, since the higher-order resummation of $\mathcal{T}_2$ provides a better description in this region. This is consistent with figure 3.11(a), where the showered GENEVA prediction agrees well with the NNLL$_B$+LO$_3$ resummed result, including uncertainties in the peak region. In the transition region in figure 3.11(b), the central value of the GENEVA showered prediction agrees with the NNLL$_B$+LO$_3$ resummed result within uncertainties; however, the uncertainties from GENEVA are smaller than the corresponding analytic ones, which suggests that in this region they may be underestimated.

In the far transition region and into the tail, the uncertainties in GENEVA generi-

cally are smaller than the corresponding analytic resummation and of order the NLO_3 scale variation, as seen for example in the $\mathcal{T}_2$, C, and ρ spectra. This difference arises because GENEVA multiplicatively interpolates to the fixed-order result, while the analytic resummation does an additive matching, as discussed in section 3.3.2.1. For an observable such as jet broadening, the lack of correlation with $\mathcal{T}_2$ means that larger values of the $\mathcal{T}_2$ spectrum contribute at smaller values of B. This can lead to an underestimate of the uncertainties from GENEVA at intermediate values of B where the resummation is still important.

Going to higher order in GENEVA in figures 3.11(c) and 3.11(d), the uncertainties of the showered prediction decrease and overlap with the NNLL_B+LO_3 uncertainties over much of the peak and transition regions. It would be interesting to compare the GENEVA prediction to the next higher-order analytic resummed jet broadening prediction to numerically test the accuracy achieved; however, this is not yet available. Determining the formal accuracy of the GENEVA prediction for a given observable and systematically including the uncertainty associated to the lack of correlation with $\mathcal{T}_2$ are next steps that we leave for future work. As mentioned in section 3.3.1.3, one possibility would be to include the size of the shift from the partonic to the showered results as a conservative estimate of the uncertainty due to the remaining showering.

The partonic GENEVA jet broadening prediction interpolates smoothly to the fixed-order NLO_3 result in the tail, with uncertainties that match the fixed-order result in this region. As for the other observables, this validates the behavior of the fully differential master formula in eq. (3.56) in this limit.

In figure 3.12, we show the hadronized GENEVA prediction for jet broadening compared to data from ALEPH and OPAL, which shows good agreement within uncertainties across the peak and transition regions and is low as expected in the far tail. The uncertainty from the PYTHIA tune and value of α_s are indicated by the central values of the tune 3 and $\alpha_s(m_Z) = 0.1184$ histograms, which agree within the perturbative uncertainties of the default GENEVA prediction across most of the transition and tail regions. As for the other observables, we see better agreement in the peak (below $B \sim 0.1$) with PYTHIA tune 1 and $\alpha_s(m_Z) = 0.1135$.

3.4 Application to hadronic collisions

In this section, we apply the framework developed in section 3.2 to hadronic collisions and present first results from the implementation in the GENEVA Monte Carlo. To accommodate hadrons in the initial state, special consideration is required for each component of our master formula. Our goal is to demonstrate that the same methods can be applied in a hadronic environment to obtain a consistent description at the next higher perturbative accuracy. We use Drell-Yan production $pp \to Z/\gamma^* \to \ell^+\ell^-$ as a concrete example to study the framework, deferring a detailed comparison with Tevatron and LHC data to later work.

In hadronic collisions, N-jettiness can be used as a jet resolution variable, with the observable taking the initial states into account. The theoretical framework exists to resum N-jettiness at hadron colliders, and this resummation has been applied to several processes [117, 41, 118]. Similarly, the techniques required to perform the next-to-leading-order calculations at hadron colliders are known. A phenomenological study additionally requires GENEVA to be interfaced with a parton shower and hadronization model that includes multiple parton interactions.

In the Drell-Yan example, the 0-jet resolution variable is beam thrust, $\mathcal{T}_0$, which is the analog to 2-jettiness, $\mathcal{T}_2$, used in the e^+e^- application.[15] The resummation of beam thrust is performed to NNLL, and the jet multiplicities at fixed order are calculated at NLO_0 and LO_1. The prediction of GENEVA is compared to the analytic resummation of $\mathcal{T}_0$ at NNLL+LO_1 as a demonstration that the program correctly describes the matching between 0- and 1-jet multiplicities. Finally, we discuss how the accuracy of these ingredients can be improved and the challenges present in applying GENEVA to hadron collisions.

Beam thrust is defined as a sum of contributions from particles in the final state [1],

$$\mathcal{T}_0 = \sum_k \min\{n_a \cdot p_k, n_b \cdot p_k\}\,, \tag{3.74}$$

where the observable is evaluated in the center-of-mass frame of the hard partonic collision. The $n_{a,b}$ are light cone vectors along the beam ($\hat{z}$) axis, with $n_a = (1, \hat{z})$ and $n_b = (1, -\hat{z})$. Beam thrust can be evaluated in any frame by performing a longitudinal boost on eq. (3.74).

With the addition of more final-state jets, the N-jettiness definition can be generalized from the 0-jet case,

$$\mathcal{T}_N = \sum_k \min\{n_a \cdot p_k,\, n_b \cdot p_k,\, n_1 \cdot p_k,\, \ldots,\, n_N \cdot p_k\}\,. \tag{3.75}$$

As for beam thrust, this observable is evaluated in the partonic center-of-mass frame. The $n_i = (1, \hat{n}_i)$ for $i = 1, \ldots, N$ are light cone vectors along the jet directions. Note that the above definition of $\mathcal{T}_N$ is a simple extension of the observable for e^+e^- collisions, which has no contribution from the beam directions but is otherwise identical.

3.4.1 Master formula and ingredients for hadronic collisions

As in the e^+e^- case, the master formula for the cross section in GENEVA is given by eq. (3.29), eq. (3.30), and eq. (3.37). To match the 0- and 1-jet multiplicities for

[15] Since we are mainly interested in QCD corrections, we have chosen the subscript on $\mathcal{T}$ to indicate the multiplicity of jets in the final state.

a general process, the master formula is

$$\frac{\mathrm{d}\sigma_{\mathrm{incl}}}{\mathrm{d}\Phi_0} = \frac{\mathrm{d}\sigma}{\mathrm{d}\Phi_0}(\mathcal{T}_0^{\mathrm{cut}}) + \int \frac{\mathrm{d}\Phi_1}{\mathrm{d}\Phi_0}\frac{\mathrm{d}\sigma}{\mathrm{d}\Phi_1}(\mathcal{T}_0)\,\theta(\mathcal{T}_0 > \mathcal{T}_0^{\mathrm{cut}})\,, \tag{3.76}$$

where the 0-jet cumulant, $\mathrm{d}\sigma/\mathrm{d}\Phi_0(\mathcal{T}_0^{\mathrm{cut}})$, and the 1-jet spectrum, $\mathrm{d}\sigma/\mathrm{d}\Phi_1(\mathcal{T}_0)$, are

$$\begin{aligned}\frac{\mathrm{d}\sigma}{\mathrm{d}\Phi_0}(\mathcal{T}_0^{\mathrm{cut}}) &= \frac{\mathrm{d}\sigma^{\mathrm{resum}}}{\mathrm{d}\Phi_0}(\mathcal{T}_0^{\mathrm{cut}}) + \left[\frac{\mathrm{d}\sigma^{\mathrm{FO}}}{\mathrm{d}\Phi_0}(\mathcal{T}_0^{\mathrm{cut}}) - \frac{\mathrm{d}\sigma^{\mathrm{resum}}}{\mathrm{d}\Phi_0}(\mathcal{T}_0^{\mathrm{cut}})\bigg|_{\mathrm{FO}}\right],\\ \frac{\mathrm{d}\sigma}{\mathrm{d}\Phi_1}(\mathcal{T}_0) &= \frac{\mathrm{d}\sigma_{\mathrm{incl}}}{\mathrm{d}\Phi_1}\left[\frac{\mathrm{d}\sigma^{\mathrm{resum}}}{\mathrm{d}\Phi_0\mathrm{d}\mathcal{T}_0}\bigg/\frac{\mathrm{d}\sigma^{\mathrm{resum}}}{\mathrm{d}\Phi_0\,\mathrm{d}\mathcal{T}_0}\bigg|_{\mathrm{FO}}\right].\end{aligned} \tag{3.77}$$

Φ_0 is the phase space for the hard scattering that produces the 0-jet final state, and Φ_1 includes the additional phase space for the final-state jet.

In GENEVA, the contributions to these cross sections are calculated separately for each parton subprocess. Because the fixed-order matching in the 0-jet cumulant is performed additively, the net weight in the 0-jet cumulant after summing over events is the same as the flavor-summed cumulant. In the 1-jet spectrum, the fixed-order matching is performed multiplicatively, meaning the sum over all events for a given $\mathcal{T}_0$ has a different cross section than if we used flavor-summed components for the different terms in the matching formula. The two approaches agree up to higher-order corrections, but the former approach is natural in the Monte Carlo. In the following subsections, we will discuss how the resummed and fixed-order contributions to the master formula are obtained.

3.4.1.1 Resummation

Like $\mathcal{T}_2$ for e^+e^- collisions, beam thrust can be factorized in SCET and the resummation can be carried out systematically to higher orders. The factorized beam thrust spectrum for Drell-Yan is given by [40]

$$\frac{\mathrm{d}\sigma}{\mathrm{d}\Phi_0 d\mathcal{T}_0} = \frac{\mathrm{d}\sigma_B}{\mathrm{d}\Phi_0}\sum_{ij} H_{ij}(Q,\mu)\int \mathrm{d}t_a\mathrm{d}t_b\, B_i(t_a,x_a,\mu)\, B_j(t_b,x_b,\mu)\, S_{ij}\Big(\mathcal{T}_0 - \frac{t_a+t_b}{Q},\mu\Big)\,, \tag{3.78}$$

where Q is the dilepton invariant mass, and Φ_0 is the phase space for the $q\bar{q} \to \ell^+\ell^-$ hard scattering. The momentum fractions $x_{a,b}$ are defined in terms of the total rapidity Y of the final state from the hard scattering,

$$x_a = \frac{Q}{E_{\mathrm{cm}}}e^{Y}\,, \qquad x_b = \frac{Q}{E_{\mathrm{cm}}}e^{-Y}\,. \tag{3.79}$$

Comparing eq. (3.78) to the e^+e^- analog, eq. (3.61), it is clear that the factorization theorems are structurally similar. The chief difference is that, while the jet functions in eq. (3.61) parametrize the collinear evolution of final-state jets, the beam functions

in eq. (3.78) parametrize the collinear evolution of the incoming partons as well as the nonperturbative process of extracting high-energy partons from the proton. The beam functions can be further factorized into a convolution between the parton distribution functions f_j and perturbatively calculable Wilson coefficients $\mathcal{I}_{ij}$ [40, 119],

$$B_i(t, x, \mu) = \sum_j \int_x^1 \frac{\mathrm{d}\xi}{\xi} \mathcal{I}_{ij}\Big(t, \frac{x}{\xi}, \mu\Big) f_j(\xi, \mu)\,. \tag{3.80}$$

Note that due to initial-state radiation, the $x_{a,b}$ are distinct from the Bjorken variable ξ appearing in the convolution above that gives the momentum fraction of the energetic partons that are liberated from the proton. The sum over partons i, j in eq. (3.78) is a sum over flavor singlet quark-antiquark combinations, such as $u\bar{u}$ or $\bar{b}b$. For each flavor, the beam functions are different, and the hard function H_{ij} differs for up- and down-type quarks due to the different electroweak couplings to the gauge boson. This flavor sum is an important consideration when implementing the master formula in GENEVA, since the Monte Carlo generates events for each flavor combination, and the flavor sum is performed in the sum over events.

For processes with final-state jets, the extension of the beam thrust factorization theorem to N-jettiness is known and has the schematic form [1, 80]

$$\frac{\mathrm{d}\sigma}{\mathrm{d}\Phi_N d\mathcal{T}_N} = \frac{\mathrm{d}\sigma_B}{\mathrm{d}\Phi_N} \mathrm{Tr} \sum_\kappa H_\kappa \left[\Big(B_a^\kappa\, B_b^\kappa\, J_1^\kappa \cdots J_N^\kappa \Big) \otimes S_{N+2}^\kappa \right] (\mathcal{T}_N)\,. \tag{3.81}$$

The trace is over the nontrivial color structures that can exist in the hard and soft functions. Additionally, there is a sum over parton channels for the hard scattering that are labeled by the index κ. The additional jets are associated with additional collinear sectors in SCET, and the factorization theorem reflects this by including additional jet functions. The soft function also changes to account for the soft radiation between the final-state jets and the initial-state radiation from the colliding partons.

The factorization theorems in eqs. (3.78) and (3.81) can be used to perform the resummation for both the spectrum and cumulant. Although these factorization theorems directly describe the spectrum in $\mathcal{T}_0$ or $\mathcal{T}_N$, they can be integrated over the observable to obtain the cumulant. The perturbative part of each function in the factorization theorem is calculable, and for many processes the functions are known to high order. Each function is associated with a scale that is connected to the physical degrees of freedom that the function describes. As in the e^+e^- case, renormalization group evolution resums the large logarithms of ratios of these scales (see table 3.2).

3.4.1.2 Fixed order

Following eq. (3.76), we need to define the 0-jet cumulant $\mathrm{d}\sigma/\mathrm{d}\Phi_0(\mathcal{T}_0^{\mathrm{cut}})$ and the 1-jet spectrum $\mathrm{d}\sigma/\mathrm{d}\Phi_1(\mathcal{T}_0)$. At the order we are interested in, the 1-jet spectrum will

be given by the tree-level cross section $B_1(\Phi_1)$ for the process $pp \to Z/\gamma^* j \to \ell^+\ell^- j$. The 0-jet cumulant is given by

$$\begin{aligned}\frac{\mathrm{d}\sigma}{\mathrm{d}\Phi_0}(\mathcal{T}_0^{\mathrm{cut}}) &= B_0(\Phi_0) + V_0(\Phi_3) + \int \frac{\mathrm{d}\Phi_1}{\mathrm{d}\Phi_0} B_1(\Phi_1)\theta(\mathcal{T}_0 < \mathcal{T}_0^{\mathrm{cut}}) \\ &\quad + \int \frac{\mathrm{d}\Phi_{1,a}}{\mathrm{d}\Phi_0} G_a(\Phi_{1,a})\theta(\mathcal{T}_0 < \mathcal{T}_0^{\mathrm{cut}}) \\ &\quad + \int \frac{\mathrm{d}\Phi_{1,b}}{\mathrm{d}\Phi_0} G_b(\Phi_{1,b})\theta(\mathcal{T}_0 < \mathcal{T}_0^{\mathrm{cut}})\,, \end{aligned} \tag{3.82}$$

where the corresponding parton distribution functions have been included into the definitions of the Born, virtual, and real emission cross sections,

$$\begin{aligned} B_N(\Phi_N) &= f_a(x_a,\mu_F) f_b(x_b,\mu_F) \mathcal{B}_N(\Phi_N)\,, \\ V_N(\Phi_N) &= f_a(x_a,\mu_F) f_b(x_b,\mu_F) \mathcal{V}_N(\Phi_N)\,. \end{aligned} \tag{3.83}$$

In addition, in order to account for the incomplete cancellations of initial-state collinear singularities, we have included one collinear counterterm $G_{a,b}$ for each initial-state parton,

$$\begin{aligned} G_a(\Phi_N) &= f_a(x_a,\mu_F) f_b(x_b,\mu_F) \mathcal{G}_a(\Phi_N)\,, \\ G_b(\Phi_N) &= f_a(x_a,\mu_F) f_b(x_b,\mu_F) \mathcal{G}_b(\Phi_N)\,. \end{aligned} \tag{3.84}$$

Assuming the UV divergences of V_0 have already been taken care of by a proper renormalization procedure, the remaining divergences present in B_1, V_0, and $G_{a,b}$ are of IR origin. We handle these divergences with the FKS subtraction procedure. After having partitioned the phase space into nonoverlapping regions m, which contain at most one collinear and one soft singularity, by means of a set of $\theta_m^{\mathcal{T}}$-functions, the final formula, including the subtraction counterterms, is

$$\begin{aligned}\frac{\mathrm{d}\sigma}{\mathrm{d}\Phi_0}(\mathcal{T}_0^{\mathrm{cut}}) &= B_0(\Phi_0) + V_0(\Phi_0) + I(\Phi_0) \\ &\quad + \sum_m \int \mathrm{d}\Phi_{\mathrm{rad}}^m \Bigg[B_1(\Phi_1^m)\theta_m^{\mathcal{T}}(\Phi_0,\Phi_{\mathrm{rad}}^m)\theta(\mathcal{T}_0 < \mathcal{T}_0^{\mathrm{cut}}) \\ &\qquad - \frac{\mathrm{d}\Phi_{\mathrm{rad}}^{m,\mathrm{s}}}{\mathrm{d}\Phi_{\mathrm{rad}}^m} B_1(\Phi_1^{m,\mathrm{s}})\theta_m^{\mathrm{s}}(\Phi_0,\Phi_{\mathrm{rad}}^{m,\mathrm{s}}) - \frac{\mathrm{d}\Phi_{\mathrm{rad}}^{m,\mathrm{c}}}{\mathrm{d}\Phi_{\mathrm{rad}}^m} B_1(\Phi_1^{m,\mathrm{c}}) + \frac{\mathrm{d}\Phi_{\mathrm{rad}}^{m,\mathrm{cs}}}{\mathrm{d}\Phi_{\mathrm{rad}}^m} B_1(\Phi_1^{m,\mathrm{cs}}) \Bigg] \\ &\quad + \int \mathrm{d}\Phi_{\mathrm{rad},a}\; G_a(\Phi_{1,a}) + \int \mathrm{d}\Phi_{\mathrm{rad},b}\; G_b(\Phi_{1,b})\,. \end{aligned} \tag{3.85}$$

As mentioned in section 3.3.1.2, we choose to partition the phase space by means of $\theta_m^{\mathcal{T}}$-functions that depend on the jet resolution variable. It is therefore crucial to evaluate the jet resolution variable and the subtraction in the same frame. This

ensures the proper cancellation of IR singularities by subtraction counterterms. The preferred frame for the fixed-order calculations is the partonic center-of-mass frame, since the subtraction is most naturally expressed in terms of variables defined in that frame. Also, the jet resolution variable, eq. (3.74), is defined in this frame and resummation can be performed in it. Therefore, our approach is to perform the entire calculation in the partonic center-of-mass frame.

At this point, all the ingredients of eq. (3.85) are known and available in the literature [102, 17]. Note that additional complications arise when extending this construction to higher multiplicities because one must use a map that preserves the value of $\mathcal{T}_0$ (up to power corrections), just as for $\mathcal{T}_2$ in the $e^+e^- \to 3$ jet case. For our $pp \to Z/\gamma^* \to \ell^+\ell^-$ study, this problem can be avoided since we currently include only up to one extra parton and, consequently, the $\mathcal{T}_0(\Phi_1)$ value is well defined. In order to obtain $\mathcal{T}_0(\Phi_N)$ with $N > 1$ in general, this issue may be addressed in a similar fashion to what has been done for e^+e^-.

3.4.2 Application to Drell-Yan production

We study Drell-Yan production in pp collisions at $E_{\text{cm}} = 8$ TeV in GENEVA, sampling the invariant mass Q of the $\ell^+\ell^-$ pair around the Z pole between $M_Z - 10\Gamma_Z$ and $M_Z + 10\Gamma_Z$, where $M_Z = 91.1876$ GeV is the mass of the Z and its width is $\Gamma_Z = 2.4952$ GeV [90]. The dominant contribution in this range of Q comes from Z exchange, although the photon does contribute. Profile scales identical to those used in the e^+e^- $\mathcal{T}_2$ resummation are used, which is justified since the logarithmic structure is the same between the two observables. The resummation is turned off just above $\mathcal{T}_0 \sim M_Z/2$, and for greater $\mathcal{T}_0$, the spectrum reproduces the fixed-order distribution.

In figure 3.13, we show the analytic beam thrust resummation at NLL and NNLL+LO_1 in the peak, transition, and tail regions. In the peak and transition regions, the resummed result converges well. At the end of the transition region and in the tail region, the pure NLL resummed distribution goes to 0 as the resummation is turned off, but the NNLL+LO_1 distribution moves into the fixed-order result.

Implementing the Drell-Yan process in GENEVA allows us to study the feasibility of the multiplicative matching for the spectrum in eq. (3.77) and compare with the analytic resummed distribution. We show this comparison in figure 3.14, where the analytic curve is evaluated at NNLL+LO_1. Additionally, we show the NNLL and LO_1 distributions separately. Overall, the partonic GENEVA distribution is quite close to the NNLL+LO_1 distribution, both in terms of the central values and the size of uncertainties. In the peak region, the spectra match closely and agree well with the pure NNLL resummed distribution. At the low end of the transition region, the resummed spectra are still in fair agreement while moving to higher $\mathcal{T}_0$ values the GENEVA partonic prediction and the NNLL+LO_1 distributions begin to systematically deviate from the NNLL distribution. This deviation arises from the LO_1 nonsingular terms

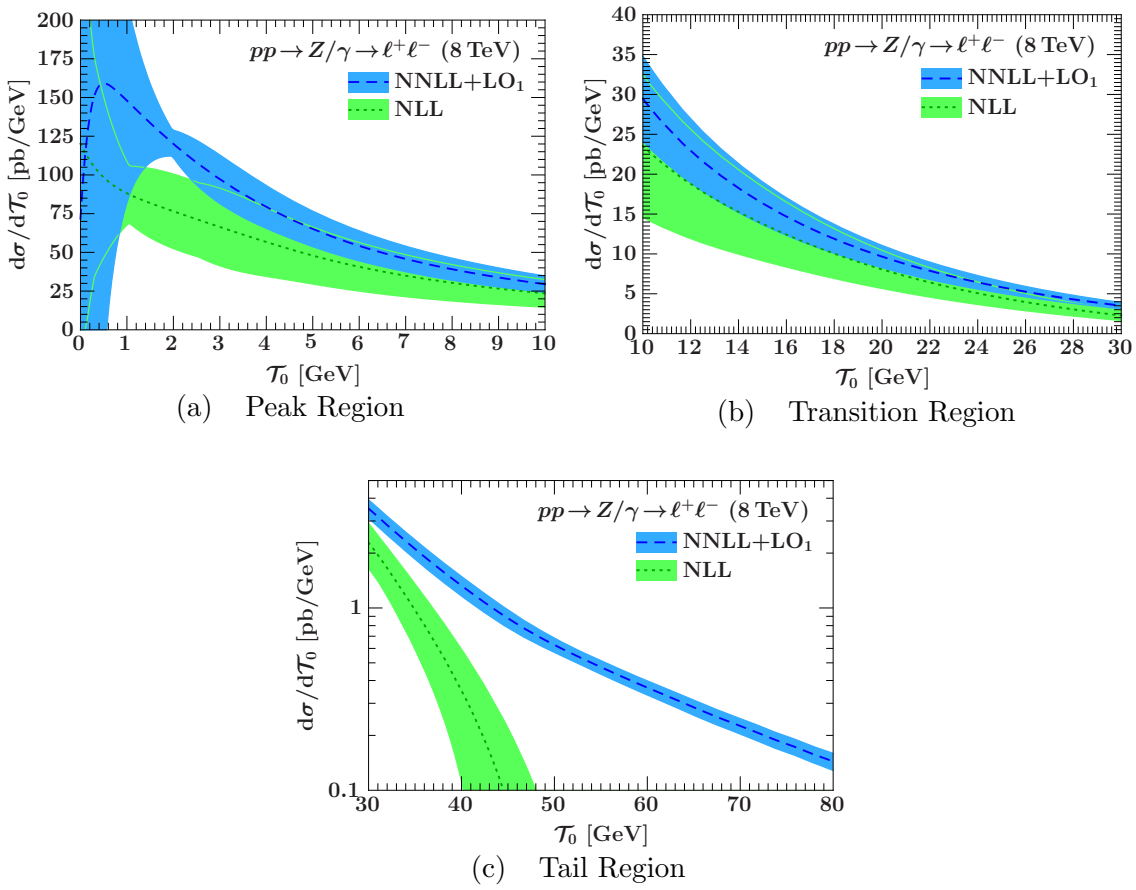

(a) Peak Region

(b) Transition Region

(c) Tail Region

Figure 3.13: Analytic resummation of $\mathcal{T}_0$ matched to fixed order in the (a) peak, (b) transition, and (c) tail regions. The central value is shown along with the band from scale uncertainties, as discussed in section 3.4.2, at NLL and NNLL′+LO$_1$.

that are present in the matched spectrum but absent in the pure resummed one. In the tail region, the GENEVA partonic and NNLL+LO$_1$ predictions move into the LO$_1$ spectrum. After the resummation has been turned off, these spectra match the LO$_1$ precisely in central value and uncertainties, as expected. Note that in the corresponding comparison in the e^+e^- case, shown in figure 3.3(a)-3.3(c), the analytic and the partonic GENEVA distributions are in closer agreement because the resummed components of the multiplicative matching in eq. (3.37) include the nonsingular terms at LO$_3$, which are known analytically. These are not included in the Drell-Yan case, and so the difference between the analytic and GENEVA distributions in figure 3.14 is more sensitive to the subleading corrections that the nonsingular terms generate.

As in the e^+e^- case, the uncertainty bands for the resummed curves and GENEVA predictions in figures 3.13 and 3.14 are obtained by adding the fixed-order and re-

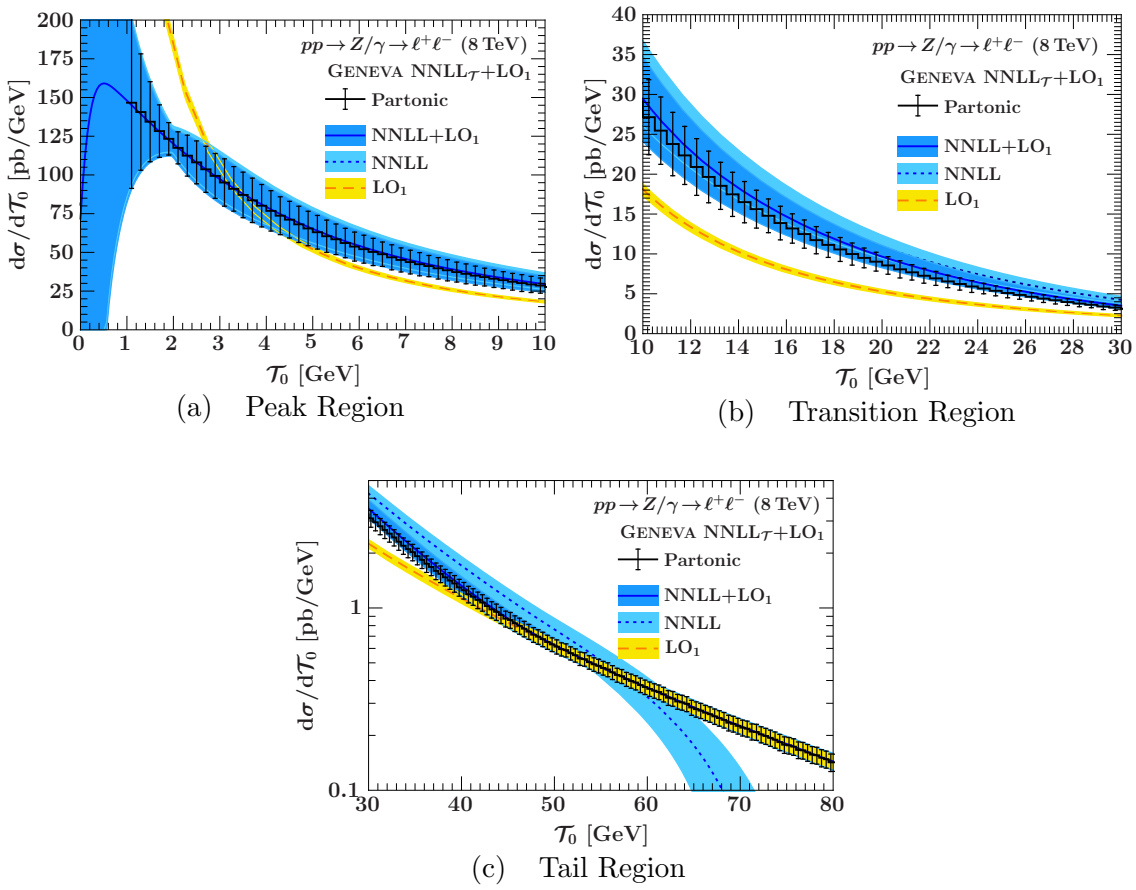

(a) Peak Region

(b) Transition Region

(c) Tail Region

Figure 3.14: The GENEVA partonic NNLL+LO$_1$ result is shown compared to the analytic resummation of $\mathcal{T}_0$ matched to fixed order at NNLL+LO$_1$ in the (a) peak, (b) transition, and (c) tail regions. Also shown for comparison is the pure resummed result at NNLL and the fixed-order LO$_1$ contribution.

summation uncertainties in quadrature. In the peak and transition regions of the distribution, the resummation uncertainties dominate, while the fixed-order uncertainty dominates as the resummation is being turned off in the tail region. Comparing the uncertainty of the resummed distributions with that of the LO$_1$ distribution, which is much smaller, one can see that the fixed-order uncertainty is an underestimate of the missing higher-order terms. The reason for this is twofold: the missing large logarithmic corrections at higher orders, whose associated uncertainties are instead included in the resummed distribution, and the partial cancellation between the renormalization and factorization scale dependence, whose variations are correlated in the results we show.

In both the e^+e^- and Drell-Yan processes, the partonic GENEVA spectrum is

determined by eq. (3.47), which for an event multiplies the fully exclusive fixed-order cross section by the ratio of the resummed cross section for the jet resolution variable divided by the fixed-order expansion of that resummation. Compared to the e^+e^- case, where each subprocess contributing to the cross section is trivially proportional, in Drell-Yan, the convolution with the PDFs requires treating every possible $q\bar{q}$ initial state separately, in both the fixed-order and the resummed cross sections. In GENEVA, the flavor sum is performed in the Monte Carlo sense, since every event has a definite flavor for the initial-state quarks and the correct flavor-summed cross section is obtained after a sum over all events. This means that the separate factors in eq. (3.47) are evaluated for an individual flavor, and the entire expression is summed over flavors. In the analytic resummation, since the matching between the resummed and fixed-order cross sections is additive, there is instead only one way to perform the sum over flavors.

A version of the master formula where both the resummed and the resummed-expanded are separately flavor summed before entering eq. (3.77) would be equally valid. We have checked, however, that this is a very minor effect and is not the main contribution to the apparent differences of the GENEVA predictions with the analytic resummed cross section. In fact, the reason for the discrepancy is in the difference of higher-order terms that are included in the GENEVA multiplicative approach with respect to the additive matching used in the analytical calculation. This can also be seen as an indication of the relative freedom in implementing the master formula in eq. (3.47) at a given perturbative accuracy. As one can evince from figures 3.3(d)-3.3(f), should the resummation and fixed-order calculations be evaluated at the next order in perturbative accuracy, the size of the yet-missing terms would decrease, and consequently, the difference between GENEVA and the analytic results would be reduced.

The GENEVA implementation in this example can be extended to higher accuracy in terms of both fixed-order matrix elements and resummation. An equivalent accuracy to the e^+e^- results shown in section 3.3 can be achieved if the fixed-order matrix elements for the 1-jet multiplicity are calculated at NLO, the 2-jet multiplicity are calculated at LO, and the resummation of beam thrust is continued to NNLL$'$. Although this is beyond the scope of this work, we nonetheless demonstrate that the GENEVA framework is capable of merging matrix elements of different jet multiplicities beyond the lowest order. As in the e^+e^- case, jet multiplicities are defined using a physical jet resolution variable, which allows for a consistent extension of the entire framework to $\mathcal{O}(\alpha_s)$ perturbative accuracy.

In section 3.3, we found that NNLL$'$ resummation of the jet resolution variable $\mathcal{T}_2$, when combined with the parton shower, was capable of describing the spectrum in other 2-jet observables with an accuracy that clearly exceeded NLL, the naive accuracy of the parton shower. The resummation of $\mathcal{T}_2$ captures an important set of logarithms that are correlated with other 2-jet observables, and, when combined with the fully exclusive, all-orders description of the parton shower, the accuracy of

other observables can be improved beyond NLL. At a hadron collider, the effective dynamic range of observables is much larger, meaning the correlation between the jet resolution variable and another observable of interest may be small. In this case, the parton shower may play a greater role in determining the spectrum, and hence the accuracy, of other observables. We will investigate these features in a future work.

3.5 Conclusions

In this chapter, we have shown how to combine higher-order resummation of a jet resolution variable with fully differential next-to-leading-order calculations to extend the perturbative accuracy of cross sections beyond the lowest order for all values of the jet resolution scale. This framework has been interfaced with a parton shower and hadronization to give the GENEVA Monte Carlo program.

Our framework provides both the versatility of fixed-order calculations and the accuracy of higher-order analytic resummation. From the point of view of Monte Carlo generators, the GENEVA approach allows the combination of higher-order resummations with higher fixed-order calculations. From the point of view of resummed calculations, it allows one to obtain a fully differential cross section that correctly resums the jet resolution variable to higher logarithmic accuracy. Since this construction maintains the higher perturbative accuracy for all values of the jet resolution scale, it naturally allows NLO calculations of different jet multiplicities to be combined with one another.

The higher logarithmic resummation of the jet resolution scale allows us to use a low cut on the jet resolution scale, much lower than the point where fixed-order perturbation theory breaks down but still above the nonperturbative regime. This is a major difference to other approaches [33, 34, 35], where the jet-merging scale has to be chosen much larger, such that $\alpha_s \ln^2 \tau^{\text{cut}} \ll 1$.

In this chapter, we have concentrated on the theoretical construction, which is valid for any number of jets, and for both e^+e^- and hadron colliders. We have shown that one has to carefully choose a jet resolution variable that is resummable to higher logarithmic accuracy. In our approach, the N-jet and $(N+1)$-jet regions are described by the same fully differential calculation without the need of an explicit jet-merging scale. The cut on the jet resolution variable is only needed due to the presence of IR divergences. We have given expressions for both the integrated cross section below the IR cutoff and the differential cross section above that properly combine the higher logarithmic resummation with a higher fixed-order calculation.

This approach has been implemented in the GENEVA Monte Carlo. As a first application, we have presented results for e^+e^- collisions. The jet resolution variable for this case was chosen to be 2-jettiness, which is directly related to thrust, and we combined its NNLL$'$ resummation with the fully differential 3-jet rate at NLO$_3$. Varying the profile scales and the renormalization scale has allowed us to obtain

event-by-event uncertainties. As a final step, we have interfaced our perturbative result with Pythia 8, which added a parton shower and hadronization to our results. The parton shower adds additional radiation beyond the highest jet multiplicity in Geneva and has been restricted to only fill out the jets of the exclusive jet cross sections at lower jet multiplicity. Since the cut on the jet resolution variable could be chosen to be very small, the effect of the perturbative shower (without hadronization) is rather small, and different tunes in Pythia do not affect the resulting distributions significantly. Hadronization has a significant effect, and the difference in final results due to different hadronization parameters is more manifest.

We have shown that Geneva correctly reproduces the higher-order resummation of the thrust spectrum, even after showering, which serves as a nontrivial validation of our approach. Using $\alpha_s(m_Z) = 0.1135$, as obtained in ref. [85] from fits to the thrust spectrum using higher-order resummation, together with tune 1 of Pythia 8, we obtain an excellent description of ALEPH and OPAL data. The same setup was then used to predict other event shape variables, namely C-parameter, heavy jet mass, and jet broadening. In all cases, our results agree remarkably well with the explicit analytical resummations, even though only the thrust resummation was used as an input. This comparison shows numerically that we achieve a higher resummation accuracy than NLL, which is what one would naively expect to obtain from the parton shower. This is especially remarkable for jet broadening, where the resummation formula has a completely different structure from the thrust resummation. Comparing our results after hadronization to the data, we again find excellent agreement for these other observables.

Finally, we have presented first results toward an implementation for hadron colliders in Geneva. Choosing the Drell-Yan process at the LHC with beam thrust as the jet resolution variable, we combined the resummation of beam thrust at NNLL with the leading-order matrix element for the emission of an extra jet. The results from Geneva agree well with analytical results, which shows the applicability of the framework to hadron colliders.

As we have shown, our theoretical framework to combine higher-order resummation with fixed-order matrix elements and parton shower Monte Carlos is very general, and there are many avenues to pursue in the future. Obvious next steps for e^+e^- collisions are to include NLO calculations for 4 jets, which would require including the logarithmic resummation for 3-jettiness [120] as well as additional tree-level matrix elements. In addition, one can consider the resummation for other jet resolution variables. For hadronic collisions, next steps are to include the resummation and NLO calculations for higher jet multiplicities, as well as adding parton showering and hadronization using the different available programs.

Chapter 4

Conclusion

The preceding chapters have described in some detail certain state-of-the-art ways that the precision of matrix-element calculations used to simulate events can be extended without sacrificing the benefits that parton shower routines have long provided to the experimental community. Doing so is not an easy task, and the discussion in section 2.3.1 articulated how the constraints that must be satisfied by a full calculation become more and more stringent as one attempts to increase the fixed-order accuracy. Further discussion in section 2.5.2.3 described new issues that arise in matching to the parton shower when pushing the fixed-order accuracy to NNLO. Nonetheless, with careful attention to the various pieces involved and the constraints that their combination must satisfy, it is possible to make progress.

The focus of chapter 2 was to detail just such a set of constraints for the extension of the fixed-order accuracy of the lowest multiplicity to NNLO. After carefully understanding the problem and constraining the solution, the general construction of an NNLO+PS framework was able to be worked out in a straightforward and systematic fashion. Indeed, the considerations presented there are sufficient to straightforwardly work out general constructions for even higher order FO+PS frameworks should there be interest in doing so. An important next step will be to flesh out the details of the general NNLO+PS construction to take practical constraints into account and to optimize the construction for ease of implementation. There are many analyses that could more fully benefit from the NNLO fixed-order calculations that are increasingly becoming available, and a concrete implementation of an NNLO+PS framework will be eagerly awaited by the experimental community.

Chapter 3 described efforts to increase the precision of event generators along a different dimension. As useful as NNLO calculations are, there are regions of phase space where fixed-order perturbation theory breaks down, and the higher fixed-order accuracy is not helpful in these regions. To address the need of extending the lowest-order matching of tree-level matrix elements with parton showers to give a complete description at the next higher perturbative accuracy in α_s at both small and large jet resolutions, higher-order resummation was employed. It was shown that extending

to the next higher perturbative accuracy *requires* the combination of the higher-order resummation at small values of the jet resolution variable in addition to the higher-precision fixed-order matrix-element corrections at large values. It was also found, interestingly, that the higher-order resummation naturally leads to a smooth connection of the NLO calculations for different jet multiplicities. This shows a relation between the first and third strategies for improving precision described in the introduction, both of which are important for increasing the power and versatility of event generators.

Progress in building a concrete implementation of such a framework in a Monte Carlo called GENEVA was also described in chapter 3. For leptonic collisions, $e^+e^- \to$ jets was used as an example of the construction. Results for this process were found to be in good agreement with LEP data for a variety of 2-jet observables. Additional work remains to be done to continue implementing the capabilities of the method. For example, it is possible, in principle, to extend the framework to any number of multiplicities at NLO, as described in section 3.2.3. Initial results were also shown for hadronic collisions in Drell-Yan production, and additional work remains to fully flesh out the capabilities of the method for hadronic collisions.

In closing, the material presented in this thesis not only advances along multiple dimensions the precision that can be attained in modern event generators for particle colliders, but it also lays the groundwork for further advances and specific implementations yet to be fully realized.

Bibliography

[1] Iain W. Stewart, Frank J. Tackmann, and Wouter J. Waalewijn. N-Jettiness: An Inclusive Event Shape to Veto Jets. *Phys. Rev. Lett.*, 105:092002, 2010.

[2] A. Heister et al. Studies of QCD at e^+e^- centre-of-mass energies between 91 GeV and 209 GeV. *Eur. Phys. J. C*, 35:457–486, 2004.

[3] G. Abbiendi et al. Measurement of event shape distributions and moments in $e^+e^- \to$ hadrons at 91-GeV - 209-GeV and a determination of alpha(s). *Eur. Phys. J. C*, 40:287–316, 2005.

[4] S. Catani, F. Krauss, R. Kuhn, and B. R. Webber. QCD matrix elements + parton showers. *JHEP*, 11:063, 2001.

[5] Leif Lönnblad. Correcting the colour-dipole cascade model with fixed order matrix elements. *JHEP*, 05:046, 2002.

[6] F. Krauss. Matrix elements and parton showers in hadronic interactions. *JHEP*, 08:015, 2002.

[7] Stephen Mrenna and Peter Richardson. Matching matrix elements and parton showers with HERWIG and PYTHIA. *JHEP*, 05:040, 2004.

[8] Michelangelo L Mangano. The so–called MLM prescription for ME/PS matching (2004). Talk presented at the Fermilab ME/MC Tuning Workshop, October 4, 2004., 2004.

[9] Andreas Schälicke and Frank Krauss. Implementing the ME+PS merging algorithm. *JHEP*, 07:018, 2005.

[10] Nils Lavesson and Leif Lönnblad. W + jets matrix elements and the dipole cascade. *JHEP*, 07:054, 2005.

[11] Stefan Höche et al. Matching parton showers and matrix elements. 2006.

[12] M. Bahr, S. Gieseke, M.A. Gigg, D. Grellscheid, K. Hamilton, et al. Herwig++ Physics and Manual. *Eur. Phys. J. C*, 58:639–707, 2008.

[13] Stefano Frixione and Bryan R. Webber. Matching NLO QCD computations and parton shower simulations. *JHEP*, 06:029, 2002.

[14] Stefano Frixione, Paolo Nason, and Bryan R. Webber. Matching NLO QCD and parton showers in heavy flavour production. *JHEP*, 08:007, 2003.

[15] Paolo Nason. A new method for combining NLO QCD with shower Monte Carlo algorithms. *JHEP*, 11:040, 2004.

[16] Stefano Frixione, Paolo Nason, and Carlo Oleari. Matching NLO QCD computations with Parton Shower simulations: the POWHEG method. *JHEP*, 11:070, 2007.

[17] Simone Alioli, Paolo Nason, Carlo Oleari, and Emanuele Re. A general framework for implementing NLO calculations in shower Monte Carlo programs: the POWHEG BOX. *JHEP*, 1006:043, 2010.

[18] Stefan Hoche, Frank Krauss, Marek Schonherr, and Frank Siegert. Automating the POWHEG method in Sherpa. *JHEP*, 1104:024, 2011.

[19] Rikkert Frederix, Stefano Frixione, Valentin Hirschi, Fabio Maltoni, Roberto Pittau, et al. Four-lepton production at hadron colliders: aMC@NLO predictions with theoretical uncertainties. *JHEP*, 1202:099, 2012.

[20] Charalampos Anastasiou, Lance J. Dixon, Kirill Melnikov, and Frank Petriello. High precision QCD at hadron colliders: Electroweak gauge boson rapidity distributions at NNLO. *Phys. Rev. D*, 69:094008, 2004.

[21] Charalampos Anastasiou, Kirill Melnikov, and Frank Petriello. Fully differential Higgs boson production and the di-photon signal through next-to-next-to-leading order. *Nucl. Phys. B*, 724:197–246, 2005.

[22] Kirill Melnikov and Frank Petriello. Electroweak gauge boson production at hadron colliders through $O(\alpha_s^2)$. *Phys. Rev. D*, 74:114017, 2006.

[23] Massimiliano Grazzini. NNLO predictions for the Higgs boson signal in the $H \to WW \to \ell\nu\ell\nu$ and $H \to ZZ \to 4\ell$ decay channels. *JHEP*, 0802:043, 2008.

[24] Stefano Catani, Leandro Cieri, Giancarlo Ferrera, Daniel de Florian, and Massimiliano Grazzini. Vector boson production at hadron colliders: a fully exclusive QCD calculation at NNLO. *Phys. Rev. Lett.*, 103:082001, 2009.

[25] Ryan Gavin, Ye Li, Frank Petriello, and Seth Quackenbush. FEWZ 2.0: A code for hadronic Z production at next-to-next-to-leading order. *Comput. Phys. Commun.*, 182:2388–2403, 2011.

[26] Stefano Catani, Leandro Cieri, Daniel de Florian, Giancarlo Ferrera, and Massimiliano Grazzini. Diphoton production at hadron colliders: a fully-differential QCD calculation at NNLO. *Phys. Rev. Lett.*, 108:072001, 2012.

[27] Michal Czakon, Paul Fiedler, and Alexander Mitov. The total top quark pair production cross-section at hadron colliders through $O(\alpha_S^4)$. *Phys. Rev. Lett.*, 110:252004, 2013.

[28] Daniel de Florian and Javier Mazzitelli. Higgs Boson Pair Production at Next-to-Next-to-Leading Order in QCD. *Phys. Rev. Lett.*, 111:201801, 2013.

[29] Aude Gehrmann-De Ridder, Thomas Gehrmann, E.W.N. Glover, and Joao Pires. Second order QCD corrections to jet production at hadron colliders: the all-gluon contribution. *Phys. Rev. Lett.*, 110:162003, 2013.

[30] Radja Boughezal, Fabrizio Caola, Kirill Melnikov, Frank Petriello, and Markus Schulze. Higgs boson production in association with a jet at next-to-next-to-leading order in perturbative QCD. *JHEP*, 1306:072, 2013.

[31] James Currie, Aude Gehrmann-DeRidder, E.W.N. Glover, and Joao Pires. NNLO QCD corrections to jet production at hadron colliders from gluon scattering. 2013.

[32] Simone Alioli, Keith Hamilton, and Emanuele Re. Practical improvements and merging of POWHEG simulations for vector boson production. *JHEP*, 1109:104, 2011.

[33] Stefan Hoeche, Frank Krauss, Marek Schonherr, and Frank Siegert. QCD matrix elements + parton showers: The NLO case. *JHEP*, 1304:027, 2013.

[34] Thomas Gehrmann, Stefan Hoche, Frank Krauss, Marek Schonherr, and Frank Siegert. NLO QCD matrix elements + parton showers in $e^+e^- \to$ hadrons. *JHEP*, 1301:144, 2013.

[35] Rikkert Frederix and Stefano Frixione. Merging meets matching in MC@NLO. *JHEP*, 1212:061, 2012.

[36] Simon Plätzer. Controlling inclusive cross sections in parton shower + matrix element merging. *JHEP*, 1308:114, 2013.

[37] Leif Lönnblad and Stefan Prestel. Merging Multi-leg NLO Matrix Elements with Parton Showers. *JHEP*, 1303:166, 2013.

[38] Keith Hamilton, Paolo Nason, Carlo Oleari, and Giulia Zanderighi. Merging H/W/Z + 0 and 1 jet at NLO with no merging scale: a path to parton shower + NNLO matching. *JHEP*, 1305:082, 2013.

[39] Gionata Luisoni, Paolo Nason, Carlo Oleari, and Francesco Tramontano. $HW^{\pm}$/HZ + 0 and 1 jet at NLO with the POWHEG BOX interfaced to GoSam and their merging within MiNLO. *JHEP*, 1310:083, 2013.

[40] Iain W. Stewart, Frank J. Tackmann, and Wouter J. Waalewijn. Factorization at the LHC: From PDFs to Initial State Jets. *Phys. Rev. D*, 81:094035, 2010.

[41] Carola F. Berger, Claudio Marcantonini, Iain W. Stewart, Frank J. Tackmann, and Wouter J. Waalewijn. Higgs Production with a Central Jet Veto at NNLL+NNLO. *JHEP*, 1104:092, 2011.

[42] Simone Alioli, Christian W. Bauer, Calvin Berggren, Frank J. Tackmann, Jonathan R. Walsh, et al. Matching Fully Differential NNLO Calculations and Parton Showers. 2013.

[43] Keith Hamilton, Paolo Nason, Emanuele Re, and Giulia Zanderighi. NNLOPS simulation of Higgs boson production. 2013.

[44] Christian W. Bauer, Frank J. Tackmann, and Jesse Thaler. GenEvA (I): A new framework for event generation. *JHEP*, 12:010, 2008.

[45] Christian W. Bauer, Frank J. Tackmann, and Jesse Thaler. GenEvA (II): A phase space generator from a reweighted parton shower. *JHEP*, 12:011, 2008.

[46] Simone Alioli, Christian W. Bauer, Calvin Berggren, Andrew Hornig, Frank J. Tackmann, et al. Combining Higher-Order Resummation with Multiple NLO Calculations and Parton Showers in GENEVA. *JHEP*, 1309:120, 2013.

[47] Leif Lönnblad and Stefan Prestel. Unitarising Matrix Element + Parton Shower merging. *JHEP*, 1302:094, 2013.

[48] Gabor Somogyi and Zoltan Trocsanyi. A New subtraction scheme for computing QCD jet cross sections at next-to-leading order accuracy. 2006.

[49] Stefano Catani and Massimiliano Grazzini. An NNLO subtraction formalism in hadron collisions and its application to Higgs boson production at the LHC. *Phys. Rev. Lett.*, 98:222002, 2007.

[50] M. Czakon. A novel subtraction scheme for double-real radiation at NNLO. *Phys. Lett. B*, 693:259–268, 2010.

[51] Radja Boughezal, Kirill Melnikov, and Frank Petriello. A subtraction scheme for NNLO computations. *Phys. Rev. D*, 85:034025, 2012.

[52] Walter T. Giele, David A. Kosower, and Peter Z. Skands. A Simple shower and matching algorithm. *Phys. Rev. D*, 78:014026, 2008.

[53] W.T. Giele, D.A. Kosower, and P.Z. Skands. Higher-Order Corrections to Timelike Jets. *Phys. Rev. D*, 84:054003, 2011.

[54] Paolo Torrielli and Stefano Frixione. Matching NLO QCD computations with PYTHIA using MC@NLO. *JHEP*, 1004:110, 2010.

[55] Stefano Frixione, Fabian Stoeckli, Paolo Torrielli, and Bryan R. Webber. NLO QCD corrections in Herwig++ with MC@NLO. *JHEP*, 1101:053, 2011.

[56] Keith Hamilton, Paolo Nason, and Giulia Zanderighi. MINLO: Multi-Scale Improved NLO. *JHEP*, 1210:155, 2012.

[57] John M. Campbell, R. Keith Ellis, Rikkert Frederix, Paolo Nason, Carlo Oleari, et al. NLO Higgs Boson Production Plus One and Two Jets Using the POWHEG BOX, MadGraph4 and MCFM. *JHEP*, 1207:092, 2012.

[58] Stefan Prestel. Matrix elements + pythia8. Talk presented at the QCD@LHC 2013 conference, `https://indico.desy.de/getFile.py/access?contribId=96&sessionId=29&resId=0&materialId=slides&confId=6889`, September 5, 2013.

[59] John C. Collins and F. Hautmann. Soft gluons and gauge-invariant subtractions in NLO parton-shower Monte Carlo event generators. *JHEP*, 03:016, 2001.

[60] John C. Collins. Subtraction method for NLO corrections in Monte Carlo event generators for leptoproduction. *JHEP*, 05:004, 2000.

[61] B. Potter and T. Schorner. Combining parton showers with next-to-leading order QCD matrix elements in deep-inelastic e p scattering. *Phys. Lett. B*, 517:86–92, 2001.

[62] Matt Dobbs. Phase space veto method for next-to-leading order event generators in hadronic collisions. *Phys. Rev. D*, 65:094011, 2002.

[63] Michael Krämer and Davison E. Soper. Next-to-leading order QCD calculations with parton showers. I: Collinear singularities. *Phys. Rev. D*, 69:054019, 2004.

[64] Davison E. Soper. Next-to-leading order QCD calculations with parton showers. II: Soft singularities. *Phys. Rev. D*, 69:054020, 2004.

[65] Zoltan Nagy and Davison E. Soper. Matching parton showers to NLO computations. *JHEP*, 10:024, 2005.

[66] Michael Krämer, Stephen Mrenna, and Davison E. Soper. Next-to-leading order QCD jet production with parton showers and hadronization. *Phys. Rev. D*, 73:014022, 2006.

[67] Rikkert Frederix, Stefano Frixione, Valentin Hirschi, Fabio Maltoni, Roberto Pittau, et al. Scalar and pseudoscalar Higgs production in association with a top-antitop pair. *Phys.Lett.*, B701:427–433, 2011.

[68] Simon Plätzer and Stefan Gieseke. Dipole Showers and Automated NLO Matching in Herwig++. *Eur. Phys. J. C*, 72:2187, 2012.

[69] Keith Hamilton and Paolo Nason. Improving NLO-parton shower matched simulations with higher order matrix elements. *JHEP*, 1006:039, 2010.

[70] Stefan Höche, Frank Krauss, Marek Schönherr, and Frank Siegert. NLO matrix elements and truncated showers. *JHEP*, 1108:123, 2011.

[71] Nils Lavesson and Leif Lönnblad. Extending CKKW-merging to One-Loop Matrix Elements. *JHEP*, 0812:070, 2008.

[72] Edward Farhi. A QCD Test for Jets. *Phys. Rev. Lett.*, 39:1587–1588, 1977.

[73] S. Catani, B.R. Webber, and G. Marchesini. QCD coherent branching and semiinclusive processes at large x. *Nucl. Phys. B*, 349:635–654, 1991.

[74] M. Dasgupta and G.P. Salam. Resummation of nonglobal QCD observables. *Phys. Lett. B*, 512:323–330, 2001.

[75] Mrinal Dasgupta and Gavin P. Salam. Accounting for coherence in interjet E(t) flow: A Case study. *JHEP*, 0203:017, 2002.

[76] Yazid Delenda, Robert Appleby, Mrinal Dasgupta, and Andrea Banfi. On QCD resummation with k(t) clustering. *JHEP*, 0612:044, 2006.

[77] Andrew Hornig, Christopher Lee, Jonathan R. Walsh, and Saba Zuberi. Double Non-Global Logarithms In-N-Out of Jets. *JHEP*, 1201:149, 2012.

[78] Randall Kelley, Jonathan R. Walsh, and Saba Zuberi. Abelian Non-Global Logarithms from Soft Gluon Clustering. *JHEP*, 1209:117, 2012.

[79] Randall Kelley, Jonathan R. Walsh, and Saba Zuberi. Disentangling Clustering Effects in Jet Algorithms. 2012.

[80] Teppo T. Jouttenus, Iain W. Stewart, Frank J. Tackmann, and Wouter J. Waalewijn. The Soft Function for Exclusive N-Jet Production at Hadron Colliders. *Phys. Rev. D*, 83:114030, 2011.

[81] G. Dissertori, A. Gehrmann-De Ridder, T. Gehrmann, E.W.N. Glover, G. Heinrich, et al. First determination of the strong coupling constant using NNLO predictions for hadronic event shapes in e^+e^- annihilations. *JHEP*, 0802:040, 2008.

[82] Thomas Becher and Matthew D. Schwartz. A Precise determination of α_s from LEP thrust data using effective field theory. *JHEP*, 0807:034, 2008.

[83] G. Dissertori, A. Gehrmann-De Ridder, T. Gehrmann, E.W.N. Glover, G. Heinrich, et al. Determination of the strong coupling constant using matched NNLO+NLLA predictions for hadronic event shapes in e^+e^- annihilations. *JHEP*, 0908:036, 2009.

[84] Yang-Ting Chien and Matthew D. Schwartz. Resummation of heavy jet mass and comparison to LEP data. *JHEP*, 1008:058, 2010.

[85] Riccardo Abbate, Michael Fickinger, Andre H. Hoang, Vicent Mateu, and Iain W. Stewart. Thrust at $\mathrm{N^3LL}$ with Power Corrections and a Precision Global Fit for $\alpha_s(m_Z)$. *Phys. Rev. D*, 83:074021, 2011.

[86] Siegfried Bethke, Andre H. Hoang, Stefan Kluth, Jochen Schieck, Iain W. Stewart, et al. Workshop on Precision Measurements of α_s. 2011.

[87] Riccardo Abbate, Michael Fickinger, Andre H. Hoang, Vicent Mateu, and Iain W. Stewart. Precision Thrust Cumulant Moments at N^3LL. *Phys. Rev. D*, 86:094002, 2012.

[88] Torbjörn Sjöstrand, Stephen Mrenna, and Peter Skands. PYTHIA 6.4 physics and manual. *JHEP*, 05:026, 2006.

[89] Torbjörn Sjöstrand, Stephen Mrenna, and Peter Z. Skands. A Brief Introduction to PYTHIA 8.1. *Comput. Phys. Commun.*, 178:852–867, 2008.

[90] J. Beringer et al. Review of Particle Physics (RPP). *Phys. Rev. D*, 86:010001, 2012.

[91] G.P. Salam and D. Wicke. Hadron masses and power corrections to event shapes. *JHEP*, 0105:061, 2001.

[92] Vicent Mateu, Iain W. Stewart, and Jesse Thaler. Power Corrections to Event Shapes with Mass-Dependent Operators. *Phys. Rev. D*, 87:014025, 2013.

[93] Christian W. Bauer, Sean Fleming, and Michael E. Luke. Summing Sudakov logarithms in $B \to X_s\gamma$ in effective field theory. *Phys. Rev. D*, 63:014006, 2000.

[94] Christian W. Bauer, Sean Fleming, Dan Pirjol, and Iain W. Stewart. An effective field theory for collinear and soft gluons: Heavy to light decays. *Phys. Rev. D*, 63:114020, 2001.

[95] Christian W. Bauer and Iain W. Stewart. Invariant operators in collinear effective theory. *Phys. Lett. B*, 516:134–142, 2001.

[96] Christian W. Bauer, Dan Pirjol, and Iain W. Stewart. Soft-collinear factorization in effective field theory. *Phys. Rev. D*, 65:054022, 2002.

[97] Sean Fleming, Andre H. Hoang, Sonny Mantry, and Iain W. Stewart. Jets from massive unstable particles: Top-mass determination. *Phys.Rev.*, D77:074010, 2008.

[98] Matthew D. Schwartz. Resummation and NLO matching of event shapes with effective field theory. *Phys.Rev.*, D77:014026, 2008.

[99] Gregory P. Korchemsky and George F. Sterman. Power corrections to event shapes and factorization. *Nucl.Phys.*, B555:335–351, 1999.

[100] Andre H. Hoang and Iain W. Stewart. Designing gapped soft functions for jet production. *Phys. Lett. B*, 660:483–493, 2008.

[101] Zoltan Ligeti, Iain W. Stewart, and Frank J. Tackmann. Treating the b quark distribution function with reliable uncertainties. *Phys. Rev. D*, 78:114014, 2008.

[102] S. Frixione, Z. Kunszt, and A. Signer. Three jet cross-sections to next-to-leading order. *Nucl.Phys.*, B467:399–442, 1996.

[103] Rikkert Frederix, Stefano Frixione, Fabio Maltoni, and Tim Stelzer. Automation of next-to-leading order computations in QCD: The FKS subtraction. *JHEP*, 0910:003, 2009.

[104] S. Catani and M. H. Seymour. The Dipole Formalism for the Calculation of QCD Jet Cross Sections at Next-to-Leading Order. *Phys. Lett. B*, 378:287–301, 1996.

[105] S. Catani and M. H. Seymour. A general algorithm for calculating jet cross sections in NLO QCD. *Nucl. Phys. B*, 485:291–419, 1997. [Erratum-ibid. **B510**, 503 (1998)].

[106] G. Parisi. Super Inclusive Cross Sections. *Phys. Lett. B*, 74:65, 1978.

[107] John F. Donoghue, F. E. Low, and So-Young Pi. Tensor analysis of hadronic jets in quantum chromodynamics. *Phys. Rev. D*, 20:2759, 1979.

[108] R. Keith Ellis, D. A. Ross, and A. E. Terrano. The Perturbative Calculation of Jet Structure in e^+e^- Annihilation. *Nucl. Phys. B*, 178:421, 1981.

[109] L. Clavelli. Jet invariant mass in quantum chromodynamics. *Phys. Lett. B*, 85:111, 1979.

[110] S. Catani, G. Turnock, and B.R. Webber. Heavy jet mass distribution in e^+e^- annihilation. *Phys. Lett. B*, 272:368–372, 1991.

[111] Paul E.L. Rakow and B.R. Webber. Transverse momentum moments of hadron distributions in QCD jets. *Nucl. Phys. B*, 191:63, 1981.

[112] S. Catani, G. Turnock, and B.R. Webber. Jet broadening measures in e^+e^- annihilation. *Phys. Lett. B*, 295:269–276, 1992.

[113] Yuri L. Dokshitzer, A. Lucenti, G. Marchesini, and G.P. Salam. On the QCD analysis of jet broadening. *JHEP*, 9801:011, 1998.

[114] Thomas Becher and Guido Bell. NNLL Resummation for Jet Broadening. *JHEP*, 1211:126, 2012.

[115] S. Catani and B. R. Webber. Resummed C-parameter distribution in e^+e^- annihilation. *Phys. Lett. B*, 427:377–384, 1998.

[116] S. Catani and B.R. Webber. Infrared safe but infinite: Soft gluon divergences inside the physical region. *JHEP*, 9710:005, 1997.

[117] Iain W. Stewart, Frank J. Tackmann, and Wouter J. Waalewijn. The Beam Thrust Cross Section for Drell-Yan at NNLL Order. *Phys. Rev. Lett.*, 106:032001, 2011.

[118] Xiaohui Liu, Sonny Mantry, and Frank Petriello. Gauge-Boson Production with Multiple Jets Near Threshold. *Phys.Rev.*, D86:074004, 2012.

[119] Iain W. Stewart, Frank J. Tackmann, and Wouter J. Waalewijn. The Quark Beam Function at NNLL. *JHEP*, 1009:005, 2010.

[120] Christian W. Bauer, Frank J. Tackmann, Jonathan R. Walsh, and Saba Zuberi. Factorization and Resummation for Dijet Invariant Mass Spectra. *Phys. Rev. D*, 85:074006, 2012.